# 16 Echocardiography

JUSTINA C. WU, LINDA D. GILLAM, AND SCOTT D. SOLOMON

*Illustrated by Bernard Bulwer*

Echocardiography remains the most commonly used comprehensive cardiac imaging modality and is often the first test of choice for assessing cardiac structure and function. When compared with other imaging methods, echocardiography can be performed quickly at bedside, with minimal patient inconvenience or risk, and provides immediate clinically relevant information at relatively low cost. Echocardiography provides detailed data on cardiac structure, including the size and shape of cardiac chambers, as well as the morphology and function of cardiac valves. Furthermore, the real-time nature of echocardiography makes it uniquely suited to immediate non-invasive assessment of systolic and diastolic function and intracardiac hemodynamics. In most echocardiography laboratories, standard *transthoracic echocardiography* (TTE) is complemented by *transesophageal echocardiography* (TEE) imaging from within the body which offers improved resolution, and by *stress echocardiography*, which is routinely used to assess myocardial ischemia and valvular function with exercise. Technical advancements in echocardiography over the past decades have led to progressively improved diagnostic capabilities. In recent years, these included advances in three-dimensional (3D) and tissue strain imaging, expanded functionality and miniaturization of systems that can be used for point of care imaging, and contrast echocardiography for better cavity visualization, augmentation of Doppler signals and assessment of tissue perfusion.

Two-dimensional (2D) echocardiography is not a tomographic technique such as cardiac computed tomography (CT) or cardiac magnetic resonance (CMR) imaging (see Chapters 19 and 20); acquisition of ultrasound images is dependent on the operator—either a sonographer or a physician. Both acquisition and interpretation of echocardiograms require substantial training and skill. Thus, echocardiography is best described as an "examination" rather than a "test." Although cardiologists receive this training routinely, a growing number of non-cardiologists, including emergency physicians, anesthesiologists, intensivists, and in-patient hospital staff are increasingly using echocardiography in their practice, in some cases with small handheld ultrasound devices (POCUS, or point-of-care ultrasound devices). Knowledge of the basic principles, utility, and limitations of echocardiography is becoming essential for all physicians who care for patients with cardiovascular problems.

## PRINCIPLES OF ULTRASOUND AND INSTRUMENTATION

### Principles of Image Generation

Echocardiography is based on the standard principles of ultrasound imaging in which high-frequency sound waves in the 1 to 10 MHz range are emitted from piezoelectric crystals housed in a transducer, traverse through internal body structures, interact with tissues, reflect back to the transducer, and are then processed by microcomputers to generate an image. An understanding of the physical principles that underlie echocardiography is essential to understanding its usefulness and limitations.[1]

Ultrasound machines measure the time required for sound waves to reflect from structures and return to the transducer, and use this data to calculate the depth of reflecting structures. This information is used to generate scan lines that depict both *location* (depth of reflection) and *amplitude* (intensity of reflection). Early ultrasound equipment projected a single beam of ultrasound, which resulted in a single scan line that could be "painted" across a moving paper or screen, with depth being depicted on the vertical axis and time on the horizontal axis. This method, known as *M-mode* (for motion) echocardiography (Fig. 16.1, lower right), has largely been replaced by 2D imaging (see Fig. 16.1, lower left). However, M-mode is still used routinely and is particularly useful for characterizing high-frequency events or making linear measurements and assessments that require precise timing with respect to the cardiac cycle.

Additional content is available online at Elsevier eBooks for Practicing Clinicians

Current 2D imaging scans sectors of the heart using phased-array transducers, in which the piezoelectric crystal is precisely diced into multiple (hundreds to thousands) of elements that emit and receive sonar pulses. Phased-array transducers steer the beam electronically through an arc side-to-side to create a scan plane (Fig. 16.2). The transducer emits pulses of ultrasound in an ordered sequence and sequentially "listens" for returning echoes, referred to as the *pulse-echo principle*.



FIGURE 16.1 Generation of ultrasound images. An ultrasound pulse transmitted from piezoelectric elements housed in a transducer **(upper left)** reflects off structures and returns to the transducer. These signals are processed and displayed based on their amplitudes **(upper right)**. Echoes with the highest amplitudes emerge from tissue interfaces such as the pericardial-pleural and endocardial-blood borders. In original A-mode scans, such signals are visualized as amplitude spikes. On B-mode, the echo amplitudes are displayed via gray scale. B-mode images can then be displayed in one dimension over time, i.e., M (motion)–mode **(bottom right),** or as a two-dimensional cross-sectional image **(bottom left)**. *IVS,* Interventricular septum; *LV,* left ventricle; *PW,* posterior wall. (Modified from Bulwer BE, Rivero JM, eds. *Echocardiography Pocket Guide: The Transthoracic Examination*. Burlington, MA: Jones & Bartlett Learning; 2011, 2013. Reprinted with permission.)

The returning sound waves are coded into electric signals, and repetition of this sequence enables reconstruction of moving images to depict the heart. The rate at which these pulses are emitted is termed the *pulse repetition frequency* (PRF). Proper interpretation of returning signals is physically limited by the speed of sound in tissues (approximately 1540 m/sec) and the depth of the tissues being interrogated, both of which dictate the time it takes for the ultrasound signal to return to the transducer. Nevertheless, improvements in processing speed have allowed "frame" rates, a major determinant of temporal resolution, to reach speeds higher than 100 image frames per second. In practice, the echo machine operator can also increase frame rate by narrowing the scan sector, imaging at shallower depths, and reducing scan line density. (On most systems, the preprocessing "zoom" feature easily narrows the sector to the region of interest to accomplish this.) 3D echocardiography extends the phased-array concept to make use of a planar waffle-like grid or matrix-array of elements (3000+), which allows both simultaneous multiplanar 2D imaging and true volumetric 3D imaging and rendering (see Three-Dimensional Echocardiography).
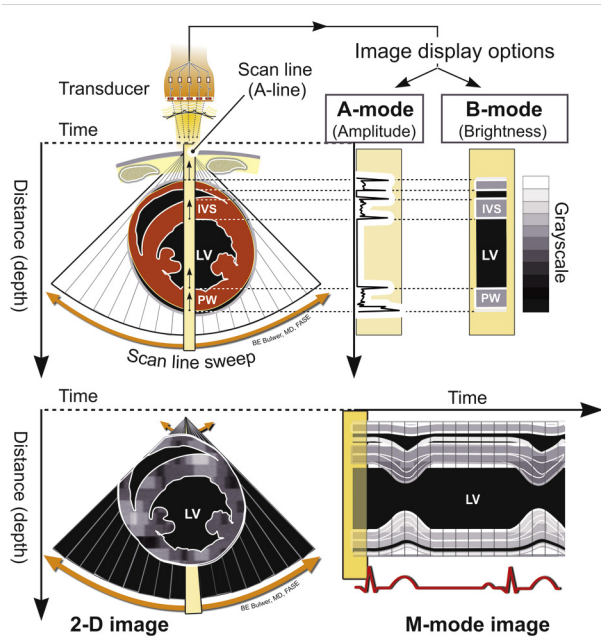
## Physical Principles of Ultrasound

The physical characteristics of ultrasound are exploited to generate images representative of the heart. The wavelength of the ultrasound used, which is inversely related to ultrasound frequency, is the principal determinant of axial imaging resolution, which equals approximately half the wavelength. The higher the ultrasound frequency (i.e., shorter the wavelength), the higher is the spatial resolution. Imaging resolution is also dependent on the depth of the structure being interrogated. Therefore, the choice of imaging frequency involves a trade-off between image resolution and target tissue depth: higher frequencies are capable of increased resolution, but at the expense of reduced tissue penetration. Most TTE machines operate across frequencies of 2.5 to 5 MHz. Higher frequencies up to 7 to 10 MHz can be used in pediatric imaging, in TEE where the transducer is closer to the heart, or when interrogating near-field structures, such as the apex of the heart from the apical window. Current broad-bandwidth transducers allow the operator to easily modify the transmit frequency (mHz), so that one may start with higher transmit frequency for better image resolution but adjust the frequency downwards during the exam if additional tissue penetration is desired.

The speed of ultrasound through body tissues averages 1540 meters per second (m/sec), essentially the speed of sound through water, but varies minutely as ultrasound waves traverse various body constituents. These slight differences in ultrasound speed through different media (e.g., blood, muscle, fat, air) result in impedance mismatches at the tissue interfaces, which produces the *specular reflections* that mark the boundaries between different tissues. The most intense reflections occur when ultrasound strikes these interfaces perpendicularly and when the tissues differ greatly in density. When ultrasound encounters inhomogeneous tissue regions, such as myocardium, liver, or other tissues, multidirectional reflection, or *backscatter*, occurs and results in speckled-appearing images. The combination of specular reflections and backscatter, together with the unique interactions between ultrasound and tissue such as refraction, interference, and attenuation, contributes to the characteristic gray-scale appearance of ultrasound images. Ultrasound
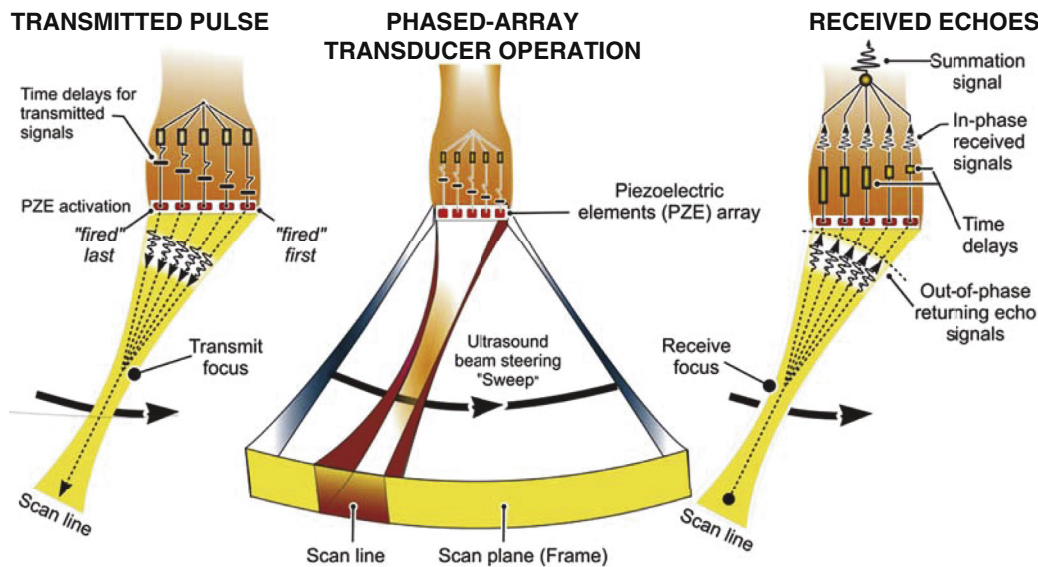


FIGURE 16.2 Phased-array transducer operation. Modern echocardiography transducers scan through a relatively wide scan sector by steering the electronic beam across the scan plane **(center)**. During transmission **(left)**, electronic time delays in firing the piezoelectric elements of the transducer cause the scan line to sweep in an arc. During reception **(right),** the returning echo signals received by each transducer element must be time-shifted or phased before being summated and processed. (Modified from Bulwer BE, et al. Physics of echocardiography. In Savage RM, Aronson S, Shernan SK, eds. *Comprehensive Textbook of Perioperative Transesophageal Echocardiography*. Philadelphia: Wolters Kluwer; Lippincott, Williams & Wilkins; 2009:1–41.)
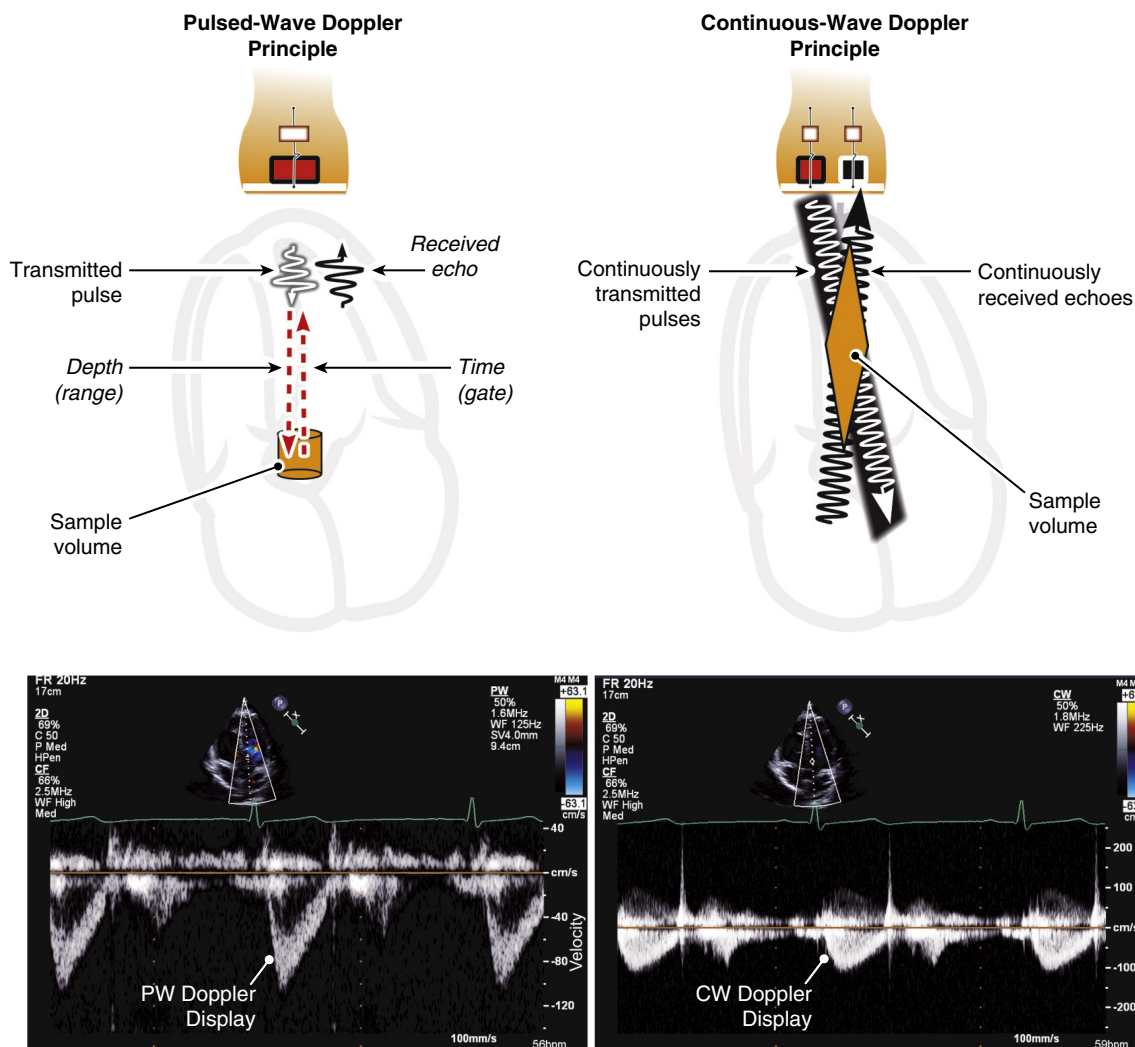
**FIGURE 16.3** Pulsed-wave (PW) versus continuous-wave (CW) Doppler. **Left,** PW Doppler technique uses a single piezoelectric element that generates the pulse, interrogates a small sample volume at a specific depth, and receives the emerging echoes within the specified time window. **Right,** CW Doppler technique uses two separate transducer elements, one continuously transmitting pulses and the other receiving echoes across a large sample volume, and thus cannot localize the depth of the site with highest velocity.

penetrates poorly through air and bone, which is one of the greatest challenges to echocardiography because the heart is surrounded by the lungs and the rib cage. The ability to circumvent these limitations during image acquisition underscores the importance of the operator's skill and the advantages of a TEE approach in specific clinical situations.

Several advances in the past decade have improved the quality of ultrasonic imaging. The higher number of elements in phased-array transducers has increased the number of scan lines and thus lateral resolution. *Tissue harmonic imaging* is now the norm, in which the receiver "listens" for returning second-harmonic ultrasound signals that are twice the fundamental frequency of the emitted ultrasound. By doing so, it effectively filters out the weaker noisy and artefactual signals and has substantially improved the definition of tissue interfaces, in particular that of the endocardial borders (eFig. 16.1), when compared to fundamental imaging.

### PRINCIPLES OF DOPPLER IMAGING
In addition to generating images of cardiac structures, ultrasound can be used to interrogate the velocity of blood flow through the heart and to assess myocardial motion. These techniques are based on the Doppler principle, which states that the perceived frequency of a waveform bounced back from a moving object will be perceived as shifted from the emitting frequency, depending on whether the object is moving toward or away from the observer. Ultrasound that is reflected from red blood cells moving toward the emitter will appear to be at a higher frequency, whereas blood flow away from the transducer will cause the perception that a lower-frequency waveform has been reflected (eFig. 16.2). This difference between the frequency emitted and that received is termed the *Doppler frequency shift* and is dependent on the speed of ultrasound through the medium and the velocity of blood flow. The basic equation for Doppler shift ($f_d$) is $f_d = f_t V/c$, where $f_t$ is the transmitted ultrasound frequency, V is the velocity of blood flow, and c is the speed of ultrasound in the tissue. For cardiac ultrasound, multiplication by a factor of 2 occurs because the Doppler shift occurs twice (when the wave goes to and from the moving object). Notably, the velocity information obtained is most accurate when the ultrasound beam is aligned parallel to the direction of blood flow (i.e., an optimal angle of insonation is 0 degrees). When the angle of insonation (θ) cannot be physically corrected, the correction factor *cos*θ may be applied. Thus the refined formula for Doppler shift is:

$$F_d = 2f_t V (\cos \theta)$$

Ultimately, the equation above is used to solve for velocity, V, of blood flow.

### Pulsed-Wave and Continuous-Wave Doppler
The two principal types of Doppler imaging are pulsed-wave (PW) and continuous-wave (CW) Doppler. In PW Doppler (Fig. 16.3, left panel), discrete pulses of ultrasound reflect off moving structures (i.e., red blood cells moving through the heart) and return to the transducer. By *gating,* or defining a specific time window during which the machine "listens"

**FUNDAMENTAL IMAGING**
Images created using echoes
with the fundamental frequency (*F*)

**HARMONIC IMAGING**
Images created using echoes with
second-harmonic frequency (*2F*)

**POOR IMAGE QUALITY:**
Much interference and artifact

**BETTER IMAGE QUALITY:**
Less interference and artifact

*F*

*2F*

**Receive at
2.5 MHz**

**Receive at
5 MHz**

**Transmit at
2.5 MHz
(*F*)**

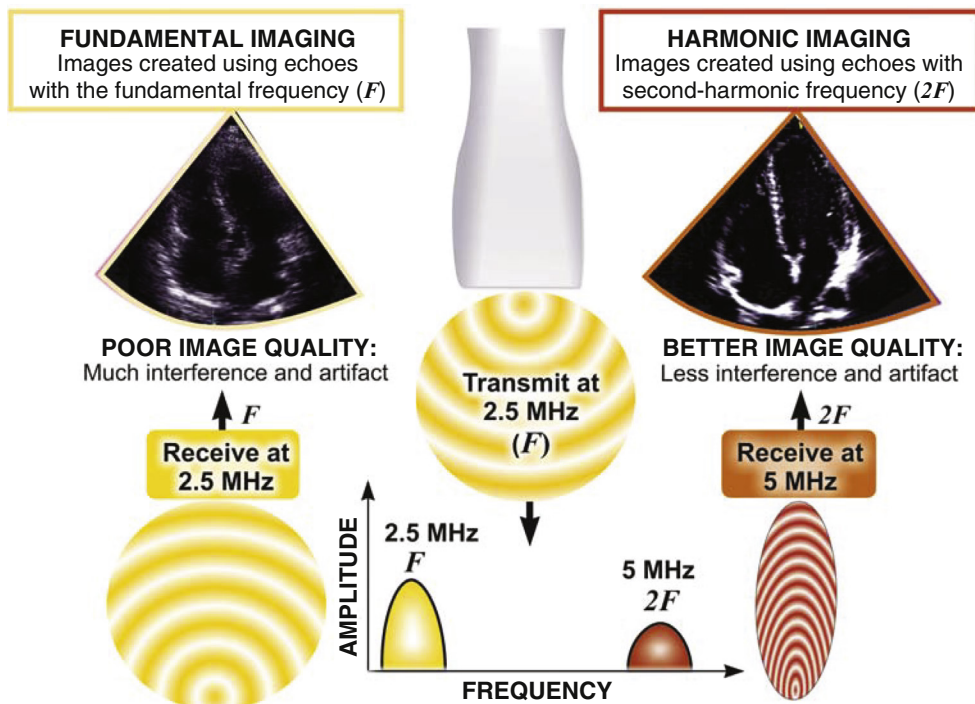AMPLITUDE

2.5 MHz
*F*

5 MHz
*2F*

FREQUENCY

**EFIGURE 16.1** Tissue harmonic imaging. Tissue harmonic imaging improves image quality by using second-order harmonics. Ultrasound causes tissues to vibrate at a the fundamental frequency **(left)** but also multiples (harmonics) of that frequency. By listening for the higher (second-order) frequency returning echoes, signal-to-noise ratio and tissue definition are dramatically improved **(right)**. The transmit and receive frequencies (e.g., 1.8/3.6 MHz) may be displayed on the echo machine screen. (Modified from Bulwer BE, et al. Physics of echocardiography. In Savage RM, et al., eds. *Comprehensive Textbook of Perioperative Transesophageal Echocardiography*. Philadelphia: Wolters Kluwer: Lippincott, Williams & Wilkins; 2009:1–41.)



**HIGHER-FREQUENCY ECHOES**

Echo
$f_R$

$f_T$ Transmitted Pulse

**Moving
*Toward transducer***

Frequency Shift / Velocity

+ve
**Doppler
shift**

***f*Doppler Signal**

**Doppler
Frequency
Shift**

Doppler     Echo     Pulse
$f_{Dop} = f_R - f_T$

**LOWER-FREQUENCY ECHOES**

Echo
$f_R$

$f_T$ Transmitted Pulse

**Moving
*Away from transducer***

Frequency Shift / Velocity

-ve
**Doppler
shift**
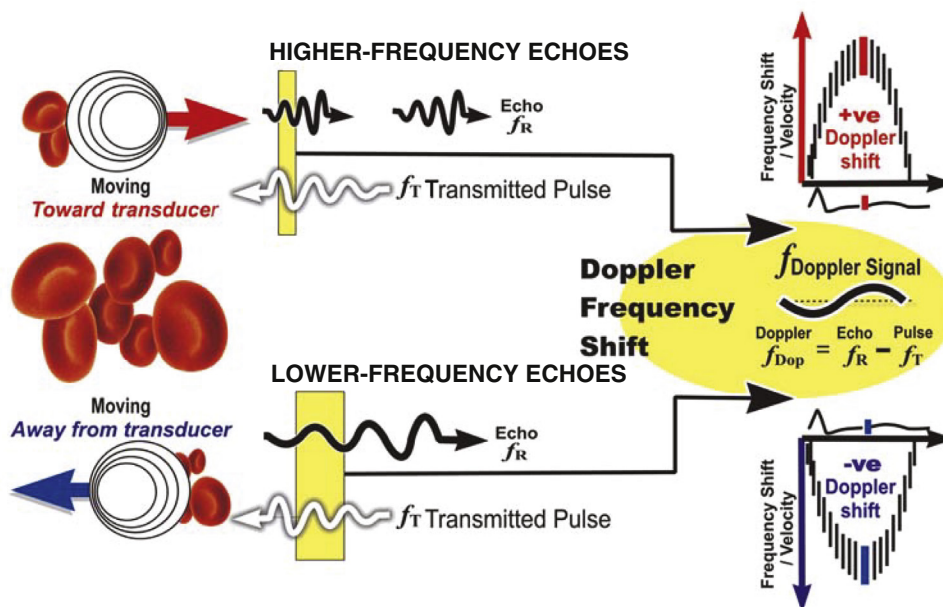
**EFIGURE 16.2** The Doppler frequency shift. Echoes reflected from blood cells moving toward the transducer will be perceived as returning at a higher frequency than the transmitted ultrasound pulse **(upper panels)**. The opposite is seen with blood moving away from the transducer **(lower panels)**. Doppler echocardiography instruments harness this shift in frequency to derive blood flow velocities. The direction of flow is displayed graphically as a time-velocity spectrum above or below the baseline (in spectral Doppler) or as color-coded velocities with color flow Doppler.

for reflected signal, this technique can be used to ascertain the velocity of blood flow at a prespecified depth within the heart. Thus, when an operator places the cursor (sample volume) on the 2D ultrasound image at a particular location, the equipment will assess the velocity at that point. Because it takes time for the pulses to reflect and return to the transducer, they cannot be transmitted too frequently, or the equipment will fail to discern whether a given pulse has returned from the defined location or some multiple of that distance from the transducer, and the velocity information obtained at that depth will be ambiguous. The PRF is essentially the sampling rate; the higher the blood flow velocity, the higher is the frequency of the Doppler shift and thus the higher the sampling rate needed to accurately sample that shift (eFig. 16.3). These physical principles limit the upper range of velocities that can be interrogated with PW Doppler. The *Nyquist limit* refers to the maximum velocity that can be accurately quantified within a given sample volume and is directly related to the PRF (the numeric value equals ½ the PRF). PRF in turn is inversely related to the distance from the sample volume to the transducer. The machine is unable to assess velocities that are higher than the Nyquist limit, because the values will go off-scale and appear to "alias" (wrap around) in the generated spectrogram; adjusting the Nyquist limit setting on the machine upward effectively adjusts the PRF upward until the physical limit is reached.

With CW Doppler (see Fig. 16.3, right panel) a dedicated piezoelectric element continuously emits ultrasound, and a separate element simultaneously continuously receives the returning signals. Because the ultrasound tone is continuous rather than pulsed, depth of the target cannot be determined from the signal received. However, unlike the situation with PW Doppler, no limit is imposed on the velocities discernible with this technique. *Thus PW Doppler is primarily used to assess flow with relatively low velocity (typically ≤1.5 m/sec) present at a specific location, whereas CW Doppler is used to assess higher velocities (typically ≥1.5 m/sec) along the transducer beam, but cannot specify at what location the highest velocity occurs.* Note that PW Doppler envelopes have a linear "hollowed-out" profile because the blood within the small sample volume tends to travel at similar velocities (laminar flow), whereas CW Doppler envelopes are "filled in" because all the varying velocities along the ultrasound beam are received and recorded.

### Color Flow Doppler

Color flow Doppler is a PW Doppler–based technique in which the velocities in a region of interest are encoded with colors that represent both mean velocities and directionality of the flow, which are superimposed on a 2D image in the region of interest (Fig. 16.4). By convention, flow moving away from the transducer is encoded in blue, and flow toward the transducer is encoded in red. Because color flow Doppler is a form of PW Doppler, it is subject to aliasing, such that high velocities (greater than the Nyquist limit) demonstrate "wraparound" in the color coding to the color of the opposite direction. Turbulent flow, in which a wide range of velocities exist, appears as a multicolored mosaic pattern (usually *green* and *yellow*). In some systems the variance in the velocities relative to the mean is color-coded in superimposed shades of *green*. Color flow Doppler allows direct real-time visualization of the movement of blood in the heart and is particularly useful for identifying blood flow acceleration and turbulence. Therefore, this technology is useful for delineating both regurgitant lesions, in which blood moves rapidly and opposite to the expected direction of flow, and discrete stenoses in which there is flow acceleration.

### Blood Flow Profiles and Doppler Signals

**Laminar Versus Turbulent Flow.** Blood flow through the normal heart and great vessels is predominantly *laminar,* meaning that the direction and velocity of flow are streamlined and uniform, even across valves. Figure 16.5 shows that the spectral Doppler flow signal observed when interrogating laminar flow is characterized by a hollowed-out waveform with a narrow outline, indicating that flow velocities throughout the sample are similar. In a Doppler assessment of the left ventricular outflow tract (LVOT), for example, the Doppler profile represents the velocity of blood flow throughout systole and is usually laminar. In contrast, valvular or vessel stenoses or obstructive lesions often cause turbulent flow, in which blood moves at different velocities and in multiple directions. In these cases, if the range of velocities is still largely within the Nyquist limit, the displayed spectrum of velocities will be wider on PW Doppler, a phenomenon termed *spectral broadening.* On color Doppler, turbulent flow appears brighter with a mixture of colors.

As illustrated by the Doppler equation and discussed earlier, the velocity of blood flow determined from the Doppler shift will change with the angle of insonation (θ). If the vector of flow is not directly in line with the ultrasound beam, the velocities calculated by the Doppler
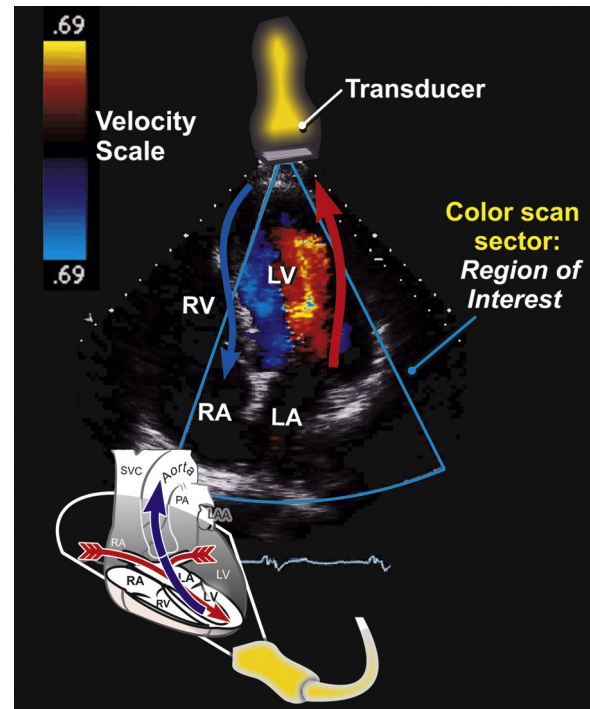


**FIGURE 16.4** Color flow Doppler. By convention, blood flow moving toward the transducer is color-coded *red* and flow away from the transducer is shown in *blue*. The color velocity scale (*upper left vertical bar*) represents increasing velocities in either direction. with higher velocities depicted in progressively brighter hues. Note the Nyquist limit (69 cm/sec) displayed above and below the color scale bar. Velocities greater than the Nyquist limit cause aliasing, i.e., an apparent wraparound in the color-coding to that of the opposite direction. *LA,* Left atrium; *LV,* left ventricle; *RA,* right atrium; *RV,* right ventricle. (Modified from Bulwer BE, Rivero JM, eds. *Echocardiography Pocket Guide: The Transthoracic Examination*. Burlington, MA: Jones & Bartlett Learning; 2011, 2013:156. Reprinted with permission.)

shift will be underestimates of those of red blood cells. This problem can be corrected by applying an angle adjustment (cosθ) that is computed at the machine level. However, the further the angle of flow deviates from the angle of the beam, the greater the likelihood for error in the calculation. In practice, for cardiac ultrasound it is recommended simply to minimize the angle of insonation as much as possible by probe and patient positioning and to avoid Doppler assessments that are substantially off-angle. It is for this reason that multiple windows are used in assessing peak flow velocities of aortic stenosis (AS) and tricuspid regurgitation (TR). Ideally, the window with the lowest angle of insonation is selected to avoid underestimation. In specific cases where flow is very laminar and insonation angles are unavoidable, such as in vascular ultrasound, the angle correction factor proves to be useful.

## Doppler Echocardiography in Practice

Doppler echocardiography is used primarily to assess blood flow velocity in the heart and blood vessels. Within the heart, the velocity of blood flow is itself dependent on the pressure gradient between cardiac chambers, with higher gradients resulting in higher velocities. This relationship can be described by the Bernoulli equation, which estimates the pressure gradient (ΔP) between two chambers separated by an orifice based on the velocity of flow through the orifice. The original Bernoulli equation (eFig. 16.4) is complex and includes variables for flow acceleration and viscous friction and a constant for fluid density. The clinical equation used in echocardiography assumes that these two factors are negligible, and that the velocity ($V_1$) proximal to an orifice is relatively low in comparison to that distal velocity. This leaves the vastly simplified equation for use in clinical echocardiography for ΔP:

$$P_1 - P_2 = 4V^2$$

For example, the peak flow velocity of a tricuspid regurgitant (TR) jet can be used to calculate the pressure gradient ΔP between the right
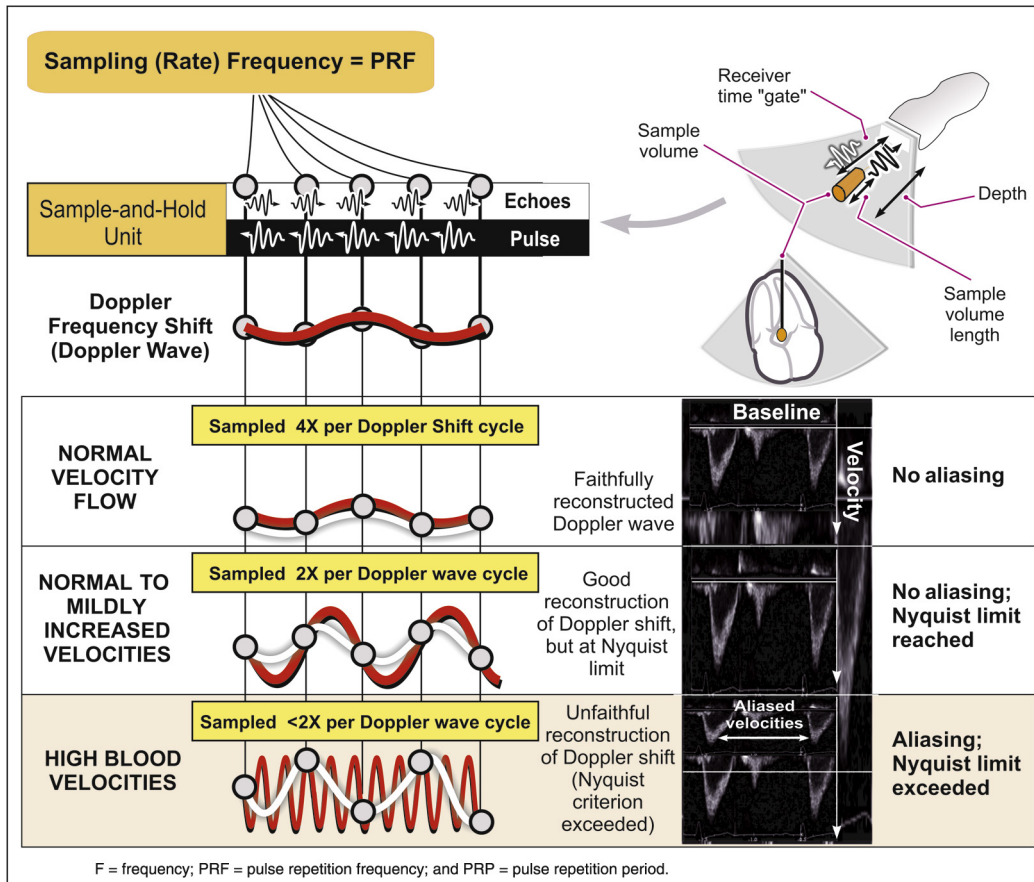
**EFIGURE 16.3** Velocities derived from Doppler frequency shifts are extracted through sampling and transformation (Fourier) before being graphically displayed. PW Doppler is subject to the limitation of aliasing when the Nyquist criterion or limit is exceeded, thus limiting the velocities that can be accurately depicted with this modality. The sampling frequency (pulse repetition frequency, PRF) must be at least twice the frequency of the sampled waveform. In Doppler ultrasound, the sampling rate must be high enough to sample the Doppler shift, which is the difference between the ultrasound frequency emitted by the transducer and the perceived ultrasound frequency returning to the transducer. As shown by the Doppler equation, $f_d = \dfrac{2f_t V \cos \theta}{C}$, this difference, the Doppler frequency shift, is directly related to the velocity of the flow being assessed. PW Doppler can accurately sample and reconstruct lower blood velocities (from the Doppler shift) with no ambiguity (aliasing) **(upper panels)**. The frequency at which waveform sampling will become ambiguous is referred to as the Nyquist limit and is half the PRF. When velocities being assessed exceed the Nyquist limit, the system cannot accurately determine these velocities, and aliasing occurs **(lower panels)**. These higher aliased velocities will appear on the opposite side of the baseline on the spectral Doppler display or will result in mosaic patterns in color flow Doppler imaging. How can this problem be minimized? Simply increasing the PRF works only up to a certain point because the farther the ultrasound pulse has to travel, the greater the time delay must be between pulses to avoid ambiguity. Newer ultrasound machines can perform high-PRF Doppler imaging, in which pulses are emitted without waiting for the original pulses to return to the transducer. This allows an unaliased signal at the expense of some range ambiguity. The technique is meant to be used in conjunction with standard PW Doppler, with the operator determining the region of highest velocity along a scan line with color Doppler and then switching to the high-PRF mode to determine this velocity.
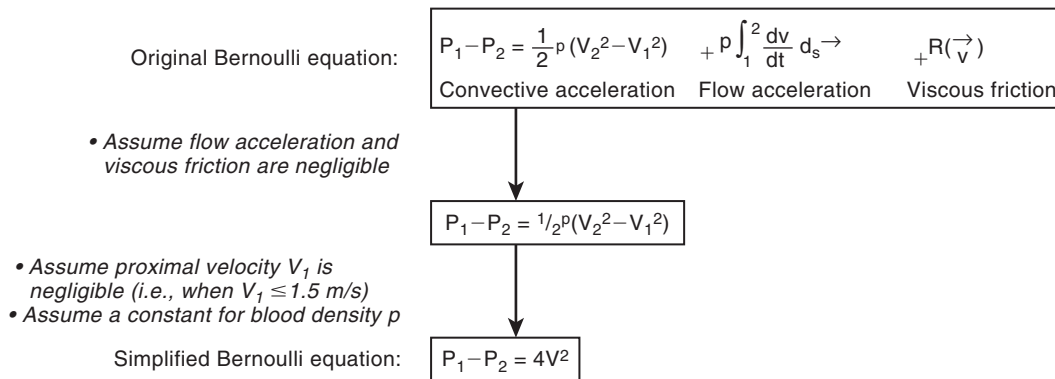


**EFIGURE 16.4** The Bernoulli equation. Derivations of the Bernoulli equation as applied to echocardiography. This equation is used to estimate the pressure difference $\Delta P = P_1 - P_2$ across orifices or stenoses in the heart. Simply put, the narrower the orifice, and the higher the change in velocity (and thus the higher the pressure gradient).
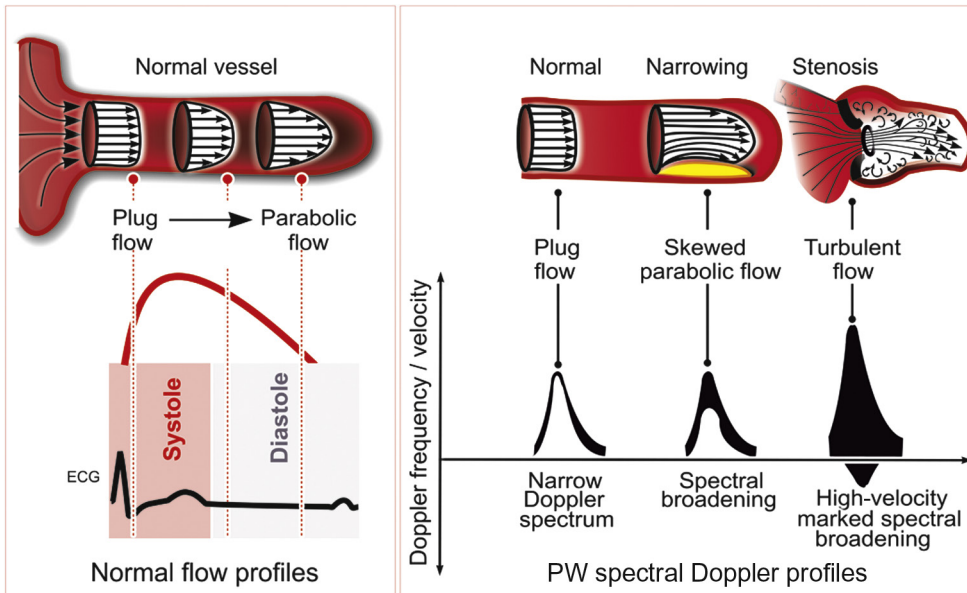
**FIGURE 16.5** Flow velocity profiles on spectral Doppler. **Left,** During the cardiac cycle, most intracardiac and large arterial flows exhibit a laminar flow profile termed "plug flow" proximally that progresses distally to a more parabolic profile because of drag force and blood viscosity. **Right,** The narrowest range or spectrum of flow velocities is seen during the initial phases of systole or when valves open (plug flow). As the vessel becomes stenotic, the turbulence causes progressively wider variation in flow velocities and directions. On spectral Doppler this manifests as a splay in velocities both above and below the baseline. (Modified from Bulwer BE, et al. Physics of echocardiography. In Savage RM, Aronson S, Shernan SK, eds. *Comprehensive Textbook of Perioperative Transesophageal Echocardiography*. Philadelphia: Wolters Kluwer; Lippincott, Williams & Wilkins; 2009:23.)
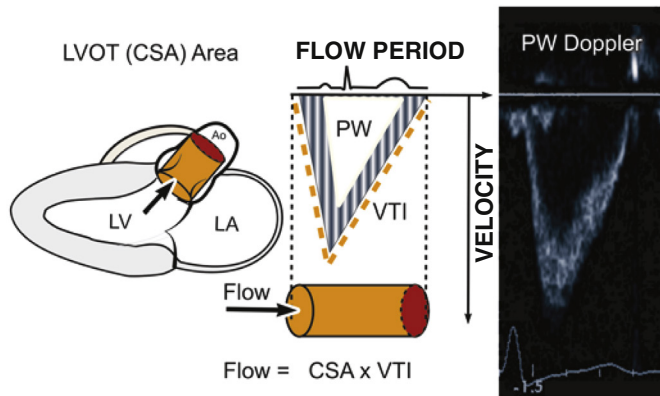


**FIGURE 16.6** Volumetric flow assessments using spectral Doppler. The volume of a cylinder is cross-sectional area (CSA) multiplied by length. Using this geometric assumption and assuming constant flow during systole, stroke volume (SV) can then be derived from the CSA of the left ventricular outflow tract (LVOT) measured on the parasternal long-axis view. This is then multiplied by the Doppler velocity-time integral (VTI) measured on apical windows. *Ao,* Aorta; *LA,* left atrium; *LV,* left ventricle.

ventricle and the right atrium, which when added to an estimate of right atrial (RA) pressure, provides an estimate of right ventricular systolic pressure (RVSP; and hence pulmonary artery systolic pressure [PASP] in most cases). Similarly, the blood flow velocity difference between the LVOT and the aorta can be used to calculate the peak instantaneous pressure gradient across a stenotic aortic valve. It is important to appreciate that Doppler echocardiography measures *velocity* but neither pressure nor flow direction. Pressure gradients are inferred from velocities based on the Bernoulli equation, but the absolute pressure within chambers cannot be directly measured as in cardiac catheterization. Similarly, the amount of flow cannot be measured directly, although there are Doppler-based methods that permit fairly accurate estimation of flow volumes (see below).

## Assessment of Flow and Continuity Equation

Doppler methods are used to assess blood flow velocities, but the magnitude of flow can also be inferred by multiplying the *velocity-time*

*integral* (VTI; i.e., integrated velocity throughout the cardiac interval) by the cross-sectional area (CSA) of the region being interrogated (Fig. 16.6). For example, stroke volume (SV) can be estimated by interrogating the LVOT region with PW Doppler and multiplying the VTI by the CSA (calculated by measuring the diameter of the LVOT and assuming a circular area $= \pi r^2$):

$$SV = VTI_{LVOT} \times Area_{LVOT}$$

The continuity principle is based on conservation of mass and states that flow in one region of the heart should be equivalent to flow in another region (assuming no intervening shunt or valve regurgitation). It can be applied to Doppler and imaging data to determine an unknown cross-sectional area, such as that of a stenotic valve. The CSA of a stenotic valve can be difficult to measure directly (i.e., by planimetry) if image quality is suboptimal. By combining the calculated CSA and measured VTI proximal to the valve with the VTI at the valve itself, the CSA of the stenosis can be calculated. Since velocities through stenotic valves are usually too high to assess with PW Doppler, CW Doppler is usually used, assuming that the highest attained velocities correspond to the narrowest region along the ultrasound beam. Because the continuity principle states that flow through the LVOT must equal flow through the aortic valve (AV);

$$VTI_{LVOT} \times Area_{LVOT} = VTI_{AV} \times Area_{AV}$$

Rearranging the equation to solve for Area$_{AV}$ will give the desired valve CSA. The accuracy of this estimate depends on the accuracy of the LVOT CSA calculation (and thus LVOT diameter measurement) and optimal positioning of the PW and CW Doppler cursors.

## THE STANDARD ADULT TRANSTHORACIC ECHOCARDIOGRAPHIC EXAMINATION

The standard adult TTE examination consists of a combination of 2D, M-mode, and Doppler imaging. The recommended comprehensive examination protocol involves a series of views, each of which is described in terms of three principal components: (1) the standard transducer position or "window," (2) the orthogonal imaging planes, and (3) the anatomic region of interest (Figs. 16.7 and 16.8). At each transducer position the operator optimally acquires 2D images with M-mode images, spectral Doppler, and color flow Doppler as indicated.

### M-Mode Echocardiography

M-mode echocardiography provides greater temporal resolution than standard 2D imaging and was traditionally the method of choice for certain linear measurements, particularly those that are collinear with the ultrasound beam. Standard reports continue to include measurements of septal and posterior wall thickness and left ventricular (LV) chamber dimensions on parasternal views. Figure 16.9A shows a normal M-mode at the basal left ventricle. Because M-mode echocardiography is essentially a one-dimensional imaging technique, it has several limitations that should be recognized. For accurate measurements the cursor scan line must be oriented perpendicular to the long axis of the left ventricle or left atrium, which may require operator steering or machine correction to achieve. For these reasons, convention has now shifted to using 2-dimensional measurements for standardization.[2,3] M-mode–based estimates of LV volume, mass, and function can also be inaccurate in patients with LV geometries that deviate substantially
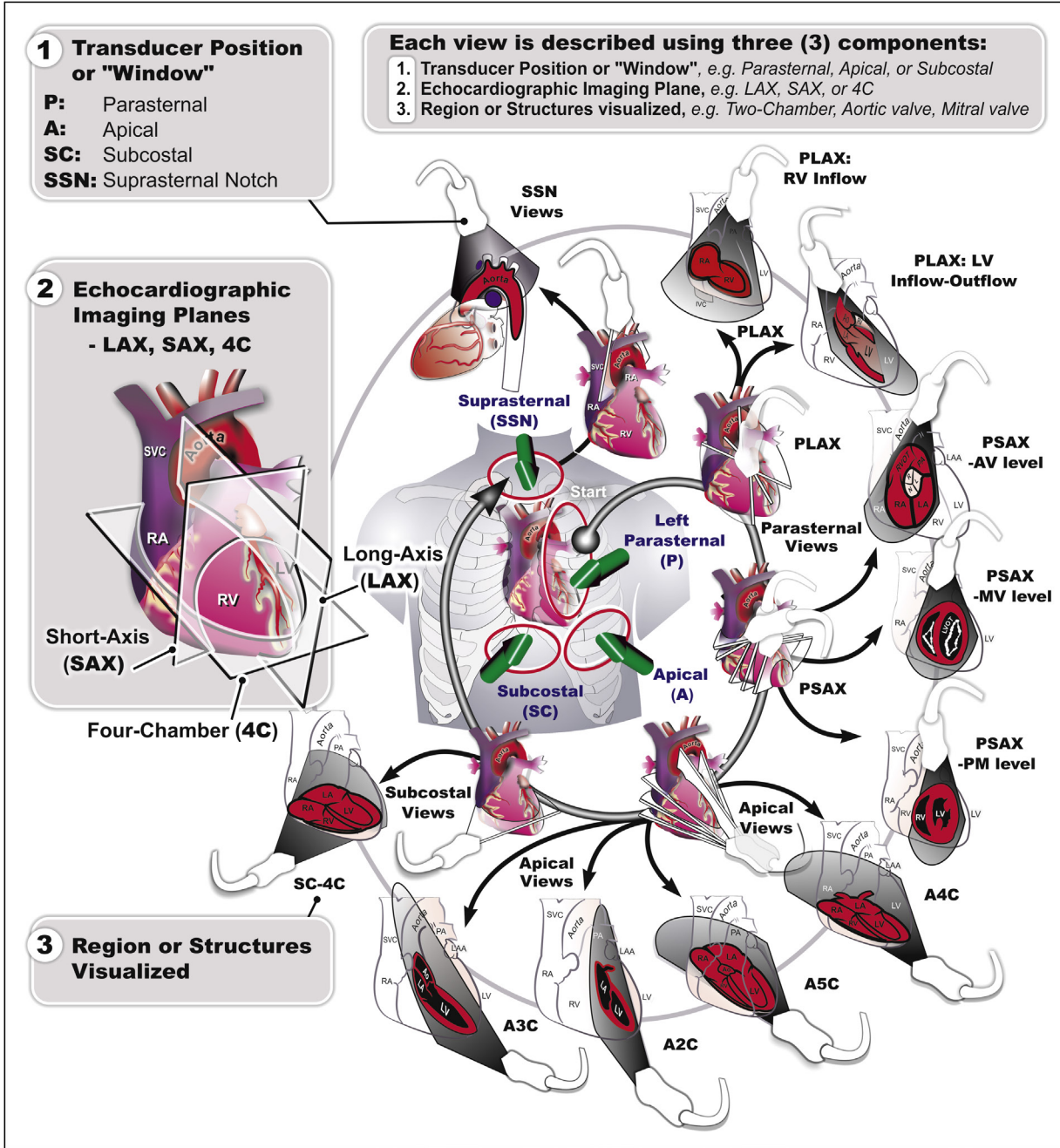
**FIGURE 16.7** Standard adult transthoracic echocardiography imaging planes, protocol, and nomenclature recommended by the American Society of Echocardiography (ASE). Each echocardiographic view can be described by three parameters: window, plane, and structure visualized. See Fig. 16.8 for abbreviations. (Modified from Bulwer BE, et al. Physics of echocardiography. In Savage RM, Aronson S, Shernan SK, eds. *Comprehensive Textbook of Perioperative Transesophageal Echocardiography*. Philadelphia: Wolters Kluwer; Lippincott, Williams & Wilkins; 2009:1–41.)

## Parasternal Long-Axis View (PLAX)

Interventricular septum
Right ventricular free wall
Postero-medial papillary muscle
Right coronary cusp
RV
Ascending aorta
Ao
LV
Non-coronary cusp
LA
Pericardium
Descending thoracic aorta

Diastole

## PSAX: Papillary Muscle (PM) Level

RV cavity
LV cavity
Posteromedial papillary muscle
Anterolateral papillary muscle
Pericardium
Inferior wall
Anterior wall
LV cavity
Septal wall
Lateral wall
**PSAX: Apical Level**
Inferior wall

Systole

## SC 4-Chamber View

LIVER
Lateral wall of right ventricle
Interventricular septum
RV
LV
Pericardium
Tricuspid valve
RA
LA
Anterolateral papillary muscle
Interatrial septum
Posterior leaflet of mitral valve

Systole

## Right Ventricular (RV) Inflow View

RV
RA
RV anterolateral (free) wall
Inferoposterior papillary muscle
RV
Anterior leaflet (Tricuspid valve)
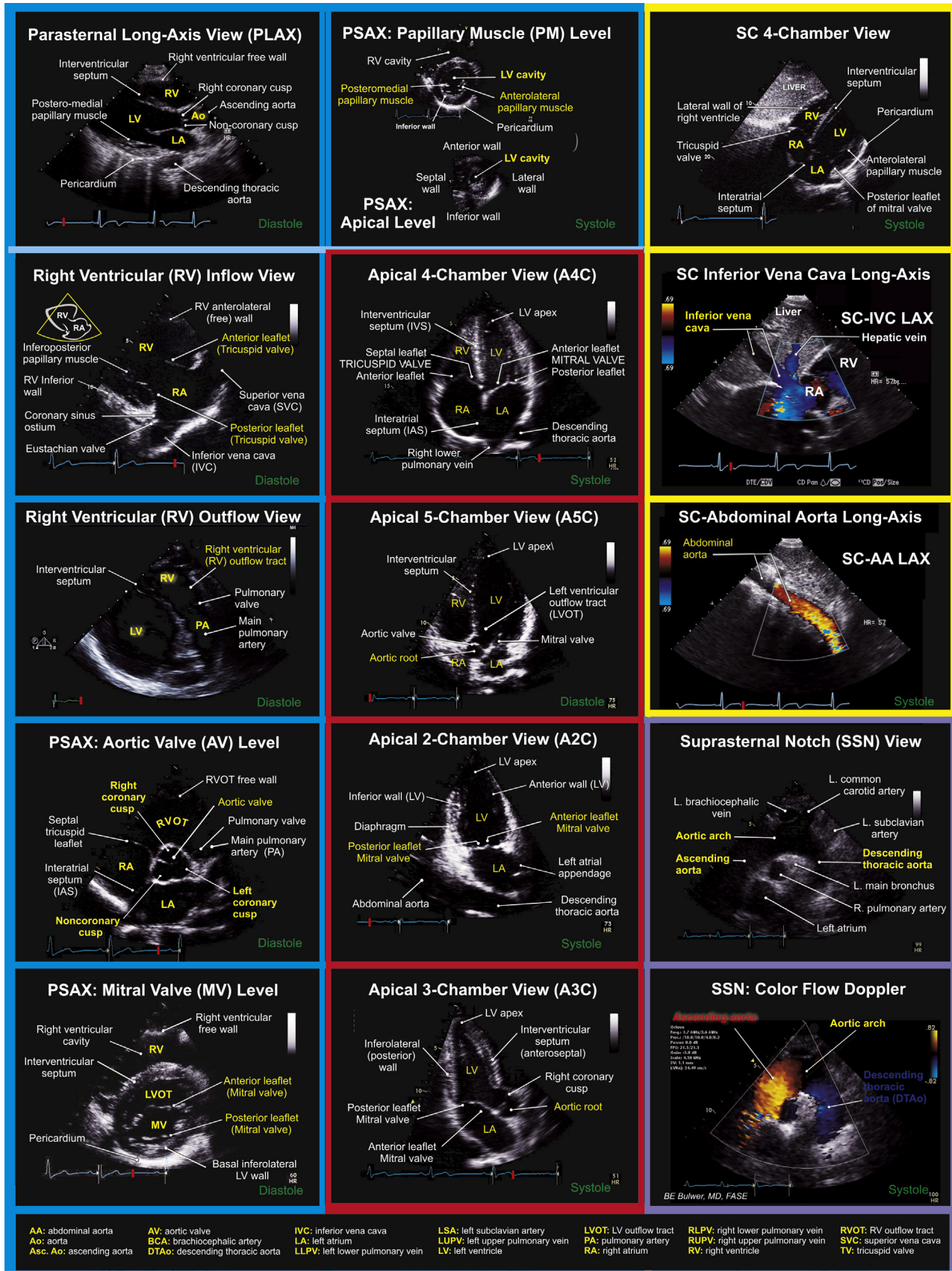RV Inferior wall
RA
Coronary sinus ostium
Superior vena cava (SVC)
Eustachian valve
Posterior leaflet (Tricuspid valve)
Inferior vena cava (IVC)

Diastole

## Apical 4-Chamber View (A4C)

Interventricular septum (IVS)
LV apex
Septal leaflet TRICUSPID VALVE Anterior leaflet
RV
LV
Anterior leaflet MITRAL VALVE Posterior leaflet
Interatrial septum (IAS)
RA
LA
Descending thoracic aorta
Right lower pulmonary vein

Systole

## SC Inferior Vena Cava Long-Axis

Inferior vena cava
Liver
SC-IVC LAX
Hepatic vein
RV
RA

## Right Ventricular (RV) Outflow View

Interventricular septum
Right ventricular (RV) outflow tract
RV
Pulmonary valve
LV
PA
Main pulmonary artery

Diastole

## Apical 5-Chamber View (A5C)

LV apex\
Interventricular septum
Left ventricular outflow tract (LVOT)
RV
LV
Aortic valve
Mitral valve
Aortic root
RA
LA

Diastole

## SC-Abdominal Aorta Long-Axis

Abdominal aorta
SC-AA LAX

Systole

## PSAX: Aortic Valve (AV) Level

Right coronary cusp
RVOT free wall
Aortic valve
Septal tricuspid leaflet
RVOT
Pulmonary valve
Main pulmonary artery (PA)
Interatrial septum (IAS)
RA
Left coronary cusp
LA
Noncoronary cusp

Diastole

## Apical 2-Chamber View (A2C)

LV apex
Inferior wall (LV)
Anterior wall (LV)
Diaphragm
LV
Anterior leaflet Mitral valve
Posterior leaflet Mitral valve
LA
Left atrial appendage
Abdominal aorta
Descending thoracic aorta

Systole

## Suprasternal Notch (SSN) View

L. common carotid artery
L. brachiocephalic vein
Aortic arch
L. subclavian artery
Ascending aorta
Descending thoracic aorta
L. main bronchus
R. pulmonary artery
Left atrium

## PSAX: Mitral Valve (MV) Level

Right ventricular cavity
Right ventricular free wall
Interventricular septum
RV
LVOT
Anterior leaflet (Mitral valve)
MV
Posterior leaflet (Mitral valve)
Pericardium
Basal inferolateral LV wall

Diastole

## Apical 3-Chamber View (A3C)

LV apex
Inferolateral (posterior) wall
Interventricular septum (anteroseptal)
LV
Right coronary cusp
Posterior leaflet Mitral valve
Aortic root
LA
Anterior leaflet Mitral valve

Systole

## SSN: Color Flow Doppler

Ascending aorta
Aortic arch
Descending thoracic aorta (DTAo)

BE Bulwer, MD, FASE
Systole

| | | | | | | | |
|---|---|---|---|---|---|---|---|
| **AA:** abdominal aorta | **AV:** aortic valve | **IVC:** inferior vena cava | **LSA:** left subclavian artery | **LVOT:** LV outflow tract | **RLPV:** right lower pulmonary vein | **RVOT:** RV outflow tract |
| **Ao:** aorta | **BCA:** brachiocephalic artery | **LA:** left atrium | **LUPV:** left upper pulmonary vein | **PA:** pulmonary artery | **RUPV:** right upper pulmonary vein | **SVC:** superior vena cava |
| **Asc. Ao:** ascending aorta | **DTAo:** descending thoracic aorta | **LLPV:** left lower pulmonary vein | **LV:** left ventricle | **RA:** right atrium | **RV:** right ventricle | **TV:** tricuspid valve |

**FIGURE 16.8** Labeled still frames of standard adult TTE views. Compare with Fig. 16.7. *Ao,* Aorta; *LA,* left atrium; *RA,* right atrium; *LV,* left ventricle; *RV,* right ventricle; *PA,* pulmonary artery; *LVOT,* left ventricular outflow tract. Labeled tricuspid valve leaflets and right ventricular walls are those typically identified from these windows, although slight differences in transducer angulation can result in the display of different wall/leaflets (e.g., the inferior rather than lateral wall seen in the subcostal view).

from normal, such as those with aneurysms or focal wall motion abnormalities. M-mode of valvular leaflets is of historical importance for diagnosis and still remains useful for demonstrating abnormalities in valvular motion, including rheumatic mitral stenosis (MS), mitral valve prolapse, and systolic anterior motion of the mitral valve as occurs in obstructive hypertrophic cardiomyopathy (HCM) (Fig. 16.9).

M-mode can also be combined with 2D imaging to reveal subtle changes in interventricular septal motion and chamber wall movement in pericardial disease, particularly with respect to timing within the cardiac cycle and relative to respirophasic changes. In combination with color flow Doppler (color M-mode), accurate information about timing and direction of flow and assessment of diastolic function can also be augmented. In apical four-chamber windows, M-mode may be applied to assess RV systolic function (see Fig. 16.17).

### IMAGING ARTEFACTS

Ultrasound imaging artefacts are ubiquitous in echocardiography and are incurred by the physical principles of ultrasound. Artefacts can include the semblance of structures that do not exist or can be caused by real structures, such as the ribs obscuring visualization of the heart. Most artefacts are caused by physical interactions between ultrasound and tissue (Fig. 16.10). Common artefacts include (1) *attenuation artefacts,* which result in acoustic "shadowing" typically caused by ribs or bony structures; (2) *side lobe artefacts,* which occur when lower-energy side beams (side lobes) aside from the main ultrasound beam reflect off of lateral structures and are mapped onto the central image; (3) *multiple reflection artefacts,* in which the sound waves bounce between a strong reflector—such as the pericardium, pleura, or aortic wall—and the transducer more than once, giving rise to mirror images (Video 16.1) or near-field clutter; and (4) *reverberation artefacts,* which are caused by continuing repetition of internal reflections, often seen behind mechanical valve prostheses or left ventricular assist device (LVAD) cannulae. One type of reverberation artefact, the comet-tail artefact, can be useful diagnostically to detect interstitial fluid in the lungs, where the specific finding is known as "B-lines" (see also Heart Failure).



FIGURE 16.9 M-mode tracings. **A**, Normal M-mode across the base of the left ventricle at the level of the mitral leaflet tips. Note the E and A waves corresponding to the anterior mitral leaflet motion in early diastole (E) and with atrial contraction (A), respectively. Compare with **B**, which shows a patient with mitral valve prolapse, where there is late systolic posterior bowing (*arrow*) of the mitral leaflets on M-mode. **C**, Rheumatic mitral stenosis, with thickened mitral leaflets that move parallel to each other, straightening of the slope after the E wave (E-F slope), and reduced leaflet opening in diastole. **D**, Hypertrophic obstructive cardiomyopathy, displaying a very thickened interventricular septum (*white double-headed arrow*) and systolic anterior motion of the mitral valve leaflets (*yellow arrow*).
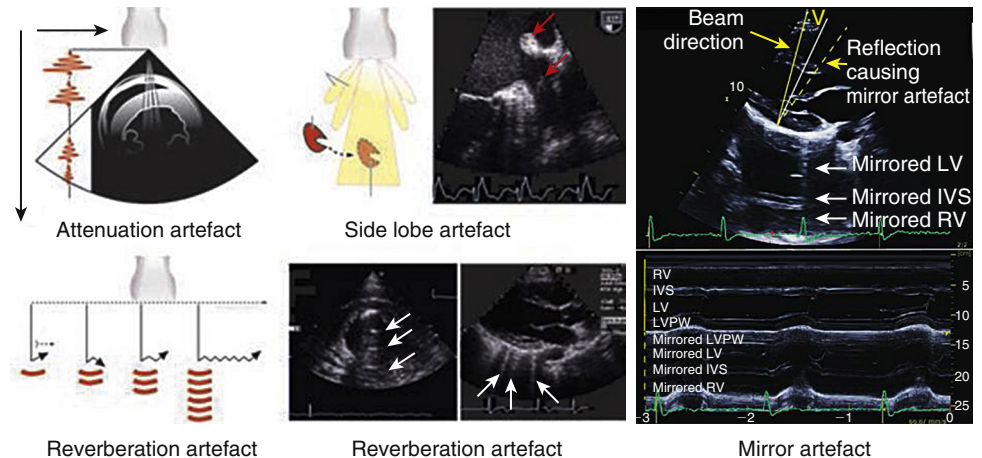


FIGURE 16.10 Common imaging artefacts seen in echocardiography. Attenuation artefacts, caused by diminution in ultrasound beam intensity with increasing depth, resulting in fading and dropout **(upper left)**. Side lobe artefacts occur when structures in the path of the side lobe beams are erroneously mapped into the image **(upper middle)**. Reverberation artefacts are common **(lower left and middle panels)**. They may be large, as in the case of reflections from the inflow tube of an LVAD (three parallel *arrows,* below center), or appear as fine comet-tail or "ring-down" artefacts because of multiple reverberations that invariably occur at the highly specular epicardial-pleural interface **(lower right)**. **Right panels,** Mirror artefact, caused by reflection between tissue interfaces and the transducer.

## Assessment of Cardiac Structure and Function

The primary goal of the echocardiographic examination remains the assessment of cardiac structure and performance. Each chamber, valve, and great vessel can be assessed qualitatively and quantitatively

to define any alterations in size, geometry, and function.[3] Measurements of cardiac structures are typically made in various locations throughout the heart, and linear, area, or volumetric measures can be obtained. These methods are often complementary to one another. For example, although volumetric measurements of the left ventricle (see later) are generally considered best suited to characterize LV size, many laboratories continue to record linear cavity measurements, because there is extensive literature correlating these measures with outcomes in numerous disease states. Moreover, linear measures may be subject to less variability than area- or volume-based measures and hence more reliable for assessing changes over time.

Tables 16.1 to 16.3 show established normal values on echocardiography. For LV linear dimensions and volume, Table 16.1 gives the normal ranges for the general population, but ideally one should take into account not only sex, but also body surface area (BSA) and age[2] (eFigs. 16.5 and 16.6). Current American Society of Echocardiography (ASE) consensus statements also provide partition values—that is, mild, moderate, and severely abnormal ranges—for LV size, mass, and ejection fraction (EF) and left atrial (LA) volume, but caution that the ranges were arrived at by experience-based consensus only, and that degree of abnormality does not necessarily connote a direct correlation with outcomes or prognosis (see Table 16.2). Normal values for LV parameters

obtained with 3D echocardiography also exist and appear accurate and reproducible when image quality is good. In general, LV volumes calculated by 3D imaging are smaller than those generated from CMR data, but correlations with trends in sex and BSA hold true.[2]

## Left Ventricular Structure: Size and Mass

Historically, LV volumes have been estimated from one of several formulas that use either linear or 2D measurements to calculate a volume based on the assumption that the left ventricle approximates a prolate ellipsoid or cylinder hemiellipsoid shape (Fig. 16.11). These approaches had the advantages of being relatively reproducible and simple to calculate. Much published research relies on M-mode data, but the estimation of LV volume is less accurate when ventricular geometry deviates from normal because of myocardial damage or remodeling. For all LV geometries, the modified biplane Simpson method of discs has been demonstrated and recommended as the most accurate method (Fig. 16.12). This method requires tracing the endocardial border in the apical four- and two-chamber views with computerized assistance to measure the diameter and height of equally distributed slices along the ventricle. With these measurements, the volume of each axial slice can be calculated, and the volume of all the slices summed to give the total chamber volume. The method is very accurate when image quality is good. However, in actual practice, suboptimal image quality can make definition of the endocardial border challenging. Moreover, foreshortening of the ventricle in one of the apical views, which can occur simply by minor changes in the transducer angle, can dramatically reduce the measured volume. The development and utilization of LV echocardiographic contrast and 3D echocardiography (see later) can

**TABLE 16.1** Normal Values for Two-Dimensional Echocardiographic Parameters of Left Ventricular Size and Function According to Sex

| PARAMETER | MALE MEAN ± SD | MALE 2-SD RANGE | FEMALE MEAN ± SD | FEMALE 2-SD RANGE |
|---|---|---|---|---|
| **Left Ventricular (LV) Internal Dimension** | | | | |
| Diastolic dimension (mm) | 50.2 ± 4.1 | 42.0–58.4 | 45.0 ± 3.6 | 37.8–52.2 |
| Systolic dimension (mm) | 32.4 ± 3.7 | 25.0–39.8 | 28.2 ± 3.3 | 21.6–34.8 |
| **LV Volumes (Biplane)** | | | | |
| LV EDV (mL) | 106 ± 22 | 62–150 | 76 ± 15 | 46–106 |
| LV ESV (mL) | 41 ± 10 | 21–61 | 28 ± 7 | 14–42 |
| **LV Volumes Normalized by Body Surface Area** | | | | |
| LV EDV (mL/m²) | 54 ± 10 | 34–74 | 45 ± 8 | 29–61 |
| LV ESV (mL/m²) | 21 ± 5 | 11–31 | 16 ± 4 | 8–24 |
| LV EF (biplane) | 62 ± 5 | 52–72 | 64 ± 5 | 54–74 |

*EDV,* End-diastolic volume; *EF,* ejection fraction; *ESV,* end-systolic volume; *SD,* standard deviation.
From Lang RM, Badano LP, Mor-Avi V et al. Recommendations for cardiac chamber quantification by echocardiography in adults: an update from the American Society of Echocardiography and the European Association of Cardiovascular Imaging. *J Am Soc Echocardiogr.* 2015;28:1.
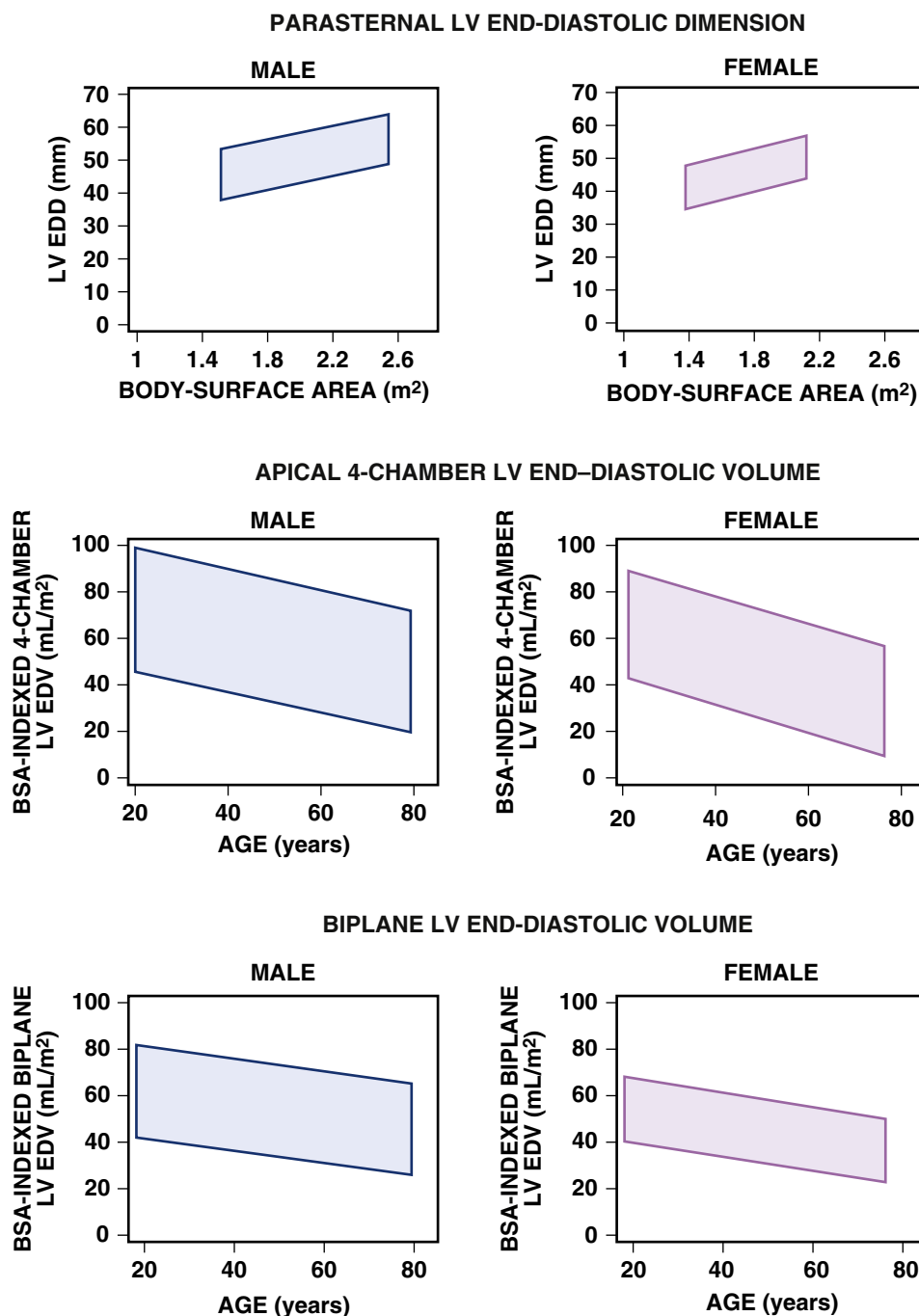
**TABLE 16.3** Normal Ranges for Left Ventricular (LV) Mass Indices

| INDEX | WOMEN | MEN |
|---|---|---|
| **Linear Method** | | |
| LV mass (g) | 67–162 | 88–224 |
| *LV mass/BSA* (g/m²) | *43–95* | *49–115* |
| Relative wall thickness (cm) | 0.22–0.42 | 0.24–0.42 |
| *Septal thickness* (cm) | *0.6–0.9* | *0.6–1.0* |
| *Posterior wall thickness* (cm) | *0.6–0.9* | *0.6–1.0* |
| **Two-Dimensional Method** | | |
| LV mass (g) | 66–150 | 96–200 |
| *LV mass/BSA* (g/m²) | *44–88* | *50–102* |

**Bold/italic values:** Recommended and best validated.
From Lang RM, Badano LP, Mor-Avi V, et al. Recommendations for cardiac chamber quantification by echocardiography in adults: an update from the American Society of Echocardiography and the European Association of Cardiovascular Imaging. *J Am Soc Echocardiogr.* 2015;28:1.
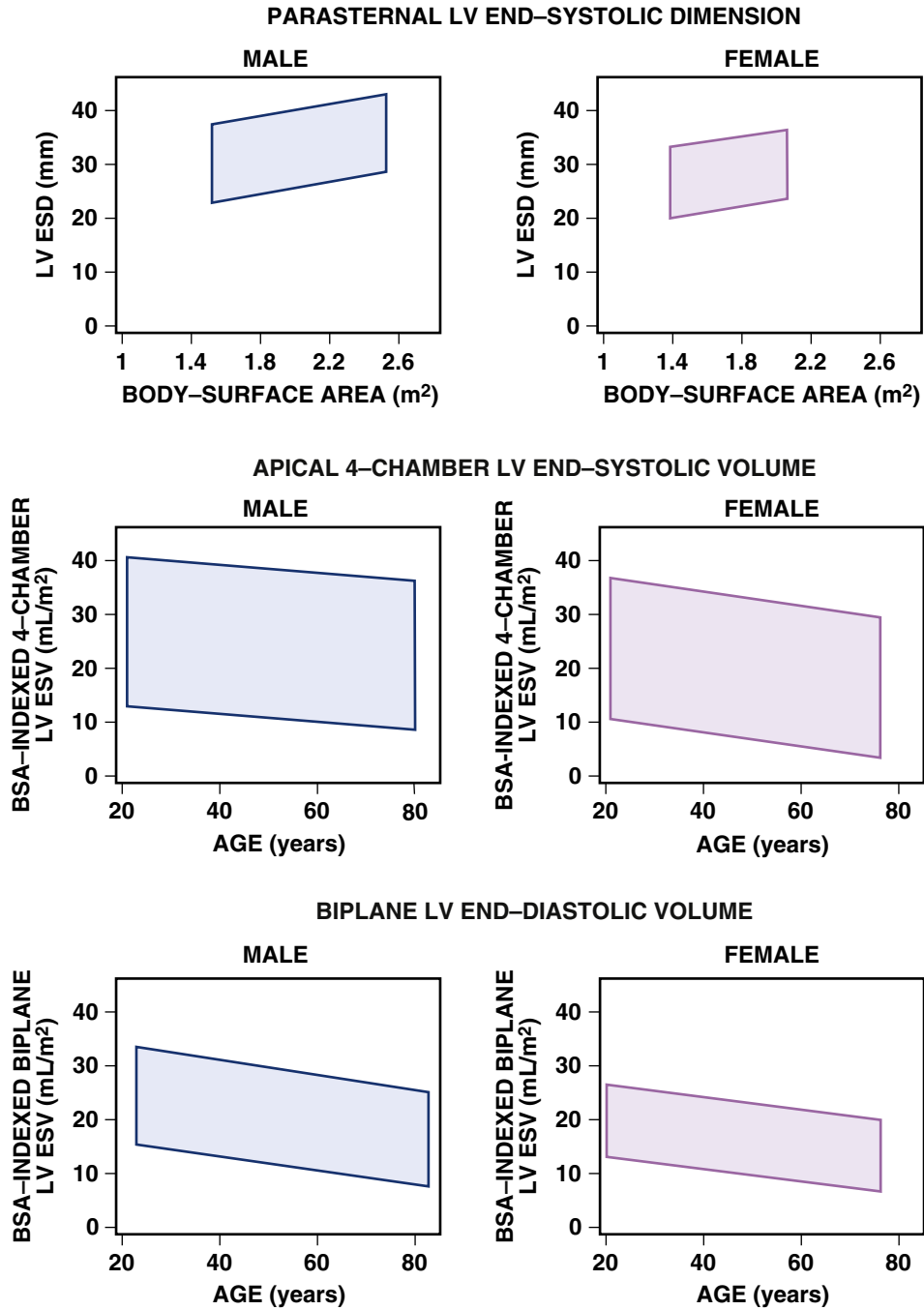
**TABLE 16.2** Normal Ranges and Severity Partition Cutoff Values for Two-Dimensional Echocardiography–Derived Left Ventricular Ejection Fraction (LVEF) and Left Atrial (LA) Volume

| | MALE NORMAL RANGE | MALE MILDLY ABNORMAL | MALE MODERATELY ABNORMAL | MALE SEVERELY ABNORMAL | FEMALE NORMAL RANGE | FEMALE MILDLY ABNORMAL | FEMALE MODERATELY ABNORMAL | FEMALE SEVERELY ABNORMAL |
|---|---|---|---|---|---|---|---|---|
| **LVEF** (%) | 52–72 | 41–51 | 30–40 | <30 | 54–74 | 41–53 | 30–40 | <30 |
| **Max LA vol/BSA** (mL/m²) | 16–34 | 35–41 | 42–48 | >48 | 16–34 | 35–41 | 42–48 | >48 |

*BSA,* Body surface area.
From Lang RM, Badano LP, Mor-Avi V, et al. Recommendations for cardiac chamber quantification by echocardiography in adults: an update from the American Society of Echocardiography and the European Association of Cardiovascular Imaging. *J Am Soc Echocardiogr* 2015;28:1.

## PARASTERNAL LV END-DIASTOLIC DIMENSION



## APICAL 4-CHAMBER LV END–DIASTOLIC VOLUME



## BIPLANE LV END-DIASTOLIC VOLUME



**EFIGURE 16.5** Normal ranges for left ventricular end-diastolic diameter (LV EDD) and volumes (LV EDV). For men **(left)** and women **(right),** the 95% confidence intervals for the following measurements are presented: LV end-diastolic dimension measured from a parasternal long-axis window on the basis of body surface area (BSA) **(top),** BSA-indexed LV EDV measured from an apical four-chamber view on the basis of age **(middle),** and BSA-indexed biplane LV EDV on the basis of age **(bottom).** For example, a normal BSA-indexed LV EDV measured from the four-chamber view in a 40-year-old woman would fall between approximately 30 and 78 mL/m². Similar charts for absolute (non-BSA indexed) LVEDV versus age (including two-chamber measurements) can be found in the following credit reference (Lang RM, et al.) and its Supplemental Fig. 1. Absolute LVEDV versus BSA (including two-chamber measurements, without breakdown for age) can also be found within the Lang RM, et al. reference, in Supplemental Fig. 3. (From Lang RM, Badano LP, Mor-Avi V, et al. Recommendations for cardiac chamber quantification by echocardiography in adults: an update from the American Society of Echocardiography and the European Association of Cardiovascular Imaging. *J Am Soc Echocardiogr.* 2015;28:1.)

**PARASTERNAL LV END–SYSTOLIC DIMENSION**

MALE

FEMALE

**APICAL 4–CHAMBER LV END–SYSTOLIC VOLUME**

MALE

FEMALE

**BIPLANE LV END–DIASTOLIC VOLUME**

MALE

FEMALE

**EFIGURE 16.6** Normal ranges for LV end-systolic diameter (LV ESD) and volumes (LV ESV). For men **(left)** and women **(right)**, the 95% confidence intervals for the following measurements are presented: LV end-systolic dimensions measured from a parasternal long-axis window on the basis of BSA **(top)**, BSA-indexed LV ESVs measured from an apical four-chamber view on the basis of age **(middle)**, and BSA-indexed biplane LV ESVs based on age **(bottom)**. Similar charts for absolute (non-BSA indexed) LVESV versus age (including two-chamber measurements) can be found within the credit reference (Lang RM et al.) and its Supplemental Fig. 2. Absolute LVESV versus BSA indexing (including two-chamber measurements, without breakdown for age) can also be found in the Lang reference and Supplemental Fig. 4. (From Lang RM, Badano LP, Mor-Avi V, et al. Recommendations for cardiac chamber quantification by echocardiography in adults: an update from the American Society of Echocardiography and the European Association of Cardiovascular Imaging. *J Am Soc Echocardiogr*. 2015;28:1.)
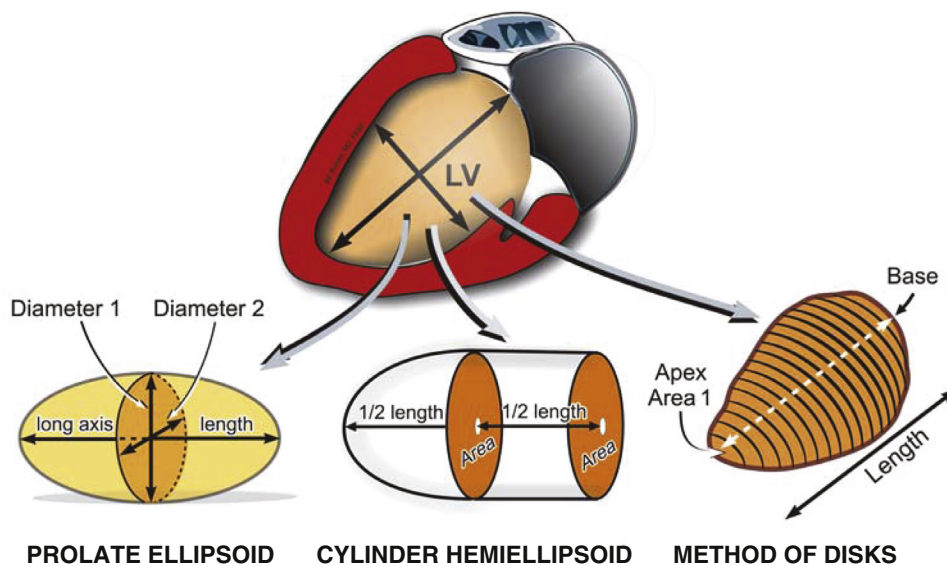
**FIGURE 16.11** Geometric models and assumptions used in quantification of volumes of the left ventricle (*LV*) in two-dimensional echocardiography. (Modified from Bulwer BE, et al. Basic principles of echocardiography and tomographic anatomy. In Solomon SD, ed. *Atlas of Echocardiography*. 2nd ed. Philadelphia: Current Science/Springer Science; 2009:1–24.)
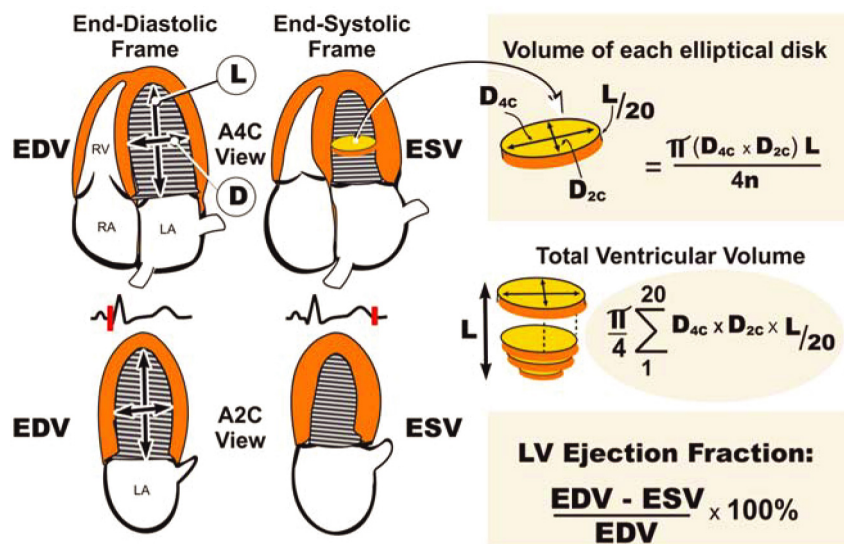


**FIGURE 16.12** Simpson method of discs for quantification of left ventricular (LV) volumes and LV ejection fraction on two-dimensional (2D) echocardiography. *A2C,* Apical two-chamber view; *A4C,* apical four-chamber view; *D,* LV diameter; *EDV,* end-diastolic volume; *ESV,* end-systolic volume; *L,* LV length; *n,* number of discs. (Modified from Bulwer BE, et al. Basic principles of echocardiography and tomographic anatomy. In Solomon SD, ed. *Atlas of Echocardiography*. 2nd ed. Philadelphia: Current Science/Springer Science; 2009:1–24.)

mitigate the impact of these limitations and appear to permit greater accuracy and reproducibility.

LV mass may be calculated by using one of several formulas that take into account both wall thickness and chamber size,[2] typically using either linear (M-mode) or 2D measurements together with geometric modeling of the shape of the LV myocardial "shell" (eFig. 16.7). These formulas have been validated in normal ventricles; however, as in volume calculations, accuracy suffers when applied to those that are abnormally shaped.

With all methods, care must be taken to measure the walls at end-diastole, because small errors may be exponentially multiplied depending on the calculation used; Table 16.3 shows currently accepted normal values. An LV mass index (derived from 2D echocardiographic measurements) of greater than 95 g/m² for women or more than 115 g/m² for men is considered abnormally high. Pathologically, LV *hypertrophy* is defined as increased overall LV mass and is distinct from wall thickness per se. However, in general, if LV diameter is not decreased, wall thicknesses of 12 mm or more correlate with LV hypertrophy. Alterations in LV size and mass can be categorized based on the ratio of relative wall thickness to the total LV mass index (Fig. 16.13). The specific pattern of ventricular remodeling has been related to prognosis in a variety of diseases, of both myocardial and valvular etiology.[5]

3D datasets, in which wall thicknesses are measured at a multitude of points and mass is calculated without assumptions about cavity geometry, ultimately appear more accurate but again depend on image quality. Normal values for LV mass index based on 3D data, validated against cardiac MRI, have emerged over the last several years. With less interobserver variability and automated calculations, these more sophisticated calculated values may have incremental value for outcome prediction in comparison to older 2D methods.[6]

## Left Ventricular Systolic Function

Echocardiography offers several methods for assessment of systolic function. The most common remains left ventricular ejection fraction (LVEF), calculated as the difference between end-diastolic volume and end-systolic volume divided by end-diastolic volume (see Fig. 16.12). LVEF is one of the best-studied measures in cardiovascular medicine for diagnosis and risk stratification. In echocardiography the volumes are preferably calculated by the modified Simpson formula (see earlier), and normal values are 52% to 72% for men and 54% to 74% for women.[2] Most echocardiography machines have basic analysis packages for automatically estimating the LVEF based on linear measurements at the base of the heart (e.g., Teicholz and Quinones formulas), which are helpful for a quick approximation but are less accurate in remodeled ventricles. In reality, the accuracy of all methods is affected by image quality, endocardial border definition, ventricular geometry, and imaging plane. When one or more of these factors are suboptimal, a visual "eyeball" estimation
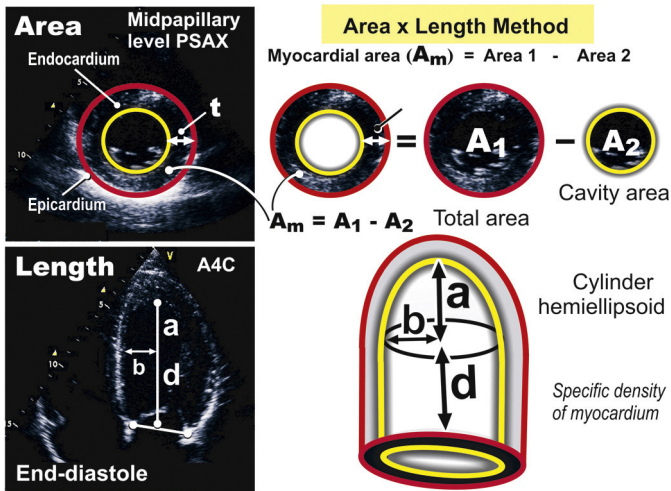
**EFIGURE 16.7** LV mass calculation in 2D echocardiography using an area-length method for a cylinder hemiellipsoid. Area 1 ($A_1$) is the total planimetered area at the mid-LV level on the parasternal short-axis (PSAX) view in diastole; area 2 ($A_2$) is the planimetered LV cavity area; $A_m$ is the myocardial "shell" area; *b,* minor axis radius; *t,* wall thickness. (Modified from Bulwer BE, et al. Basic principles of echocardiography and tomographic anatomy. In Solomon SD, ed. *Atlas of Echocardiography*. 2nd ed. Philadelphia: Current Science/Springer Science; 2009:1–24.)
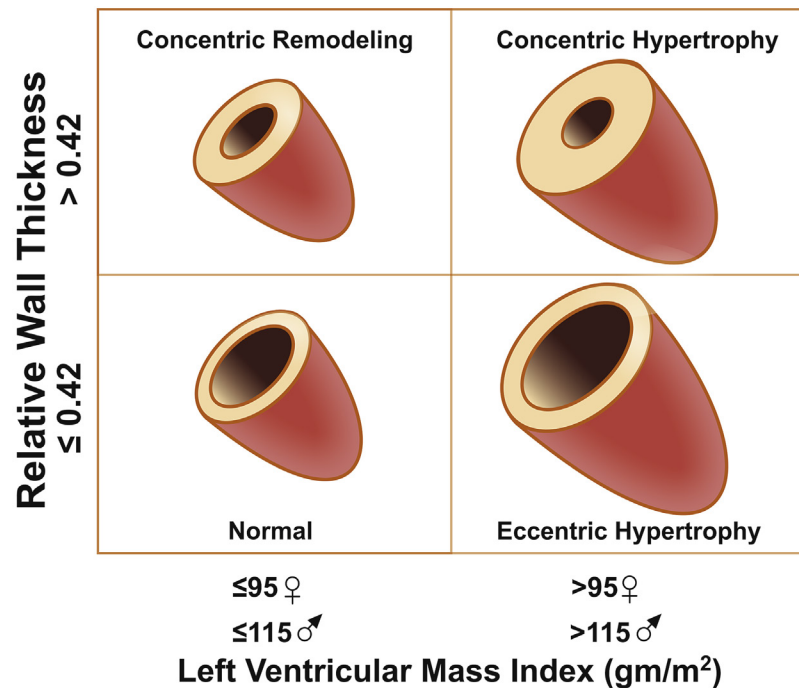
**FIGURE 16.13** Patterns of left ventricular (LV) remodeling. Three patterns of adverse LV remodeling can be defined based on measurement of left ventricular mass index (LVMI) and relative wall thickness (RWT): concentric remodeling (normal LVMI and increased RWT), eccentric hypertrophy (increased LVMI and normal RWT), and concentric hypertrophy (both LVMI and RWT are increased). (Modified from Konstam MA, Kramer DG, Patel AR, et al. Left ventricular remodeling in heart failure. current concepts in clinical significance and assessment. *J Am Coll Cardiol Imaging*. 2011;4:98.)

by experienced echocardiographers can be reliable and sufficient for most clinical scenarios. Although this is common practice and can actually be more accurate than mathematical computation in many cases, the presence of intra- and interobserver variability needs to be acknowledged, and reproducibility should be monitored.[7] Current echocardiography systems can now automatically calculate the LVEF using the Simpson's method of discs from 2D or 3D datasets, which are accurate and reproducible, but only in patients with good image quality. 3D volumes can also be used to calculate LVEF (Video 16.2).[2]

Other approaches are commonly used in addition to LVEF to assess systolic function. Stroke volume can be determined from 2D or 3D images by subtracting end-systolic volume from end-diastolic volume. An alternative method is to use Doppler data (discussed earlier), in which the VTI within the LVOT is multiplied by the LVOT CSA to calculate SV (see Fig. 16.6). Multiplication of SV by the heart rate gives the cardiac output.

Several other methods have been proposed for assessment of both LV and RV function. The *myocardial performance index* (MPI), also known as the Tei index, is defined as the sum of isovolumic relaxation time (IVRT) and isovolumic contraction time divided by ejection time, and this method takes into account both systolic and diastolic performance (eFig. 16.8). A higher index is associated with worse function.[2] In adults, values of LV MPI greater than 0.40 and RV MPI greater than 0.43 are considered abnormal. This measure has been related to outcomes in a variety of conditions, including heart failure and following myocardial infarction (MI). *Doppler tissue imaging* (DTI) can be used to assess myocardial contraction velocity, or S′, although this technique is also frequently used in assessment of diastolic function (see later).

### Myocardial Strain Imaging
Myocardial deformation, or strain imaging, has evolved to become a sensitive method for assessment of cardiac function. *Strain* refers to the percent deformation between two regions, such as shortening of myocardial muscle in systole or lengthening in diastole.[2] It was initially measured by Doppler of the myocardial tissues to derive the change

in distance between points, but an alternate method, 2D speckle-tracking has been found to be more robust and reliable and has proven its utility in clinical applications. The technique has been validated by sonomicrometry and takes advantage of the coherent speckle within the myocardial tissue digital signature (eFig. 16.9) to determine regions that are contracting versus those that are moving passively. Strain can be estimated in the longitudinal, circumferential, and radial directions by using the appropriate imaging plane (Fig. 16.14). Normal values for longitudinal and circumferential strain are negative whereas for radial strain, values are normally positive reflecting the normal change in the relative positions of myocardial targets in each of these directions.

Current equipment can assess regional strain and then calculate global longitudinal strain (GLS) either by averaging regional strain values or by determining the percent difference in the endocardial perimeter between systole and diastole (Fig. 16.15). Longitudinal deformation reflects function of the subendocardial myocardial fiber bands primarily, whereas circumferential deformation, best assessed on short-axis views, may reflect the function of more epicardial layers.

Global strain, particularly *global longitudinal strain* (GLS, or the maximal deformation of the LV myocardium at peak systole averaged over the entire ventricle), has emerged as an important measure of cardiac performance that adds incremental predictive value to standard measures such as the LVEF (Video 16.3).[8] GLS is expressed as a percentage, and since the overall deformation is towards compression (negative), values closer to zero represent worse function. Several diseases have been associated with a reduction in GLS, including hypertension, diabetes mellitus, renal insufficiency, infiltrative cardiomyopathies, HCM, and valvular heart disease. This measure also appears to predict survival or the development of heart failure in patients following MI. Global strain measurements are also useful in assessing the effect of cardiotoxic chemotherapies on individual patients over time, and may be useful in identifying acute subclinical rejection in cardiac transplant patients.

Myocardial deformation imaging has been used for the evaluation of cardiac synchrony by assessing the time to peak strain (maximal contraction) across many cardiac regions (eFig. 16.10). Both regional timing, reflecting synchrony, and myocardial peak strain, reflecting contractile function, have prognostic significance in patients undergoing cardiac resynchronization therapy (CRT) (see Chapters 50 and 69). The identification of patients who will benefit most from CRT has been a challenge. No single echocardiographic parameter has been found to date that can unequivocally predict response, although radial strain appears to more accurate than other parameters. Ultimately, utilizing regional strain data during CRT placement to help guide optimal lead position may be a more effective approach.[8]

In addition to assessment of global function, strain imaging can be used to assess and quantify regional function. Regional strain correlates with the degree of myocardial scar in patients with ischemic heart disease (see Chapter 36) and in HCM[8,9] (Chapter 54). These measures can also be used to assess ischemia during stress echocardiography. Moreover, a pattern in which strain is preserved apically relative to that at the midventricular and basal levels is suggestive of amyloid cardiomyopathy.[8] An offshoot of myocardial strain imaging has been the quantitative assessment of ventricular twist and torsion, or the wringing motion of the heart during contraction and relaxation (eFig. 16.11).[10]

There are several limitations of strain imaging based on 2D echocardiography. First, myocardial deformation occurs in three dimensions, and out-of-imaging plane movement is lost. Second, these measures are subject to the same limitations as conventional ultrasound images, including frame rate and image quality, with limited temporal resolution at high heart rates. Third, the technique, data acquisition and calculations, and normal values were initially not standardized among the many vendors, making it difficult to compare data in individual cases. The industry has now converged to provide consensus on standardization as well as automated strain measurements, which has amplified the utility of this tool in routine clinical practice.[9]

### Left Ventricular Regional Function
Although measures of global LV function provide quantification of overall cardiac performance and carry prognostic value, regional
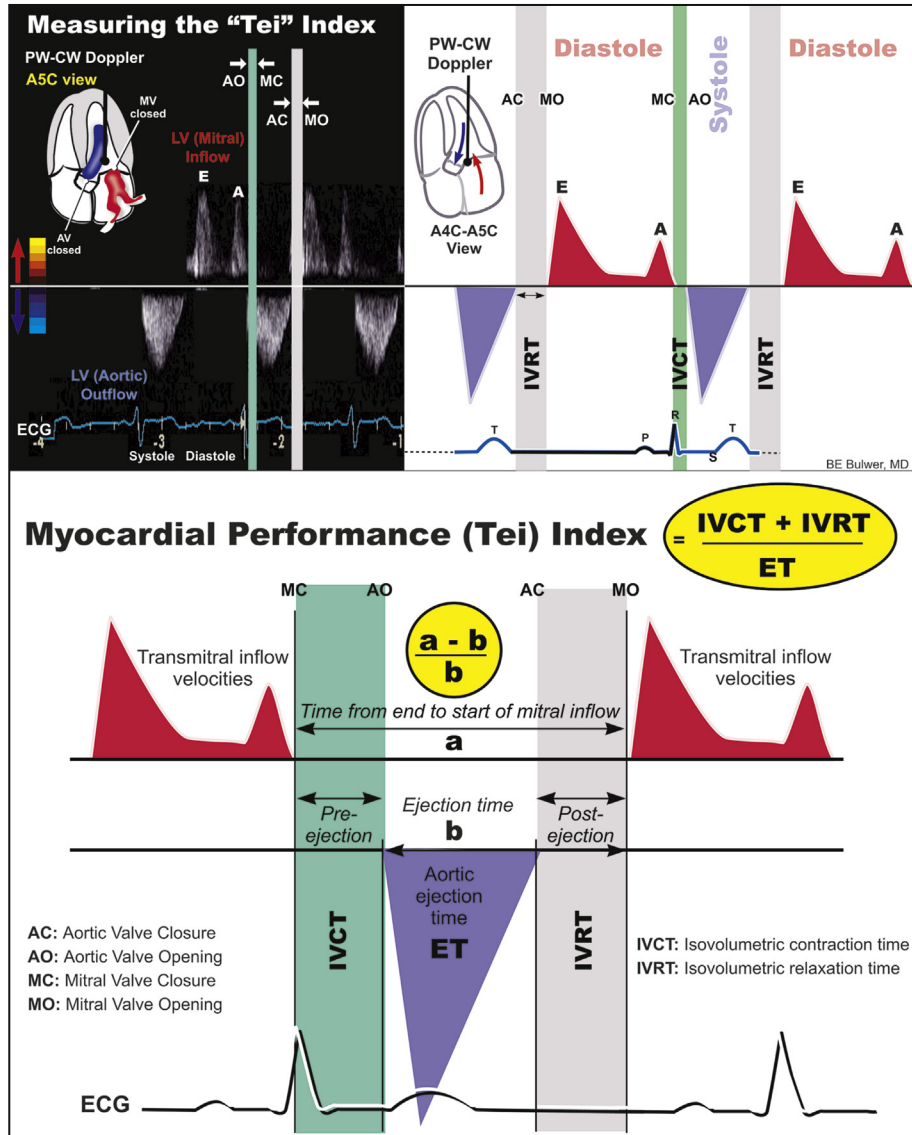
**EFIGURE 16.8** Myocardial performance (MPI), or Tei, index. This is a measure of both global systolic and diastolic ventricular function and can be calculated from spectral Doppler tracings of mitral valve inflow and left ventricular (LV) outflow. It is equal to the sum of the isovolumetric contraction and relaxation times (IVCT and IVRT, respectively) divided by the ejection time (ET). A4C, Apical four-chamber; A5C, apical five-chamber; CW, continuous wave spectral Doppler; LV, left ventricle; PW, pulsed wave. For spectral Doppler method: normal LV Tei index is ≤0.40. Similar calculations can be performed for the right heart, and normal RV Tei index is ≤0.43. (From Bulwer BE, Solomon SD. Assessment of Left Ventricular Systolic Function. In: Gillam LD et al, eds. *Essential Echocardiography: A Companion to Braunwald's Heart Disease*. Philadelphia, Elsevier, 2019. Courtesy of Bernard E. Bulwer, MD, FASE.)
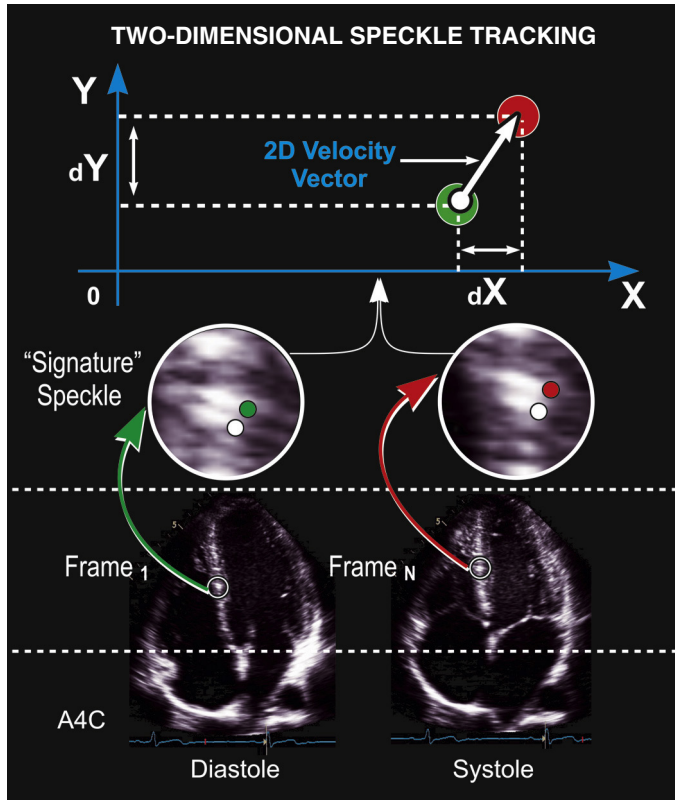
**EFIGURE 16.9** Two-dimensional (2D) speckle tracking methodology. Speckles are inhomogeneous interference patterns that result from the interaction of ultrasound with the myocardium. Each area of myocardium, with its unique signature speckle, can be tracked during the myocardial deformation cycle. Unlike Doppler-based deformation imaging measures, speckle tracking–derived deformation measures are angle independent. *A4C,* Apical four-chamber view.
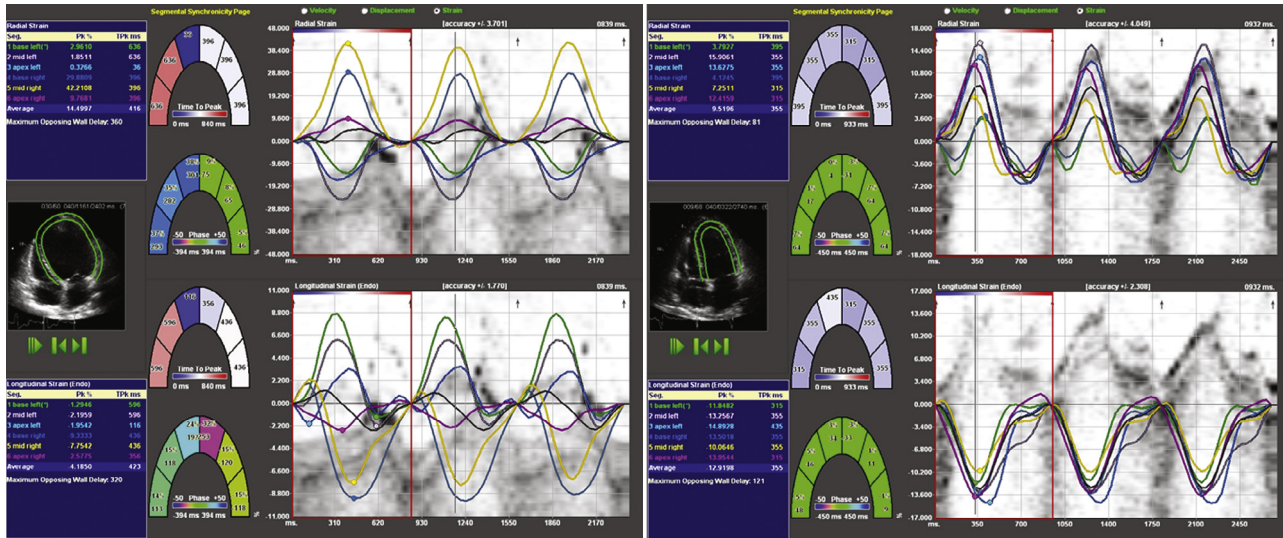


**EFIGURE 16.10** Dyssynchrony versus synchrony, as assessed by myocardial strain before and after CRT. Average radial and longitudinal strain is calculated from six different regions in the ventricle on apical four-chamber views. The waveforms depicted demonstrate both timing and magnitude of peak strain in these regions. **Left panel** shows a patient with cardiomyopathy before therapy with a cardiac resynchronization device. **Right panel** shows same patient after 12 months of CRT with dramatic improvement in ventricular synchrony.
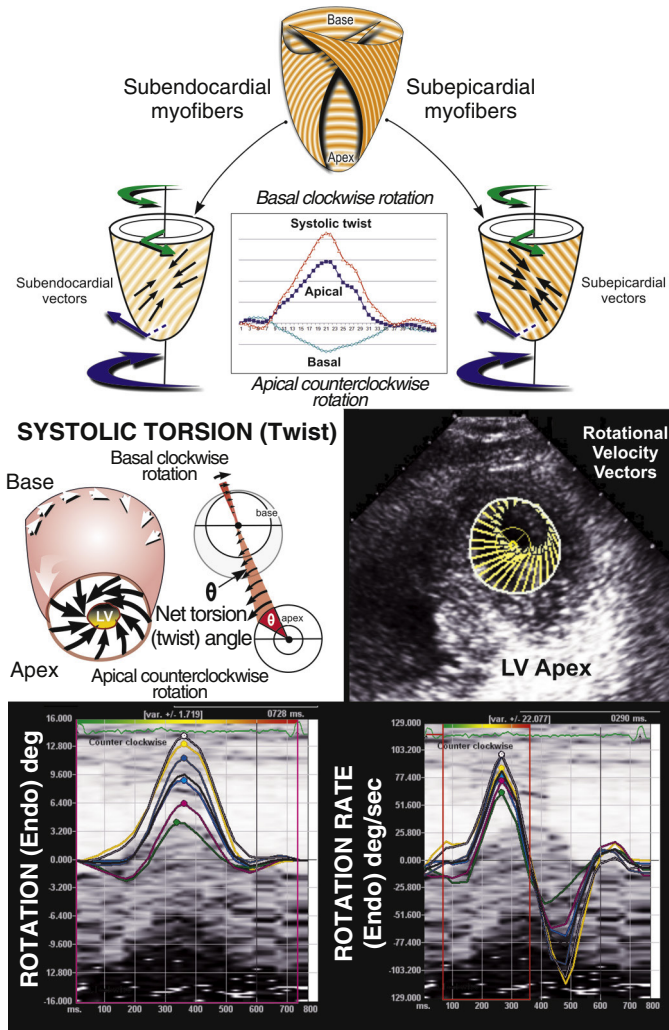
**EFIGURE 16.11** Ventricular torsion (or twist) can be assessed by comparing the rotation occurring at the base of the heart with that occurring at the apex using speckle tracking. Rotation and the rate of rotation can be assessed and displayed. (Modified from Bulwer BE, Solomon SD. Assessment of systolic function. In: Solomon SD, ed. *Atlas of Echocardiography*. 2nd ed. Philadelphia: Current Science/Springer Science; 2009:63.)
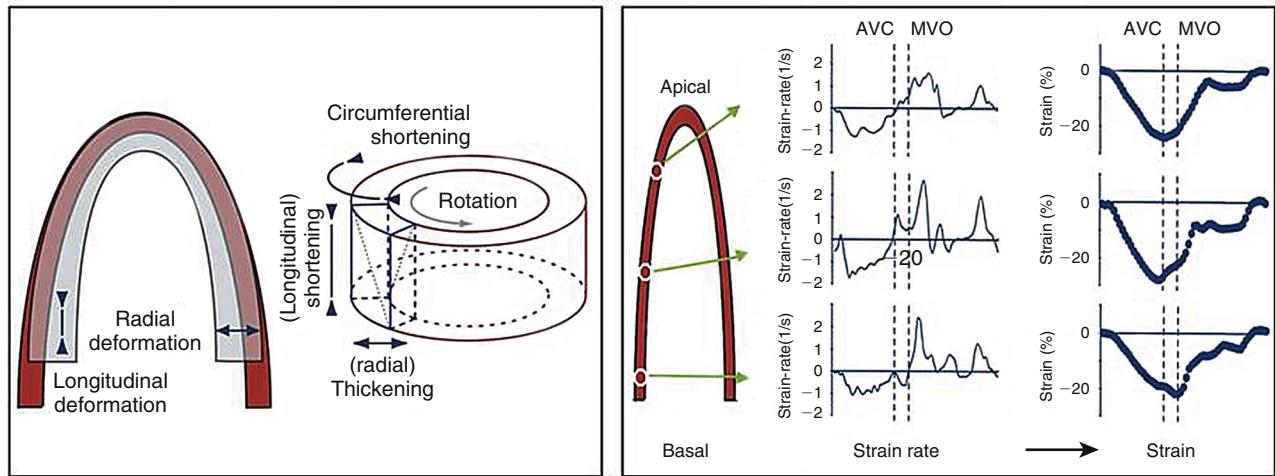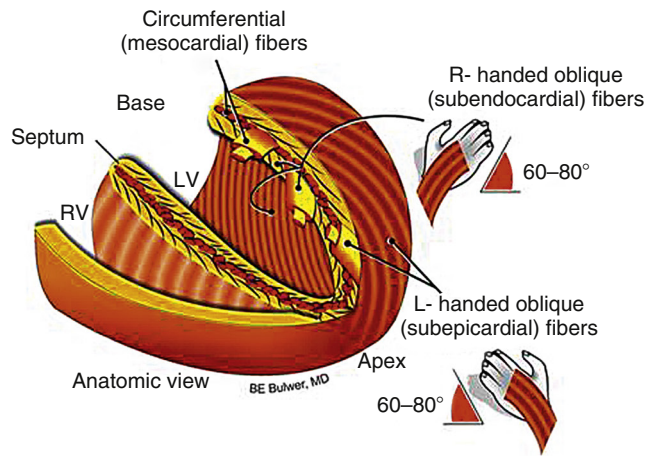
FIGURE 16.14 Normal myocardial fiber orientation, deformation planes, and typical longitudinal strain rate and strain traces. **Upper panel,** Left ventricular endo- and epicardial longitudinal fibers and their opposing oblique directions, midmyocardial circumferential fibers. **Lower panel: Left,** The three planes of myocardial motion and deformation at systole: longitudinal shortening, radial thickening, and circumferential shortening. **Right,** Typical traces of longitudinal strain rate and strain from a healthy adult. *AVC,* Aortic valve closure; *MVO,* mitral valve opening. (From Cikes M, Solomon SD. Beyond ejection fraction: an integrative approach for assessment of cardiac structure and function in heart failure. *Eur Heart J.* 2016;37:1642.)
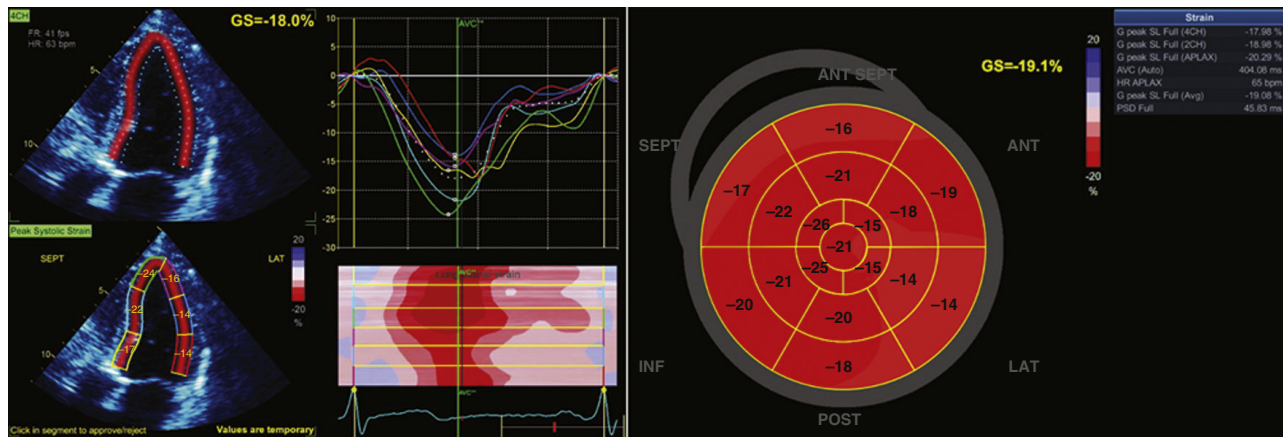


FIGURE 16.15 Global longitudinal strain (GLS) GLS is measured in the three apical planes, mapped onto a bulls-eye plot, and averaged.

function can vary substantially, particularly when affected by ischemic heart disease or other focal processes. Acute MI can cause segmental wall motion abnormalities, that is, altered contractility—visualized on echocardiography as an inwards centripedal segmental motion or wall thickening—of a focal segment of the myocardium. Although there is variability, each specific myocardial region has a typical coronary artery blood supply (see later, Myocardial Infarction). Regional wall motion may be assessed qualitatively or semiquantitatively with a scoring system (eFig. 16.12). The most popular current scoring system is based on a 17-segment model advocated by the ASE in which each segment is scored as normal (1 point), hypokinetic (2 points), akinetic (3 points), or

dyskinetic (4 points). The *wall motion score index* (WMSI) is equal to the sum of these grades divided by the number of segments visualized, so a normally contracting ventricle should have a score of 1.0. A WMSI of 1.7 or higher is usually associated with the physical examination findings of heart failure. A higher score is also an independent predictor of mortality and morbidity, including increased hospitalization for heart failure following MI.

One main goal of detecting regional myocardial dysfunction is to identify patients with coronary artery disease (CAD). The hallmark of a significant MI is the appearance of discrete regions of severe hypokinesis (decreased systolic thickening), akinesis (no thickening), or even
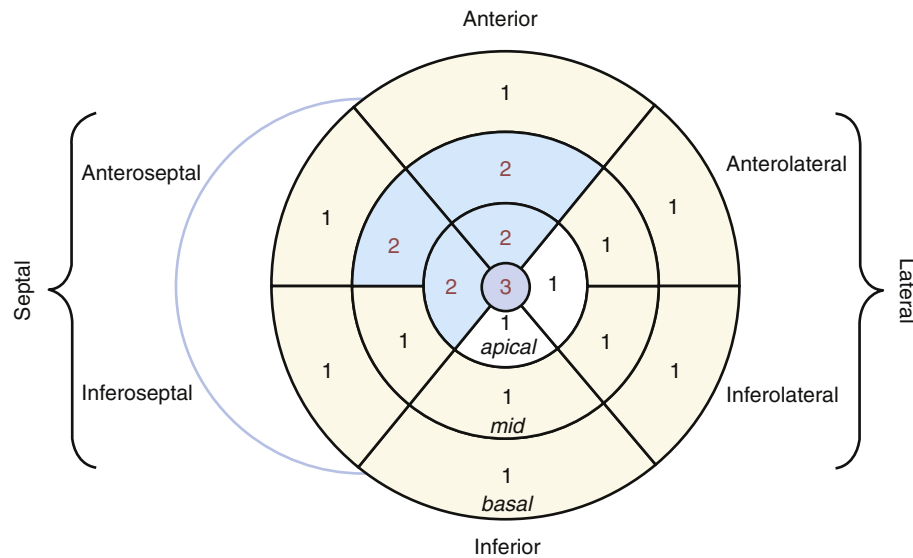
ASE Wall motion score index (WMSI) = Σ17 scores/17 segments

For this case:                    WMSI =          23/17              = 1.35

Points:     1 = normal
            2 = hypokinetic (reduced wall thickening)
            3 = akinetic (absent or negligible wall thickening, i.e., scar)
            4 = dyskinetic (systolic thinning or stretching, i.e., aneurysm)

**EFIGURE 16.12** Wall motion score index (WMSI). A polar map or "bulls-eye" view, one way to schematically depict the area of regional wall motion abnormalities (WMA) and calculation of the wall motion score index. Scores are 1 = normokinetic, 2 = hypokinetic, 3 = akinetic, and 4 = dyskinetic. The example displayed here is of mid-to-distal anteroseptal and anterior hypokinesis with an akinetic apex, giving a WMSI of 1.35. See **Fig. 16.27** in text for coronary distributions.

dyskinesis (bulging outwards in systole). Hypokinesis as a focal wall motion abnormality can be apparent even within the first few minutes of acute MI, thus making echocardiography particularly suited for diagnosis in the acute setting, for example, in patients with acute chest pain and equivocal abnormalities on the electrocardiogram (ECG) in whom a new discrete wall motion abnormality might argue for early intervention (see Chapters 38 and 39). Ultrasound cannot easily distinguish between old and new wall motion abnormalities, although local myocardial thinning and increased echo-brightness would be suggestive of chronic infarction and scar tissue. Although MI, either acute or old, is the most prevalent reason for regional wall motion abnormalities, other conditions such as myocarditis, stress cardiomyopathy (Takotsubo syndrome) or sarcoidosis can affect the myocardium regionally, but these generally will not present in a clear coronary distribution. The LV dysfunction that can accompany valvular or hypertensive heart disease may also have some minor regional variability.

Assessment of regional wall motion is particularly important in stress echocardiography, in which induced focal wall motion abnormalities in the setting of exercise-induced or pharmacologic stress indicate myocardial ischemia. For stress echocardiography, regions are compared before and after stress in a side-by-side fashion, and wall segments with unchanged or worsening systolic function are compared qualitatively and scored (see later).

## Left Ventricular Diastolic Function

Diastolic dysfunction is extremely prevalent in patients with hypertension and in older adults (see Chapter 26 and 51). It is described mechanistically as impaired LV relaxation and increased LV stiffness. The historical "gold standard" for assessment of diastolic function has been the invasively obtained pressure-volume loop, in which diastolic function is assessed as the instantaneous relationship between pressure and volume. By echocardiography, assessment of, left atrial pressure, left ventricular end-diastolic pressure (LVEDP) and diastolic dysfunction is multifaceted and can be nuanced. (Age-adjusted reference values are shown in eTable 16.1.)[11] Analysis of diastolic dysfunction must be carried out with acknowledgment that (1) there are no absolute cutoffs for echo values that define the presence and degree of diastolic dysfunction at any LVEF; (2) the age, hemodynamics, and presence of other cardiac disease (particularly mitral disease) may affect many values; and (3) no single index is accurate in isolation.

### Mitral Inflow Patterns

Mitral inflow Doppler can be used to assess flow from the left atrium to the left ventricle during diastole (eFig. 16.13). The transmitral inflow velocity at a given point in time correlates with the pressure gradient between the chambers. The E wave occurs during early diastole when the ventricle is filling passively. The A wave represents the velocity of blood flow during late diastole during atrial contraction. Initial classification of diastolic function has been based on the pattern (i.e., relative heights) of the E and A waves. E wave velocity is dependent on the transmitral pressure gradient and is thus directly related to LA pressure and inversely related to LV compliance. The height of the A wave is additionally dependent on the strength of atrial contraction. Normally in individuals younger than 65, E wave height is greater than A wave height, with ratios of 1.0 or higher. LV compliance declines with age, and so the E wave generally diminishes. Simultaneously, the A wave typically increases as atrial contraction augments to compensate for the reduced LV compliance. Moreover, the deceleration time (DT) of the E wave increases as compliance worsens initially (eFig. 16.14). However, as diastolic function continues to worsen and LA pressures rises, the E wave will heighten again, and the size of the A wave declines as LV pressure rises and LA function begins to worsen, so the E/A ratio may revert to relatively normal (*pseudonormalization*). Because pseudonormal patterns can appear similar to normal patterns, E and A measures alone can be misleading. Further worsening of diastolic function leads to the so-called restrictive pattern, in which the descending slope of the E wave becomes very steep (rapid DT) because of abrupt cessation of mitral inflow. Thus, both the pattern of the E and the A waves and the mitral DT follow a biphasic course as diastolic function worsens, which limits the usefulness of these measures alone in assessment of diastolic function.

### Doppler Tissue Imaging

DTI applies Doppler imaging principles to the assessment of myocardial contraction and relaxation. Rather than assessing signals from rapidly moving red blood cells, DTI uses filters to optimize reception of the higher-amplitude signals that arise from the much slower-moving myocardium. When applied to assess myocardial motion at the mitral annulus (typically at both medial and lateral sampling points), the Doppler velocities are recorded over the cardiac cycle. Three distinct waveforms are seen: systolic contraction (the S′ wave) toward the relatively fixed apex, followed by early (e′) and late relaxation (a′) signals in diastole. The timing of the e′ and a′ waves is coincident and analogous in many ways to standard Doppler of mitral inflow, but the movement is in the opposite direction to blood flow and of much lower velocity. The e′ peak value is inversely related to tau ($\tau$), the time constant of ventricular relaxation. The e′ velocity ranges up to greater than 20 cm/sec in children and young adults but declines rapidly in early adulthood and beyond. Values less than 5 cm/sec are seen in patients with severe diastolic dysfunction (e.g., amyloidosis).

Because E velocity reflects the atrial-to-ventricular pressure gradient, it is dependent on both LV compliance and LA pressure (i.e., preload dependent). In contrast, DTI e′ in principle is a measure of LV compliance alone. Therefore, dividing E by e′ yields a measure that reflects LA pressure, which usually approximates LVEDP. An E/e′ ratio greater than 14 is considered abnormally high at any age and is usually indicative of elevated LVEDP. However, this ratio may be insensitive to acute changes and thus may not be suitable for monitoring patients during therapy.[11]

### Pulmonary Venous Doppler Flow Patterns

Pulmonary flow patterns are complementary to mitral inflow Doppler patterns for assessment of diastolic function. Pulmonary vein flow has three components: (1) the S wave, which consists of forward flow from the pulmonary veins to the left atrium during ventricular systole; (2) the D wave, which consists of passive flow during ventricular diastole; and (3) the AR wave, which is the slight flow reversal into the pulmonary veins during atrial contraction. Patients with impaired LV relaxation will demonstrate blunting of the S wave relative to the D wave. Reduced LV compliance may also result in greater flow into the pulmonary veins during atrial contraction (broader A wave).

A number of other Doppler parameters change with declining diastolic function. The *isovolumic relaxation time* represents the period between closure of the aortic valve and the start of ventricular filling (i.e., end of LVOT flow and beginning of mitral inflow E wave; see eFig. 16.8). Prolongation of the IVRT is associated with abnormal relaxation, and shortening of the IVRT can occur in patients with restrictive LV filling. Mitral E wave DT (see eFig. 16.14) is the interval from peak to no mitral inflow in early diastole. In early diastolic dysfunction, DT can actually increase. However, in patients with severe restrictive physiology where the stiff ventricle reaches its volume limit suddenly, the DT will be very rapid (<140 ms). This has been associated with an adverse prognosis in patients with heart failure and after MI (i.e., in patients with both systolic and advanced diastolic dysfunction).

### Color M-Mode and Flow Propagation

Color M-mode can be used to assess transmitral flow propagation velocity (Vp). While performing color flow Doppler through the mitral valve in apical windows, one can initiate the M-mode function to superimpose the color flow information onto the M-mode image (eFig. 16.15). The slope of the E wave flow (Vp) represents flow propagation, which correlates inversely with tau, the time constant of relaxation. Patients with impaired active relaxation will have a reduced "suction" action of the left ventricle, with abrupt slowing of blood once it enters the ventricle. On color M-mode, this manifests as a more shallow slope of Vp (abnormal is considered <0.45 in middle-aged adults, and <0.55 in younger adults). In practice, despite refinements in calculation of parameters based on flow propagation, Vp measures have lower reproducibility and appear reliable only in patients with depressed LVEF.[11]

### Assessing Diastolic Function in Clinical Practice

In clinical practice, assessment of diastolic function requires an integrated approach. Main parameters and rough cutoffs for initial

**ETABLE 16.1** Age-Adjusted Reference Range for Diastolic Function Parameters

| | AGE GROUPS (yr) | | | | | |
|---|---|---|---|---|---|---|
| | **45–49** | **50–54** | **55–59** | **60–64** | **65–69** | **≥70** |
| *Mitral Inflow Parameters* | | | | | | |
| E (m/sec) | 0.7 (0.5–0.9) | 0.6 (0.5–0.9) | 0.7 (0.5–0.9) | 0.7 (0.5–0.9) | 0.6 (0.4–0.8) | 0.6 (0.4–1.0) |
| A (m/sec) | 0.5 (0.3–0.7) | 0.5 (0.4–0.8) | 0.6 (0.4–0.9) | 0.6 (0.4–0.9) | 0.7 (0.4–1.0) | 0.8 (0.5–1.1) |
| E/A | 1.3 (1.0–2.0) | 1.2 (0.8–2.0) | 1.2 (0.7–1.8) | 1.0 (0.7–1.6) | 1.0 (0.6–1.5) | 0.8 (0.6–1.3) |
| DT (msec) | 208 (180–258) | 217 (178–266) | 210 (183–287) | 222 (180–282) | 227 (188–298) | 242 (188–320) |
| *TDI—Mitral Annulus* | | | | | | |
| *Septal* | | | | | | |
| $e'_s$ (m/sec) | 0.10 (0.07–0.14) | 0.09 (0.06–0.14) | 0.09 (0.05–0.12) | 0.09 (0.06–0.13) | 0.08 (0.05–0.11) | 0.07 (0.05–0.11) |
| $E/e'_s$ | 6.67 (4.62–11.25) | 7.00 (4.55–11.67) | 7.78 (4.62–13.33) | 7.64 (5.00–12.00) | 8.57 (5.45–13.33) | 8.57 (4.55–16.67) |
| *Lateral* | | | | | | |
| $e'_L$ (m/sec) | 0.13 (0.09–0.17) | 0.12 (0.08–0.16) | 0.11 (0.07–0.15) | 0.10 (0.07–0.15) | 0.09 (0.07–0.12) | 0.08 (0.05–0.11) |
| $E/e'_L$ | 5.38 (3.75–7.78) | 5.45 (3.75–8.89) | 6.00 (3.85–10.00) | 6.67 (4.62–8.89) | 7.00 (4.17–11.25) | 7.78 (5.00–14.00) |
| *Pulmonary Vein Flow Parameters* | | | | | | |
| $P_S/P_D$ | 1.25 (0.86–2.00) | 1.40 (1.00–2.00) | 1.40 (1.00–2.00) | 1.50 (1.00–2.25) | 1.60 (1.00–2.50) | 1.67 (1.00–2.50) |
| $PVAR_{dur}$ (msec) | 118 (100–140) | 122 (103–142) | 123 (105–157) | 123 (103–160) | 127 (110–152) | 130 (112–170) |

Data are median (5th and 95th percentile).

*A,* Late diastolic mitral flow velocity; *DT,* deceleration time of early diastolic mitral flow; *E,* early diastolic mitral flow velocity; $e'_L$, early diastolic lateral annular velocity; $e'_s$, early diastolic septal annular velocity; $P_D$, pulmonary vein diastolic flow velocity; $P_S$, pulmonary vein systolic flow velocity; $PVAR_{dur}$, duration of pulmonary vein atrial flow reversal; *TDI,* tissue Doppler imaging;

Modified from Munagala VK, Jacobsen SJ, Mahoney DW, et al. Association of newer diastolic function parameters with age in healthy subjects: a population-based study. *J Am Soc Echocardiogr* 2003;16:1049.
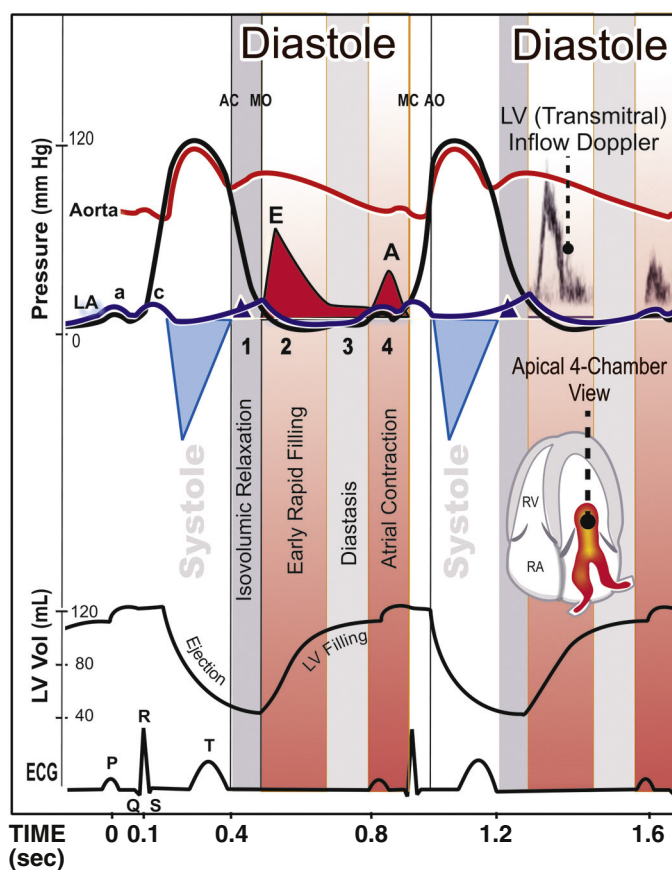


**EFIGURE 16.13** The cardiac cycle and phases of diastole. *AC,* Aortic closure; *AO,* aortic opening; *MC,* mitral closure; *MO,* mitral opening; *RA,* right atrium; *RV,* right ventricle.
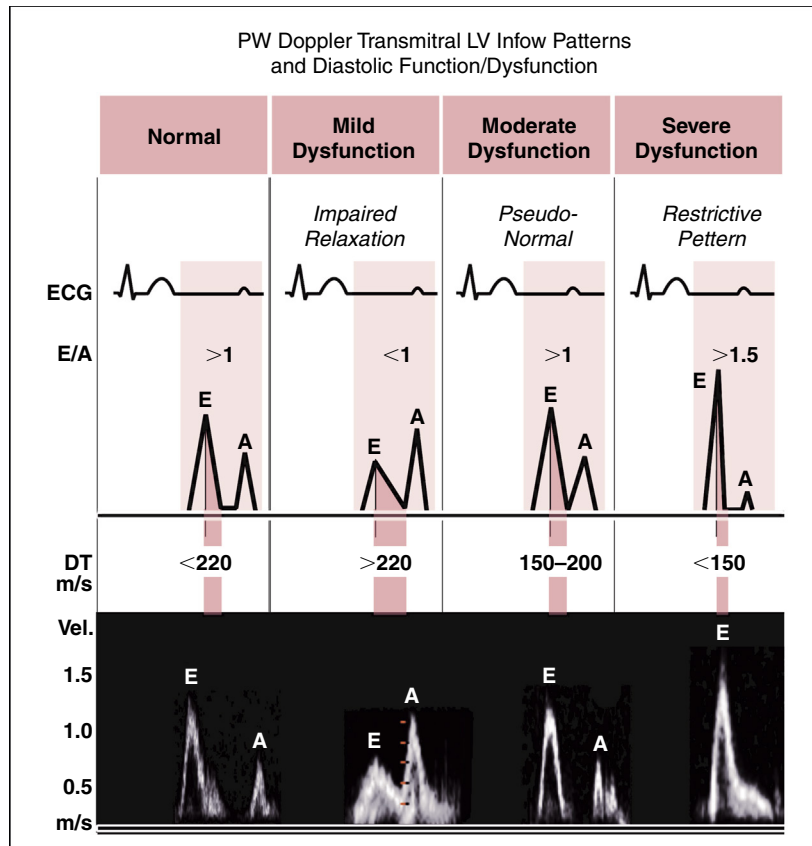
**EFIGURE 16.14** Mitral inflow Doppler waveforms in diastolic dysfunction. Left ventricle diastolic filling patterns (normal, impaired relaxation, pseudonormal, and restrictive filling). See text for details. *ECG*, Electrocardiogram; *LV*, left ventricle; *PW*, pulsed wave. (Modified from Ho CY, Bulwer BE. Echocardiographic assessment of diastolic function. In: Solomon SD, Bulwer BE, eds. *Essential Echocardiography. A Practical Handbook with DVD*. Totowa, NJ: Humana Press; 2007:124.)
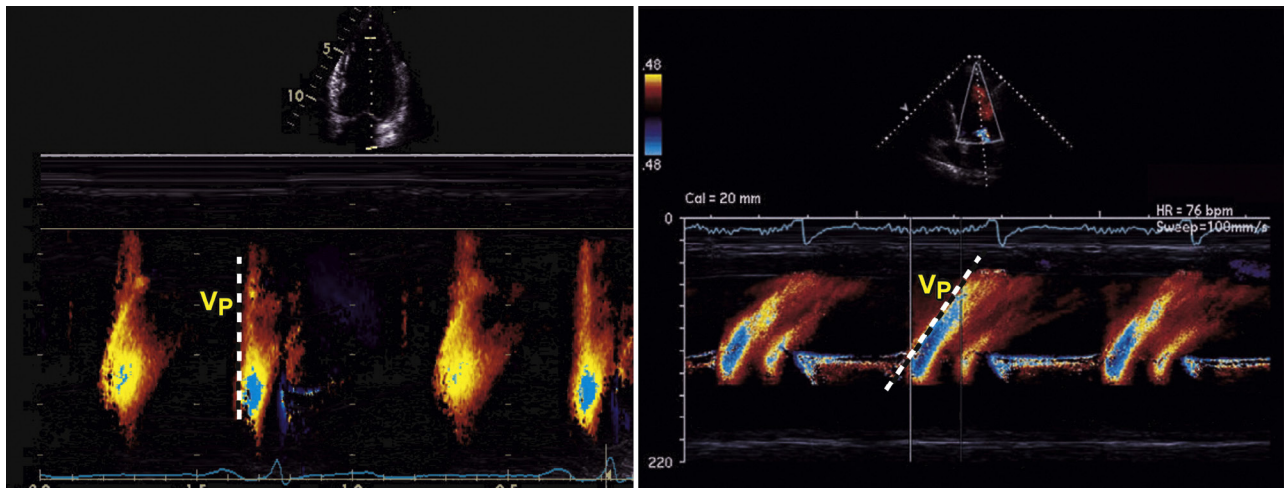


**EFIGURE 16.15** Transmitral flow propagation demonstrated by color M-mode. Flow propagation velocity is assessed as the linear slope of the isovelocity contour (the aliasing portion) of the mitral inflow pattern at 4 cm into the LV cavity. This slope will be more shallow when velocity is impaired (as in **right panel**). Vp is transmitral flow propagation velocity. Determination of Vp is often more difficult when the early diastolic flow velocities form a curved isovelocity inflow pattern, rather than a single straight slope.

**TABLE 16.4** Expected Findings for Left Ventricular (LV) Relaxation, Filling Pressures, and Two-Dimensional and Doppler Findings According to LV Diastolic Function

| PARAMETER | NORMAL | GRADE I | GRADE II | GRADE III |
|---|---|---|---|---|
| LV relaxation | Normal | Impaired | Impaired | Impaired |
| LA pressure | Normal | Low or normal | Elevated | Elevated |
| Mitral E/A ratio | ≥0.8 | ≤0.8 | >0.8 to <2 | >2 |
| Average E/e′ ratio | <10 | <10 | 10–14 | >14 |
| Peak TR velocity (m/sec) | <2.8 | <2.8 | >2.8 | >2.8 |
| LA volume index | Normal | Normal or increased (>34 ml/m²) | Increased | Increased |

*LA,* Left atrial; *TR,* tricuspid regurgitation.
From Nagueh SF, Smiseth OA, Appleton CP, et al. Recommendations for the evaluation of left ventricular diastolic function by echocardiography: an update from the American Society of Echocardiography and the European Association of Cardiovascular Imaging. *J Am Soc Echocardiogr.* 2016;29:277.

**TABLE 16.5** Normal Values for Right Ventricular (RV) Chamber Size

| PARAMETER | MEAN ± SD | NORMAL RANGE |
|---|---|---|
| RV basal diameter (mm) | 33 ± 4 | 25–41 |
| RV mid diameter (mm) | 27 ± 4 | 19–35 |
| RV longitudinal diameter (mm) | 71 ± 6 | 59–83 |
| RVOT PLAX diameter (mm) | 25 ± 2.5 | 20–30 |
| RVOT proximal diameter (mm) | 28 ± 3.5 | 21–35 |
| RVOT distal diameter (mm) | 22 ± 2.5 | 17–27 |
| RV wall thickness (mm) | 3 ± 1 | 1–5 |
| RVOT EDA (cm²) | | |
| Men | 17 ± 3.5 | 10–24 |
| Women | 14 ± 3 | 8–20 |
| RV EDA indexed to BSA (cm²/m²) | | |
| Men | 8.8 ± 1.9 | 5–12.6 |
| Women | 8.0 ± 1.75 | 4.5–11.5 |
| RV ESA (cm²) | | |
| Men | 9 ± 3 | 3–15 |
| Women | 7 ± 2 | 3–11 |
| RV ESA indexed to BSA (cm²/m²) | | |
| Men | 4.7 ± 1.35 | 2.0–7.4 |
| Women | 4.0 ± 1.2 | 1.6–6.4 |
| RV SEDV indexed to BSA (mL/m²) | | |
| Men | 61 ± 13 | 35–87 |
| Women | 53 ± 10.5 | 32–74 |
| RV ESV indexed to BSA (mL/m²) | | |
| Men | 27 ± 8.5 | 10–44 |
| Women | 22 ± 7 | 8–36 |

*BSA,* Body surface area; *EDA,* end-diastolic area; *ESA,* end-systolic area; *PLAX,* parasternal long-axis view; *RVOT,* RV outflow tract.
From Lang RM, Badano LP, Mor-Avi V, et al. Recommendations for cardiac chamber quantification by echocardiography in adults: an update from the American Society of Echocardiography and the European Association of Cardiovascular Imaging. *J Am Soc Echocardiogr.* 2015;28:1.

assessment include mitral inflow Doppler (particularly E/A ratio) and tissue Doppler (é and E/é′ ratio) criteria, but also estimates of PASP and LA volume (Table 16.4 and eFig. 16.16). A majority of evidence (initially at least two of four) of these abnormal parameters is required to parse diastolic dysfunction, with use of additional parameters as needed for corroboration.[11] Several schemes have been developed to grade diastolic function based on these parameters (Table 16.4). Their application, particularly for assessing LV filling pressures, should also take into consideration LV systolic function and the presence of underlying cardiomyopathies. Although these schemes allow for some standardization in description of diastolic dysfunction, data on the relationship between specific grades, resting hemodynamics, and clinical outcomes remain limited. Abnormalities in diastole are extremely prevalent in patients with hypertension and in elderly patients but are not necessarily associated with clinical symptoms or overt heart failure.[11,12] Assessment of diastolic function during exercise, termed the "diastolic stress test," may help unmask abnormalities that contribute to symptoms only during exertion.[12]

### Right Ventricular Structure and Function

Assessment of the right ventricle has proved especially challenging for 2D echocardiography. Whereas the left ventricle is relatively easily characterized as a prolate ellipsoid, the odd crescentic shape of the right ventricle makes modeling of volumes considerably more complex. Moreover, because visualization of the entire right ventricle is not encompassed by any single 2D plane, multiple measurements from multiple views are necessary to fully assess this chamber (eFig. 16.17). Normal linear RV measurements are shown in Table 16.5. Under normal conditions, the right ventricle is accustomed to low pulmonary vascular resistance (PVR) and is thus extremely sensitive to changes in afterload. Conditions that increase PVR acutely, such as pulmonary embolism (see Chapter 87), will cause marked RV dilation and dysfunction. Conditions that cause a chronic increase in PVR will lead to RV hypertrophy and dilation, but RV function is usually maintained until the late stages of disease (see Chapter 88).

Several methods are commonly used to assess global RV function initially on conventional echocardiography (Table 16.6).[2] RV fractional area change (FAC) (Fig. 16.16) is easily determined by calculating the RV area in diastole (RVAd) and systole (RVAs) on the apical four-chamber view:

$$FAC = (RVAd - RVAs)/RVAd$$

Assessment of RV function by FAC has been shown to provide incremental prognostic value in patients with heart failure and following MI.[13] *Tricuspid annular plane systolic excursion* (TAPSE) is a measure of RV contractility that is readily measured with M-mode imaging in the apical four-chamber view (Fig. 16.17). This longitudinal motion of the tricuspid annulus can similarly be assessed with pulsed or tissue Doppler as the peak velocity of the systolic wave, S′ (see Fig. 16.17, right). Also exactly analogous to the left ventricle, an RV Tei index and RV GLS values can similarly be obtained. RV regional, as opposed to global, dysfunction has particular importance in conditions in which RV afterload increases abruptly, such as pulmonary embolism (see later), in which regional RV function is often preserved in the apical and basal free wall segments but dyskinetic or akinetic in the midregion. Both global and segmental RV wall motion abnormalities also notably occur in RCA infarcts and RV cardiomyopathies.

3D imaging of the right ventricle is now available, and reconstructed views beautifully illustrate its geometric complexity (Fig. 16.18). 3D imaging allows for calculation of volumes that are not as angle dependent as all the measures previously discussed. Image acquisition still relies on an experienced sonographer, and the volume measurements require additional training, are only semiautomatic, and must be done off-line. However, normal reference values for RV volumes and RV ejection fractions now exist (see Tables 16.5 and 16.6).[2] Similar to LV volume data, the accuracy appears comparable with that of CMR imaging, although volumes tend to be lower on echocardiography.

**In patients with normal LV EF**

1-Average E/e' > 14
2-Septal e' velocity < 7 cm/s or
Lateral e' velocity <10 cm/s
3-TR velocity > 2.8 m/s
4-LA volume index > 34 mL/m$^2$

<50%
positive

50%
positive

>50%
positive

**Normal Diastolic
function**

**Indeterminate**

**Diastolic
Dysfunction**

A

**Mitral Inflow**

E/A≤0.8 + E≤50 cm/s

E/A≤0.8 + E>50 cm/s
or
E/A>0.8-<2

E/A≥2

3 criteria to be evaluated*

2 of 3 or 3 of 3
Negative

1-Average E/e'<14
2-TR velocity>2.8 m/s
3-LA Vol. index>34 mL/m$^2$

2 of 3 or 3 of 3
Positive

When only 2 criteria are available

2 negative

1 positive and
1 negative

2 positive

Normal LAP
Grade I Diastolic
Dysfunction

Cannot determine
LAP and Diastolic
Dysfunction
Grade*

↑ LAP
Grade II Diastolic
Dysfunction

↑ LAP
Grade III Diastolic
Dysfunction

*If Symptomatic*

Consider CAD, or
proceed to diastolic
stress test

B

(* : LAP indeterminate if only 1 of 3 parameters available. Pulmonary vein S/D ratio <1 applicable to conclude elevated
LAP in patients with depressed LV EF)

**EFIGURE 16.16** ASE algorithm for diagnosis of LV diastolic dysfunction in (**A**) subjects with normal LVEF; (**B**) in patients with depressed LVEF and patients with myocardial disease and normal LVEF after consideration of clinical and other 2D data. (From Nagueh SF, et al. *J Am Soc Echocardiogr.* 2016:29.)
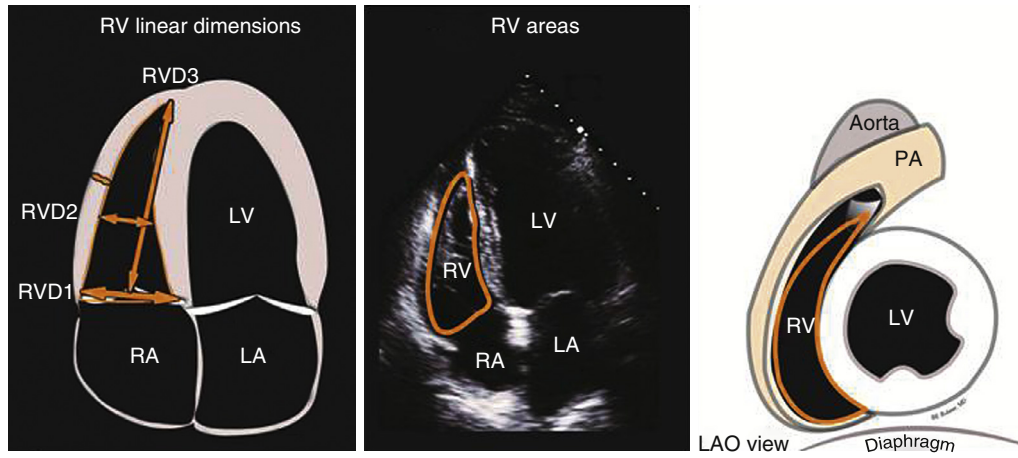
**EFIGURE 16.17** Right ventricular linear and area measurements on 2D echocardiography. The right ventricle is a tripartite shape, with a half-crescent shape in long-axis windows and a crescentic cross section in short-axis views. As a rough guide, from RV-focused apical views (which display the largest basal RV diameter but still center the LV apex at the top of the scanning sector) an RV basal diameter greater than 41 mm and midlevel diameter greater than 35 mm is indicative of RV enlargement (see Table 16.5). *LA,* Left atrium; *LV,* left ventricle; *PA,* pulmonary artery; *RA,* right atrium; *RV,* right ventricle. (Modified from Bulwer BE, Solomon SD. Assessment of systolic function. In Solomon SD, ed. *Atlas of Echocardiography*. 2nd ed. Philadelphia: Current Science/Springer Science; 2009:65.)

## Left and Right Atria

LA enlargement has been associated with adverse cardiovascular outcomes. The left atrium enlarges under several pathologic conditions, including LV systolic and diastolic dysfunction and atrial fibrillation (AF). Other frequent causes of LA enlargement include hypertension and mitral valve regurgitation or stenosis. LA size is thought to reflect LV filling pressure and thus has been considered a useful indicator of diastolic function over time. Indeed, left atrial volume (corrected for BSA) is a key element of the assessment of diastolic function in the ASE guidelines. Several methods can be used to quantify LA size. A linear measurement of the left atrium is traditionally obtained on the parasternal long axis view and in the early days of echocardiography was the initial screen of LA size. A longstanding reference standard for parasternal long-axis LA dimension has been 3.8 cm as the upper limit of normal in women and 4.0 cm in men (or 2.3 cm/m$^2$ BSA for both). Other axes in the apical windows may also be measured. However, any single linear measurement is inadequate, and LA area is more fully assessed from orthogonal apical views, with volume subsequently calculated by applying the Simpson biplane method.

**TABLE 16.6** Normal Values for Parameters of Right Ventricular (RV) Function

| PARAMETER | MEAN ± SD | ABNORMALITY THRESHOLD |
|---|---|---|
| TAPSE (mm) | 24 ± 3.5 | <17 |
| Pulsed Doppler S wave (cm/sec) | 14.1 ± 2.3 | <9.5 |
| Color Doppler S wave (cm/sec) | 9.7 ± 1.85 | <6.0 |
| RV fractional area change (%) | 49 ± 7 | <35 |
| RV free wall 2D strain* (%) | −29 ± 4.5 | >−20† |
| RV 3D EF (%) | 58 ± 6.5 | <45 |
| Pulsed Doppler MPI | 0.26 ± 0.085 | >0.43 |
| Tissue Doppler MPI | 0.38 ± 0.08 | >0.54 |
| E wave deceleration time (msec) | 180 ± 31 | <119 or >242 |
| E/A | 1.4 ± 0.3 | <0.8 or >2.0 |
| e′/a′ | 1.18 ± 0.33 | <0.52 |
| e′ | 14.0 ± 3.1 | <7.8 |
| E/e′ | 4.0 ± 1.0 | >6.0 |

*Limited data; values may vary depending on vendor and software version.
†<20 in magnitude with the negative sign.
MPI, Myocardial performance (Tei) index; TAPSE, tricuspid annular plane systolic excursion.
From Lang RM, Badano LP, Mor-Avi V, et al. Recommendations for cardiac chamber quantification by echocardiography in adults: an update from the American Society of Echocardiography and the European Association of Cardiovascular Imaging. J Am Soc Echocardiogr. 2015;28:1.
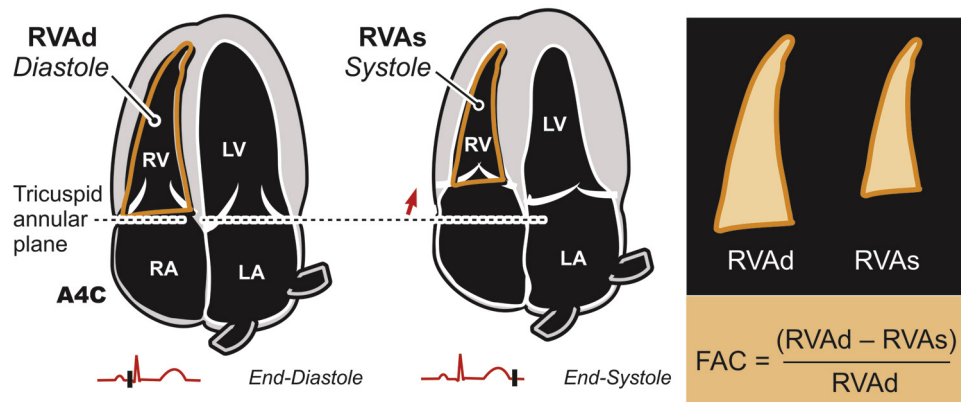
Volumes are typically indexed to BSA (see Table 16.2). LA function contributes to overall cardiac performance and is itself also affected by LV compliance.

Assessment of the right atrium is best performed from the apical and subcostal views. RA size is a reflection of right-sided filling pressure and volume. The most frequent causes of RA enlargement are AF and TR. Isolated right heart enlargement should always raise the question of whether interatrial (left-to-right) shunting is occurring, and a search for an atrial septal defect should be undertaken with intravenous (IV) saline contrast if necessary. Biatrial enlargement can occur with AF or with restrictive cardiomyopathy.

Indexed RA volumes based on volumetric assessment are similar to LA volumes in healthy men and are slightly smaller in healthy women (eTable 16.2). Assessment of both the right atrium and the inferior vena cava (IVC) is important in the estimation of RA pressure, which is essential for calculating PASP from TR velocity. Qualitative evidence of elevated RA pressure includes a dilated right atrium, dilation of the IVC, or attenuation of IVC collapse during inspiration. Several methods have been used to estimate RA pressure by echocardiography, but most involve a combination of IVC size and the amount that the IVC collapses with inspiration. A rough scale of RA pressure has been developed that combines assessment of IVC size using a cutoff of 2.1 cm and respirophasic collapse (Table 16.7) using a cutoff of 50%. Notably, the IVC is occasionally dilated in healthy young individuals and in athletes, particularly when imaged completely supine. It does not provide a consistent measure of RA pressure in mechanically ventilated patients due to positive end-expiratory pressure.[14]

## TRANSESOPHAGEAL ECHOCARDIOGRAPHY

TEE is an alternative method to obtain ultrasound images of the heart in which a smaller ultrasound transducer is introduced into the patient's esophagus through a manipulable flexible probe. Similar to transthoracic scanning, multiplane 2D and 3D, color flow, and spectral Doppler imaging can be performed at the bedside, but with a higher-frequency transducer and from a position that is posterior and closer to the heart than can be achieved with TTE. The result is superior image quality and spatial resolution with less artefact, particularly when assessing the left atrium and left-sided valves, which are directly adjacent to the esophagus. Because it is semi-invasive, TEE is generally used as an adjunctive or follow-up test to an initial TTE if additional information is sought or the TTE images are inconclusive. Table 16.8 summarizes the advantages and disadvantages of TTE versus TEE.

TEE is particularly useful in the evaluation of valve dysfunction, diagnosis or follow-up of endocarditis (see Chapter 80), searching for potential causes of stroke, and for better characterization of cardiac masses and congenital heart disease.[15,16] In some circumstances, TEE is appropriately the first test of choice, such as evaluation of aortic pathology and assessment for LA appendage thrombi (see Diseases of the Aorta and Cardiac Masses).[17] TEE can be used to determine the presence of thrombus in patients in whom rapid cardioversion of AF is necessary (see Chapter 66) or when elective atrial arrhythmia ablation/cardioversion is planned, particularly in the patient found to be underanticoagulated or at high risk for stroke (eTable 16.3). In addition, TEE has a major role in optimizing and evaluating cardiac surgical and percutaneous procedures, particularly with respect to valvular procedures, closure of intracardiac shunts, implantation of LVADs, and left atrial appendage occlusion.



$$FAC = \frac{(RVAd - RVAs)}{RVAd}$$

**FIGURE 16.16** Right ventricular area (RVA) measurement and fractional area change (FAC) used to assess RV function with the apical four-chamber view (A4C). LA, Left atrium; LV, left ventricle; RA, right atrium; RV, right ventricle.

**ETABLE 16.2** Normal Right Atrial (RA) Size Obtained From Two-Dimensional (2D) Echocardiographic Studies

|  | WOMEN | MEN |
|---|---|---|
| RA minor axis dimension (cm/m²) | 1.9 ± 0.3 | 1.9 ± 0.3 |
| RA major axis dimension (cm/m²) | 2.5 ± 0.3 | 2.4 ± 0.3 |
| 2D echocardiographic RA volume (mL/m²) | 21 ± 6 | 25 ± 7 |

Data are expressed as mean ± SD.
From Lang RM, Badano LP, Mor-Avi V, et al. Recommendations for cardiac chamber quantification by echocardiography in adults: an update from the American Society of Echocardiography and the European Association of Cardiovascular Imaging. *J Am Soc Echocardiogr* 2015;28:1.

**ETABLE 16.3** Indications for Transesophageal Echocardiography–Guided Cardioversion

| APPROPRIATE | INAPPROPRIATE |
|---|---|
| CHF exacerbation or hemodynamic compromise | Stable with therapeutic anticoagulation >3 weeks |
| Symptomatic from AF | AF <48 hours (insufficient time for thrombus to form) |
| Hospitalized and symptomatic | Permanent AF (sinus rhythm unable to be sustained after cardioversion) |
| New-onset AF (first-time diagnosis) | Hospitalized but asymptomatic |
| High stroke risk (including history of stroke or TIA, previous history of LA thrombus, rheumatic heart disease, HOCM) | |
| Subtherapeutic anticoagulation (INR <2) within preceding 3 weeks, or significant interruption in NOAC therapy | |
| Miscellaneous (including need for TEE unrelated to AF but otherwise appropriate, such as evaluation of valve function or endocarditis, with timing of TEE coincidentally helpful for expediting cardioversion) | |

*AF,* Atrial fibrillation; *CHF,* congestive heart failure; *HOCM,* hypertrophic obstructive cardiomyopathy; *INR,* international normalized ratio; *TIA,* transient ischemic attack; *NOAC,* non–vitamin K antagonist oral anticoagulant.

M-mode | Tissue Doppler
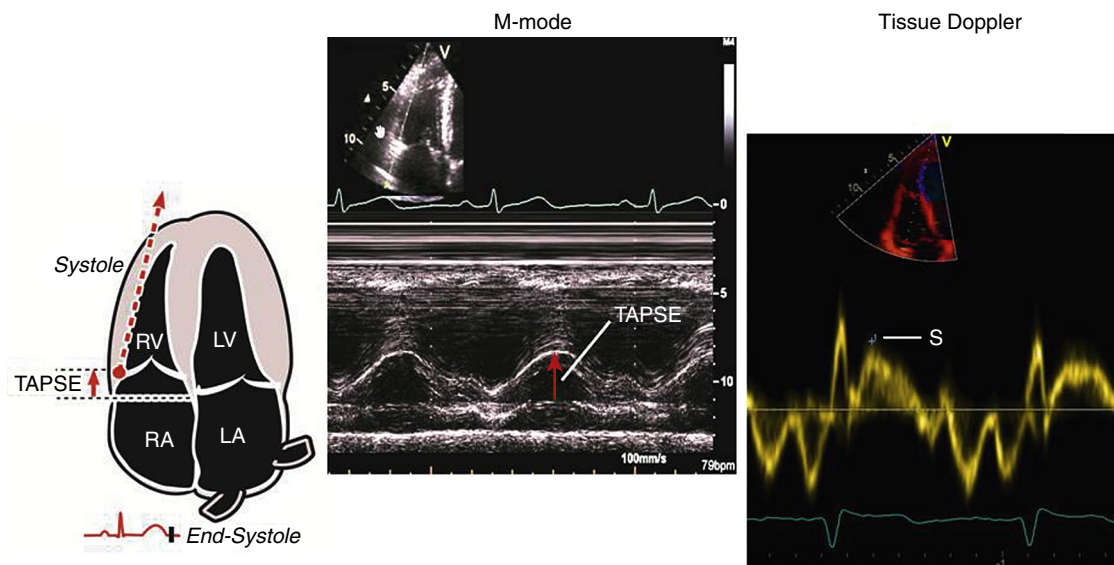


**FIGURE 16.17** M-mode and Doppler tissue imaging (DTI) measurements of RV systolic function. **Left and middle panels,** On M-mode, the tissue annular plane systolic excursion (TAPSE) can be measured. **Right,** DTI is used to map tricuspid annular motion, where *S* is the analogous measurement to TAPSE.
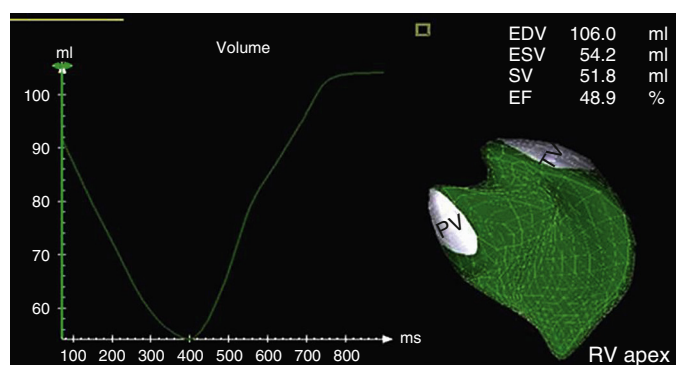


**FIGURE 16.18** Three-dimensional measurements of right ventricular (RV) volume and function. A 3D echocardiographic reconstruction of the RV shape and volume, as viewed from the septal surface. The graph at *left* shows RV volumes plotted against time over the cardiac cycle, with data obtained from RV-focused apical four-chamber windows. RV stroke volume (SV) = EDV − ESV. RV ejection fraction (EF) = SV/EDV. *EDV,* end-diastolic volume; *ESV,* end-systolic volume; *PV,* pulmonic valve; *TV,* tricuspid valve.

**TABLE 16.7 Estimation of Right Atrial Pressure Based on Inferior Vena Cava (IVC) Diameter and Collapse**

| VARIABLE | NORMAL (0–5 [3] mm Hg) | INTERMEDIATE (5–10 [8] mm Hg) | HIGH (15 mm Hg) | |
|---|---|---|---|---|
| IVC diameter | ≤2.1 cm | ≤2.1 cm | >2.1 cm | >2.1 cm |
| Collapse with sniff | >50% | >50% | <50% | <50% |
| Secondary indices | | | | Restrictive filling by tricuspid valve inflow |
| | | | | Tricuspid E/e′ >6 |
| | | | | Diastolic flow predominance in hepatic veins (systolic filling <55%) |

Ranges are provided for low and intermediate categories, but for simplicity, midrange values of 3 mm Hg for normal and 8 mm Hg for intermediate are suggested. Intermediate (8 mm Hg) RA pressures may be downgraded to normal if no secondary indices of elevated RA pressure are present, upgraded to high if minimal collapse with nasal inhalation (<35%) and secondary indices of elevated RA pressure are present, or left at 8 mm Hg if uncertain.
From Rudski LG, Lai WW, Afilalo J, et al. Guidelines for the Echocardiographic Assessment of the Right Heart in Adults: A Report from the American Society of Echocardiography. *J Am Soc Echocardiogr.* 2010:23:685.

TEE may be performed on an inpatient or outpatient basis, and most patients require topical anesthesia and/or IV conscious sedation for comfort. This is usually achieved with IV midazolam and fentanyl or alternatively with propofol if issues with respiratory or hemodynamic stability or patient comfort are anticipated. Risks are relatively low but include trauma to the oropharynx and esophagus, aspiration, bronchospasm or laryngospasm, accidental tracheal intubation, and arrhythmia, as well as risks associated with sedation (transient hypotension) and theoretically with neck manipulation. General anesthesia is used for patients in the operating room and during some transcatheter procedures and, in this context, TEE may be associated with higher complication rates (as high as 1.2% for major complications), particularly during prolonged procedures.[17,18] The most serious complication is upper gastrointestinal perforation, which typically occurs in the esophagus or hypopharynx. Patients with esophageal diverticula or strictures, significant thoracic radiation-induced fibrosis, distorted anatomy of the mediastinal organs, or difficult probe placement are at higher risk. TEE may also cause bleeding (0.02% to 1.0%) from direct abrasion or laceration of the mucosa, esophageal varices, or tumor. The overall risk for major adverse events with TEE is 0.2% to 0.5% in the nonsurgical setting, and the overall mortality rate is exceedingly low (0.0004%). These risks may be minimized by screening patients for potential contraindications (eTable 16.4); if one is found, TEE is best deferred until the

situation can be better assessed or ameliorated. Alternatively, another imaging modality (e.g., intravascular ultrasound [IVUS] or epiaortic scanning, CT or CMR) or management strategy could be considered if an underlying risk factor cannot be mitigated.

## The Standard Transesophageal Echocardiographic Examination

Figure 16.19 shows a standard TEE examination. It is usually prudent to address the main indication first in the event that the examination must be aborted because of clinical instability. If the patient remains stable, a comprehensive examination is performed, with the majority of the images at the midesophageal level (probe tip approximately 35 cm from the incisors). For a frame of reference with respect to the imaging planes, at midesophageal level with the transducer angle set at 0 to 30 degrees and the probe flexed, the imaging plane cuts the heart in

**ETABLE 16.4** **Relative Contraindications to Transesophageal Echocardiography and Potential Strategies**

| RELATIVE CONTRAINDICATION | POTENTIAL STRATEGIES |
|---|---|
| Esophageal strictures or diverticula | GI consultation to evaluate, consider use of a pediatric TEE probe or limited TEE only to a depth proximal to the lesion |
| Esophagitis, especially radiation induced | GI consultation to evaluate, consider alternative procedure (e.g. CT angiography, IVUS, PET, CMR) |
| Esophageal varices or recent UGI bleeding | GI consultation to evaluate, correct any coagulopathy, limit TEE only to a depth proximal to the lesion, avoid unnecessary probe manipulation or locking of probe in flexed position, freeze image when probe not being used, use real-time 3D imaging when possible to expedite procedural time |
| Recent esophageal dilation or UGI surgery | GI/surgery consultation, consider delaying TEE to at least 4–6 weeks, consider limited TEE proximal to the intervention |
| Unstable airway and/ or hemodynamically tenuous or unstable | Consider intubation and pressors, place probe under direct laryngoscopy |
| Unstable cervical spine (e.g., after trauma) | Stabilize with a cervical spine collar, consider paralysis, neurologic and/or orthopedic consultation to clear |
| Uncooperative patient, restricted cervical mobility | Anesthesia consultation for intravenous propofol, consider higher levels of sedation or general anesthesia |
| History of significant opioid use/abuse | Anesthesia consultation for intravenous propofol |
| Severe coagulopathy or thrombocytopenia | Consider correction with blood products and vitamin K |

*CMR*, cardiac MRI; *GI,* Gastrointestinal; *IVUS*, intravascular ultrasound; *PET*, positron emission tomography; *UGI,* upper GI.

**TABLE 16.8** Advantages and Disadvantages of Transesophageal Echocardiography (TEE) Relative to Transthoracic Echocardiography (TTE)

| ADVANTAGES | DISADVANTAGES |
|---|---|
| Useful in percutaneous and surgical procedures, as well as at the bedside | Semi-invasive—usually requires sedation, hence associated risks with probe intubation (gastrointestinal and pulmonary implications) and sedation effects (hypotension). Long procedures may necessitate general anesthesia. |
| | Generally a minimum of two staff members required: one operator and one person to monitor the sedation needed. |
| | Aerosol-generating procedure (risk of transmission of airborne pathogens) |
| Higher resolution: better to definitively detect vegetations, thrombi, masses, and intracardiac shunts. Superior imaging of valves, especially the mitral and aortic, left atrium and appendage, left ventricle, thoracic aorta and arch, and interatrial septum, as well as the pulmonary veins | May not view the LV apex or right-sided structures well (structures that are further from probe, particularly in large patients) |
| "Continuous" acoustic window when compared with TTE (no ribs to cause acoustic shadowing) | "Blind spot" of acoustic shadowing where the trachea is interposed between the esophagus and heart |
| | Much of the abdominal aorta is out of range |
| Superior imaging of the mitral valve and mitral prostheses in general, with the ability to precisely localize valvular and paravalvular defects | Mechanical aortic prostheses can cause excessive shadowing |
| | May be technically difficult to achieve the best angle of insonation (i.e., less reproducible and accurate) for assessing aortic stenosis gradients |
| | Maneuvers to increase or decrease preload may be more difficult (e.g., Valsalva maneuver), although most patients can cooperate |
| | Real-time 3D imaging and reconstruction dependent on a slow regular heart rate and "stable" window (i.e., still patient) |

a short-axis (transverse) plane. A TEE transducer angle of 90 to 120 degrees corresponds to a long-axis (longitudinal, or sagittal) plane.

Most transesophageal examinations start with the standard four-chamber view of the heart, similar to the transthoracic apical four-chamber view. At midesophageal level, 0 degrees, this is achieved by slight retroflexion of the probe to tilt the imaging plane in order to include the cardiac apex. At this level the multiplane "omni" controller is used to rotate the scanning plane counterclockwise to slice the left ventricle into two-chamber (approximately 90-degree) and then three-chamber (long-axis or 120-degree) views. These views are optimal for assessing the left ventricle, left atrium, and mitral valve structure and function. If desired, the LA appendage may be thoroughly examined by withdrawing the probe slightly cephalad, centering the image sector on the appendage, and scanning from 30 to 150 degrees. To examine the aortic valve, the operator retracts the probe slightly, and the aortic valve should be imaged just superior to the mitral valve, at approximately 30 degrees for short-axis images and 120 degrees for long-axis views. The tricuspid valve may be examined at approximately 45 degrees, with subsequent views of the right ventricular outflow tract (RVOT), pulmonary artery and valve, and pulmonary bifurcation sought by gradually increasing the omni angle up toward 120 degrees. The tricuspid valve may be best seen by advancing the probe to about 40 cm from the incisors which typically is in the vicinity of the gastroesophageal junction. Minor additional manipulations of the TEE probe and transducer angle will provide views of the pulmonary veins, right atrium, interatrial septum, superior vena cava (SVC), IVC, coronary sinus, and abdominal aorta. For transgastric windows, the TEE probe is advanced gently past the gastroesophageal sphincter with the transducer plane reset back to 0 degrees and the probe in a neutral position (unflexed). One can view the left ventricle and mitral valve in the short axis and also obtain transaortic gradients from an apical five- or three-chamber view if needed. By increasing the omni angle up to 90 degrees and rotating the transducer plane to the right, more detailed views of the tricuspid valve and right side of the heart are attainable. Lastly, the thoracic aorta is usually examined in cross-sectional and longitudinal views as the probe is withdrawn, to document any significant atherosclerosis or other pathology.

## THREE-DIMENSIONAL ECHOCARDIOGRAPHY

Acquisition and display of 3D images have been a long-term goal of echocardiography. Although 3D datasets can be obtained by reconstruction from transthoracic or transesophageal rotational 2D acquisition, true 3D echocardiography is accomplished by using a matrix-array transducer that emits and receives stacked beams of ultrasound which allows the real-time acquisition of a pyramidal dataset in three dimensions (Fig. 16.20). Matrix-array probes for both transthoracic and transesophageal use are available. The 3D datasets can be used to display simultaneous orthogonal 2D images (e.g., four- and two-chamber apical views, Video 16.4) or a 3D-rendered image (Video 16.5). 3D echocardiography offers the potential to better orient valvular structures (see Valvular Heart Disease) or congenital abnormalities and can be particularly useful in planning surgical and percutaneous interventions. As discussed earlier, 3D echocardiography can also improve the accuracy of quantification of LV and RV volume and function. Useful 3D imaging depends heavily on good 2D images, and in fact there is some loss of spatial and temporal resolution in comparison. However, 3D echocardiography has become extremely useful as a way to delineate complex structures that extend beyond one plane or to find and localize measurements and abnormalities that are difficult to encompass using 2D images. Examples include finding clefts and localizing prolapsed segments in the mitral valve, delineating paravalvular leaks, measuring the distance of the coronary artery origins from the aortic valve, and providing comprehensive quantitative analysis of the valve leaflets and annuli (Fig. 16.21 and Video 16.6), as well as guiding percutaneous device implantation (see Transcatheter Interventions). 3D acquisition is now becoming standard in echocardiography and in the operating room.

## ULTRASOUND ENHANCING AGENTS

Contemporary echocardiographic enhancing agents, also called ultrasound "contrast" agents, are stabilized gas microspheres of 1.1 to 4.5 µm, similar in size to red blood cells, and can move through the circulatory system accordingly after IV injection. Currently approved agents consist of high-molecular weight gases, chosen because of their resistance to diffusion into the blood, which are enclosed within either albumin or phospholipid shells. Unlike the larger bubbles created by agitating saline, commercial contrast bubbles are uniform in size and small enough to transit the pulmonary vascular bed and are therefore capable of opacifying the left side of the heart.

Because their shells are somewhat resilient, contrast bubbles will contract in response to the peak acoustic pressure of the sinusoidal ultrasound wave and expand when acoustic pressure is lowest. Optimal
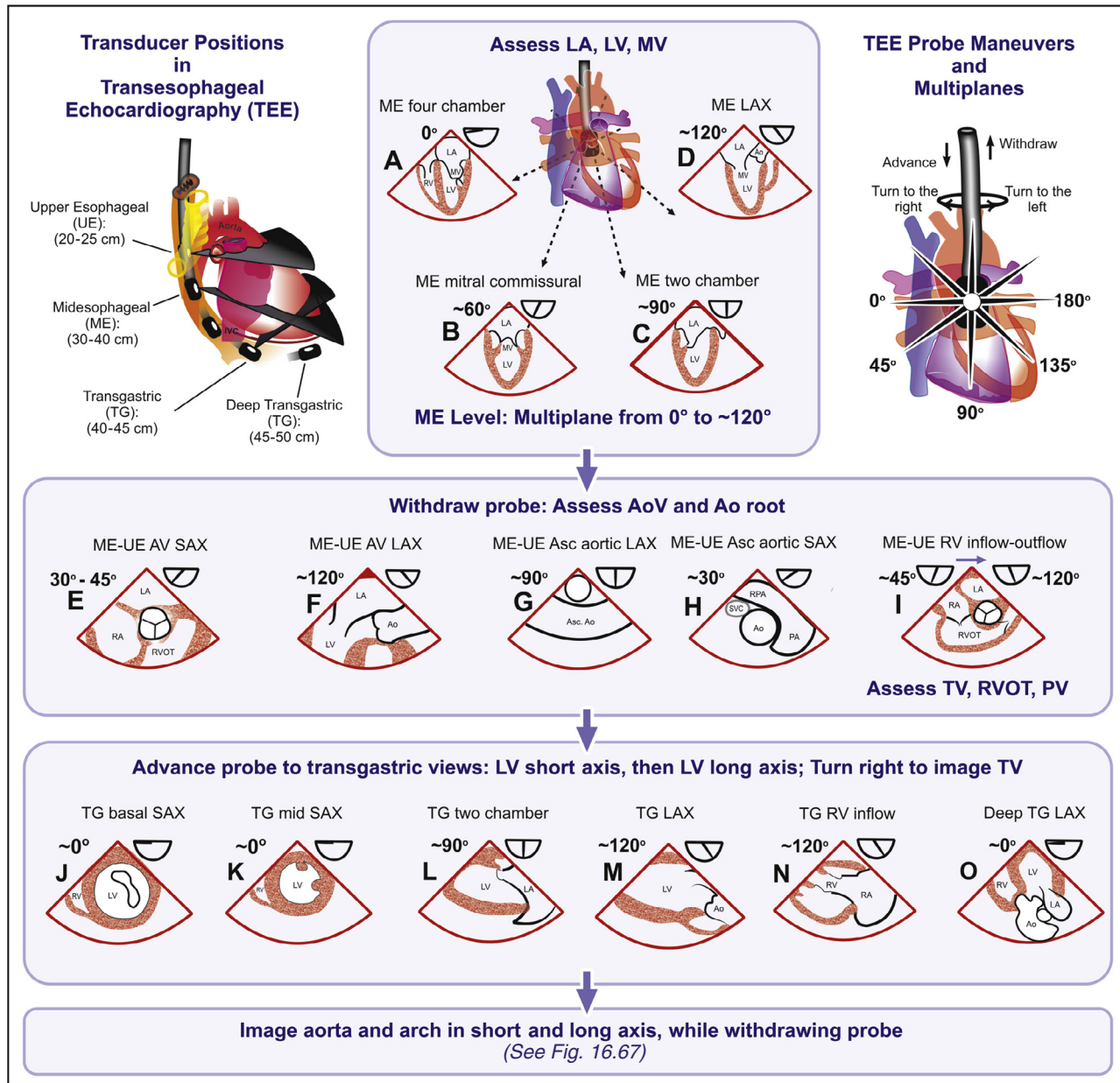
**FIGURE 16.19** A suggested standard TEE examination, showing basic probe positioning, manipulations, and views. The sequence illustrated allows a basic survey of all the cardiac chambers and valves. Additional views are obtained as required for the specific indication. *Ao,* Aorta; *AoV,* aortic valve; *Asc,* ascending; *AV,* aortic valve; *Desc,* descending; *LAX,* long axis; *ME,* midesophageal; *PV,* pulmonic valve; *SAX,* short axis; *TG,* transgastric; *TV,* tricuspid valve; *UE,* upper esophageal.

imaging of contrast agents capitalizes on the way in which this oscillation in size varies with ultrasound system transmit power (mechanical index). When exposed to sound waves at lower mechanical indices, the bubbles will undergo resonant oscillation in a linear fashion and reflect sound at the same fundamental frequency. With higher transmit frequencies, the bubbles will resonate in a nonlinear fashion and reflect sound at both fundamental and harmonic frequencies, multiples of the fundamental frequency. At even higher transmit powers, the bubbles will be destroyed, thereby generating very strong nonlinear backscatter of extremely short duration (eFig. 16.18). Therefore, to distinguish bubbles from surrounding tissue, ultrasound systems are set at low mechanical indices (0.15 to 0.3) that will generate nonlinear resonance without bubble destruction and then selectively "listen" only at harmonic frequencies, thereby improving the strength of the bubble signal relative to that of tissue.

By opacifying the blood pool, ultrasound enhancing agents improve detection of the endocardial–blood pool interface and thus facilitate assessment of ventricular volume, as well as global and regional ventricular function (Fig. 16.22).[20] It has been demonstrated that enhancing agents can convert nondiagnostic (defined as inadequate visualization of two or more of six LV segments seen on apical views) to diagnostic studies in up to 90% of patients. This can be particularly helpful in the intensive care unit (ICU), as well as with stress echocardiography, in which obtaining adequate images in the immediate postexercise period may be challenging. By better delineating the cardiac anatomy, enhancing agents facilitate the discovery of aneurysms and diverticula, mechanical complications of MI such as free wall rupture and pseudoaneurysms (Video 16.7), apical hypertrophy, transient apical ballooning, endomyocardial fibrosis, and the spongelike trabeculations of noncompaction cardiomyopathy. Contrast is also helpful in
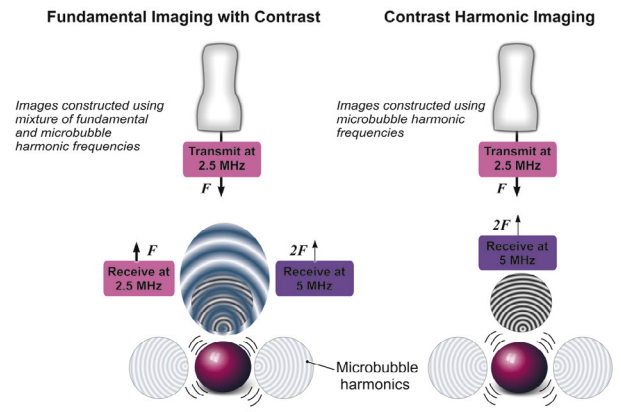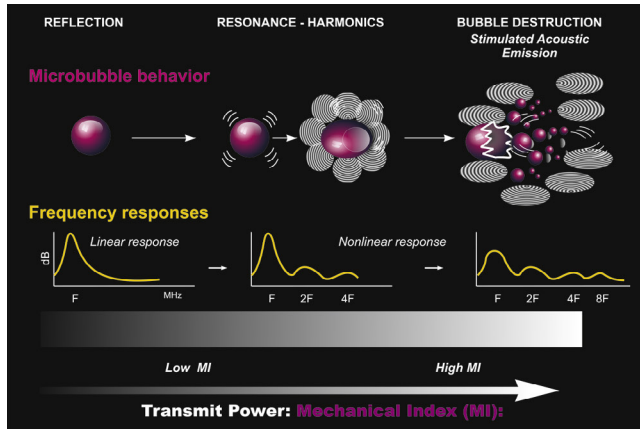
**EFIGURE 16.18** Principles of contrast-enhanced imaging.
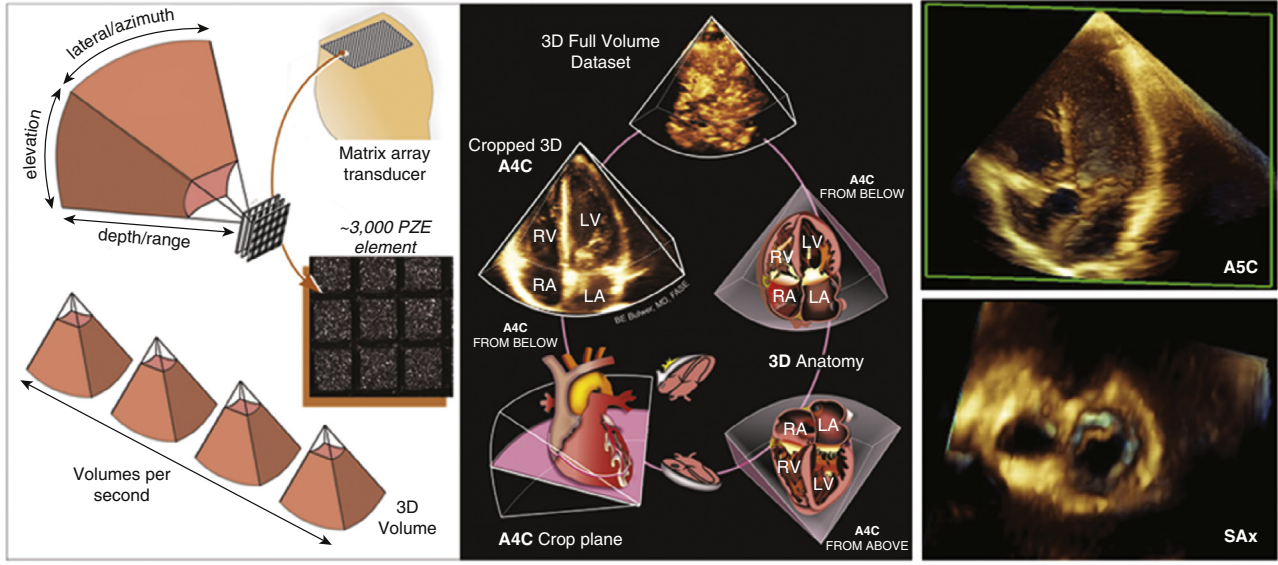
**FIGURE 16.20** Three-dimensional echocardiography using a matrix-array transducer. A waffle-like matrix array **(left panel)** is used to obtain pyramidal "volumes" for real-time 3D data sets that can be cropped **(middle panel)** and rendered in three dimensions. Alternatively, two-dimensional planes can be "cut" through any part of the 3D data set (**right panels**, showing apical 5 chamber cut plane on top and short-axis cuts across the mitral and tricuspid valves on bottom). *A4C,* Apical four-chamber view; *A5C,* Apical five-chamber view, *SAx,* short-axis view. (Modified from Bulwer BE, Rivero JM, eds. *Echocardiography Pocket Guide: The Transthoracic Examination*. Burlington, MA: Jones & Bartlett Learning, 2011, 2013:208. Reprinted with permission.)
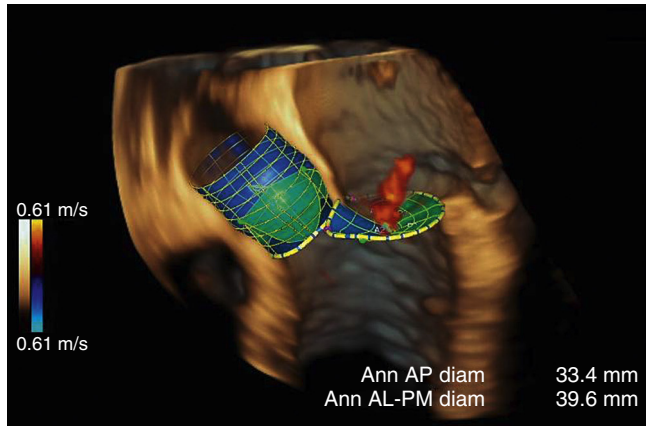


**FIGURE 16.21** Three-dimensional TEE reconstructed view of the heart, showing the aortic and mitral valve geometry with mitral regurgitant jet (*red*) originating between the midscallops of the mitral valve. (See Video 16.6 for corresponding 4D images.)



**FIGURE 16.22** Unenhanced **(left)** and contrast-enhanced **(right)** apical four-chamber systolic images. In the unenhanced image it is impossible to define the endocardium, whereas with contrast enhancement the endocardium is clearly delineated and the straight margin characteristic of a sessile apical thrombus (*arrow*) is appreciated.



**FIGURE 16.23** Apical four-chamber unenhanced **(left)** and contrast-enhanced **(right)** images. In the unenhanced image a thrombus-like structure is visualized in the apical region (*arrow*). The enhanced version shows that there is no filling defect, thus suggesting that this was an acoustic artefact and not a true thrombus.

detecting intracardiac masses such as thrombi and tumors and assessing their vascularity. In addition, these agents may help distinguish imaging artefact from pathology (Fig. 16.23). Ultrasound enhancing agents may also be used (off-label) to intensify spectral Doppler signals, which may be particularly helpful in defining TR signals and gradients in AS (eFig. 16.19), and can delineate extracardiac pathology such as vascular dissection. Finally, in patients undergoing alcohol septal ablation for obstructive HCM (see Chapter 54), contrast agents are used to delineate the perfusion bed of target septal perforators.

Myocardial perfusion contrast-enhanced echocardiography is another application that is based on the ability of ultrasound to detect contrast bubbles within the myocardial vasculature. Approaches depend on the fact that a burst of ultrasound with a high mechanical index "flash" will predictably destroy all microbubbles in the sector,
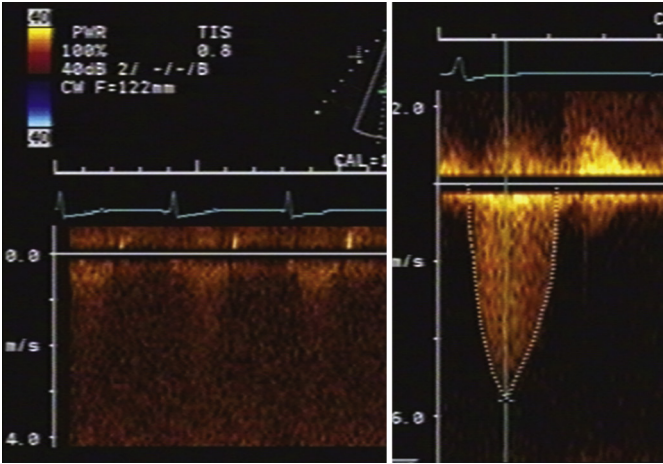
**EFIGURE 16.19** Use of echocardiographic contrast to enhance CW envelopes. Baseline unenhanced Doppler spectra **(left panel)** in this patient with valvular aortic stenosis are indistinct. Following administration of contrast material **(right panel)**, the CW spectra are clearly defined.
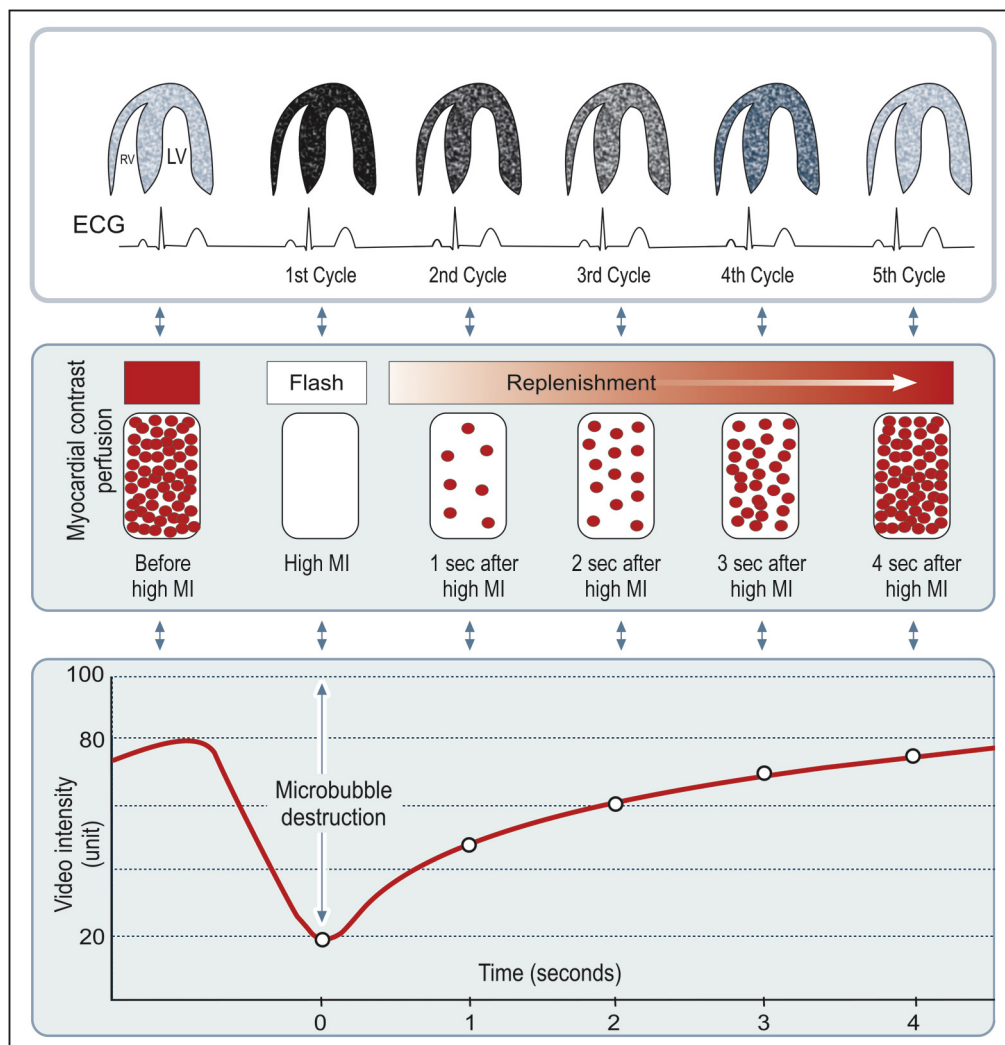
**FIGURE 16.24** Myocardial contrast-enhanced echocardiography: schematic demonstrating the approach to myocardial perfusion imaging during steady-state infusion of a contrast agent. A high–mechanical index impulse (MI) destroys all the intramyocardial bubbles to yield an unenhanced image that will serve as the reference baseline. Subsequently, bubbles will return by coronary perfusion and progressively enhance the myocardium until a steady-state concentration is reached. This may be monitored by either a triggered approach in which imaging is performed on end-systolic images at increasing numbers of beats after the flash (1, 2, 3, 4, etc.) or by using low-MI continuous imaging. Enhancement will increase until a steady-state level is achieved (in this hypothetical example, at a five-beat pulsing interval or after 4 seconds of low-MI imaging). The rate at which replenishment occurs and the degree of enhancement under steady-state conditions, as quantitated by video intensity, reflect myocardial perfusion. (Modified from Wei K, Jayaweera AR, Firoozan A, et al. Quantification of myocardial blood flow with ultrasound-induced destruction of microbubbles administered as a constant venous infusion. *Circulation.* 1998;97:473.)

available today. Therefore, TTE or TEE is often the first tool used in emergency situations such as cardiac tamponade, aortic dissection, peri-infarct or postoperative complication, and shock, in which rapid assessment of a very unstable patient may be carried out at the bedside. When a large number of patients need to be screened or patients need to be monitored long term with serial examinations, the fact that ultrasound imaging involves no ionizing radiation or potentially toxic contrast is a particularly important consideration. It is thus ideal for monitoring valvular dysfunction, cardiotoxic chemotherapy, and cardiomyopathies. Although the spatial resolution of other modalities such as CMR or CT may be greater than that of echocardiography, the superior temporal resolution of TTE and TEE render these techniques ideal for detection of small mobile vegetations, thrombi, and fibrinous strands in the heart, which move too rapidly to be easily visualized by techniques with slower frame rates. Echocardiography also allows the simultaneous assessment of the impact of these lesions on valvular function, i.e., extent of regurgitation.

On the other hand, PET with ^{18}F-fluorodeoxyglucose (FDG) has emerged as a sensitive method for detecting inflammation and abscesses (see Chapter 80) when suspicion of endocarditis and intracardiac abscess is high but TEE is nondiagnostic.[16,22] Use of contrast-enhanced CT for diagnosis of aortic dissections has increased over the past two decades, largely because of the increasing accessibility of high-speed scanners and their ability to scan the entire aorta expeditiously. More recently, CT angiography has emerged as a feasible alternative for detecting left atrial and prosthetic valve thrombus, as well as for device surveillance after endovascular left atrial appendage closure.[23] These radiologic modalities serve as a useful alternative or adjunct, particularly if the patient has contraindications to TEE, or if risk of aspiration or aerosolization of contagious pathogens are a large concern (as in the recent Covid-19 pandemic).

and the rate at which myocardial contrast will subsequently be replenished depends on myocardial blood flow (Fig. 16.24). There are two options for imaging protocols following the high–mechanical index flash: continuous low–mechanical index real-time imaging, which preserves the ability simultaneously to see wall motion in the segment, versus a higher–mechanical index approach with progressively longer intervals between ultrasound frames, which enhances the perfusion signal but at the expense of attaining wall motion information. Although myocardial perfusion imaging has been shown to be of value in both rest and stress imaging for detecting ischemia (eFig. 16.20) and identifying viable but stunned or hibernating myocardium,[21] contrast perfusion imaging requires expertise and special machine capabilities, which currently limits its mainstream use.

### ECHOCARDIOGRAPHY IN THE CONTEXT OF CARDIAC IMAGING

The arsenal of noninvasive cardiovascular imaging modalities includes nuclear imaging (single-photon emission computed tomography [SPECT] and positron emission tomography [PET]), cardiac CT, and CMR (see Chapters 18 to 20) and will undoubtedly continue to expand. Of these choices, echocardiography continues to hold the major advantage of being the most rapid, portable, and real-time imaging modality

In addition to diagnosing structural abnormalities of the myocardium, pericardium, valves, and vessels, echocardiography can directly demonstrate the consequent physiologic and hemodynamic derangements. This is particularly true for pericardial effusions (see Chapter 86), in which echocardiography can demonstrate evidence of impending or actual tamponade in real time within seconds. For more refined tissue characterization, CMR often offers higher resolution and specificity in defining tumor characteristics such as tissue density and vascularity, infiltrative/inflammatory processes, and nontransmural fibrosis. CT is particularly useful in defining calcified cardiac structures, and CT angiography is capable of imaging the coronary arteries along their full extent much more reliably than echocardiography (provided that the patient has a relatively slow and regular heart rate). Defining the thickness of the pericardium is also another "Achilles heel" of echocardiography; CT and CMR provide a more sensitive and comprehensive method of evaluation. However, echocardiography remains the first-line modality for detecting the characteristic respirophasic septal bounce and respiratory variation in cardiac output caused by constriction and continues to be the mainstay of follow-up regardless of treatment.[24]

Acoustic shadowing from prosthetic valves, ventricular assist devices (VADs), calcification, or air between the transducer and the far-field
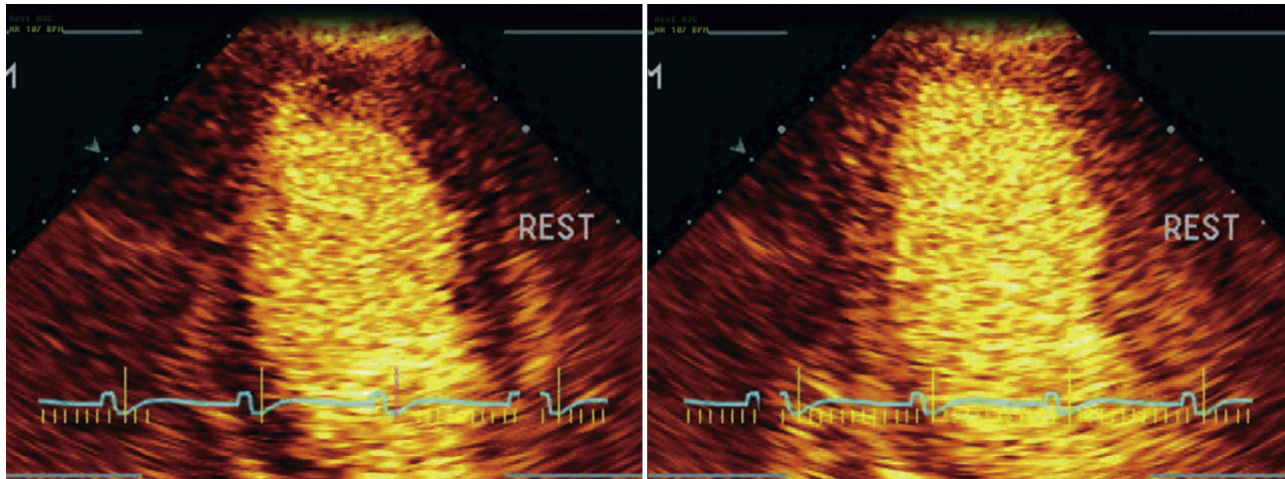
**EFIGURE 16.20** Apical three-chamber views showing real-time myocardial perfusion imaging. **Left,** Unenhanced baseline immediately after a high–mechanical index impulse flash. **Right,** Uniform enhancement consistent with normal perfusion. (Courtesy F. Xie and T. Porter, University of Nebraska Medical Center.)

portions of the heart can preclude adequate visualization of portions of the heart by echocardiography. In these cases, fluoroscopy and CT are useful alternative or adjunctive modalities. A common example would be the dysfunctional mechanical aortic prosthesis, which can be difficult to visualize directly on TEE because of acoustic shadowing. However, the valve discs and disc excursion are easily visible on fluoroscopy or CT angiography. Similarly, because the sternum and ribs impede transthoracic ultrasound imaging and the air-filled trachea produces a "blind spot" on TEE, echocardiographic evaluation of the aorta is limited to the proximal root, arch, and segments of the thoracic and abdominal aorta. However, for unstable patients (e.g., after a motor vehicle accident or those in profound shock), TTE or TEE is often the only suitable bedside tool and is sufficient to diagnose or rule out most type A dissections (see Chapter 42). With TEE one can also expeditiously determine whether the proximal coronary arteries and arch vessels are patent without the use of nephrotoxic contrast material.

Stress echocardiography using either treadmill, bicycle, or pharmacologic (dobutamine or vasodilator) stress has proved to be more accurate than the exercise ECG alone for diagnosing flow-limiting CAD, particularly in women and patients with LV hypertrophy.[25] When compared with nuclear imaging, stress echocardiography is equally sensitive and specific. It also has the advantage of allowing simultaneous assessment of hemodynamics, valvular disease (particularly aortic and MS), and estimation of PASPs in the same examination. However, the presence of previously infarcted segments, known multivessel CAD, and a left bundle branch block (LBBB) may decrease the sensitivity and specificity of stress echocardiography because of difficulty interpreting wall thickening in the presence of resting regional dysfunction and translational motion.

It should be emphasized that in many cases the use of two or more modalities is appropriate and complementary to diagnose more definitively the nature and extent of a pathology and plan appropriate treatment.[15] This is particularly true in cases of ischemic and nonischemic cardiomyopathy for which CMR, SPECT and FDG PET methods can more clearly define the locations of hypertrophy, fibrosis, or inflammation. Extensive aortic dissections in which one needs to define precisely the extent to which major coronary, head, and systemic arteries are involved also often calls for multimodality imaging.[26] Nuclear molecular imaging is also useful for confirming or refuting suspected diagnoses of sarcoidosis and ATTR amyloidosis (see Chapter 53) made initially on clinical and echocardiographic grounds.

Significant valvular pathology may necessitate the use of other modalities after initial echocardiographic assessment (see Multimodality Imaging, later): CT calcium scores have been found useful to risk-stratify calcific AS that may benefit from aortic valve replacement.[27] In patients with valvular regurgitation, where the degree of regurgitation appears significant but unclear, CMR is indicated to determine the regurgitant volume.[16] Fusion imaging, in which images from different modalities (e.g., TEE and fluoroscopy, or FDG-PET and CT angiography) are hybridized, has been shown to be feasible for real-time images and may more accurately guide the deployment of devices in transcatheter structural heart disease interventions.[28,29]

Echocardiography can unfortunately render a variety of artefacts that mimic masses, thrombi, tumors, or mobile tissue flaps. Although most can be discerned as false findings by experienced echocardiographers, a minority may require additional tailored echocardiographic views in varying tissue planes to put the question to rest. The adjunctive use of 3D echocardiography and echocardiographic enhancing agents can often reveal the true nature of these artefacts without the nephrotoxic effects of the iodinated and gadolinium agents used in radiologic imaging.

Currently, the newer techniques for assessing tissue strain, dyssynchrony, and diastolic function have evolved in almost parallel fashion in echocardiography and CMR.[30] These techniques have been used extensively in research and are being validated in a clinical setting with larger populations. In summary, although ultrasound and radiology continue to advance, familiarity with the relative advantages and limitations of each imaging modality greatly assists in determining which tool is best suited to answer the clinical question at hand.

## MYOCARDIAL INFARCTION

Echocardiography plays an essential diagnostic and prognostic role in assessing patients during and after acute MI. Normal wall contractility (normokinesis) is seen as wall thickening caused by the contraction of individual myocardial fibers during systole. On echocardiography

the radial distance between the epicardial and endocardial borders normally increases by at least 20% during systole. Global LVEF, as calculated by 2D echocardiography and preferably by the 2D biplane method of discs, provides an indication of overall infarct size and its impact on function. It has remained the single measure with the greatest prognostic and clinical significance during and after MI.[31]

Myocardial ischemia affects LV systolic function both focally and globally. Focal hypokinesis—decreased systolic thickening—occurs within seconds of the onset of myocardial ischemia, before chest pain and changes on the ECG. This pathognomonic finding will occur in the region of the left and/or right ventricle supplied by the compromised artery (at least 70% stenosis) and give the appearance of a hinge point compared with adjacent perfused segments (Video 16.8). Ischemia may also manifest as delayed contraction of a segment (tardokinesis). Ischemia may be a dynamic condition, and if sufficient blood flow is restored in time, either through a decrease in metabolic demand (as when a stress test ends) or through reperfusion, contractility of the affected segment can recover rapidly. However, after reperfusion, a marked reduction in LVEF during the initial few days after MI can be secondary to myocardial stunning rather than permanent myocardial dysfunction and can improve substantially over days to weeks (see Chapter 36).

Persistence or increasing severity of the wall motion abnormality after the initial insult implies that the tissue is becoming nonfunctional (i.e., not metabolically active or hibernating) or nonviable (infarcted). Akinetic myocardial segments do not thicken at all, and dyskinetic segments bulge paradoxically outward in systole, thus implying that no functioning myocardium is present. Thinning of the walls to less than 6 mm, echo brightness, and dyskinesis usually indicate scar. Sudden dilation of the left ventricle and a decrease in the LVEF are predictive signs of larger areas of ischemia (more proximal and/or multivessel disease). More refined techniques, including IV echocardiographic contrast enhancement to examine myocardial perfusion, low-dose dobutamine echocardiography, or regional strain analysis, may be useful in demonstrating whether segments that are still akinetic after reperfusion remain viable but hibernating.[31]

Specific regions in the heart can be mapped to specific coronary artery territories (Fig. 16.25), thereby allowing determination of the infarct-related vessel in patients with MI or detection of ischemic territory during stress echocardiography (see later, Stress Echocardiography). Very proximal CAD can actually be detected by examining the ostia of the coronary arteries with TEE. A proximal coronary artery stenosis will cause wall motion abnormality in a large territory (i.e., an entire wall from base to apex), whereas more distal blockage will affect only more apical segments. An acute left main occlusion will result in such extensive dysfunction (anterior septum, anterior and lateral walls) that if untreated, it is usually lethal. Proximal right coronary artery (RCA) lesions can additionally cause RV dysfunction and infarction (Video 16.9). The presence of previously existing CAD can modify the extent of new wall motion abnormalities seen during acute MI. Collateral vessels from other unobstructed coronary arteries can develop and perfuse the peripheral territory of affected vessels, thus diminishing the dysfunctional region. Wall motion scoring can be used as a complementary tool to the EF for quantifying the extent and severity of LV systolic function (see eFig. 16.12).

## Practical Considerations in Assessment of Regional Wall Motion

It is important to distinguish carefully between wall thickening as opposed to just epicardial or endocardial border movement during systole. The many pitfalls in diagnosing wall motion abnormalities include false-positives because of poor visualization of the endocardium, superior angulation of the probe such that the membranous nonmuscular portion of the upper interventricular septum is misinterpreted as an akinetic myocardial segment, extracardiac compression of the inferior wall by ascites or abdominal contents ("pseudodyskinesis"), and paradoxical or dyssynchronous septal motion as a result of bundle branch block or the postsurgical state. False-negatives, such as missing a wall motion abnormality that is present, can also occur
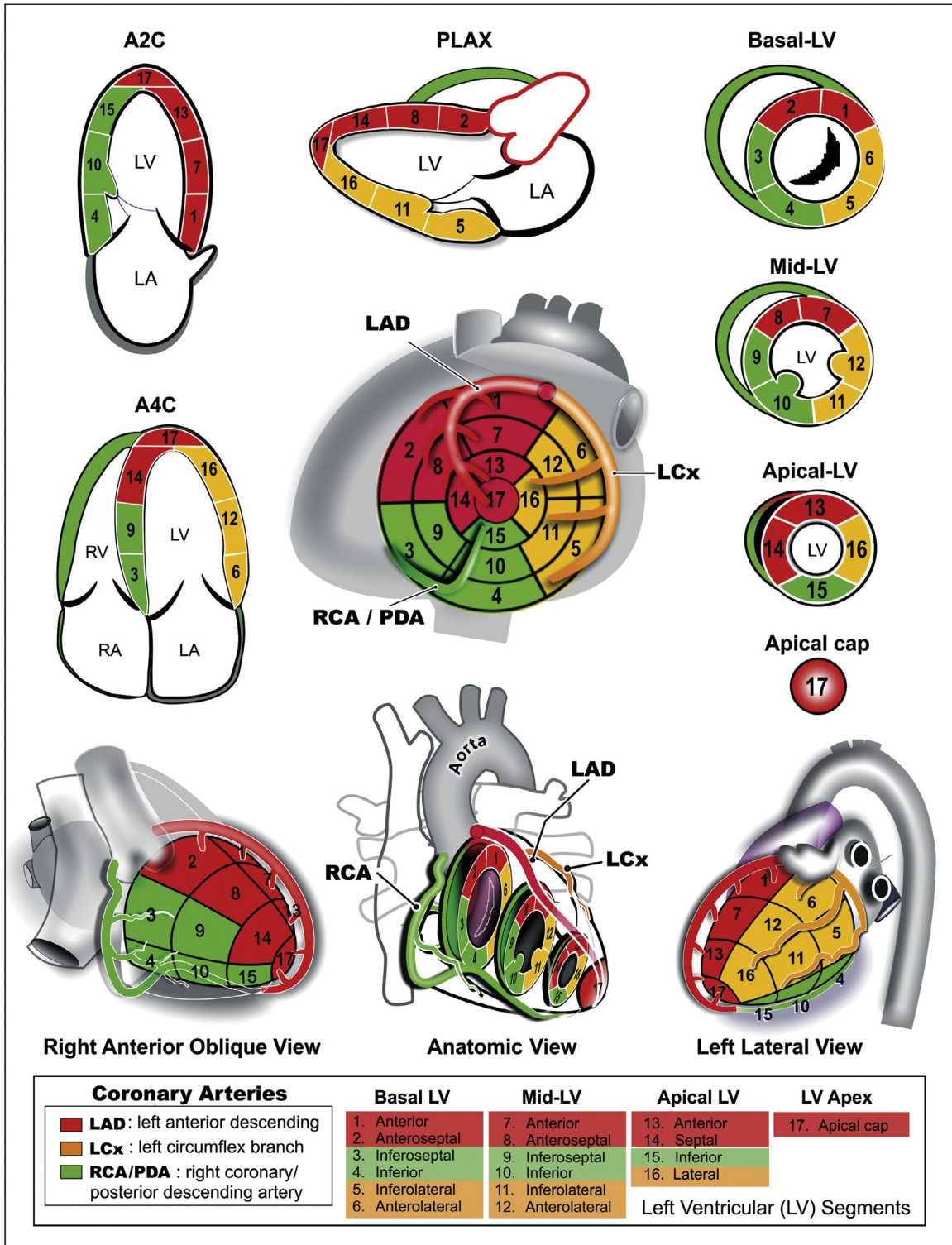
**FIGURE 16.25** Coronary artery territories. The main epicardial coronary arteries each supply distinct myocardial territories, which may be mapped and evaluated during the ultrasound examination. For standardization, the left ventricle (LV) is divided along the long axis into anterior, inferior, septal, and lateral quadrants. At the basal and midventricular levels, the septal and lateral walls are further subdivided into anterior and inferior segments. Each wall is further sectioned in short-axis planes into basal, middle, and apical thirds, with the distal apex beyond the LV cavity forming a cap segment, to yield a total of 17 wall segments. Most of the blood supply to the heart is from the left main coronary artery, which divides into the left anterior descending (LAD) and left circumflex (LCx) arteries. The LAD supplies most of the anterior ventricular wall, and its septal branches supply the anterior two thirds of the septum. In addition, diagonal branches of the LAD supply the anterolateral wall. Large LADs may wrap around the apex of the heart and supply the distal-most portion of the inferior wall. The LCx runs in the atrioventricular groove, and its obtuse marginal branches supply the inferolateral wall. The right coronary artery (RCA) supplies blood to the inferior third of the septum and the inferior wall. The RCA also supplies the right ventricle. *A2C,* apical two-chamber view; *A4C,* apical four-chamber view; *LA,* left atrium; *PDA,* posterior descending artery; *PLAX,* parasternal long axis; *RA,* right atrium; *RV,* right ventricle. (Modified from Bulwer BE, Rivero JM, eds. *Echocardiography Pocket Guide: The Transthoracic Examination*. Burlington, MA: Jones & Bartlett Learning; 2011, 2013:131. Reprinted with permission.)

because of poor image quality or off-axis imaging. Injection of an IV ultrasound enhancing agent can often help delineate the endocardial borders.

Notably, echocardiography in a patient who is free of chest pain at the time of imaging may not reveal a resting wall motion abnormality (because of decreased demand or reperfusion at that point in time). Furthermore, this technique is relatively insensitive for small areas of subendocardial or microvascular ischemia. Nevertheless, when a patient has ongoing acute chest pain but echocardiography does not reveal new wall motion abnormalities, a broader differential diagnosis than epicardial coronary artery occlusion must be entertained. Possible non-ischemic cardiac causes of chest pain that can be also diagnosed by cardiac ultrasound include aortic or coronary aneurysm or dissection, myocarditis, cardiac contusion, and ruptured mitral chordae. Taken in context, the presence of a pericardial effusion may support a diagnosis of pericarditis. Noncardiac causes include pulmonary emboli (which can cause acute right-sided heart dysfunction in a distinctive pattern), as well as gastroenterologic processes (reflux, peptic ulcer disease, esophageal spasm), pleuritis, and costochondritis.
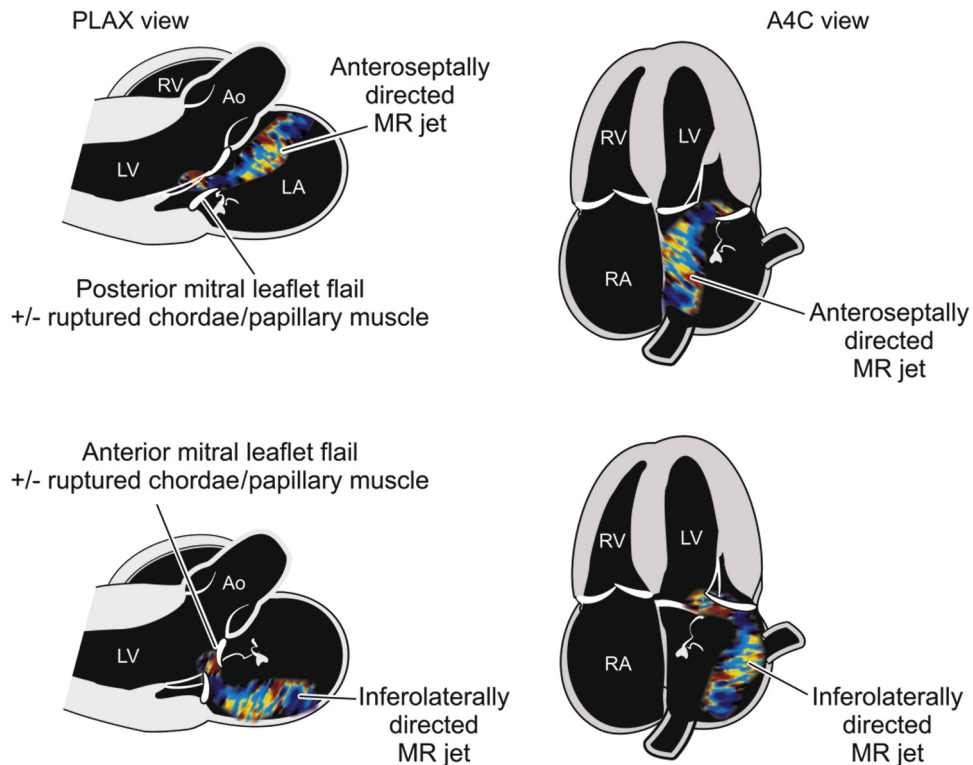


**FIGURE 16.26** Acute structural mitral regurgitation (MR). The consequences of rupture of the posterior papillary muscle and chordae **(upper figure)** versus the anterior papillary muscle and chordae **(lower figure)** are shown with respect to the direction of the MR jet. Posterior mitral leaflet flail will cause a very eccentric jet to be directed anteroseptally, and this can occasionally cause clinicians to erroneously detect a "new aortic stenosis" murmur. Anterior mitral leaflet flail will cause the MR jet to be directed inferolaterally, and this murmur may be missed unless one auscultates the back. *A4C,* Apical four-chamber; *Ao,* aorta; *LA,* left atrium; *LV,* left ventricle; *PLAX,* parasternal long axis; *RA,* right atrium; *RV,* right ventricle.

## MECHANICAL COMPLICATIONS AFTER MYOCARDIAL INFARCTION

MI can cause serious collateral damage from tissue necrosis and bleeding, which is often heralded by cardiogenic shock (see Chapter 38). These events may appear within days of the initial infarct or may be delayed by years. All cardiologists should be familiar with causes of infarct-related shock and their appearance on echocardiography (eFig. 16.21).[14,32]

### Mitral Regurgitation

Acute severe mitral regurgitation (MR) is most often caused by infarction and consequent rupture of a papillary muscle. It results in "flail" of the associated mitral leaflet into the left atrium during systole with valve incompetence (eFig. 16.21A and Videos 16.10 and 16.11). The anterolateral papillary muscle receives dual blood supply from both the left anterior descending (LAD) coronary artery and its diagonals and the left circumflex artery (see Chapter 21); thus a very large infarct would be required to disrupt this papillary muscle, which supports more of the anterior mitral leaflet. In contrast, the posterior descending artery, which arises from the RCA in right-dominant individuals, is the sole blood supply of the posteromedial papillary muscle. For this reason, papillary muscle rupture and flail posterior leaflet occur more frequently with inferior infarcts. There is, however, overlap between the papillary muscle support of the leaflets, and only one head or a tip of a papillary muscle may be disrupted rather than the entire trunk. Thus, in small infarcts there may be a focally flail segment or just the tip of an opposing mitral leaflet affected. The jet of MR is eccentric and directed *away* from the affected mitral leaflet; that is, posterior leaflet flail directs the MR jet anteroseptally, whereas anterior leaflet flail directs the regurgitant jet posterolaterally (Fig. 16.26). *If clinical suspicion for acute infarct-related MR is high and TTE is not definitive, proceeding expeditiously to surgical consultation and TEE is recommended.*

### Ventricular Septal Defect

Defects in the ventricular septum may appear as discrete areas of echo dropout with interventricular flow coursing through, as demonstrated by color Doppler (eFig. 16.21B and Video 16.12). Echocardiography should define the location, type (simple or complex), and size of the defect. Anterior ventricular septal defects (VSDs) tend to be simple (i.e., direct slitlike perforations through both sides of the septum at the same level) and are usually located more apically. In contrast, inferior infarctions often involve the adjacent basal inferior septum or even the right ventricle and can be complex (with serpiginous or multiple fissures). Unless the defect is very large, 2D echocardiographic images alone may only be suggestive of thinned or focally absent myocardium, but color flow Doppler can definitively demonstrate both location and extent of the shunt at the "break" area (Video 16.13). A small (restrictive) VSD will have a high interventricular pressure gradient, whereas a large (unrestrictive) VSD will have lower gradients and is more likely to be associated with further tissue damage, including even papillary muscle rupture or free wall rupture in catastrophic cases. By applying the Bernoulli equation, the pressure gradient across a restrictive VSD can be calculated. RV systolic pressure should be equal to systolic blood pressure minus the interventricular pressure gradient. Significant and prolonged shunting across the VSD can lead to biventricular failure and eventually cause right-sided pressures to increase and the amount of left-to-right shunting paradoxically to decrease over time.

### Pseudoaneurysm

A pseudoaneurysm is a ventricular free wall perforation that is locally contained by adjacent pericardium and adhesions. Pseudoaneurysms appear more often after inferior MI, although they may arise in the lateral and apical regions. On echocardiography, pseudoaneurysms appear as echo-free spaces or extra chambers adjacent to and continuous with the LV cavity (eFig. 16.21C and Video 16.14). The appearance can be similar to that of a true LV aneurysm or diverticulum, but unlike these two pathologies, the definitive feature of a pseudoaneurysm is disruption of all three layers: endocardium, myocardium, and epicardium. Thus a pseudoaneurysm is more likely to have distinguishing traits such as a narrower neck with more ragged edges and turbulent bidirectional
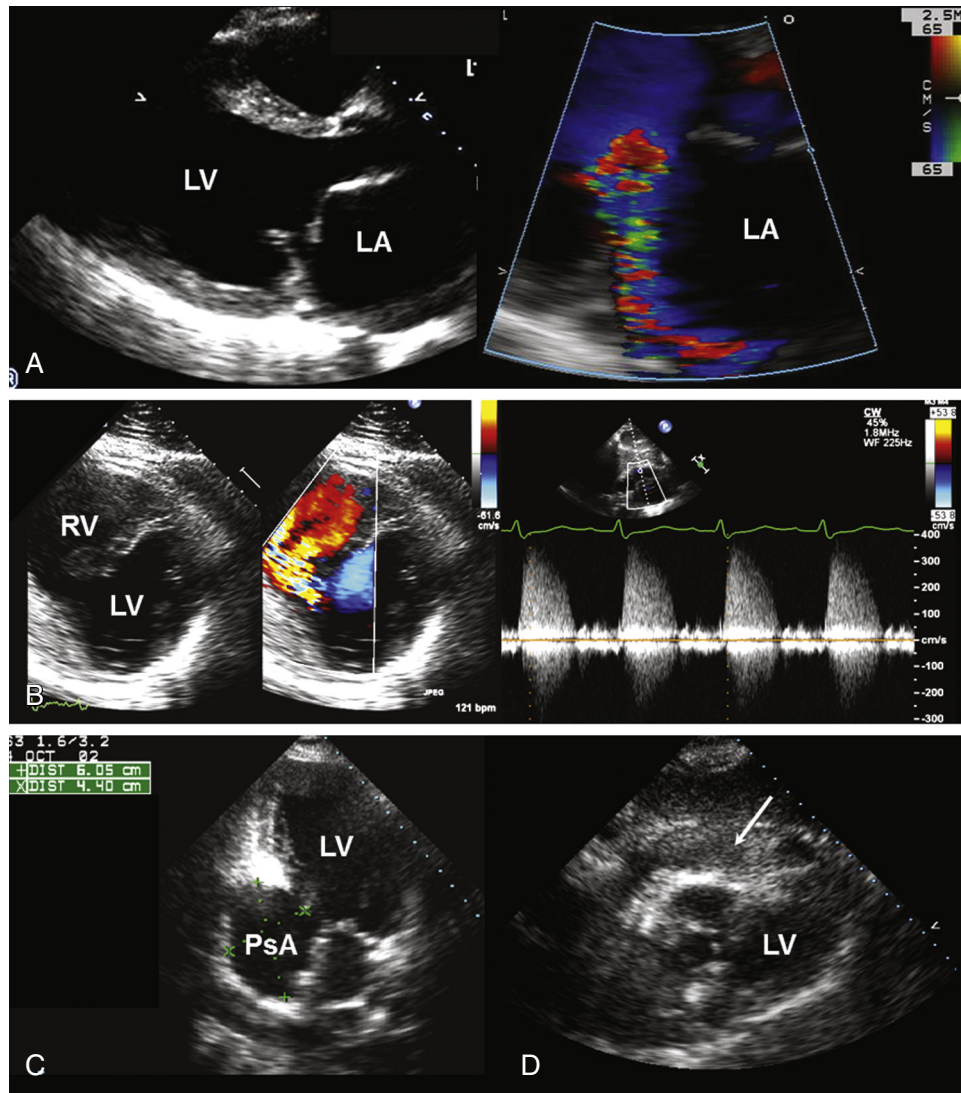
**EFIGURE 16.21** Acute complications of myocardial infarction. **A,** Flail mitral leaflet **(left panel)** with severe mitral regurgitation **(right panel). B,** Ventricular septal defect **(left panel)** in the basal inferoseptum with **(right panel)** an intraventricular pressure gradient of 58 mm Hg by spectral Doppler. **C,** Pseudoaneurysm (*PsA*) of the basal inferior wall. **D,** Hemopericardium (*arrow*) caused by free wall rupture. *LA,* Left atrium; *LV,* left ventricle; *RV,* right ventricle.

flow (as opposed to the smoother margins and flow pattern typically seen with true aneurysms). However, no single echocardiographic criterion is specific enough to distinguish false from true LV aneurysms definitively. IV ultrasound enhancing agents can be very helpful in delineating the area of the perforation and extravasation into the pericardial space if the patient is sufficiently stable (see Video 16.7). Although pseudoaneurysms are typically subacute complications of MI and may hemorrhage suddenly, a fair percentage of pseudoaneurysms are surprisingly stable and go undetected for months and even years. In stable patients, historically LV angiography was used to confirm pseudoaneurysm, but contemporary use of CMR or CT angiography can noninvasively render higher resolution anatomy and also assess for regional myocardial viability.

### Free Wall Rupture

Free wall rupture is usually so acutely lethal that it is rarely imaged, but findings consist of a sudden new pericardial effusion in a patient with marked thinning and akinesis at the terminal myocardial territory of the occluded artery. Echocardiographic features of tamponade are usually present. The pericardial effusion may contain spontaneous echocardiographic contrast or organized clot (*hemopericardium*) (Video 16.15). Demonstration of low-velocity color Doppler flow or extravasation of IV echocardiographic contrast from the LV cavity into the effusion (eFig. 16.22) would confirm wall rupture, but care must be taken not to confuse rupture with the low-velocity color signal generated within pericardial fluid by the adjacent moving heart.

### Tamponade

Mechanical causes of tamponade related to infarcts include pseudoaneurysm and free wall rupture, as previously described, but also aortic dissection (in some cases caused iatrogenically by percutaneous intervention). All cause frank bleeding into the pericardial sac. Hemopericardium is associated with a distinctive gel-like appearance of pericardial fluid on echocardiography (eFig. 16.21D and Video 16.15). Fully organized thrombus found in otherwise echolucent pericardial effusions may be indicative of past wall rupture that has been sealed off in the interim (i.e., intermittent bleeding).

### Other Causes of Cardiogenic Shock in Myocardial Infarction

In addition to the mechanical complications described earlier, there are other potential explanations for hypotension in the setting of acute MI.[32] Simple loss of pump function in large infarcts is probably the most common reason. RV infarction can occur concomitantly with inferoposterior injury or as isolated RV injury in a patient with occlusion of a nondominant RCA (see Chapter 38). It may reveal itself when nitroglycerin is administered and decreases preload. The most reliable echocardiographic sign of RV infarction is new dilation and hypokinesis of the right ventricle. Typically, the lateral, diaphragmatic or posterior RV walls are most affected (the posterior wall represents the distal most RCA territory), with sparing of the apex (which is also supplied by the distal LAD). Depressed RV function can often be illustrated by a low tissue Doppler peak systolic velocity of the tricuspid annulus (S′ wave) or by a slow upstroke to the TR Doppler envelope (low dP/dT), and can be quantified by a low RV ejection fraction or FAC.[13] Annular dilation may cause associated TR and RA dilation with relatively low or normal peak TR flow velocity (because of low or normal RV systolic pressure). Because RV walls are thinner than those of the left ventricle, the right ventricle can recover relatively quickly from ischemic insults and return to normal function after revascularization. Other potential causes of hypotension and cardiogenic shock include reocclusion of coronary arteries with infarct expansion, related effusive pericarditis (Dressler syndrome), and acute dynamic LVOT obstruction with mitral systolic anterior motion, when the basal portion of the heart becomes hypercontractile as compensation for more apical wall motion abnormalities in patients with upper septal hypertrophy.

### LATE COMPLICATIONS OF MYOCARDIAL INFARCTION

Even after an MI is completed, ongoing changes in heart structure and function can cause negative sequelae that can be clinically silent. *Left ventricular aneurysms* are discrete dyskinetic outpouchings of the left ventricle with preservation of the integrity of the three heart layers (endocardium, myocardium, and epicardium). The most common locations of LV aneurysms are the basal inferior wall and the apex, where they may grow to a size that rivals the other cardiac chambers

(Video 16.16). Spontaneous echocardiographic contrast within the aneurysms signifies local stasis of blood flow.

In the absence of anticoagulation, ongoing stagnant flow within an LV aneurysm may lead to the formation of *left ventricular thrombus* (Fig. 16.27A). Patients with large aneurysms, anterior MIs, or LVEF less than 40% are at particular risk for LV thrombus. Intracavitary thrombi may be detected within the first 1 to 2 weeks after MI and appear as discrete, homogeneously echogenic, deformable masses abutting the endocardial border of an akinetic or dyskinetic wall segment. Earlier studies indicated that the sensitivity and positive predictive value (PPV) of echocardiography for LV thrombus were decently high, compared with surgical/pathologic or radionuclide imaging. However, compared with CMR, the sensitivity and PPV appear to be significantly less than originally assumed.[33] Accuracy is undoubtedly affected by pretest probability, image quality, and the size and type of thrombus (the mural type being more difficult to detect). The use of IV ultrasound enhancing agents can double the detection rate of intracavitary thrombi (sensitivity up to 60%, and PPV increases to 93%) and is highly recommended (see Fig. 16.22). Thrombi may appear mural (i.e., fixed, flattened, and adherent to the endocardial wall, as in Fig. 16.27A) or may have independently mobile and protuberant portions (Video 16.17). Larger and more mobile thrombi, as well as those residing adjacent to hyperkinetic myocardial segments, are more likely to embolize. As the thrombi age, they tend to become less mobile, more compact, and echobright in appearance. With anticoagulation, LV thrombi have been observed to resolve in almost 50% of patients by 1 year and in approximately 75% by 2 years of follow-up.

The left ventricle can continue to expand in size and mass and display hypokinesis in noninfarcted areas, even after the initial insult has ended, a process termed *left ventricular remodeling*. In the broadest context, remodeling is defined as an increase in LV volume, but concomitant changes in the geometry of the ventricle are also frequently observed. An increase in the globular shape of the heart is quantified by the *sphericity index.* On 2D echocardiography, this is the ratio of the long-axis dimension to the short-axis dimension. Sphericity index is 1.5 or higher in normal hearts but approaches 1.0 in globular hearts (see later, Dilated Cardiomyopathy).

*Ischemic* MR refers to mitral incompetence in the setting of ischemic LV dysfunction and in the absence of structural abnormalities, such as prolapse, thickening, calcification, or papillary muscle rupture that would otherwise cause regurgitation (see Chapter 76). It is a subset of secondary (functional) MR. This process has been intensively studied, and there appears to be interplay between the LV, mitral, and subvalvular components, as well as the left atrium, all of which contribute to the pathophysiology of MR and an imbalance between the closing and tethering forces that normally maintain valve competence.[34] Displacement of the papillary muscle positions inferiorly and toward the apex contributes to tethering of the mitral leaflets at abnormal angles that restrict leaflet closure. Impaired LV systolic function reduces closing forces. Mitral annular and LA dilation and decreased LV basal myocardial rotation all appear to play a role in enhancing ischemic MR as well (Fig. 16.27B). The imaging hallmark of ischemic MR is pathologic systolic leaflet tethering which may be associated with a hockey-stick appearance. Dysfunction of the papillary muscles per se does not cause ischemic MR and may, in fact, mitigate leaflet tethering. Quantitation of ischemic MR may be challenging but the *effective regurgitant orifice area* (EROA) derived from color and spectral Doppler measurements has a direct correlation with overall mortality (see later, Mitral Regurgitation).

# Echocardiographic Prognostic Indicators After Myocardial Infarction

After acute MI, echocardiography can assist in assessing (1) the prognosis for patients at risk for recurrent ischemia and heart failure and (2) overall risk for morbidity and mortality. LVEF is one of the most important predictors of overall morbidity and mortality after acute MI and is used as a surrogate endpoint in most major clinical trials of medical and procedural interventions. As LVEF declines, the rate of sudden cardiac death (SCD) increases. Based on current evidence, an LVEF of ≤30% to 40% (cutoff varies depending on other clinical characteristics) is a Class I indication for implantation of an implantable cardioverter-defibrillator (ICD)
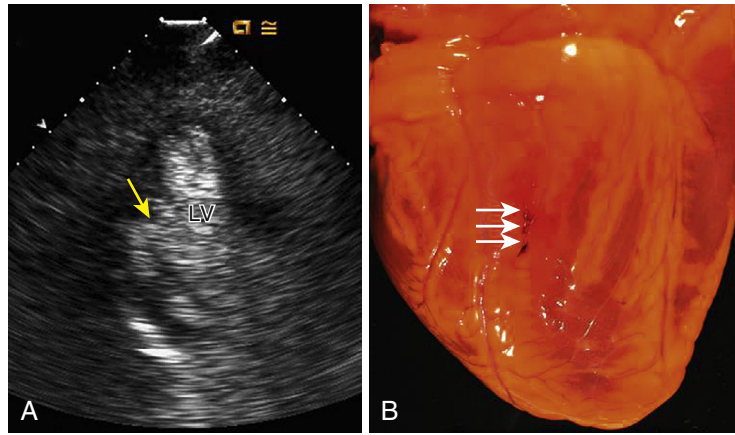
**EFIGURE 16.22** LV wall rupture, as demonstrated by **A,** extravasation of intravenous echo contrast from the LV cavity through a slitlike orifice (*arrow*) into the pericardium inferolaterally, on this apical three-chamber view. **B,** Posterior view of the heart, with the site of rupture (*arrows*) at the posterolateral left ventricle, causing this patient's demise 5 days after diagnosis of a large posterolateral myocardial infarction.
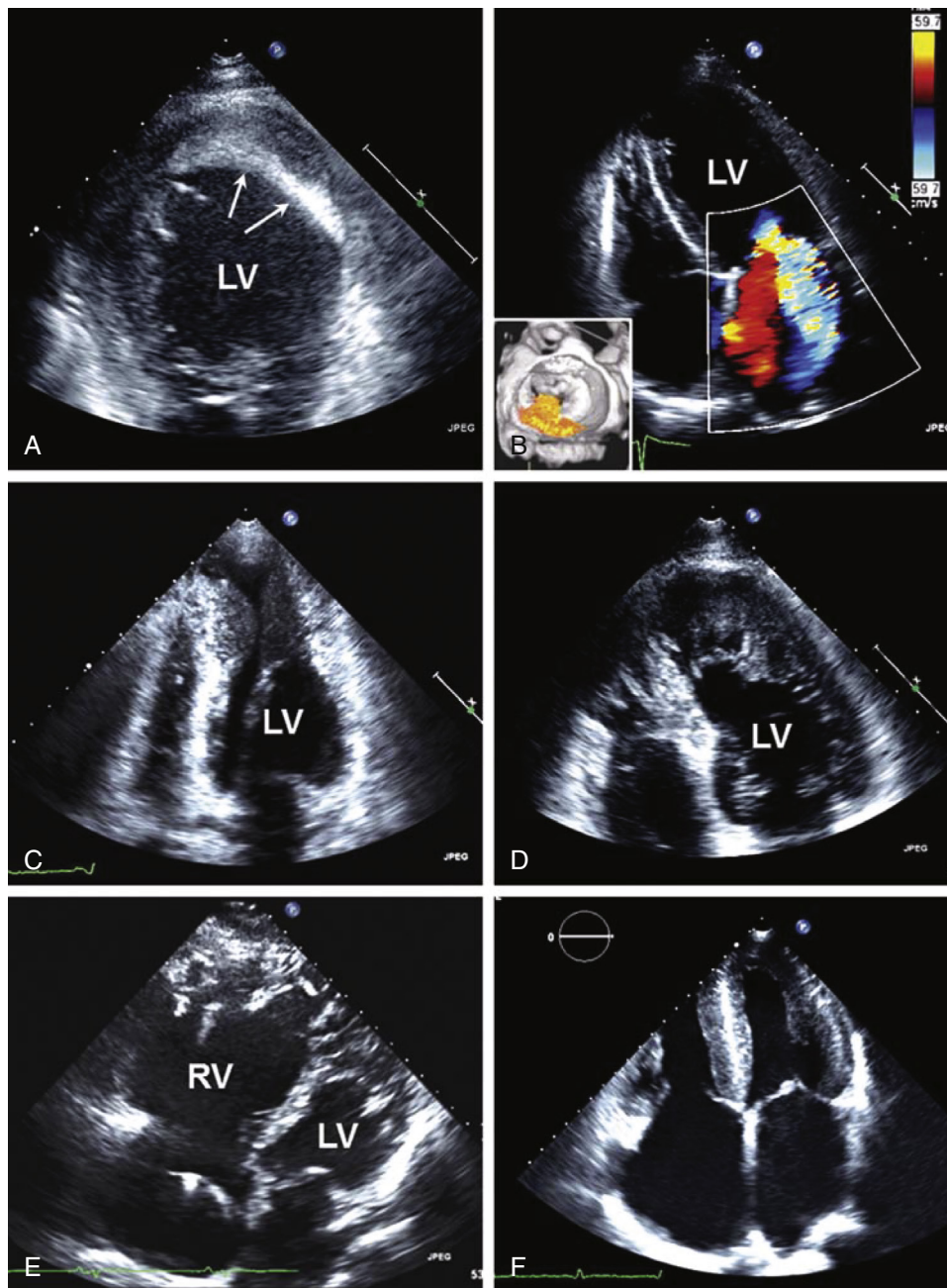
**FIGURE 16.27** Cardiomyopathies. **A,** Ischemic cardiomyopathy illustrating an apical aneurysm and thrombus (*arrows*). **B,** Ischemic cardiomyopathy illustrating severe functional MR. **C,** Apical hypertrophic cardiomyopathy with midcavity systolic obliteration and an apical aneurysm. **D,** LV noncompaction. **E,** Arrhythmogenic RV dysplasia. **F,** Amyloid heart disease. *LV,* Left ventricle; *RV,* right ventricle. (See Videos 16.21 to 16.28.)

independently predictive of heart failure in patients with stable CAD include increasing LV mass index (LVMI >90 g/m²), a restrictive pattern of diastolic dysfunction (E/é' ratio >15, DT <130 msec), an LVOT VTI less than 22 mm, an LA volume index greater than 32 mL/m², and estimated PASP greater than 35 mm Hg. The presence of at least moderate MR (especially if EROA ≥20 mm² or regurgitant volume ≥30 mL) is now well established as an independent predictor of cardiac mortality as well as heart failure. RV systolic function, in particular an RV GLS ≤–22%, also appears to be associated with increased risk.[31]

The WMSI may be a more discriminatory measure than LVEF (as measured by echocardiography or nuclear methods) in predicting cardiac events, in particular, rehospitalization for heart failure. On resting echocardiography, WMSI higher than 1.5 that persists after treatment of MI suggests a substantial (>20%) perfusion defect and increased risk for complications. In stress echocardiography, WMSI higher than 1.7 at peak stress and LVEF of 45% or less are independent markers of patients at high risk for recurrent MI or cardiac death. When there is a question of whether revascularization will improve akinetic but viable areas, dobutamine or contrast-enhanced echocardiography may delineate the extent of myocardium that is hibernating (hypocontractile yet viable and still perfused)[25] (see later, Stress Echocardiography).

Finally, it should be noted that wall motion abnormalities are indicative of focal myocardial dysfunction but are not entirely specific for atherosclerosis-related MI. Vasospasm, inflammation, or fibrosis secondary to myocarditis; swelling from intramural hematoma or edema; Takotsubo cardiomyopathy (see Chapter 52); and any focal myocardial insult are also causes of wall motion abnormality. A comprehensive synthesis of the history, clinical and physical examination findings, and ECG together with appropriate cardiac imaging will allow the clinician to narrow down the differential diagnoses and pursue appropriate therapy.

for primary prevention in selected patients, with an increasing proportion receiving biventricular pacing (CRT) as well (see Chapters 50, 58, and 69).[35] As mentioned previously, after reperfusion, stunned or hibernating myocardium may recover function days to weeks later, so it is generally recommended that one wait at least 40 days after acute MI, or as long as 3 months after coronary artery bypass graft (CABG) or percutaneous revascularization, to reevaluate LVEF before making a decision on ICD implantation for primary prevention. Reduced global longitudinal (GLS <–14%) and circumferential strain have emerged as important risk indicators for death or heart failure after MI. A high degree of dyssynchrony, quantitated by the same technique, is also a risk factor.[2,5,31,35] In addition to LVEF, overall LV size (as assessed by LV end-diastolic diameter and volume) and sphericity are important prognostic indicators. Other measures

# CARDIOMYOPATHIES

## Dilated Cardiomyopathy

Dilated cardiomyopathies share the common characteristics of an enlarged LV and/or RV cavity with systolic dysfunction (see Chapter 52). Left ventricular end-diastolic (LVED) and end-systolic volumes, as well as LVED dimensions and overall LV mass, are increased (with normal or thinned walls), and the overall LVEF is subnormal. With persistence of the underlying condition, the left ventricle becomes less ellipsoid and more globular in shape, and the sphericity index
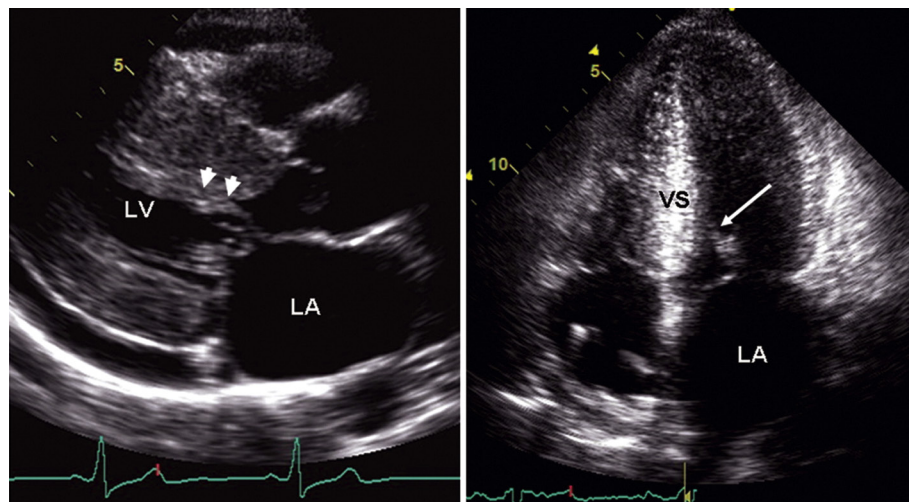
**FIGURE 16.28** Hypertrophic cardiomyopathy. A parasternal long-axis view **(left)** shows markedly increased septal wall thickness and systolic anterior motion of the mitral valve (*arrows*), also visualized in the apical four-chamber view **(right)**. Note the sigmoid, banana-shaped septum. *LA,* Left atrium; *LV,* left ventricle; *VS,* interventricular septum. (See Videos 16.23 and 16.24.)

decreases toward 1. The actual SV and cardiac output may remain preserved because of increased overall ventricular volumes, as well as increased heart rate.

Dilated cardiomyopathies due to viral, postpartum, genetic, chemotherapeutic, tachycardia-mediated, and toxic-metabolic causes typically display diffuse LV hypokinesis; those caused by more focal processes such as sarcoidosis are more likely to have discrete areas of hypokinesis or akinesis (Video 16.18). Ischemic heart disease is often accompanied by focal wall motion abnormalities in a coronary distribution, as well as visible atherosclerotic plaque in the aortic root and other portions of the aorta. One clue to the presence of focal inflammatory processes is wall motion abnormalities that do not follow a coronary distribution and associated thickening secondary to edema. Approximately half of symptomatic patients with Chagas disease classically have segmental abnormalities such as an apical or inferobasal aneurysm, but more advanced cases feature global hypokinesis and RV dysfunction.[37] *Takotsubo cardiomyopathy,* which appears to be a stress- or neuroendocrine-mediated process, is unique in displaying a distinctive pattern of apical ballooning and basal hyperkinesis in the majority (>80%) of patients (Video 16.19).[38] Although the degree of dysfunction can be impressive in stress cardiomyopathy, remarkable and complete resolution often occurs within days to weeks. Rarer "reverse" or alternate patterns of stress cardiomyopathy have also been encountered, in which basal or midventricular wall motion abnormalities occur with preservation of apical function. Video 16.20 is an example, which happens to be the same patient as in Video 16.19 just 3 months later, demonstrating that disparate patterns can occur in the same individual. With sustained left-sided heart failure (and thus secondary pulmonary hypertension) or systemic causes of myocardial dysfunction, the right ventricle may also become dilated and hypokinetic, and enlargement of both atria—and thus four-chamber enlargement—is also common.

The degree of impairment in LV contractility is quantifiable by several means (see earlier, Assessment of Cardiac Structure and Function). Historically, M-mode findings such as increased separation of the mitral E point from the interventricular septum, decreased mitral leaflet opening, and early closure of the aortic valve are known to correlate with poor cardiac output. A universally used measure of systolic function is LVEF, which is considered subnormal if less than 50%. The total SV of the ventricle (reflected by $VTI_{LVOT}$) may be diminished, and tissue Doppler S′ (systolic) excursion is diminished. RV size and contractility may be assessed by parallel means (see Tables 16.5 and 16.6), although it is more difficult to assess RV volume without the use of 3D echocardiography. One easily obtainable measure of RV function is TAPSE, which reflects shortening in the long-axis dimension of RV myocardial fibers; a TAPSE of less than 17 mm is considered abnormal, and 14 mm or less confers a worse prognosis in patients with dilated cardiomyopathy.

Functional (secondary) MR with incomplete leaflet coaptation, caused by multiple processes similar to that seen with ischemic cardiomyopathy, often accompanies and exacerbates dilated cardiomyopathy (see Fig. 16.27B and Videos 16.21 and 16.22).[34] If the patient begins to experience right-sided heart failure because of left-sided heart failure (i.e., elevated LVED pressure), the pulmonary venous inflow patterns will show diminution of systolic inflow (the S wave) because of elevated atrial pressure, and this may precede a rise in estimated PASP (as reflected by TR velocity).

Regardless of cause, a worse prognosis is associated with declining LVEF and elevated end-diastolic and end-systolic volume, increasing LV mass, the development of restrictive physiology by Doppler indices, and the presence of right-sided heart failure, pulmonary hypertension, and severe TR.[11,39] If the LVEF is 35% or lower and the patient has an intraventricular conduction delay and clinical heart failure, CRT (see Chapters 58 and 69) may improve pump cardiac output, reverse the LV remodeling, and improve functional MR[40] (see later, Echocardiography in Heart Failure). Whereas chamber enlargement and systolic dysfunction are the prominent features in dilated cardiomyopathies, in *hypertrophic* and *restrictive cardiomyopathies* the ventricles are not dilated, but diastolic filling of the ventricle is impaired. Declining systolic function and chamber enlargement typically appears only very late in the process. Both cardiomyopathies typically have thickened LV walls, caused by infiltration, myocyte hypertrophy, or both. Biatrial enlargement is frequent because the atria become the low-compliance reservoirs for cardiac inflow, particularly if AF is present.

## Hypertrophic Cardiomyopathy

HCM is a primary, genetic disease of the sarcomere in which the ventricular walls are inappropriately hypertrophied and frequently asymmetrically thickened (see Chapter 54). HCM should be distinguished from the more common *focal upper septal hypertrophy,* a discrete septal bulge frequently observed in older adults, not usually associated with significant LVOT obstruction, and with a benign prognosis. In contrast, the most common forms of HCM of the obstructive type show these echocardiographic features (Fig. 16.28): a small, hyperdynamic left ventricle with a thick sigmoid septum and/or banana-shaped cavity, asymmetric septal hypertrophy (septal thickness ≥1.6 times the thickness of the posterior wall), a relatively small LVOT, elevated flow velocity in the LVOT that peaks in late systole (when the LVOT is smallest), systolic anterior motion of the mitral valve, and often a significant amount of posteriorly directed MR (Videos 16.23 and 16.24). The LVOT gradient (ΔP) is calculated from PW Doppler LVOT peak velocity by the Bernoulli equation $\Delta P = 4(V_{LVOT})^2$. It reflects the degree of outflow obstruction caused by altered LV and mitral valve geometry. The combination of small LVOT area and motion of a relatively large, anteriorly positioned, slack mitral apparatus causes the mitral leaflets to be pushed into the LVOT in early systole by flow drag forces and, to a lesser extent, by suctioning via the LVOT gradient and Venturi effect. A maximum wall thickness greater than 30 mm or a resting LVOT gradient greater than 30 mm Hg is associated with increased risk for SCD and progression to New York Heart Association (NYHA) Functional Class III heart failure. The LVOT obstruction is highly dynamic: in some individuals the LVOT obstruction and gradient can be significantly augmented by conditions that decrease preload and consequently also diminish LVOT size. Such movements include the Valsalva maneuver, sudden standing, and exercise, all of which may be performed during echocardiographic evaluation of these patients.

Other forms of HCM may easily be recognized by echocardiography and facilitated with the use of an ultrasound enhancing agent. In *apical* HCM, basal wall thickness may be normal, but the midventricular and apical portions are unusually thickened, and a midcavity gradient may exist; in more advanced cases, a distal apical aneurysmal area may develop (see Fig. 16.27C and Video 16.25) and may be associated with a higher incidence of arrhythmias, stroke, and SCD.[41] In a minority (10% to 15%) of patients with HCM, systolic dysfunction ultimately develops, and the heart becomes progressively more dilated and globally hypokinetic. For screening purposes, it is important to keep in mind that some patients with HCM by genotype may have normal or only slightly increased wall thickness or may not manifest hypertrophy until late in adulthood.[42,43]

## Other Cardiomyopathies With Regional or Global Variations in Myocardial Composition

### Left Ventricular Noncompaction

LV noncompaction is a myocardial phenotype that is thought in many cases to be genetically determined. It is characterized by abundant trabeculations and deep endothelial-lined recesses extending into the myocardial layer that have failed to compact. On echocardiography this confers a double-layered architecture to the myocardium: there is a "spongy" appearance to the inner layer, whereas the outer layer closer to the epicardium has the normal "compacted" morphology (see Fig. 16.27D and Video 16.26). Using color flow Doppler and/or echocardiographic contrast enhancement, blood extending between the intratrabecular recesses and the LV cavity can be demonstrated. With noncompaction there is a spectrum of expression: the condition may affect the entire mid- and apical ventricle or merely a portion of the apicolateral wall in less affected individuals, and the severity of trabeculation may vary. There is rising awareness of the condition, but to complicate the issue there is also a high prevalence of trabeculations that appear to be acquired in patients with chronically increased LV preload and afterload, and even in athletes. Hence, the appearance may resemble or overlap that of genetic or sporadically occurring noncompaction and may represent a common end-pathway. Accordingly, the definitive imaging and clinical criteria for noncompaction continue to be debated. There is general agreement that on echocardiography, a ratio of trabeculated/compacted layer thickness of greater than 2 as measured on short-axis views at the mid- and apical levels, is likely to be consistent with noncompaction.[44] More specific sets of criteria are listed in Chapter 52.

### Arrhythmogenic Cardiomyopathy

Arrhythmogenic cardiomyopathy (ACM) appears in many cases to be caused by autosomal dominant mutations in a gene encoding desmosomal proteins. It is distinct from the other nonischemic cardiomyopathies in that the right ventricle is usually primarily affected (see Chapter 52), hence the older term arrhythmogenic right ventricular dysplasia (ARVD). However, as use of CMR and familial screening has increased, we now know that biventricular or even LV-predominant expressivity also occurs in up to 76% of patients. In the most classic form, RV dilation (RVOT long-axis dimension ≥32 mm or short-axis dimension ≥36 mm) is the most commonly associated abnormality, and RV global hypokinesis (FAC ≤33%) is present in most (see Fig. 16.27E and Video 16.27). Segmental wall motion abnormalities, including thinning, akinetic areas, and aneurysms, may be present and are caused by fibrofatty infiltration. The inferoposterior wall of the RV inflow tract is the most frequent segment affected. RV trabecular derangement and subsequent TR secondary to annular dilation is common. Echocardiography alone is insufficiently sensitive or specific for the diagnosis of ACM, and other causes of right-sided heart dilation and arrhythmia need to be considered.[44,45]

### Restrictive Cardiomyopathies

Systemic diseases that can infiltrate the heart may lead to restrictive cardiomyopathies (see Chapters 52 and 53); the most common is *amyloidosis.* Deposition of amyloid proteins in the heart causes a very distinct appearance on echocardiography, including increased LV and RV wall thickness in association with a very finely granular or "scintillating" echobright appearance of the myocardium and initially a preserved LVEF (see Fig. 16.27F and Video 16.28). Advanced diastolic dysfunction is manifested both by Doppler indices and by worsening longitudinal strain measured by speckle tracking. Features that distinguish infiltrative cardiomyopathy from true LV hypertrophy include the concomitant presence of diffusely thickened valves, biatrial enlargement ("owl eyes" pattern), RV hypertrophy, pericardial effusion, and low voltage on the ECG. Although LVEF can appear to be normal even in clinically affected individuals, there is often marked systolic dysfunction in the longitudinal axis, as detected by both tissue Doppler and strain imaging. Amyloidosis in particular has a characteristic regional pattern of severely reduced longitudinal strain at the base of the left ventricle, but relatively preserved apical strain ("apical sparing") (see Chapter 53).[46] The classic echocardiographic features of amyloid are not specific enough to distinguish between the types of amyloidosis (i.e., light chain from transthyretin amyloidosis), and clinical features and additional MRI or radionuclide imaging often need to be incorporated into a diagnostic and treatment plan.

Apart from amyloid heart disease, echocardiography is frequently used to screen for cardiac involvement by other infiltrative diseases.[47] It may reveal abnormalities ranging from dilated to restrictive phenotypes, but no specific pattern is pathognomonic of any single cause. Heart failure develops in more than one third of patients with idiopathic or hereditary *hemochromatosis,* and their echocardiograms reveal LV and LA dilation and global hypokinesis with normal LV wall thickness. A restrictive filling pattern may occur earlier than the manifestations of systolic heart failure. All these parameters of function have been shown to improve with iron removal therapy. *Fabry disease* is associated with accumulation of glycosphingolipid in the heart and a high incidence of cardiovascular signs and symptoms in addition to renal, dermatologic, and neurologic abnormalities. More than 80% of individuals with Fabry disease will display concentric LV hypertrophy (men earlier and more prominently than women), although concentric remodeling and asymmetric hypertrophy, as well as RV hypertrophy occur in a smaller proportion. The presence of LV hypertrophy is associated with lower alpha-galactosidase activity and more cardiovascular symptoms. Longitudinal strain reduction in one or more segments has been shown to correlate with regions of fibrosis on MRI in patients with Fabry disease. Mitral leaflet thickening and significant MR are common, and focal or global LV systolic dysfunction occurs in a minority of patients. Fabry disease may mimic the findings of HCM.

*Endomyocardial fibrosis,* also termed *Loeffler endocarditis*, is a rare restrictive cardiomyopathy frequently accompanied by peripheral eosinophilia, which may be idiopathic or associated with helminthic infection in the tropics. Eosinophilic endocarditis and infiltration of the myocardium lead to changes that can be striking on echocardiography. LV size and systolic function may be preserved, but a hallmark of this condition is the formation of prominent diffuse thrombi along the endocardium in one or both LV apices that may embolize and can grow large enough to actually obliterate the cavities (Video 16.29). The ventricular cavities themselves are small with restrictive physiology because of the fibrotic process. Patients may display retracted and incompetent atrioventricular valves and marked biatrial enlargement. Because most patients are identified relatively late in the disease, the time course of development of these changes is unclear.

## Heart Failure

Echocardiography is key in the diagnosis and management of patients with heart failure (see Chapters 50 and 51). Determination of LVEF is the primary method to distinguish heart failure with reduced ejection fraction (HFrEF) from heart failure with preserved ejection fraction (HFpEF), with the former generally being considered when the LVEF is 40% or less. The exact EF cutoff for HFpEF has been subject to debate, and recent guidelines have used the term heart failure with mid-range ejection fraction (HFmrEF) to denote patients in the LVEF range of 40% to 49%.[48] Echocardiography can help distinguish among the different types and narrow down the potential causes of heart failure.

Abnormalities in diastolic function are common in patients with heart failure and either reduced or preserved LVEF and may have prognostic implications. MR can occur in heart failure patients secondary to apical displacement of the papillary muscles, annular dilation, or both, and progressive ventricular dilation can develop in patients with primary valvular MR (see Chapter 76). Increasing degrees of MR are associated with a poor outcome in patients with heart failure.

## Assessment of Ventricular Synchrony

CRT is used to reduce heart failure and death in patients with reduced LV function and a wide QRS complex (see Chapters 58 and 69). Use of CRT can reverse ventricular remodeling and improve pump performance; in numerous studies it has also been associated with marked improvement in LV end-diastolic and end-systolic volume, EF, RV function, and LA size. While the benefit of CRT is seen most often in patients with LVEF ≤30% to 35%, QRS greater than 130 msec on ECG, and heart failure symptoms, 30% to 35% of those treated turn out to be nonresponders. Although echocardiography has been used to identify patients for CRT placement, no single parameter reliably predicts a positive clinical or echocardiographic response to CRT in the referred population.[48]

Nevertheless, echocardiography is useful in quantifying dyssynchrony and cardiac function before and after CRT. In patients with LBBB, significant dyssynchrony can be grossly visualized as an early systolic movement of the interventricular septum towards the center of the LV, followed immediately by movement in the opposite direction (a paradoxic motion). Because this affects only the basal and midportion, as the apex continues to move inwards throughout systole it may appear to rock relative to the proximal septum translating outwards (Video 16.30); a key distinction is that the septum will still thicken overall in systole if myocardium is viable and functional, unlike a true wall motion abnormality. Also, in the normal LV, all segments contract and thicken simultaneously, but with LBBB, the time to activate the more lateral segments increases and these will thicken later than the septal segments, contributing to the rocking appearance. Because these abnormal motion patterns are subtle, visual assessment alone is only qualitative and subjective. However, longitudinal and radial strain measured by speckle-tracking has been shown to be quantitative and reproducible in assessing baseline dyssynchrony and demonstrating improvement due to CRT. Prior to or during device implantation, echocardiography may be used in select patients to discriminate appropriately paceable regions from scar and thereby optimize placement of the LV and coronary venous leads. Post-CRT implant, echocardiography is sometimes used to quantify both LVOT stroke volume and degree of MR at bedside, so that atrioventricular intervals and interventricular intervals may be tailored to produce the best forward cardiac output. In summary, LVEF remains a cornerstone for CRT patient selection, and echocardiography and myocardial deformation imaging may be useful on a case-by-case basis for optimizing CRT and quantifying the effects on heart mechanics and remodeling.[49]

## Assessment After Orthotopic Heart Transplantation

Echocardiography is used both to certify that cardiac structure and function are normal in potential heart donors and to monitor for rejection in cardiac transplant recipients (see Chapter 60).[50] After uncomplicated orthotopic heart transplantation, the "normal" transplanted heart should display normal LV size and systolic function, although mild LV hypertrophy is common. GLS is often slightly lower than normal reference values. The RV is usually mildly enlarged with reduced measures of RV systolic function and free wall strain, although some recovery is often seen within a year after transplant. In patients who have undergone the standard Shumway-Lower technique of transplantation, the resultant atria are very enlarged and deformed because of the retained upper portion of the dilated native heart. In these patients the anastomosis between the donor and recipient heart may be visible as a thickened ridge of plicated tissue that encircles the atria. The ridge may be mistaken for thrombus by inexperienced observers. Newer surgical methods retain no recipient myocardium (i.e., total atrioventricular transplantation) or retain only a limited cuff of LA wall with pulmonary vein ostia (in the bicaval technique) and thus preserve

more normal atrial architecture with less obvious suture lines. A "normal" transplanted heart often has slight paradoxical septal motion—anterior motion of the septum in systole and a slight decrease in septal systolic thickening—that persists in the postoperative state. Over time, in part because of distortions in atrial geometry, supraventricular arrhythmias, and repeated endomyocardial biopsies causing incidental damage to the tricuspid valve, significant TR and MR, as well as atrial thrombi, may develop in the allograft heart.

Cardiac allograft dysfunction may result from acute rejection, coronary artery vasculopathy, myocardial fibrosis, acute myocarditis from opportunistic infections, or tachycardia-mediated cardiomyopathy. Cardiac ultrasound may detect the "downstream" effects of these pathologic mechanisms. Acute cellular rejection, which results in edema and interstitial infiltrates in the myocardium, has been shown to cause detectable increases in LV wall thickness and mass, systolic dysfunction, and Doppler indices of elevated LA pressure and restrictive physiology (increased E wave velocity, decreased IVRT and mitral DT), but these changes are of insufficient sensitivity and specificity to rely on for routine clinical screening. Speckle tracking has shown that that in addition to EF, GLS is generally lower in patients with rejection, but the differences in a given individual are not significant enough to detect biopsy-proven rejection.[51] For now the gold standard for detecting acute rejection remains endomyocardial biopsy, although echocardiography and GLS evaluation have an appropriate supplementary role in monitoring for graft dysfunction and other complications after transplantation.

For detecting cardiac allograft vasculopathy, coronary angiography is the standard of care, with coronary IVUS as the ultimate gold standard at experienced centers, if more specific imaging is needed. Among noninvasive imaging techniques, echocardiography is the most widely investigated and used.[52] The presence of depressed LVEF or focal wall motion abnormalities on a *resting* echocardiogram is relatively specific (>80% in multiple studies) for allograft vasculopathy but has poor (<50%) sensitivity. Some centers use dobutamine stress echocardiography (DSE), which is preferred over exercise stress echocardiography because denervation of the allografted heart blunts the heart rate response to exercise. Meta-analysis of the published data on the accuracy of DSE indicates a pooled mean sensitivity between 60% and 70% and a specificity of 86%.[53,54] The use of longitudinal strain rate imaging or myocardial echocardiographic contrast enhancement with DSE may increase the sensitivity. For prognostic purposes, however, normal findings on DSE have been shown to have a high negative predictive value for adverse cardiac events (0.6% incidence) over short-term follow-up. Conversely, worsening findings on serial DSE confer increased risk in comparison to stable findings. Currently, therefore, DSE (as well as SPECT) is considered by the International Society of Heart and Lung Transplantation as possibly being useful (class IIa, level of evidence B) in transplant recipients who are unable to undergo invasive evaluation. Some centers use DSE to minimize exposure of transplant patients to coronary angiography, although currently no noninvasive imaging modality is sufficiently accurate to supplant it.

### Assessment of Left Ventricular Assist Devices

The advent and increasing use of a variety of VADs for both bridge and destination therapy (see Chapter 59) have mandated that echocardiography play an integral role in assisting in the optimal selection of patients for left and right VADs, implantation, optimization, and troubleshooting. Here we address the principles for the more widely used HeartMate devices, which are now continuous-flow pumps with the latest models using centrifugal design.

All LVADs work by unloading the ventricle (i.e., removing some or all of the inflow and pumping it to the aorta). Echocardiography is useful for evaluation of the patient *preoperatively* for VAD implantation and for evaluating LV as well as RV function.[55] If RV failure is too severe, as may be indicated by a number of parameters such as RV FAC, TAPSE, and the RV Tei index (see earlier), there will be insufficient preload to fill the VAD and left ventricle. The incidence of right-sided heart failure is 20% to 30% in patients implanted with an isolated LVAD, and a preoperative RV FAC less than 20% is associated with RV failure on activation of the LVAD. In addition, echocardiography (TTE and/or TEE) can identify aortic insufficiency, intracardiac shunting, thrombi in the LV or LA appendage, or structural problems with inflow and outflow site

cannulation such as excessive necrosis or atherosclerotic plaque, which are detrimental to proper LVAD function. *Intraoperatively*, TEE is used to ensure proper LV apical coring, de-airing, and cannula position and to reassess RV function on initial start-up of the LVAD. Extreme RV failure may mandate placement of an RV assist device (RVAD) as well.

*Postoperatively* the echocardiogram may be used to identify causes of LVAD dysfunction and fine-tune its operation[56]. When the LVAD is working properly, the ventricle should be "decompressed," that is, smaller than its original dilated size with the interventricular septum in a neutral position. The aortic valve in a completely decompressed heart stays completely closed throughout the cardiac cycle. Thickening and fusion of the aortic valve often occurs over time with nonpulsatile LVADs; it is desirable to adjust flow settings to permit at least occasional opening of the aortic valve (i.e., on a 1:3 or smaller cyclic ratio) to avoid this valvulopathy and associated aortic regurgitation (AR, which develops in approximately 25% of patients). This is ideally assessed with both M-mode and 2D imaging of the aortic valve over multiple beats. Enlargement of the left ventricle, distention of the interventricular septum rightward, and rising estimated PASP are signals of a relatively underfunctioning device that may be caused by an inadequate pump rate, worsening ventricular function, AR, volume overload, or systemic factors (e.g., sepsis). If the left ventricle appears small with a left-shifted interventricular septum, this indicates inadequate preload to the ventricle, and factors such as RV failure, pulmonary embolus, tamponade, hypovolemia (e.g., bleeding) should be sought. Obstruction of the inflow cannula is another important complication and may be caused by LV thrombus, a papillary muscle or chorda, or bending or slippage of the cannula or outlet graft. Such abnormalities may be demonstrated by 2D imaging or by increased velocities and turbulence seen with Doppler evaluation at the cannula/graft orifices. The LVAD inflow cannula should be visible at the apex, and the outflow graft/cannula can occasionally be detected by angling into the ascending aorta with a right parasternal view. Occasionally, positional kinks in the LVAD cannulae or the aortic outflow graft, which tend to occur in smaller patients, can be demonstrated by scanning the patient in the supine, sitting, and standing positions. In some patients, echocardiography "ramp" studies are performed for continuous-flow LVADs, in which the aforementioned parameters (LV and RV dimensions, septal position, aortic valve opening, valvular insufficiency, and calculated PASP) are tracked at incrementally varying pump rpm settings, with the aim of optimizing LV unloading and diagnosing malfunction, in particular thrombosis.[55,56] Assessing the IVC as a surrogate for RA filling pressure may also be useful. In the latest centrifugal pump (HeartMate 3), much narrower speed ranges are needed to optimize hemodynamics, leading to a decreased need to perform routine ramp tests in these patients.

*Percutaneously implanted ventricular assist devices* (PVADs) are often used to provide temporary or partial support for the left ventricle. These are increasingly replacing intra-aortic balloon pumps for short-term LV support. Echocardiography is useful for confirming that the cannulas are positioned appropriately across the interatrial septum (in the case of the TandemHeart PVAD, CardiacAssist, Pittsburgh, PA) or the aortic valve/LVOT (for the Impella), with vigilance for either obstruction or prolapse. The Impella is placed retrograde across the aortic valve into the LVOT, where it takes blood from the left ventricle and pumps it into the ascending aorta just distal to the valve. Echocardiographic imaging and color Doppler are frequently used to optimize device placement (eFig. 16.23). As imaged in the parasternal long axis view, the inflow portion (a teardrop-shaped cage) of the Impella should be in the LV approximately 3.5 cm from the aortic annulus and color mosaic flow generated from the outlet portion of the cannula should be seen above the aortic valve.

Extracorporeal membrane oxygenation (ECMO) uses a pump to circulate blood through an oxygenator in order to provide short-term support for the lungs and heart in patients with acute severe respiratory failure (e.g., ARDS) or refractory cardiogenic shock (e.g., post MI or cardiac arrest, or failure to wean from cardiopulmonary bypass). There are two types of ECMO, venovenous (VV, in which a cannula takes blood from the femoral vein and returns oxygenated blood to the right atrium via the IVC or SVC) and venoarterial (VA, in which the return catheter is placed into the femoral artery to bypass a failing right ventricle). Catheters may also be placed more centrally, directly into the right atrium and ascending aorta, if a sternotomy is being performed. Transthoracic or TEE is used to evaluate left and RV function and ensure no significant valvular regurgitation is present in candidates for ECMO. Echocardiography is also used to select and confirm cannula positioning sites, assess RV function, and rule out cannula obstruction or thrombus.

### Lung Ultrasound in Heart Failure

Lung ultrasound is a technique that can provide semiquantitative assessment of lung fluid in patients with heart failure. *B-lines* are vertical echogenic reverberation artefacts that arise from the pleural line and extend raylike to the far field of the imaging window with respirophasic movement. They are caused by reverberations at the interface between interstitial/alveolar fluid and air, and hence are markers of increased extravascular lung water (eFig. 16.24 and Video 16.31). B-lines are most frequently seen in pulmonary edema but also in other processes such as acute respiratory distress syndrome and pulmonary fibrosis.[57] In patients with heart failure, the presence of B-lines appears more sensitive for lung congestion than even lung auscultation and chest x-ray, and correlates with N-terminal pro-brain natriuretic peptide (NT-proBNP) levels. B-lines within prespecified thoracic segments also clear contemporaneously with treatment. In patients admitted with acute heart failure, an increased number of B lines found early in admission is a prognostic marker for in-hospital adverse events. The number present at discharge is associated incrementally with increased short-term hospital readmission for heart failure and death.

The simplicity and availability of this ultrasound technique make it attractive for early diagnosis and monitoring of therapy, particularly in limited-resource environments. During the COVID-19 pandemic, lung ultrasound performed with portable ultrasound units was helpful in qualitatively assessing the burden of lung pathology, and had the added advantage of reducing the potential for viral transmission throughout hospitals. B-lines alone did not clearly distinguish between congestive heart failure and ARDS in patients with COVID respiratory distress. However, the concomitant presence of pleural thickening and irregularity and subpleural consolidations together with preserved LV systolic function seen on POCUS was indicative of significant interstitial-alveolar damage and correlated with lung CT findings of ground-glass opacities and COVID pneumonia. Lung ultrasound is also a very effective tool for rapid diagnosis of pneumothorax, an occasional complication of the positive-pressure ventilation frequently needed to treat patients with severe heart failure or COVID-19 pneumonia.[32]

## The Athlete's Heart

Physiologic changes, including enlargement of the heart and bradycardia, can be induced in the heart through intensive athletic training. Echocardiography, along with ECG and ECG exercise testing, is often used to distinguish the athlete's beneficial cardiac adaptive changes from pathologic entities such as hypertrophic, arrhythmogenic, or other cardiomyopathies that are associated with SCD. Different forms of exercise are hypothesized to favor different remodeling patterns: endurance athletes have been well documented to develop LV (and actually four chamber) dilation together with a balanced increase in wall thickening (eccentric hypertrophy), whereas strength/isometric training is predisposed towards concentric hypertrophy (LV walls thickened relative to LV diameter, or RWT >0.42).[58] Although strict cutoff values for normal LVED diameter are not advocated for distinguishing physiologic from pathologic remodeling (a variable percentage of athletes have diameters >60 mm), absolute wall thicknesses greater than 15 mm in men or 12 mm in women are unusual even in elite athletes and should trigger further investigation for HCM, particularly if the hypertrophy is asymmetric. Typically, the resting LVEF is in the low-normal (approximately 50%) range in trained athletes. The standard flow and tissue Doppler metrics of diastolic dysfunction are normal or even supranormal (higher E' velocities and transmitral E/A >2) in athletes compared with HCM patients, and speckle-based local and GLS parameters are generally higher as well. Further CMR testing, exercise testing (to confirm LV augmentation and document high exercise capacity), and in "gray-zone" cases even a period of detraining (to see if LV hypertrophy regresses) may be necessary to distinguish the athlete's heart from a true cardiomyopathy.[59]

## STRESS ECHOCARDIOGRAPHY

Stress echocardiography is a well-validated tool for the evaluation of ischemia. In particular, it is an appropriate first-line test in patients who
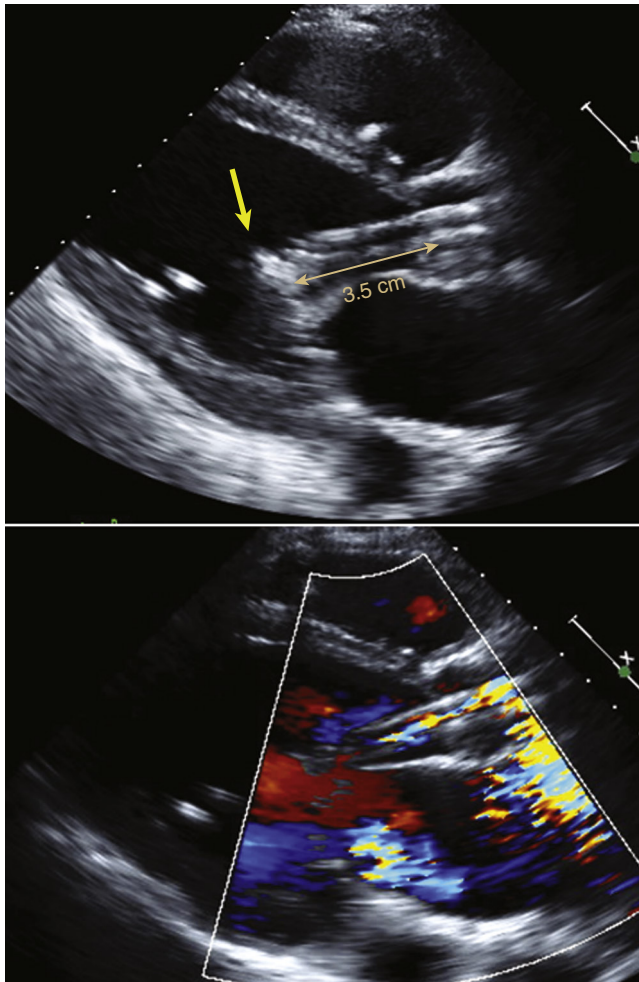
EFIGURE 16.23 Impella PVAD, seen on parasternal long-axis window. **Top panel**, The fenestrated inflow portion (*arrow*) of the Impella cannula appears as a more bulbous "teardrop" on echocardiogram, above the more distal thinner and less visible pigtail portion, and should be positioned ~3.5 cm from the aortic annulus. **Bottom panel**, Appropriate positioning is also confirmed by seeing color Doppler flow appropriately within the cannula and above the aortic valve; note there is also mitral regurgitation.
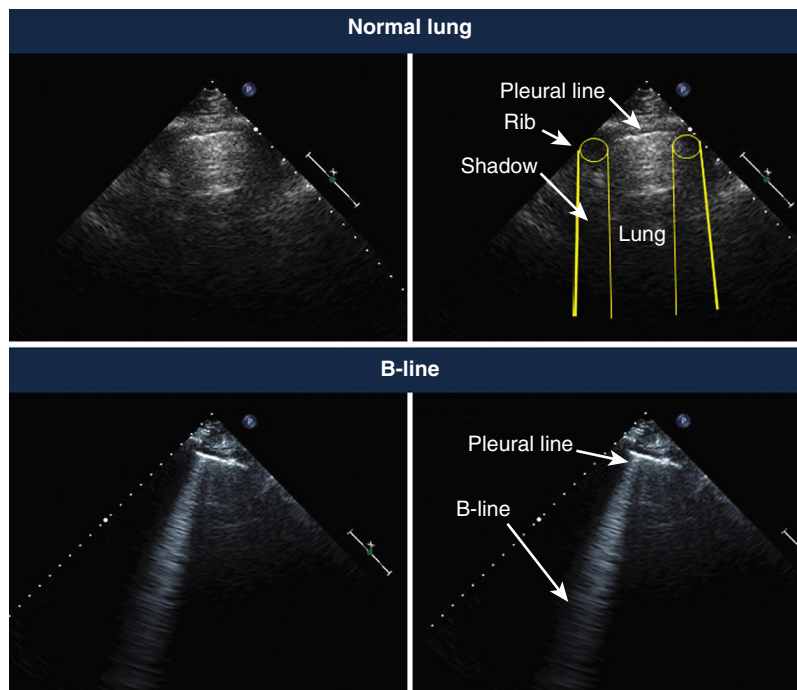


EFIGURE 16.24 B-lines on lung ultrasound. For studies, typically the number of B-lines are summed from two to eight segments of the chest using a 1.5- to 7.5-mHz transducer. **Top panels,** Normal lung. **Bottom panels,** Example of B-line. Annotated images are on the right. (Courtesy Dr. Elke Platz, Brigham and Women's Hospital.)

have baseline abnormalities on the ECG that preclude interpretation of exercise ECGs, and it is both time- and cost-efficient. The accuracy of stress echocardiography is similar to that of stress radionuclide perfusion imaging (see Chapter 18). From meta-analyses, as well as from comparisons of the accuracy of stress echocardiography and nuclear imaging in the same patient population, the sensitivity of stress echocardiography for significant CAD (generally defined as >50% coronary artery stenosis by angiography) averages approximately 88% and its specificity is 83%.[60] The specificity of stress echocardiography appears to be higher than that of nuclear imaging for left main and triple-vessel CAD. As with other tests, stress echocardiography is best used for diagnosis or to identify the extent, severity, and location of ischemia in patients with an intermediate pretest probability of disease.

### The Stress Echocardiographic Protocol

In the standard stress protocol, baseline images are obtained at rest, before the patient exercises on either a treadmill or stationary bicycle. The same Bruce protocol used for routine (ECG only) exercise stress tests is standard (see Chapter 15), with echocardiographic imaging performed at rest and during immediate recovery as close to the peak exercise time as possible. If a stationary (upright or supine) bicycle is used, the workload is increased by 25 W every 2 or 3 minutes, and echocardiographic images can be monitored continuously and captured precisely at the time of peak stress. The test endpoint is exercise-limiting symptoms or completion of the protocol (reaching at least 85% of the age-predicted maximal heart rate). Absolute indications to terminate the test early include moderate to severe angina, ST-segment elevation, sustained ventricular tachycardia, near-syncope or signs of poor perfusion, a drop in systolic blood pressure of more than 10 mm Hg from baseline when accompanied by any other evidence of ischemia, and patient request to stop (intolerable symptoms). Relative indications to stop early include a hypertensive response (systolic blood pressure >220 mm Hg and/or diastolic blood pressure >120 mm Hg).[60]

Patients who cannot exercise can undergo pharmacologic stress with a graded dobutamine infusion of up to 40 μg/kg/min (and added atropine, if necessary, to achieve the target heart rate), which increases the heart rate and myocardial contractility. This method, although less physiologic than exercise, produces a smaller rise in blood pressure and also allows imaging exactly at the time of peak stress. Vasodilator stress with dipyridamole and pacing stress—via a preexisting permanent pacemaker or a transesophageal pacing catheter—are also possible but less widely used. If not combined with myocardial contrast perfusion techniques, vasodilator stress echocardiography relies on ischemia-associated wall motion abnormality to define a positive test unlike nuclear vasodilator stress test which addresses flow redistribution.

The risks associated with exercise echocardiography or DSE are very low. In the largest survey to date, the overall rate of life-threatening events was 1 per 1000 examinations (0.015% for exercise and 0.18% for dobutamine).[25] The most frequent complications were acute MI or ventricular tachycardia or fibrillation.

If a previous echocardiogram has not been performed, a brief survey of the ventricular chambers, valves, and aortic root should be performed to screen for significant pathology or contraindications to stress and to ensure adequate image quality (usually obtainable in at least 90% of patients with harmonic imaging). If endocardial resolution is poor in two or more segments, IV echocardiographic contrast enhancement should be used to improve accuracy. Images of the left ventricle are then obtained in the parasternal long, parasternal short, and apical windows at rest and then with stress. Side-by-side comparison of the baseline versus stress digitized images, which are gated by the ECG and synchronized in systole, allows quantification of overall LV size and systolic function, as well as identification of regional wall motion abnormalities. The standard 17-segment ASE model is used as the guide for grading function in each segment as normal, hyperkinetic, hypokinetic, akinetic, or dyskinetic at rest and with exercise or increasing doses of dobutamine. A normal ventricle has normal size and wall thickness and an EF of 50% or higher with no focal wall motion abnormalities (WMSI = 1.0); with stress the ventricle should become hypercontractile and the cavity size should shrink. The presence of baseline wall motion abnormalities that remain "fixed" (unchanged) with stress is indicative of a previous infarct. The development of a new or worsening wall motion abnormality indicates a flow-limiting stenosis in the coronary artery supplying the abnormal segment or segments (Fig. 16.29 and Video 16.32). A large ischemic territory—such as left main or multivessel disease—will manifest as diminished global LVEF and chamber dilation with stress (i.e., transient ischemic LV dilatation).
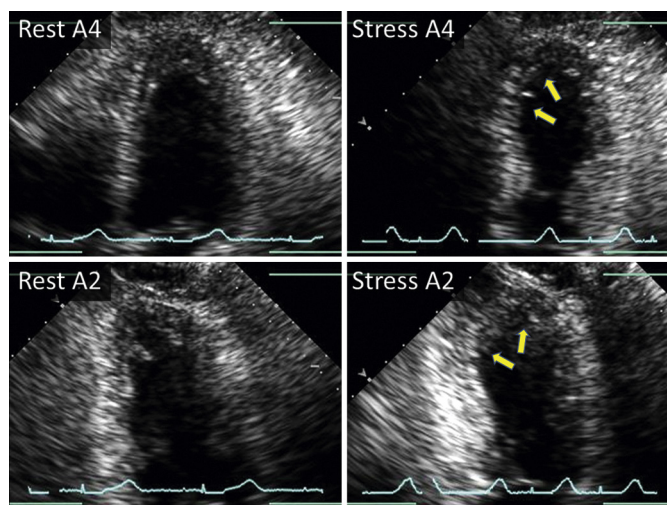


**FIGURE 16.29** Stress echocardiography showing evidence of ischemia in the left anterior descending (LAD) distribution. Resting and stress echocardiograms in the apical four-chamber (*A4*) and apical two-chamber (*A2*) views reveal new severe mid to distal septal, apical, and distal inferior LV hypokinesis (*arrows*). This patient was found to have greater than 90% mid-LAD stenosis on cardiac catheterization. (See Video 16.32.)

### Limitations of Stress Echocardiography

When compared with the gold standard of coronary angiography, the results of stress echocardiography can be discrepant. The primary causes of a false-negative result include suboptimal level of stress (from inadequate exercise capacity or beta-blocker use), limited image quality, a small area of ischemia (particularly for single-vessel or left circumflex disease), or preexisting conditions such as marked LV hypertrophy or a hyperdynamic state. False-positive results may also occur, particularly when the pretest probability is low. Diagnosis of wall motion abnormalities is particularly challenging in patients with LBBB or septal dyssynchrony (e.g., as a result of pacing or the postoperative state). In these patients, because exercise can exaggerate the abnormal septal motion and thereby obfuscate interpretation, DSE is recommended. A focus on wall thickening rather than on endocardial excursion may also be helpful in such situations. Other conditions that can cause nonspecific or nondiagnostic findings include the presence of preexisting wall motion abnormalities that tether adjacent segments, severe hypertension, HCM, and other cardiomyopathies in which myocardial perfusion reserve is diminished as a result of microvascular disease.[60]

### Risk Stratification with Stress Echocardiography

Numerous studies have demonstrated that in patients who complete normal exercise or pharmacologic stress echocardiograms (demonstrating good exercise capacity and/or reaching target heart rate), the risk for cardiac events is very low and at or close to that of a "normal" population (<1% per year for exercise and <2% per year for pharmacologic tests). In patients with suspected or known CAD, both the extent of resting wall motion abnormalities and the extent of ischemia—specifically quantified by an increase in WMSI, four or more LV wall segments affected, and/or no change or decrease in exercise LVEF—correlate with a fourfold or greater increased risk for cardiac death or MI.[60]

### Assessment of Myocardial Viability

DSE can also be used to quantify viability (contractile reserve) and thus functional recovery after reperfusion.[60] Although its overall sensitivity appears to be slightly lower than that of nuclear and CMR studies, DSE has better specificity for predicting recovery of systolic function of viable segments. A biphasic response, in which improvement in wall thickening occurs at low-dose dobutamine but then deteriorates with high-dose dobutamine, is the most specific sign. However, any improvement in wall motion abnormality by at least one grade in two or more

segments during stress is likely to signify viability (either stunned or hibernating myocardium).

### Coronary Flow Reserve and Perfusion

To provide additional prognostic information, it is feasible to assess coronary flow and flow reserve (see Chapter 36), most reliably in the LAD territory, by using Doppler TTE and vasodilators (adenosine or dipyridamole). Coronary flow reserve reduced to less than 1.9 to 2.0 in the LAD territory correlates with greater than 70% angiographic stenosis and is a predictor of future adverse cardiac events. Microperfusion of the myocardium at rest and with stress echocardiography may also be demonstrated with the use of ultrasound enhancing agents on 2D and 3D images (see Ultrasound Enhancing Agents and Fig. 16.24). In laboratories with expertise, both techniques of assessing myocardial perfusion appear to have acceptable agreement compared with angiography and nuclear stress tests. However, technical challenges and a learning curve presently exist, which has currently limited widespread adoption of these methods.[25,60]

Stress echocardiography is also used to assess factors beyond LV systolic function, particularly in patients who are dyspneic for unclear reasons. Valvular disease, diastolic function, pulmonary hypertension, and hemodynamics may all be assessed under stress conditions.[60,61]

### Stress Echocardiography in Valvular Heart Disease

Resting echocardiography may lead to conflicting interpretations of the degree of AS in patients with very calcified valves and low LVEF, because leaflet excursion and both the LVOT and the aortic velocities are diminished simply by low forward flow (see Chapter 72). In patients with "low-gradient, low-output aortic stenosis" and LV dysfunction (defined classically as a calculated aortic valve area (AVA) by Doppler ≤1.0 cm$^2$ [0.6 cm$^2$/m$^2$]), mean transaortic gradient <40 mm Hg, and reduced LVEF, variably defined as <45% or 50%, DSE can be used to assess both the true severity of AS and the amount of LV contractile reserve (see later, Aortic Stenosis). In this test, dobutamine is infused in graded doses from 5 to 20 μg/kg/min, typically for longer stages than used for ischemia testing, to allow for steady-state measurements of PW Doppler of the LVOT and CW Doppler across the aortic valve. SV is calculated from VTI$_{LVOT}$. An increase of 20% or higher in SV is indicative of significant contractile reserve. The test is indeterminate if little or no augmentation of LV function takes place (no contractile reserve, or ΔSV <20%). AVA is calculated at both baseline and with dobutamine; in true AS, the transvalvular gradients increase and the valve area remains in the severe AS range, whereas in "pseudosevere" or "functional" AS, the aortic gradients change relatively little while the LVOT VTI increases, and the calculated valve area increases as the leaflets open more. Patients with true severe AS generally benefit from aortic valve replacement, but if contractile reserve is absent or concomitant CAD is present, surgical mortality is high.[61,62] TAVR may provide a valuable option in this patients.

A subset of patients with advanced AS have been described who have "paradoxical" low-gradient/low-flow states despite preserved LVEF (see Chapter 72).[62] These are defined as having AVA ≤1.0 cm$^2$ (0.6 cm$^2$/m$^2$), mean transaortic gradient <40 mm Hg, LVEF ≥50% and BSA-corrected forward SV <35 cc/m, measured when the systolic BP is <140. While there are many causes of low flow despite preserved LVEF including MR or stenosis, AF and constriction, these patients are often women with small ventricles and hypertension. DSE has limited utility for these patients as it may be difficult to augment SV but where there is a response, those with true AS tend to maintain low AVAs and demonstrate modest gradient augmentation. These patients have a poor prognosis, which is improved by aortic valve replacement. The explanation appears to be pronounced LV concentric remodeling and myocardial fibrosis that results in severe restrictive physiology and low SV. Optimizing antihypertensive therapy is important as higher gradients may emerge with better BP control. Given its limited utility, DSE has largely been replaced by CT with calcium scoring or hybrid CT-Doppler imaging in evaluating these patients.[63]

Patients with rheumatic or calcific MS may have severe exertional symptoms despite relatively modest gradients on the resting echocardiogram. Conversely, sedentary patients with severe MS may be relatively asymptomatic because they are inactive. Valve gradients are notoriously dependent on the flow rate and heart rate. Stress
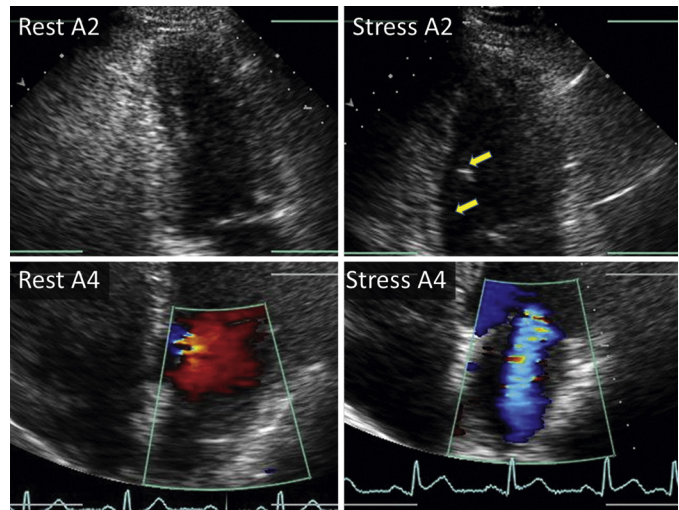


**FIGURE 16.30** Stress echocardiography with evidence of ischemia in the right coronary artery (RCA) territory and acute ischemic MR. Resting and stress echocardiograms in the apical two-chamber (*A2*) and apical four-chamber (*A4*) views with color Doppler reveal new stress-induced inferior hypokinesis (*arrows*) in the area containing the posteromedial papillary muscle and increased MR. This patient was found to have 90% stenoses of the RCA and left circumflex artery on cardiac catheterization. (See Video 16.33.)

echocardiography can define the true exercise capacity and quantitate the degree of valvular stenosis and regurgitation. A rise in the mean transmitral pressure gradient greater than 15 mm Hg or an increase in calculated PASP to greater than 60 mm Hg is correlated with significant MS, and such patients should be considered for valvotomy (if the cause is rheumatic and there is no more than mild MR) or mitral valve replacement (see Chapter 75).[61,64] Mitral valve surgery might also be considered if severe MR is elicited with stress. If symptoms and PASP increase markedly while transmitral gradients remain low, however, a pulmonary cause should be sought.

In patients with MR, stress echocardiography may be instrumental in revealing worsening ischemic MR caused by inferior wall ischemia (Fig. 16.30 and Video 16.33). This would characteristically be associated with stress-induced inferior wall motion abnormalities and improvement in both abnormalities during recovery. In chronic severe primary MR, stress echocardiography may unmask exercise induced LV dysfunction as well as assess exercise capacity. An exercise induced PASP of ≥60 mm Hg has been proposed for risk stratification but does not appear in current guidelines for intervention.[64]

Stress echocardiography may be refined or tailored in other conditions. In patients with HCM, exercise can bring out latent gradients and is also used to monitor response to therapy and assess symptoms such as syncope (see Chapter 54). In patients or family members of those with known or suspected pulmonary hypertension, stress echocardiography may also be helpful and should include calculation of PVR as well as PA pressure. In conjunction with cardiopulmonary testing, stress echocardiography may aid in identifying other causes of dyspnea and fatigue, such as diastolic dysfunction. Delayed diastolic relaxation, as measured by strain and strain rate imaging, may also be a more sensitive and persistent indicator of exercise-induced ischemia than wall thickening. With the advent of real-time 3D and four-dimensional (4D) imaging, automatic endocardial border tracking, and volumetric imaging, there is now the capability to capture images of LV systolic and diastolic function simultaneously at peak exercise, thereby potentially improving the sensitivity, accuracy, and reproducibility of this test for ischemia.

# VALVULAR HEART DISEASE (SEE PART VIII)

## Mitral Valve (see Chapters 75 and 76)

### Mitral Valve Anatomy

The mitral valve apparatus is a complex structure consisting of two leaflets attached to the left atrium by the mitral annulus and to the left
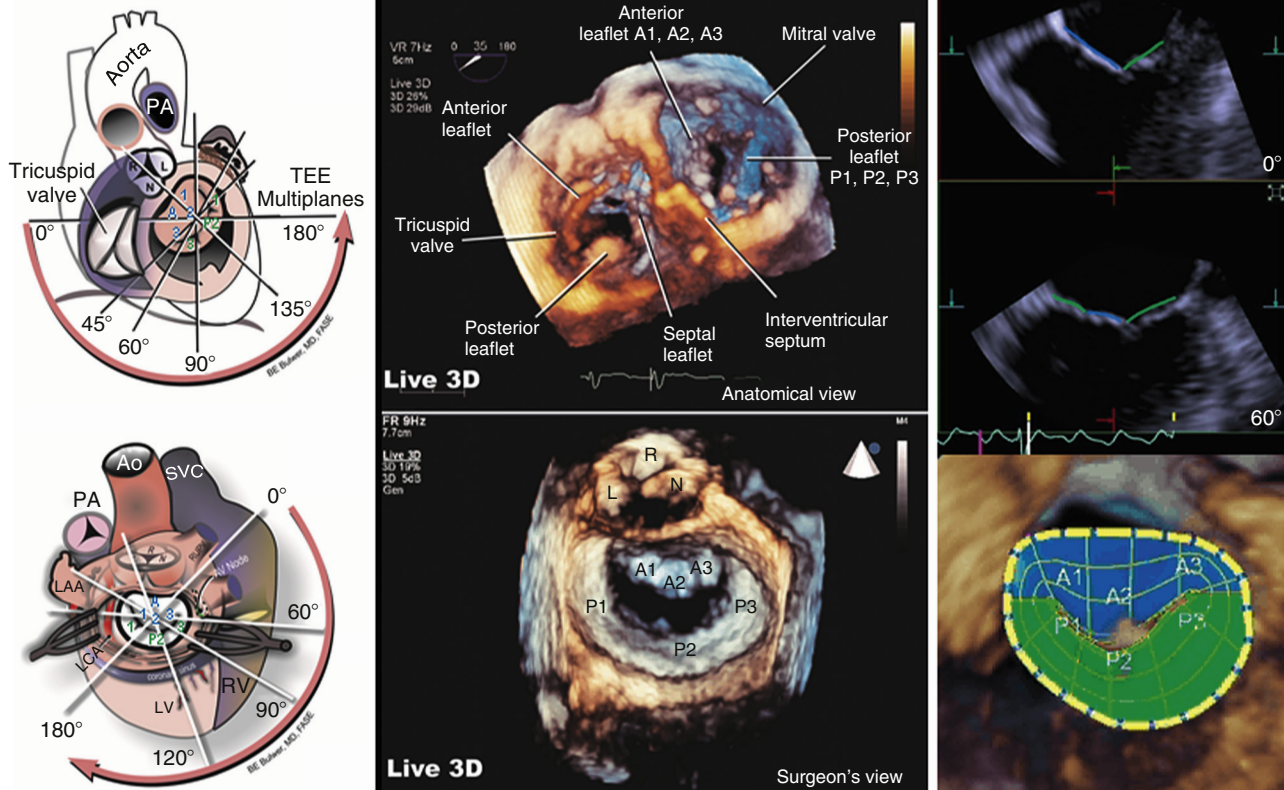
**FIGURE 16.31** Mitral valve anatomy from TEE. **Left,** Two-dimensional (2D) TEE approach involving adjustment of probe position and omni orientation (degrees), sweeping to image all scallops. **Middle,** Three-dimensional (3D) appearance of the valve from the TEE view **(upper)** and surgeon's view **(lower)** with the mitral leaflet scallops labeled. **Right,** 3D TEE images delineating the mitral valve scallops at 0 degrees (four-chamber) and 60 degrees (two-chamber) planes, and below superimposed 3D analysis of leaflet areas from the left atrial aspect. *Ao,* Aorta; *PA,* pulmonary artery, *LAA,* left atrial appendage. The aortic valve right (*R*), left (*L*), and non- (*N*) coronary cusps are also shown. (See Video 16.34.)

ventricle through the mitral chordae and papillary muscles. The posterior leaflet is divided naturally into three scallops termed P1, P2, and P3 (using the Carpentier nomenclature), with P1 being lateral and P3 being medial. Opposing scallops of the anterior leaflet are termed A1, A2, and A3. Localization of pathology to specific scallops is important, particularly in surgical decision making for primary degenerative MR. The annulus is a nonplanar saddle-shaped structure, with its highest points seen on the parasternal long-axis view and its nadir seen in the apical four-chamber view (see Fig. 16.21). The chordae consist of a complex arcade of primary (first-order) and secondary (second-order) chordae radiating from both papillary muscles, with the former being inserted along the free margin of both leaflets and the latter serving as strut supports to the leaflet undersurfaces. Tertiary (third-order) chordae arise from the ventricular wall and insert into the base of the posterior leaflet only (Fig. 16.31 and eFig. 16.25).

Although it is possible to identify each of the scallops with 2D TTE on the parasternal short-axis view at the level of the mitral valve, it may be challenging to identify the scallops in the other views. Consequently, TEE plays a particularly important role in assessment of the mitral valve. 3D TEE has rapidly become an essential tool because of its ability to provide images that replicate the surgeon's view of the valve (see Fig. 16.31), as well as improved methods for assessing mitral pathophysiology in a variety of disease states. Leaflet morphology, focal disruptions, and detailed measurements can now be made virtually real-time (Video 16.34). Congenital anomalies of the mitral valve are unusual, but those that might be newly diagnosed in adulthood include double-orifice and parachute mitral valve, as well as isolated clefts.

## Mitral Stenosis
### Echocardiographic Features
Commissural fusion, chordal thickening and fusion, as well as leaflet thickening and calcification that develop in patients with rheumatic MS result in narrowing of the mitral orifice, classically with a fish-mouth configuration (Fig. 16.32). Other pathognomonic echocardiographic features of rheumatic mitral disease are best appreciated on the parasternal long- and short-axis views and apical views. Commissural fusion results in restricted diastolic excursion of the tips of the
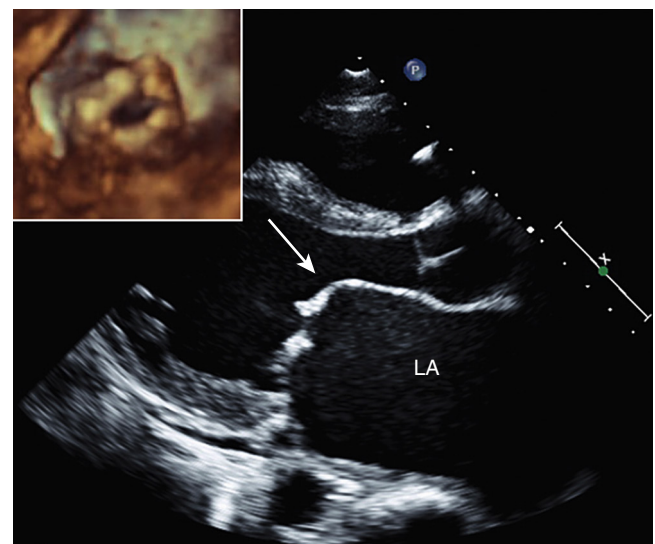


**FIGURE 16.32** Rheumatic mitral stenosis. Parasternal long-axis view (diastolic frame) of a rheumatic mitral valve. Diastolic doming of the anterior mitral leaflet (*arrow*) is present, as well as a fixed posterior leaflet. *Inset,* Doming and fish-mouth appearance of the valve, as seen by 3D TTE from the LV aspect. *LA,* Left atrium. (See Videos 16.35 and 16.36.)

leaflets, with relatively preserved mobility of the belly of the leaflet, particularly in early or milder forms of the disease. The result is a pattern of opening in which excursion of the midsection of the leaflet exceeds that of the leaflet tips, termed *doming*. Doming is also seen in rheumatic tricuspid stenosis and congenital anomalies of the aortic valve (discussed later). In rheumatic mitral disease, anterior leaflet doming is more readily appreciated because the posterior leaflet is shorter and
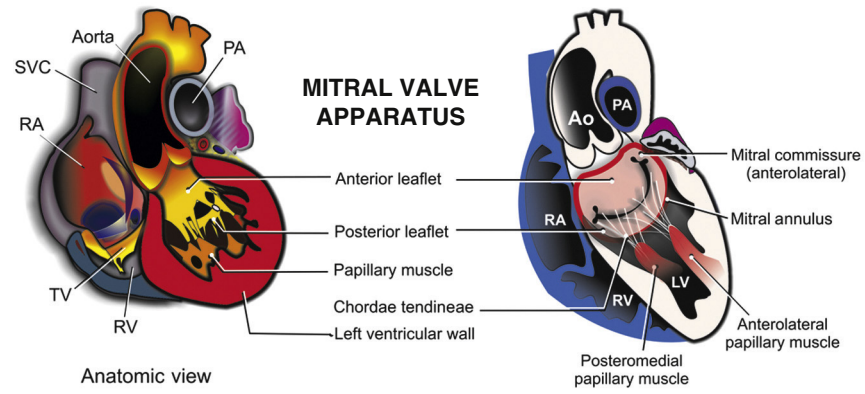
**EFIGURE 16.25** Normal mitral valve anatomy. *Ao,* aorta; *LV,* left ventricle; *PA,* pulmonary artery; *RA,* right atrium; *RV,* right ventricle; *SVC,* superior vena cava; *TV,* tricuspid valve. (Modified from Bulwer BE, Rivero JM, eds. *Echocardiography Pocket Guide: The Transthoracic Examination*. Burlington, MA: Jones & Bartlett Learning; 2011, 2013:132. Reprinted with permission.)

tends to become immobilized early in the rheumatic process (Videos 16.35 and 16.36). Leaflet and chordal thickening with or without calcification is also seen. Despite the fact that degenerative mitral annular calcification is a very common anomaly that occurs with aging and renal disease, it infrequently causes significant MS unless very severe.

### Quantification of Severity

The normal mitral valve area (MVA) is 4 to 5 cm$^2$, and severe MS usually correlates with MVA ≤1.0 to 1.5 cm$^2$.[65] Direct planimetry of the orifice area from a parasternal short-axis view was first validated in the pre-Doppler era. It relies on meticulous positioning of the imaging plane at the level of the flow-limiting orifice; misleadingly larger-appearing "orifices" will be captured if the plane used is at the level of more mobile leaflet segments. It is equally important for the gain to be set at the lowest possible setting that will provide a complete orifice. Overgained images will underestimate the true MVA. 3D echocardiography has proved to be a valuable tool because it provides a robust means of precisely identifying the valve orifice (Fig. 16.33).

Determination of the mean gradient is the simplest Doppler method for assessing the severity of MS. Given the degree to which gradients are influenced by flow rate, it is important to report the heart rate at which the gradient was determined and to be cognizant of the impact of concomitant MR, which can increase overall transmitral flow (and hence the inflow gradients, leading to overestimation of MS). Conversely, abnormalities that increase LV diastolic pressure independent of transmitral flow, such as reduced LV compliance and AR, can attenuate the transmitral gradient and result in underestimation of the severity of MS.

Doppler echocardiography also provides alternative methods to planimetry for determining MVA. The most widely used approach is the pressure half-time (PHT) method, which relies on the rate at which LA and LV pressures equalize. Using a simplified derivation of a catheterization laboratory–validated method, MVA is calculated as 220 divided by PHT, with 220 being an empirically derived constant. PHT is the time that it takes the initial transvalvular gradient to fall to half its initial value. This calculation can rapidly be done online with the basic analysis packages available on echocardiographic machines (Fig. 16.34). There are caveats: the PHT method should not be used in the immediate postvalvuloplasty setting because acute changes in both the LA-LV compliance relationship and in the initial transmitral gradient may have occurred. As discussed, it may also be invalid in the setting of significant AR and reduced LV compliance, each of which will result in overestimation of MVA. Additionally, the PHT may be indeterminate when the mitral inflow Doppler spectrum has a biphasic contour. Finally, this method has not been validated for other causes of MS, such as mitral annular calcification, or for prosthetic valves.

An alternative method is the *proximal isovelocity surface area* (PISA) approach (Fig. 16.35), in which MVA = $2(\pi r^2)(V_{aliasing})/(\text{Peak } V_{mitral}) \times \alpha/180$, where $\alpha$ is the angle formed by the doming cusps, or a simplification of this equation in which $\alpha$ is assumed to be 100 degrees. A 2D/Doppler-based method based on the principle of flow continuity may also be used, which calculates MVA = $\pi(D_{LVOT}/2)^2(VTI_{LVOT}/VTI_{MV})$, where D is the diameter of the LVOT measured on the parasternal long-axis view. As with other forms of valvular heart disease, an approach that integrates imaging and Doppler findings will optimize assessment of mitral stenotic severity.
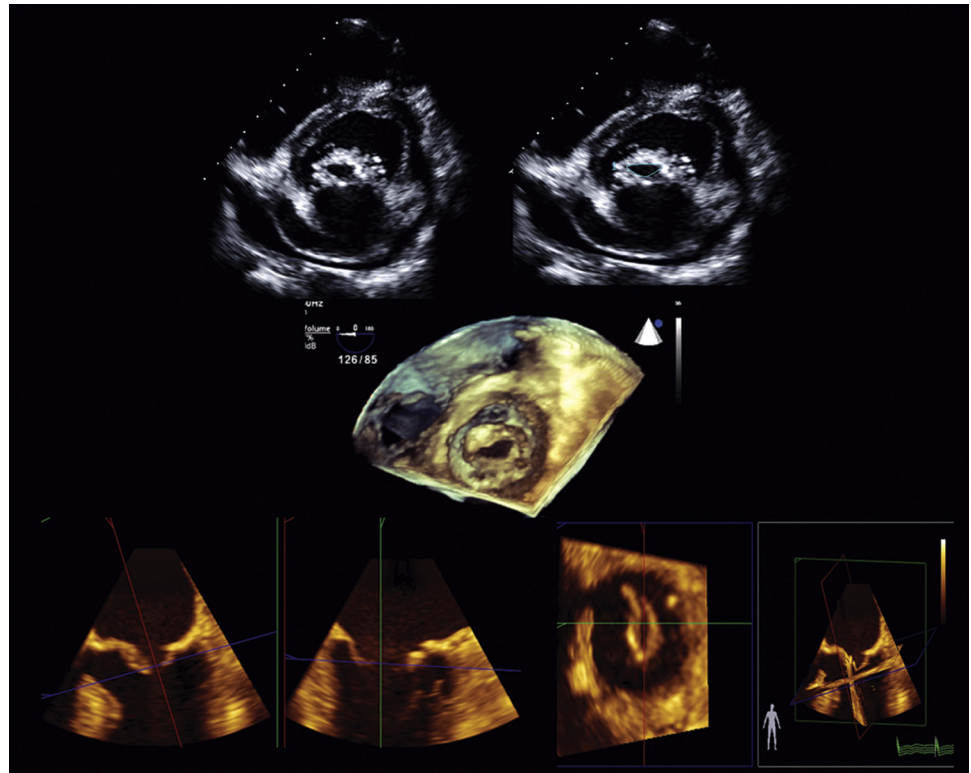


**FIGURE 16.33** Approaches to planimetry of the mitral valve area (MVA) in rheumatic mitral stenosis. **Top,** Planimetry of 2D parasternal short-axis images. **Middle,** 3D TEE view of the stenotic orifice from the perspective of the left ventricle, which can be directly planimetered. **Bottom,** Multiplanar reconstruction of 3D TEE volumes can ensure that a short-axis view precisely at the level of the limiting orifice is selected for planimetry.
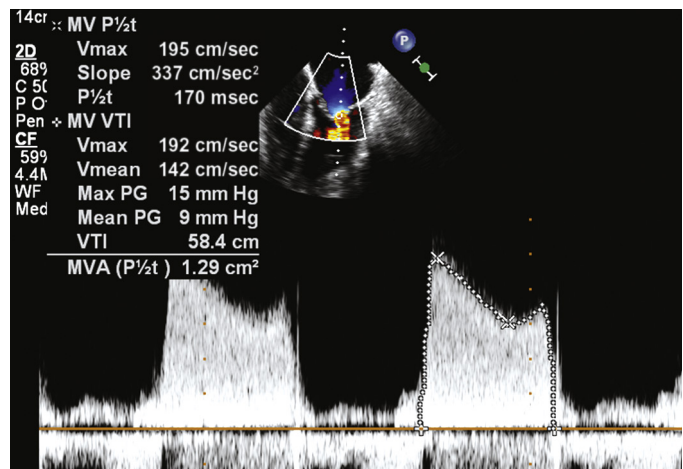


**FIGURE 16.34** Tracing the CW mitral stenotic spectrum (*dotted line*) for VTI provides the mean transvalvular gradient, whereas assessment of the rate at which the gradient between the left atrium and left ventricle falls (marked by the two Xs) can be used to calculate valve area from the pressure half-time method ($P^1/_2 t$). *MV,* Mitral valve; *MVA,* MV area; *PG,* pressure gradient.

### Patient Selection for Balloon Valvuloplasty

In patients with severe MS in whom transcatheter intervention is planned, the Wilkins echocardiographic scoring system is useful in determining the likelihood of overall procedural success (Table 16.9); the less widely used Padial scoring system is useful in predicting freedom from severe MR. A Wilkins score greater than 8 or Padial score of 10 or more are predictors of poorer outcomes. It is also important to determine the amount of associated MR on echocardiography, because percutaneous balloon mitral valvotomy will increase the severity of regurgitation by at least one grade; thus the presence of moderate or greater MR should deter one from pursuing
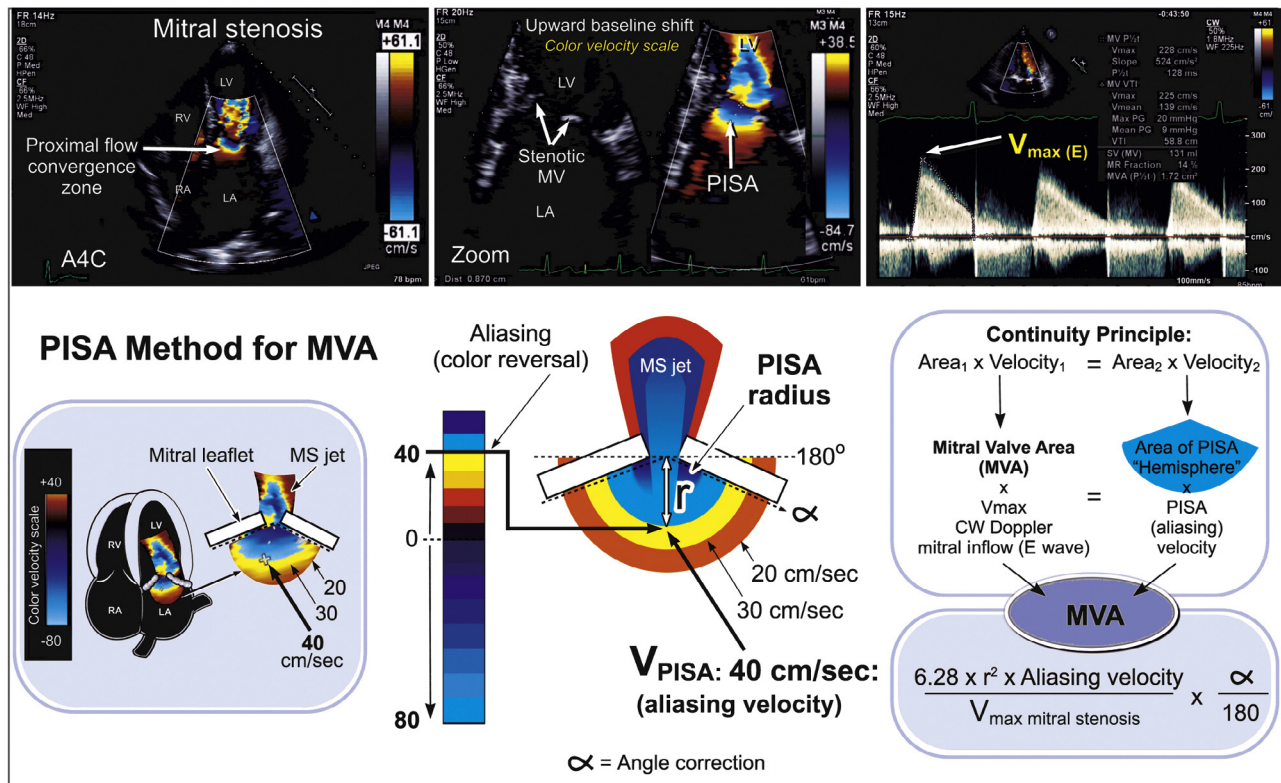
**FIGURE 16.35** Proximal isovelocity surface area (PISA) method for calculation of MVA. In patients with mitral stenosis (MS), flow acceleration proximal to the stenotic orifice will result in a flow convergence zone that is characterized by color aliasing and a PISA shell **(upper left)**. The definition of the PISA shell and thus accuracy of the PISA radius measurement can be improved by shifting the baseline Nyquist limit in the direction of flow **(upper middle)**. In the **lower left** and **middle panels,** the aliasing velocity is 40 cm/sec. Application of the continuity equation allows MVA to be calculated as MVA = $[2(\pi r^2)(V_{aliasing})/(Peak\ V_{mitral})] \times \alpha/180$. The angle correction is used to correct for deviation of the shell from hemisphericity. *A4C,* Apical four-chamber view.

**TABLE 16.9** Wilkins Scoring System for Mitral Valvuloplasty

| GRADE | LEAFLET MOBILITY | VALVE THICKENING | CALCIFICATION | SUBVALVULAR THICKENING |
|---|---|---|---|---|
| 1 | Highly mobile | Minimal thickening | Single area of brightness | Minimal chordal thickening |
| 2 | Reduced mobility | Thickened tips | Scattered areas at leaflet margins | Chordal thickening up to one-third |
| 3 | Basal leaflet motion only | Entire leaflet thickened | Brightness extends to mid leaflets | Distal third of chordae thickened |
| 4 | Minimal motion | Marked leaflet thickening | Extensive leaflet brightness | Extensive thickening to papillary muscles |

A desirable score is 8 or lower.

a percutaneous approach. The presence of LA appendage thrombus, which must be ruled out by TEE, is also a contraindication to percutaneous intervention because of the risk of embolization from guidewires and catheters.

## Mitral Regurgitation

### Causes of Mitral Regurgitation

Minor leakage of the mitral valve is a common physiologic finding. There are many causes of pathologic regurgitation, and echocardiography should be used not only to diagnose and quantify MR, but also to determine the underlying functional disturbance and, when possible, to identify the disease causing the disturbance (see Chapter 76). Carpentier proposed a useful classification system based on the pathophysiology of MR that lends itself to an echocardiographic approach. In type I, leaflet motion is normal, and the most common abnormalities are leaflet perforation, alteration in coaptation because of bulky vegetation, or annular dilation secondary to chronic AF. In type II, at least one leaflet overrides the most superior plane of the annulus, that is, mitral prolapse or flail on the basis of either intrinsic valvular abnormality or rupture of either the chordae or papillary muscles. In type IIIA, leaflet motion is restricted during both systole and diastole, usually because of rheumatic disease, whereas in type IIIB, motion is limited in systole because of pathologic tethering on the basis of LV systolic dysfunction

and remodeling. This is the most common scenario in secondary or functional MR.

### Primary (Degenerative) Mitral Regurgitation

Mitral prolapse or flail that is attributable to primary leaflet and/or chordal pathology is termed *degenerative* MR. Echocardiography is the gold standard for the diagnosis of mitral prolapse or flail, distinguished as follows: in mitral flail, the unsupported free edge of the mitral leaflet falls back into the left atrium because of loss of chordal support, whereas in mitral prolapse, the free edge remains tethered by chordae, and the body of the leaflet billows pathologically into the left atrium. The diagnosis of prolapse is made from the parasternal long-axis view when any part of the leaflet extends 2 mm above a line drawn from the insertion of the anterior and posterior leaflets (Fig. 16.36 and Video 16.37). This line represents the most superior aspect of the saddle-shaped annulus (see Fig. 16.21 for 3D mitral valve shape). In the apical four- and two-chamber views, some extension of leaflet tissue above the annular boundaries is a normal variant. Hence these views should not be used to diagnose or define prolapse, although they may demonstrate the classic billowing motion of a truly prolapsing mitral valve. It may be difficult to differentiate between mitral prolapse and flail with TTE alone, but TEE can assist in making the correct diagnosis.
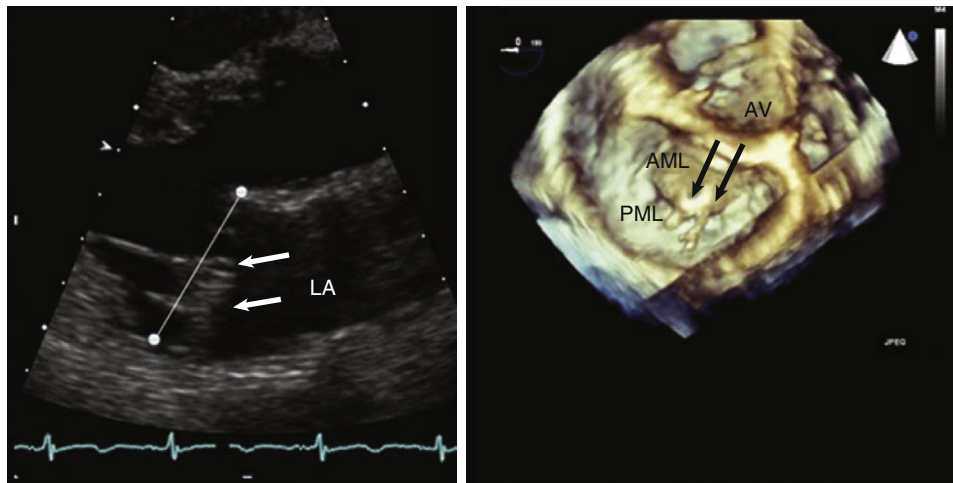
FIGURE 16.36 Degenerative MR. **Left,** Parasternal long-axis view showing bileaflet prolapse, as evidenced by billowing of both leaflets (*arrows*) above the annular plane, defined by the insertion of the anterior and posterior leaflets (*line*). **Right,** 3D TEE image of the mitral valve from the left atrial perspective. There is a large flail segment of the anterior mitral leaflet (*AML*). *Arrows* point to ruptured chordae. *AV,* Aortic valve; *LA,* left atrium; *PML,* posterior mitral leaflet.
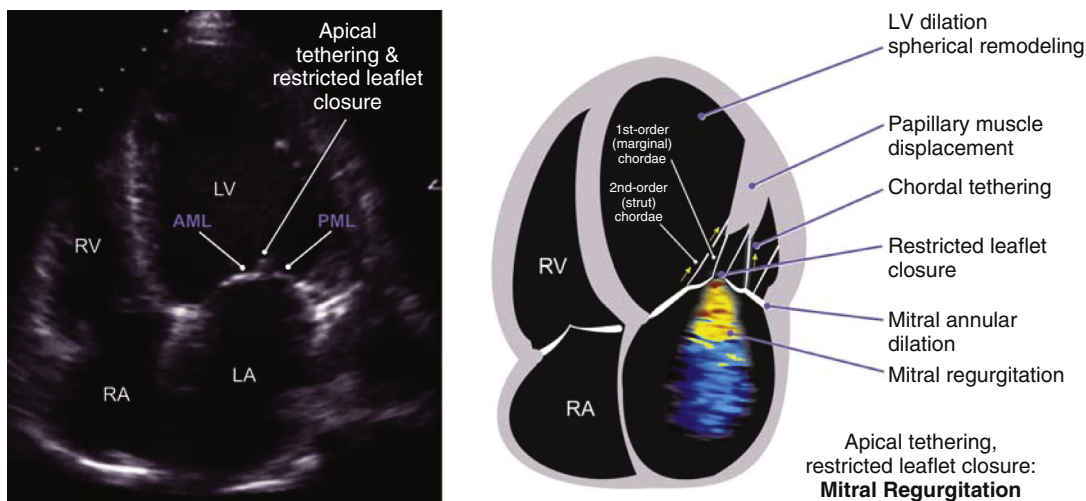


FIGURE 16.37 Functional/ischemic MR. Mitral tethering forces are increased because of both annular dilation and papillary muscle traction, which occur as a result of LV remodeling. Closing forces are reduced because of impaired LV systolic function. The end result is apical displacement of leaflet coaptation, as shown in the apical four-chamber view on the left. *AML,* Anterior mitral leaflet; *LA,* left atrium; *LV,* left ventricle; *PML,* posterior mitral leaflet; *RA,* right atrium; *RV,* right ventricle.

The anatomic substrate for degenerative MR spans the spectrum from diffuse myxomatous change (Barlow) to localized abnormalities characterized as fibroelastic deficiency. Mitral valve prolapse is more prevalent in patients with Marfan syndrome, Ehlers-Danlos syndrome, osteogenesis imperfecta, and other connective tissue disorders. 3D echocardiographic assessment of the extent of billowing has been reported to be useful in characterizing the nature of the pathology but, more importantly, has assumed a key role in determining precisely which scallop(s) are prolapsing or flail. This information is essential in predicting the likelihood of successful repair, whether surgical or with transcatheter approaches. Isolated P2 pathology is the most common pattern, and successful repair is highly probable. Next in frequency and ease of repair is A2 disease, followed by abnormalities in the medial and lateral scallops. 3D TEE (see Video 16.34) is also helpful in identifying involvement of multiple scallops or unexpected associated anomalies such as localized mitral valve clefts. The latter are particularly important in mitral clip repair as they may impact effective leaflet grasping. In the absence of 3D capability, a systematic approach to assessment of all three scallops via 2D TEE can be used (see Fig. 16.31). Complete assessment of the mitral scallops is difficult with TTE, although when achievable, high-quality 3D TTE images may be used for this purpose.

### Secondary (Functional) Mitral Regurgitation

The term *secondary or functional* MR is used when the leaflets, chords and papillary muscles are structurally normal. Most commonly, the root cause of functional MR is LV systolic dysfunction and remodeling (Carpentier Type IIIB). When the dysfunction is on the basis of CAD, the term *ischemic MR* is used. Recently, functional MR that occurs with preserved ventricular function has been recognized when the primary abnormality is annular dilation, typically due to AF (Carpentier Type I), termed "atrial functional MR." 3D echocardiography has shown that functional MR reflects an imbalance between the forces that close versus those that tether the mitral leaflets (Fig. 16.37).[33] The end result is pathologic tethering seen as apical displacement of leaflet coaptation. This pattern, which is appreciable on parasternal long-axis or apical views, is the echocardiographic hallmark of functional MR (see Video 16.21). Reduced closing forces are attributable to impaired LV systolic function, whereas pathologic tethering forces can occur because of traction on the mitral leaflets from either their annular insertion (as a result of annular dilation and/or reduced annular contraction) or from their chordal connection to the papillary muscles. The latter has been shown to result from geometric displacement of the papillary muscles either apically (in the case of global remodeling) or inferiorly (due to regional remodeling from focal infarct). It has been shown convincingly that papillary muscle contractile dysfunction per se does not cause functional/ischemic MR.

### Quantitation of Mitral Regurgitation

The ASE recommends an integrated approach to the quantitation of MR[66] that incorporates semiquantitative measures such as assessment of jet area (ratio of jet area to LA area), the size of the peak mitral E
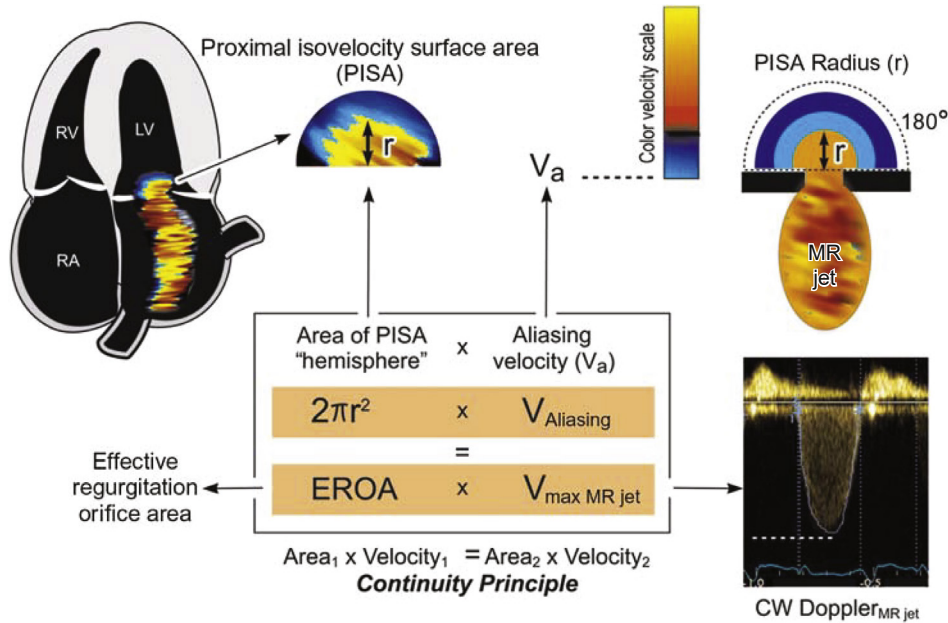
FIGURE 16.38 PISA approach to quantitating the effective regurgitant orifice area (EROA) for MR. To optimize the PISA shell, the baseline is shifted in the direction of the jet. EROA is computed as EROA = $2(\pi r^2)(V_{aliasing})/(V_{MaxMR})$. Regurgitant volume can be calculated as EROA × $VTI_{MR}$, where $VTI_{MR}$ is the velocity-time integral of the MR spectrum.



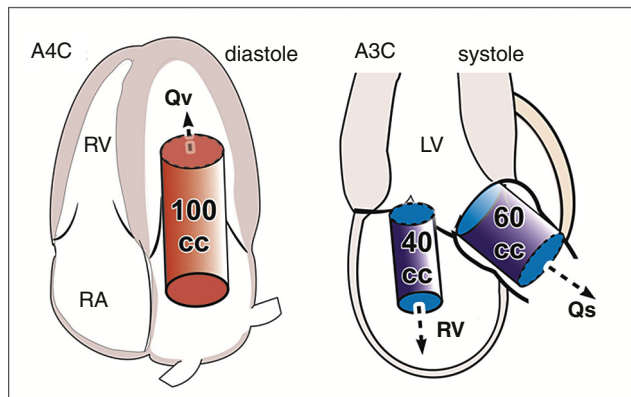FIGURE 16.39 Quantitative Doppler approach to assessing the severity of MR. Regurgitant volume (RV) is calculated as the difference between total transmitral flow (Qv) and antegrade flow across the LVOT (Qs). Qv and Qs are calculated via the continuity method approach (CSA × VTI). Alternatively, Qv, which is identical to LV SV in the absence of a ventricular shunt or aortic regurgitation, may be calculated as LVEDV – LVESV, where LVEDV and LVESV are the LV end-diastolic and end-systolic volumes, respectively. *A4C,* Apical four-chamber view; *RA,* right atrium.

wave, vena contracta diameter, and pulmonary venous flow patterns in addition to the imaging appearance of the mitral valve, left atrium and left ventricle (eFig. 16.26). The peak E velocity reflects the initial diastolic gradient between the left atrium and left ventricle and will be elevated when MR has resulted in elevation of LA pressure. The vena contracta is the narrowest region of a jet and is best assessed in zoom mode on the parasternal long-axis view. Pulmonary venous flow patterns reflect the impact of the MR jet on flow into the left atrium with, in some cases, severe regurgitant systolic flow reversal. Quantitation of regurgitant volume and the EROA is possible with the PISA approach, which is based on the concept of acceleration of flow proximal to the regurgitant orifice (Fig. 16.38). The quantitative Doppler approach that uses the continuity equation provides a means of calculating regurgitant volume and fraction by comparing the total antegrade flow across the mitral valve with that across a nonstenotic nonregurgitant reference valve, typically the aortic valve (Fig. 16.39). In general, an EROA of ≥0.4 cm² and RV volume of ≥60 mL is indicative of severe MR.

Even though the color jet size approach is easy and widely utilized, it is influenced by machine settings and many other factors.[66] It underestimates MR severity with eccentric jets and overestimates severity with non-holosystolic MR. It should not be the only tool used to quantitate more than mild MR. The PISA method is limited in situations where the assumption of a hemispheric PISA shell and circular regurgitant orifice is invalid; this is often true for eccentric jets caused by degenerative MR, as well as for functional MR cases where the PISA shell is flatter and hemi-elliptical. In fact, for functional ischemic MR, the PISA values that correlate with poor clinical outcome are lower than those used for primary MR. This is in part because studies have consistently shown that any degree of ischemic MR is prognostically important, but also because the regurgitant orifice is elliptical rather than circular, causing 2D PISA measures to commonly underestimate ischemic MR severity. 3D planimetry may provide a superior method of determining the EROA.[65] Conversely, in nonholosystolic MR (e.g., late systolic MR that frequently occurs in MV prolapse), the EROA calculated with the PISA approach will overestimate severity because it reflects the maximum EROA rather than the EROA averaged over all of systole. The major limitation of the quantitative Doppler technique lies in the assumption of circular or oval mitral orifice geometry in calculating transmitral flow. The use of LV SV calculated from echocardiographically measured LV volume versus aortic outflow has been suggested as an alternative approach. The advent of 3D echocardiography has provided methods for direct planimetry of regurgitant orifices, an approach that is increasingly used but that typically requires the spatial resolution of TEE. 3D techniques for optimizing assessment of nonhemispheric PISA shells have also been reported but are not yet widely used clinically.

It is important to recognize that secondary, and to a lesser degree primary, MR is afterload dependent, and thus determination of severity must take into account LV systolic pressure. Clinical decision making based on echo parameters made under general anesthesia is to be avoided, because anesthesia is associated with a predictable fall in systemic vascular resistance which may dramatically reduce the degree of regurgitation.

## Aortic Valve (see Chapters 72 to 74)

### Aortic Valve Anatomy
The normal aortic valve consists of three symmetric cusps that are supported by the aortic annulus and extend into the aortic root. The right and left coronary cusps lie within the sinuses of Valsalva that give rise to the corresponding coronary arteries, and the remaining cusp is termed the *noncoronary* cusp. The ideal views for assessing aortic valvular anatomy are the parasternal short- and long-axis views (see Fig. 16.8) and their comparable views on TEE (see Fig. 16.19E,F). The short-axis view shows all three cusps, which when open create a triangular-shaped orifice and when closed have a Y-shaped appearance. The long axis typically displays the right and noncoronary cusps, which when normally open will flatten against the walls of the aortic root and with normal closure will meet centrally without prolapse below the plane of the aortic annulus.

The most common congenital abnormalities of the aortic valve result from failure of cusp development and include, in order of decreasing frequency, bicuspid, unicuspid, and quadricuspid valves (Fig. 16.40). There are several approaches to the classification of congenitally abnormal valves. The most widely used is the Sievers classification based on the number of raphes (vestigial commissures) and their orientation. Type 0 is the classic bicuspid valve with no raphe, Type 1 (one raphe) is the most common with left-right fusion the most prevalent orientation. Type 2 is least common and corresponds to a functionally unicuspid valve. Quadricuspid valves are not included in this classification. Because of the inability of bicuspid valves to open fully, the systolic orifice of a bicuspid aortic valve is oval when seen in short axis, whereas the long-axis view demonstrates convex bulging of the leaflet midportions into the aortic lumen
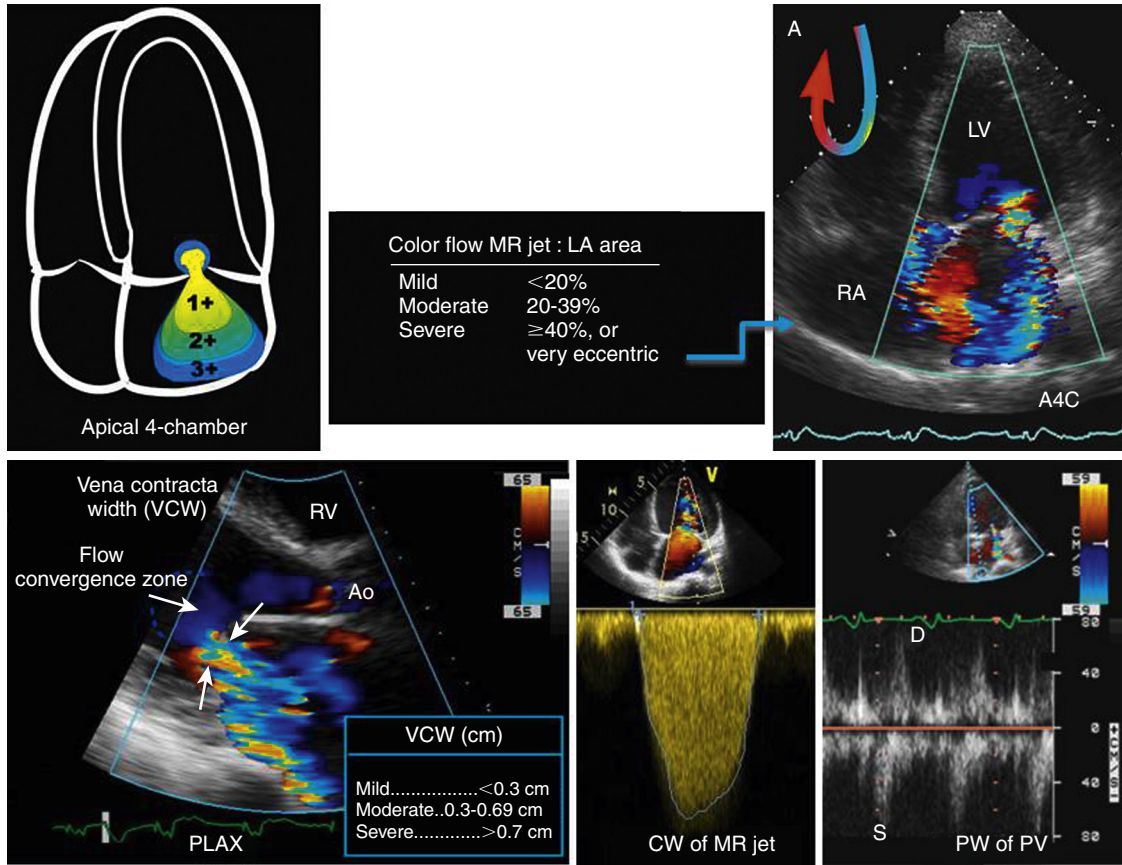
**EFIGURE 16.26** Mitral regurgitation (MR) grading by semiquantitative parameters. **Top panels,** A time-honored technique of grading simple central mitral regurgitant jets by freezing the apical window when the color flow jet is greatest (at usual Nyquist limits of 50 to 70 cm/sec), then tracing the area of the jet and expressing it as a ratio to the area of the left atrium. Ideally this is done in two orthogonal planes and the results averaged. If the jet is very eccentric (i.e., "hugs a wall"), the grade is generally increased by one grade in this scale. **Bottom panels: Left**, Vena contracta, or "neck," of color flow Doppler is measured ideally in the parasternal long-axis window (or alternatively, apical three-chamber window), and is a linear estimate that correlates with the actual orifice size of the mitral valve during systole. **Middle,** MR CW Doppler jet is very dense, consistent with more severe mitral regurgitation. **Right,** There is systolic flow reversal (the S wave is negative, or below the baseline) in the right upper pulmonary vein on PW Doppler.
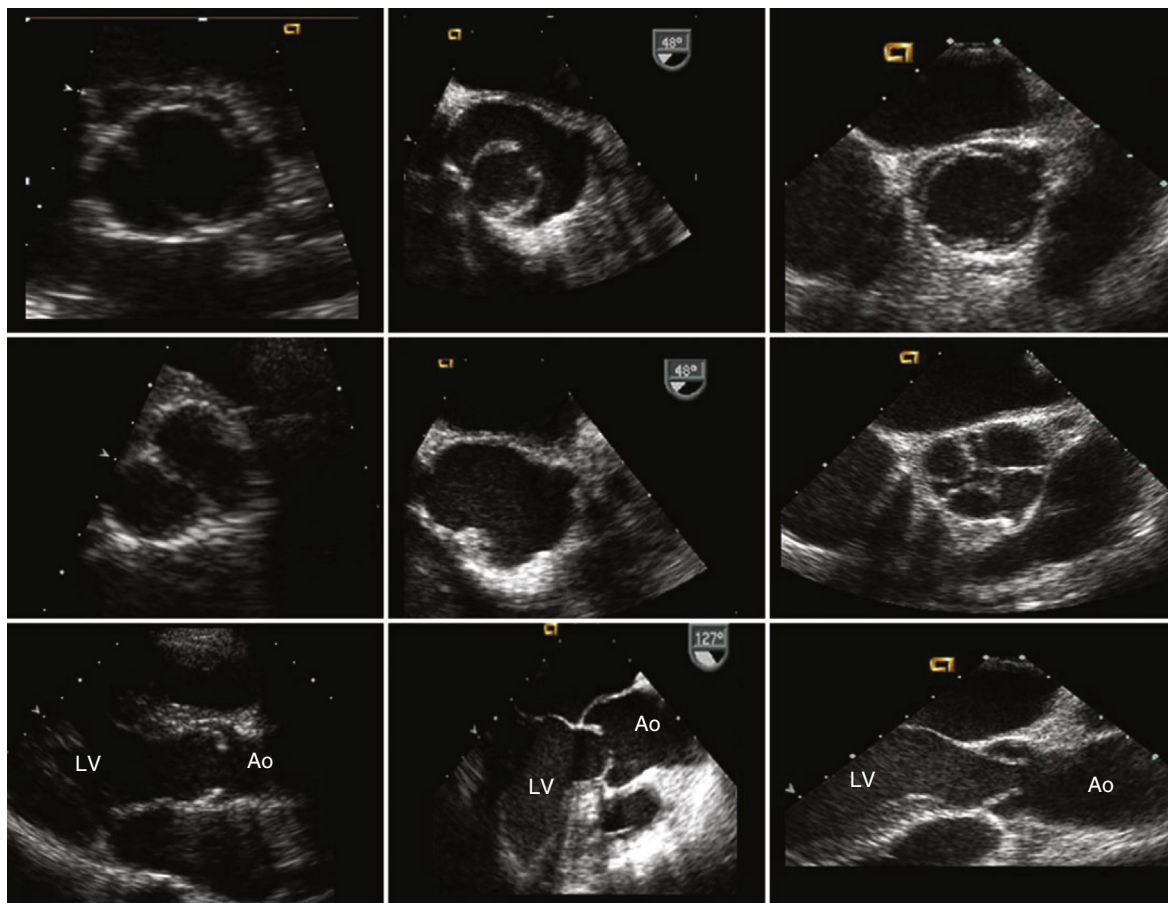
**FIGURE 16.40** Congenital abnormalities of the aortic valve with (*top to bottom*) systolic short-axis, diastolic short-axis, and systolic long-axis views. **Left panels,** Bicuspid aortic valve. **Middle panels,** Unicuspid unicommissural aortic valve. **Right panels,** Quadricuspid aortic valve. *Ao,* Aorta; *LV,* left ventricle.
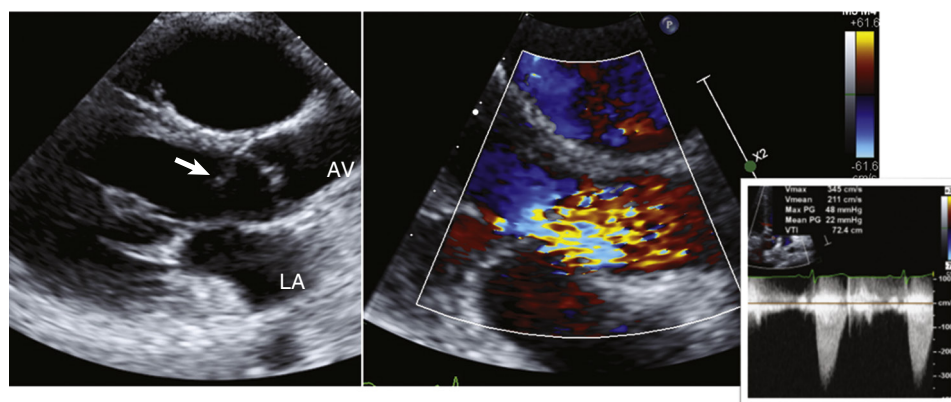


**FIGURE 16.41** Parasternal long-axis view demonstrating **Left,** a subaortic membrane (*arrow*) extending from the anterior mitral leaflet to the septum. The aortic valve (*AV*) is about to open. *LA,* Left atrium. **Right,** color Doppler showing turbulent brisk flow across the membrane. Right inset, CW Doppler showing a peak gradient across the LVOT of 48 mm Hg.

(doming) (Videos 16.38 and 16.39). Although bicuspid aortic valves classically have a single line of closure and no raphe (type 0), these account for only 7% of cases. The majority (88%) have an echogenic ridge or raphe that represents a vestigial commissure between two "would-be" cusps on a trileaflet valve. The closed appearance of such valves may be echocardiographically indistinguishable from a tricuspid valve. Thus, bicuspid aortic valve is a systolic diagnosis (see Videos 16.38 and 16.39). Unicuspid valves (Type 2) (Video 16.40) typically have circular openings that may be central or asymmetrically positioned, and quadricuspid valves (Video 16.41) have a square appearance in systole and a crosslike appearance in diastole.

Congenital abnormalities of the LVOT include subaortic membranes, characterized by linear echoes extending from the anterior mitral leaflet to the septum or fibromuscular tunnels in which there is an echogenic ridge extending into the LVOT (Fig. 16.41). The presence of subaortic systolic turbulence on color Doppler should prompt close inspection of the

LVOT for evidence of obstruction. Associated valvular AR is seen frequently and results from valve trauma caused by the subaortic stenotic jet. Supravalvular AS is a rare phenomenon that consists of localized or diffuse narrowing of the ascending aorta distal to the sinuses of Valsalva.

## Aortic Stenosis
Although the impeded cusp excursion of a congenitally bicuspid or unicuspid aortic valve is the most frequent cause of AS in young patients, calcium deposition on a previously structurally normal tricuspid aortic valve is a common cause of AS in elderly adults. The echocardiographic appearance is restricted cusp excursion with irregular nodular cusp thickening (Fig. 16.42).

### Quantitation of Severity
The normal AVA is 3 to 4 cm². In adults, severe AS usually occurs with an AVA less than 1.0 cm². Indexing of the AVA for BSA (<0.6 cm²/m² for severe AS) is important in children and small adults.[67] Application of the Bernoulli equation to CW Doppler interrogation of transvalvular flow provides accurate measures of the mean and peak instantaneous gradients in AS. Typically, the simplified form of the equation ($\Delta P = 4V^2$) may be used, but when LVOT velocity significantly exceeds 1 m/sec, the expanded version, $\Delta P = 4 (V_2^2 - V_1^2)$, where $V_2$ is transaortic velocity and $V_1$ is LVOT velocity, should be used.

In recognition of the importance of recording Doppler signals parallel to flow, aortic gradients are best recorded from the apical five- or three-chamber, suprasternal notch, and right parasternal windows;
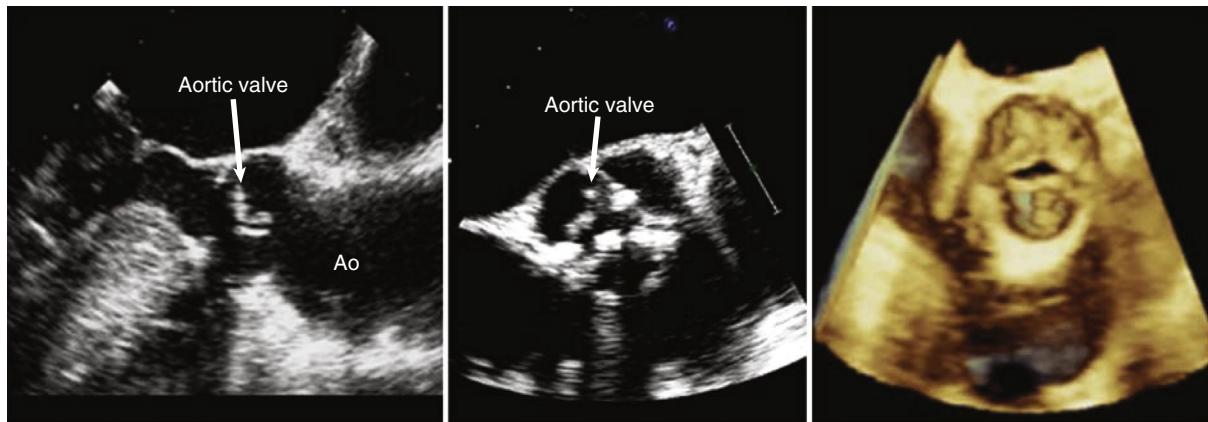
**FIGURE 16.42** Systolic TEE images of calcific aortic stenosis in a patient with a tricuspid valve. **Left,** Two-dimensional long axis. There is minimal opening of the valve. *Ao,* Aorta. **Middle,** Short axis. **Right,** Three-dimensional image. The latter two views better demonstrate the distribution of calcium.
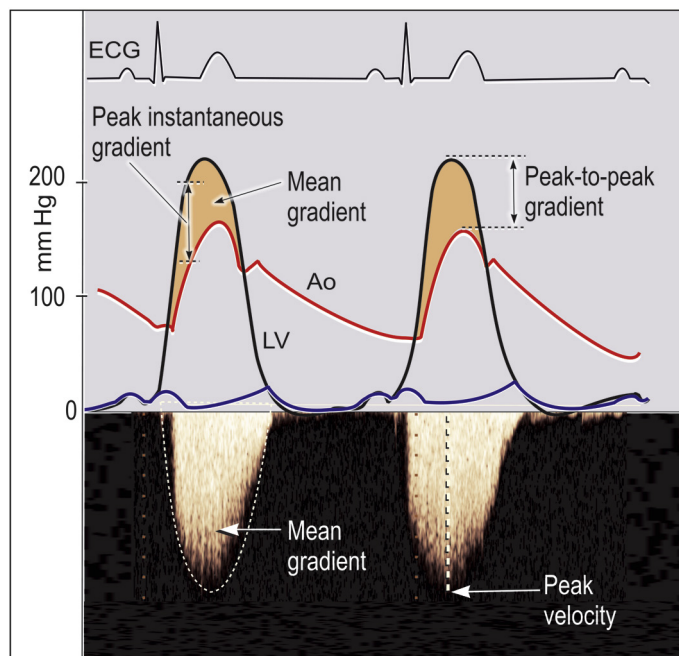


**FIGURE 16.43** Doppler methods provide peak instantaneous and mean gradients. The peak instantaneous gradient is typically higher than the peak-to-peak gradient calculated from invasively measured peak left ventricular (*LV*) and aortic (*Ao*) pressure, which is not instantaneous, although mean gradients measured with both techniques are identical.



**FIGURE 16.44** Continuity equation approach to calculating aortic valve area. The cross-sectional area (CSA) of the aortic valve ($CSA_{AV}$) is calculated as ($CSA_{LVOT} \times VTI_{LVOT}$)/$VTI_{AV}$). LVOT CSA is calculated as $\pi(D/2)^2$, where *D* is LVOT diameter. LVOT VTI should be measured from the modal rather than the maximal velocity (see Fig. 16.45).

typically, the highest velocities are found on the right parasternal view. The nonimaging Pedoff probe has a small footprint, making it essential for optimal assessment of patients with AS. When TEE is used, velocities are recorded from the deep transgastric views (see Fig. 16.19, position O). It should be noted that although echocardiographically derived mean gradients are generally identical to those obtained invasively, the echocardiographically derived peak *instantaneous* gradient is typically higher than the *peak-to-peak* gradient calculated in the catheterization laboratory (see Chapter 22). The latter is the arithmetic difference between peak LV and aortic pressure (Fig. 16.43), which may not be coincident in time.

Although gradients alone provide a reasonable assessment of the severity of AS when transaortic flow is normal, they may underestimate severity in the setting of low-flow states and overestimate severity when flow is elevated (e.g., high-output states such as those caused by sepsis and anemia). For this reason it is important to determine AVA. Direct planimetry of TEE images may be used for this purpose, but TTE planimetry is not sufficiently accurate. The most common approach is
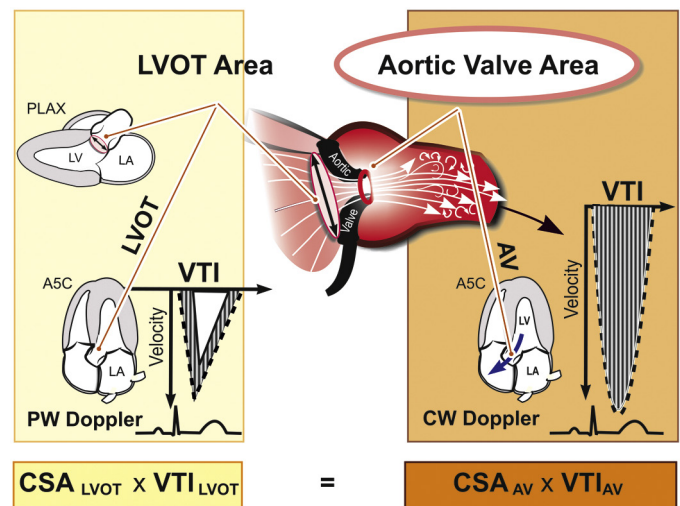
therefore by application of the continuity equation (Fig. 16.44). AVA is calculated as follows:

$$AVA = (CSA_{LVOT} \times VTI_{LVOT})/VTI_{AV}$$

Less desirable is the simplified version:

$$AVA = (CSA_{LVOT} \times V_{LVOT})/V_{AV}$$

where V represents peak velocity. The CSA of the LVOT is typically calculated by assuming circular geometry with the formula $CSA = \pi(D/2)^2$, where D is the systolic LVOT diameter measured on the parasternal or TEE-equivalent long-axis view. According to the ASE convention, the diameter is measured just proximal to the aortic annulus. It is cautioned that because the LVOT velocity incorporated into the calculation is the *modal* velocity, displayed as the densest part of the pulsed Doppler envelope, the VTI should not be traced by using the outer edge of the spectrum, which represents the maximal (not modal) velocity at each time point (Fig. 16.45). Optimal sample volume placement for pulse wave Doppler is in the LVOT immediately proximal to the site of subvalvular flow acceleration, typically 1 to 2 mm proximal to the valve on the apical five- or three-chamber (TTE) or deep transgastric (TEE) views.

### Low-Gradient Severe Aortic Stenosis
In the setting of reduced SV because of LV systolic dysfunction, leaflet excursion may appear reduced and calculated effective orifice area may be small despite low gradients, and it becomes important to
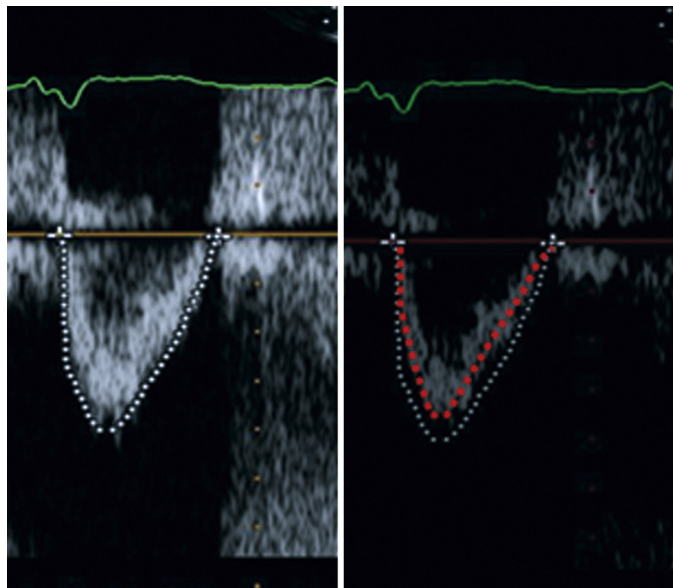
**FIGURE 16.45** Doppler spectra demonstrating the error that may be introduced if the maximal (*white dotted line*) rather than the modal (*red dotted line*) velocity is measured. The modal velocity (the most commonly occurring velocity) corresponds to the brightest portion of the Doppler spectrum.



**FIGURE 16.46** Doppler methods of quantitating aortic regurgitation (AR). A pressure half-time (PHT) greater than 500 msec suggests mild AR, 200 to 500 msec suggests moderate AR, and less than 200 msec suggests severe AR. Holodiastolic flow reversal in the descending thoracic aorta, as shown here, is consistent with at least moderate AR. *S,* Systole; *D,* diastole.

determine whether the valve obstruction is fixed (true severe AS) or the valve is intrinsically capable of opening more fully at higher flow rates (pseudosevere AS). As noted previously, DSE is routinely used in this setting, typically with close physician supervision to determine the true AVA as well as LV contractile reserve (i.e., augmentation of segmental and global contractility). The effective orifice area may also be severely reduced despite low gradients when the LVEF is within the normal range but SV is impaired, so-called paradoxical low-gradient, preserved–EF, severe AS (discussed earlier) that can occur with small restrictive ventricles or other causes of reduced forward flow including MS or regurgitation, constrictive physiology, or poorly controlled AF[62,64]

#### Subvalvular or Supravalvular Aortic Stenosis

CW Doppler echocardiographic assessment of peak and mean gradients is the cornerstone in evaluating patients with LVOT obstruction below or above the valve (see Fig. 16.41). However, by demonstrating the site of flow acceleration relative to the 2D images, color Doppler may provide a clue that the obstruction is not at the level of the valve and prompt more detailed imaging investigation of the pathophysiology. In some patients, evaluation is complicated by the presence of obstruction at multiple levels, such as the presence of both subaortic and valvular AS. In such cases, because of the trade-off between range resolution and the inability to measure accurately high velocities that is inherent in the PW Nyquist limit, it may be impossible to precisely quantitate the gradients created at each level of obstruction.

### Aortic Regurgitation (see Chapter 73)

AR may result from abnormalities in the valve cusps, normal cusps whose coaptation is altered by enlargement of the annulus and/or sinuses, or rarely, prolapse of an aortic dissection flap through the valve (see Diseases of the Aorta). Echocardiographic imaging (TTE and TEE) will establish a causative diagnosis and typically demonstrates LVED enlargement if the regurgitation is hemodynamically significant. High-frequency fluttering of the anterior mitral leaflet caused by the impact of the regurgitant jet may be evident on M-mode, and in cases of acute severe regurgitation, the mitral valve may close prematurely before ventricular systole because of a rise in LV pressure exceeding the LA pressure before ventricular contraction (eFig. 16.27).

The diagnosis of AR is most easily made when a diastolic color Doppler jet is seen in the LVOT. Small transient jets can be normal variants. Again, an integrated approach is best for determining the severity of AR, with elements including evidence of LV enlargement, color jet dimensions, spectral Doppler signal intensity, PHT, vena contracta, and
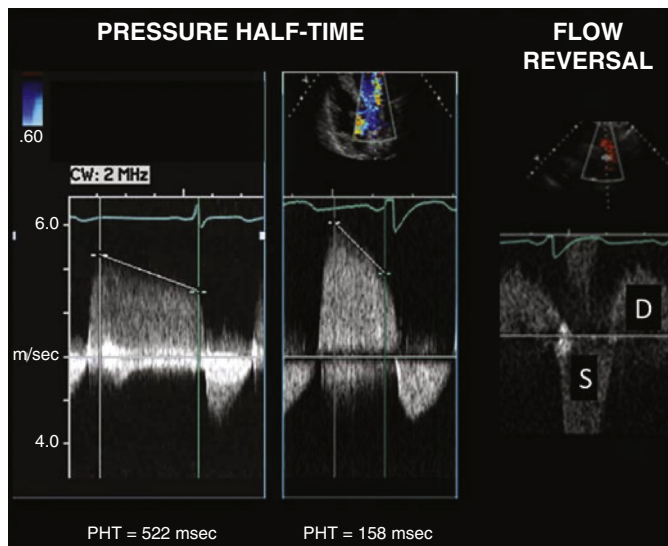
diastolic flow reversal in the descending thoracic or abdominal aorta (eFig. 16.28). Color jet dimensions should be assessed with Nyquist settings of 50 to 60 cm/sec.

The best color jet predictors of angiographic severity are the jet area/LV short-axis area ratio (parasternal short-axis view) and jet diameter indexed to LVOT diameter immediately proximal to the valve (parasternal long-axis view), but these may be misleading with eccentric jets. Jet length is not a reliable index of severity. The PHT reflects the rate at which aortic and LV pressures equalize and is most reliable in the setting of acute AR, as long as care is taken to ensure that the early diastolic velocity is captured accurately (Fig. 16.46). The vena contracta is the waist (smallest diameter) of the regurgitant flow jet at the level of the valve measured in zoom mode on a parasternal long-axis or TEE-equivalent view. A measurement > 6 mm generally correlates with severe AR. Holodiastolic flow reversal in the descending thoracic aorta as detected with the pulsed Doppler is a marker of at least moderate AR (see Fig. 16.46 and eFig. 16.28). Reversal of comparable duration as measured in the abdominal aorta generally reflects severe AR. Regurgitant volume and fraction can be calculated using a continuity-based 2D/Doppler approach (eFig. 16.29). This approach calculates regurgitant volume by comparing flow through the LVOT with that across a competent nonstenotic valve; it is most robust when the pulmonic valve is used as the reference for normal flow (image quality permitting). The mitral valve can theoretically be used as the reference but is more geometrically complex and thus more prone to error. Alternatively, both measures and EROA may be calculated with the PISA approach similar to the principles used in MR. A regurgitant volume of ≥60 mL and EROA of ≥0.30 cm² are consistent with severe AR.[64,65]

## Tricuspid Valve (see Chapter 77)

#### Tricuspid Valve Anatomy

The tricuspid valve is the largest cardiac valve and is anatomically complex, with anterior, posterior, and septal leaflets extending from a saddle-shaped tricuspid annulus to chordae and variable papillary muscle/trabecular attachments. Even though the anterior and septal leaflets are well seen on multiple echocardiographic views, the posterior leaflet is visualized only on the RV inflow tract view and on short-axis views of the right ventricle (which can display all three leaflets). Because of its importance in imaging the tricuspid valve, on TTE the RV inflow tract view must be acquired in a manner that displays the inferior (diaphragmatic) wall but avoids the interventricular septum and septal leaflet of
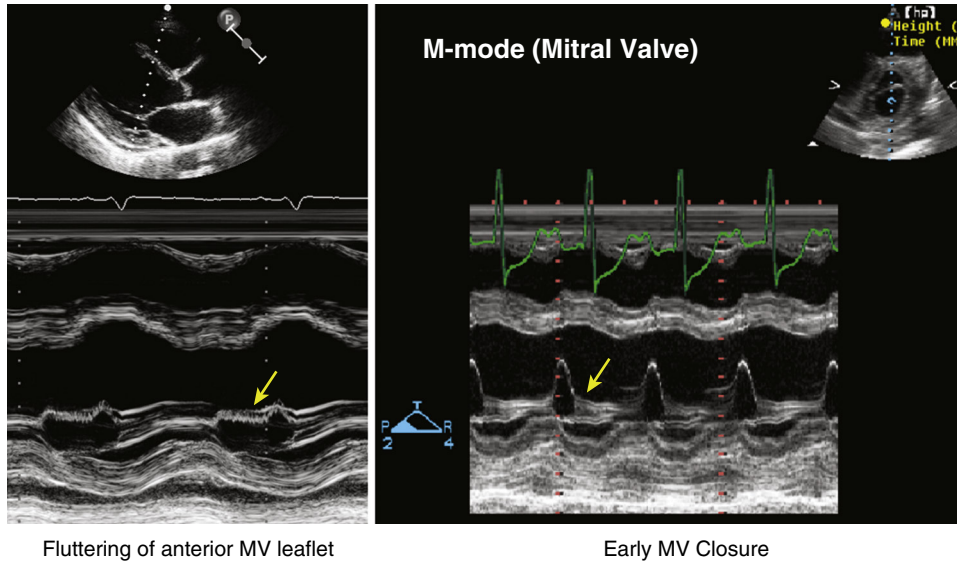
Fluttering of anterior MV leaflet                    Early MV Closure

**EFIGURE 16.27** Severe aortic insufficiency affects M-mode of the mitral valve. **Left,** Anterior mitral valve leaflet fluttering in diastole. **Right,** Early closure of the mitral valve (*arrows*).
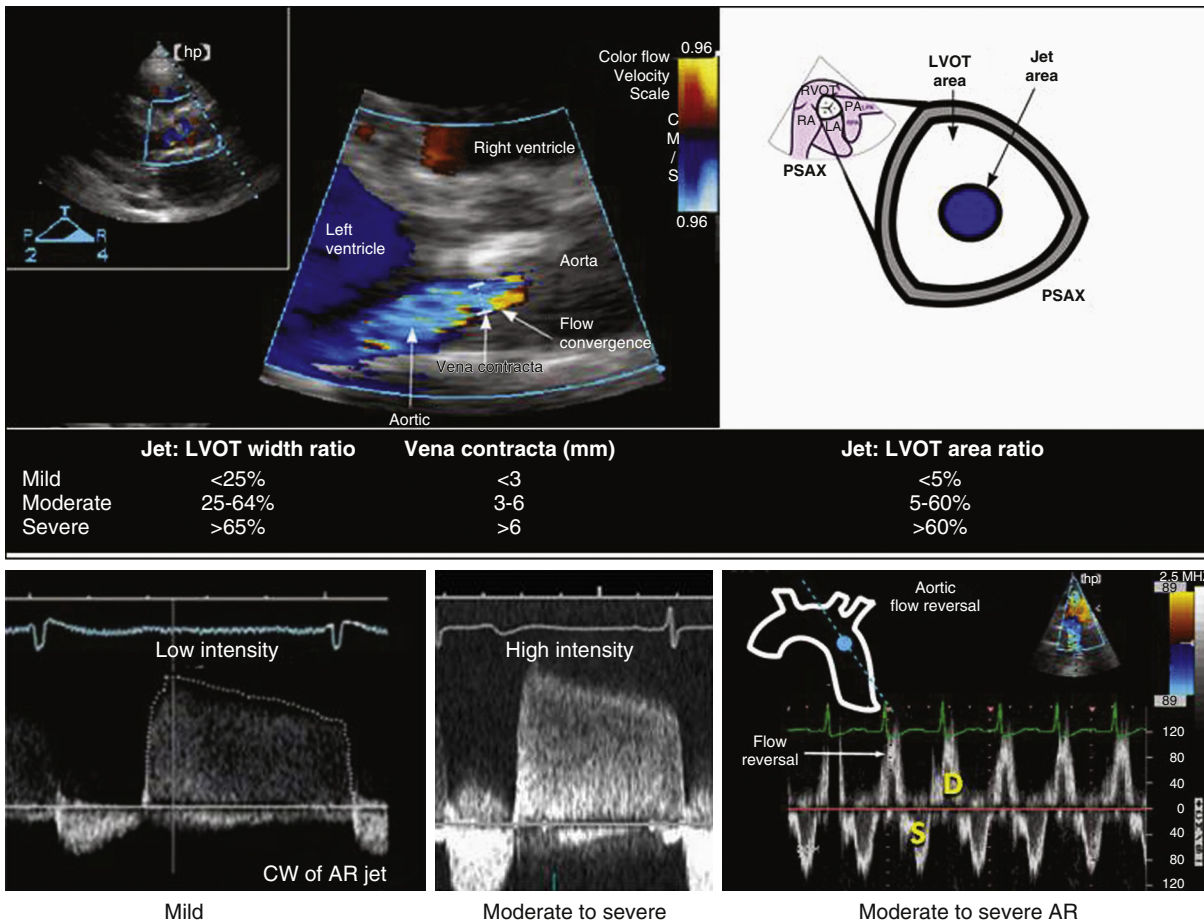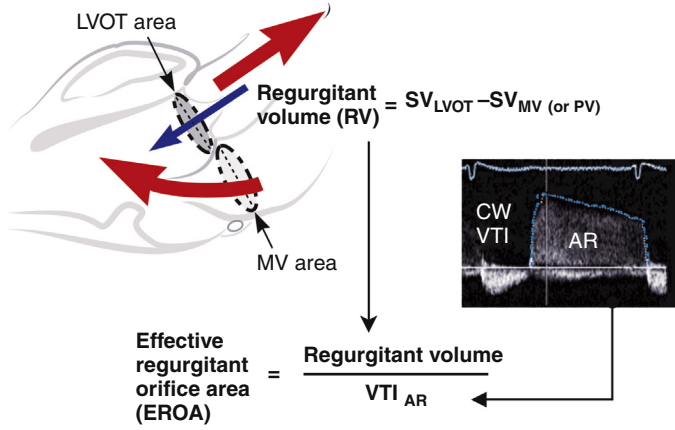


| | Jet: LVOT width ratio | Vena contracta (mm) | Jet: LVOT area ratio |
|---|---|---|---|
| Mild | <25% | <3 | <5% |
| Moderate | 25-64% | 3-6 | 5-60% |
| Severe | >65% | >6 | >60% |

**EFIGURE 16.28** Aortic regurgitation (AR) grading by semiquantitative parameters. **Top panel,** Color Doppler zoomed in on the parasternal long axis (*left*) view of the aortic valve showing the AR jet. Parameters that correlate roughly with grades of AR are shown in the chart below each measurement. The jet height and left ventricular outflow tract (LVOT) height are measured directly on the images. The jet area can be traced by planimetry. LVOT area is calculated as $0.785 \times (\text{LVOT diameter}/2)^2$. **Bottom: Left panels,** CW Doppler of the jet in apical five-chamber view, showing that the density of the CW jet in diastole, relative to the forward-flow envelope, correlates roughly with the severity of AR. **Right panel,** PW Doppler with the pulse sample volume placed in the descending thoracic aorta near the origin of the left subclavian artery, showing that there is diastolic flow reversal suggestive of at least moderate AR. If diastolic flow reversal is seen even more distally, in the abdominal aorta, the AR is likely severe.

EVALUATION OF THE PATIENT

III



LVOT area

Regurgitant volume (RV) $= SV_{LVOT} - SV_{MV \text{ (or PV)}}$

MV area

CW VTI   AR

Effective regurgitant orifice area (EROA) $= \dfrac{\text{Regurgitant volume}}{VTI_{AR}}$

| | EROA (cm²) | RV(ml) |
|---|---|---|
| Mild | <0.10 | <30 |
| Moderate | 0.10–0.29 | 30–59 |
| Severe | >0.30 | >60 |

**EFIGURE 16.29** Calculation of the aortic effective regurgitant orifice area (EROA), using quantitative Doppler methods based on the continuity equation. The EROA represents the average size of the defect in the aortic valve during diastole and is proportional to regurgitant severity. The regurgitant volume (RV) across the aortic valve may be calculated as the difference between the LVOT volume ($SV_{LVOT}$) and the transmitral volume ($SV_{MV}$) or transpulmonic volume ($SV_{PV}$), assuming there is no significant mitral (or pulmonic) regurgitation. Alternatively $SV_{LVOT}$ may be calculated as LVEDV – LVESV, where LVEDV and LVESV are the LV end-diastolic and end-systolic volumes traced from endocardial borders and calculated by modified Simpson's equation, respectively.
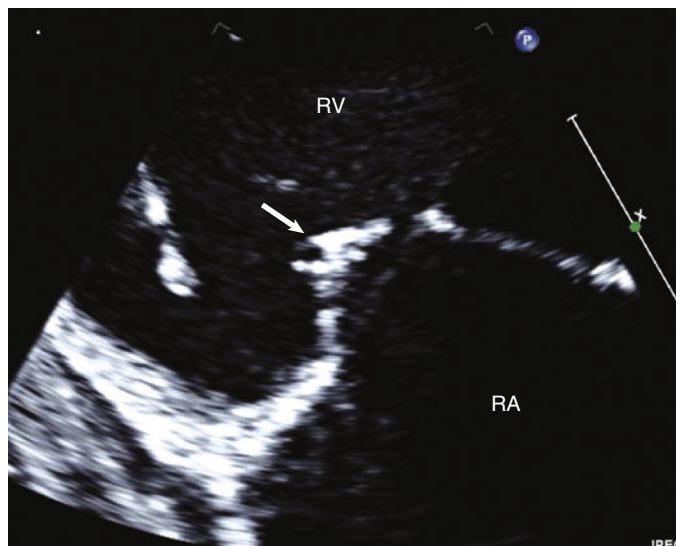
FIGURE 16.47 Right ventricular inflow tract view demonstrating diastolic doming of the posterior leaflet (*arrow*) characteristic of rheumatic tricuspid valve disease. *RA,* Right atrium; *RV,* right ventricle.

the tricuspid valve (see Fig. 16.8). Although all 3 leaflets can often be seen in transgastric TEE views, 3D echocardiography more reliably permits visualization of all the leaflets in an en-face view from the atrial or RV side.

### Acquired Disorders of the Tricuspid Valve

Tricuspid stenosis occurs in approximately 11% of patients with rheumatic mitral disease and is characterized by diastolic leaflet doming, as well as by leaflet and chordal thickening (Fig. 16.47 and Video 16.42). Severity is best assessed by Doppler-derived mean gradients. Methods for calculating valve area, including the PHT approach, have not been validated for tricuspid stenosis (see Chapter 77).

Pathologic TR most frequently occurs on a functional basis, that is, attributable to RV (and RA) enlargement or dysfunction. RV pathology, in turn, may be due to pulmonary hypertension and left-sided cardiac abnormalities. Isolated RA and tricuspid annular enlargement may be the consequence of AF. The echocardiographic hallmark of functional TR is apical tethering, which when severe may result in a visible regurgitant orifice (noncoaptation of the leaflets) (Fig. 16.48). Under these conditions the regurgitant jet could be laminar (nonturbulent) and relatively low velocity because of the almost complete equalization of pressures between the right ventricle and the right atrium and could lead to underestimation of the severity of the TR. Similarly, estimation of PASP from TR jet velocity will be inaccurate in this situation.

Myxomatous tricuspid valve disease, the most common cause of primary TR, has been less well studied than mitral disease. It accompanies MVP in 20% of patients. Because there is great variability in the mobility and size of the three tricuspid leaflets, there are less clear-cut criteria for the diagnosis in the TV. Unlike the mitral valve, spontaneous flail of the tricuspid valve virtually never occurs. Less common acquired causes of primary TR include carcinoid, rheumatic disease, endocarditis, trauma (including iatrogenic injury to the valve during RV biopsy as well as blunt trauma), and deformation or damage by pacemaker and defibrillator wires. The characteristic echocardiographic appearance of carcinoid heart disease is drumstick-like, rigid, and shortened leaflets with at times a visible regurgitant orifice (Fig. 16.49 and Video 16.43). Carcinoid involvement of the tricuspid valve may be associated with mixed tricuspid stenosis and regurgitation; the pulmonic valve may be similarly involved. Carcinoid involvement of the mitral valve is rare and suggests either pulmonary metastases or a right to left shunt. Absence of concomitant mitral involvement may help distinguish carcinoid from rheumatic tricuspid disease.

### Quantitation of Tricuspid Regurgitation

Quantitation of TR is similar to that for MR and consists of an integrated parametric approach,[66] including measures of jet size, vena contracta, and PISA-derived regurgitant volume and EROA. Systolic flow reversal into the hepatic veins is specific for severe TR and may be appreciated with color and PW Doppler or with saline contrast.

## Pulmonic Valve (see Chapter 77)

### Pulmonic Valve Anatomy

The normal pulmonic valve is tricuspid with a structure that is similar to that of the aortic valve. The cusps are named right, left, and anterior, although it is unusual to be able to see all three cusps simultaneously with 2D imaging. The pulmonic valve can be seen on parasternal and subcostal views, as well as on anteriorly oriented apical views. TEE windows include the midesophageal, deep transgastric, and high esophageal (at the level of the aortic arch). The most common congenital anomaly is valvular stenosis, based on developmental abnormalities that mimic those of a bicuspid aortic valve (eFig. 16.30). It is characterized by systolic doming and a jump rope–like appearance of the valve (Video 16.44). Congenital pulmonic stenosis may be isolated or may occur as a feature of more complex congenital anomalies. Acquired pulmonic disease is rare with causes that include carcinoid and endocarditis, as well as iatrogenic regurgitation due to disruption of the valve from balloon or surgical valvuloplasty for congenital stenosis.

### Quantitation of Valve Dysfunction

Pulmonic stenosis is most reliably quantitated with mean and peak gradients, although the continuity equation provides a means of calculating valve area. Pulmonic regurgitation is usually graded on the basis of jet dimensions, with the caveat that there may be little turbulence in the setting of severe regurgitation with normal pulmonary pressure, which can lead to inadvertent underestimation of the true severity. Using Doppler, a wide color jet origin width plus laminar regurgitant flow and rapid diastolic flow deceleration on spectral Doppler are clues to severe regurgitation. (Figs. 16.49E and 16.50). Mild-to-moderate degrees of pulmonic regurgitation may be seen in patients with dilatation of the pulmonary artery and pulmonary hypertension.

## Prosthetic Valves (see Chapter 79)

Echocardiographic assessment of prosthetic valves requires an understanding of valve design, normal functional characteristics, and the imaging artefacts introduced by valve elements.

The most commonly encountered mechanical valves are bileaflet or single, tilting disc valves. Ball-and-cage valves, which are no longer implanted, are now quite rare. Most bioprosthetic valves are stented porcine or bovine pericardial valves, although freestyle (stentless) xenograft, cadaveric homograft, autograft (Ross procedure), and transcatheter and sutureless surgical valves are also available. Prosthetic annular rings are also often used for mitral and tricuspid repair. The sewing rings of all valves, as well as the occluders of mechanical valves, may cause acoustic shadowing that limits imaging and Doppler assessment; the exceptions to this are the stentless, homograft, and autograft valves, which may be indistinguishable from native valves. Additionally, the material of the ball in ball-and-cage valves transmits sound more slowly than human tissue does, with the result that the ball appears much larger than its actual size when imaged echocardiographically.

Even normally functioning prostheses tend to be intrinsically stenotic, with the degree of stenosis inversely related to valve size. Additionally, trivial degrees of valvular regurgitation are normal findings, and although not normal, trivial paravalvular regurgitation is not uncommon. Intraventricular microcavitations (apparent "microbubbles," thought to be caused by transient localized pressure drop at the site of prosthetic valve closure vaporizing blood) are often seen in the left heart in the presence of mechanical valves and are considered normal. Figures 16.51 to 16.53 and Video 16.45 demonstrate the normal echocardiographic appearance of the most common
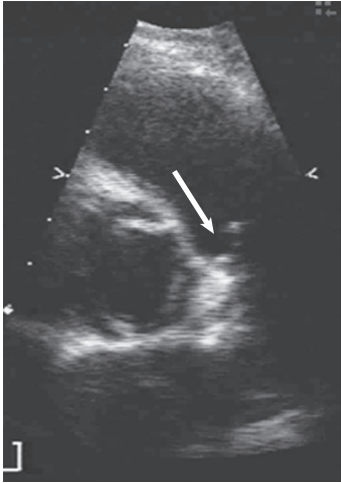
**EFIGURE 16.30** Systolic parasternal short-axis view demonstrating systolic dom-ing of this congenitally stenotic pulmonic valve (*arrow*). In real time the valve has a jump rope appearance.
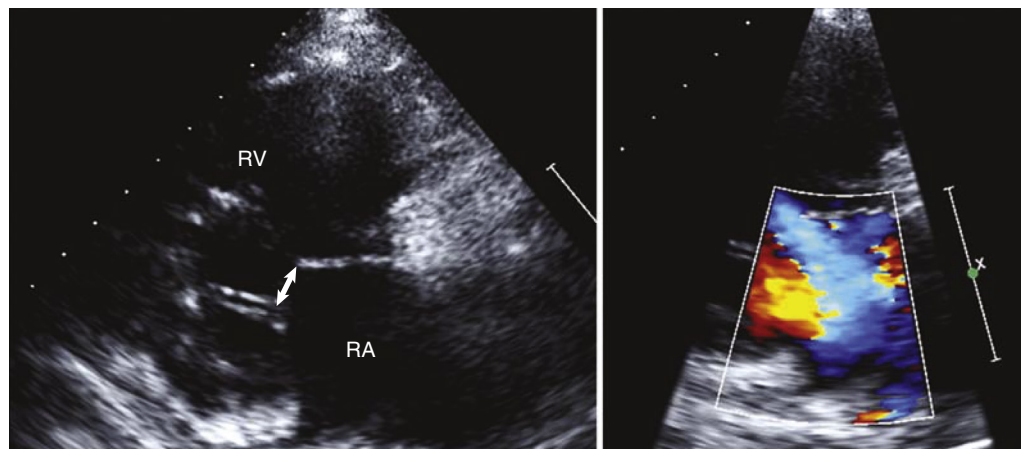
FIGURE 16.48 **Left,** Right ventricular inflow tract view showing failure of coaptation of the anterior and posterior leaflets (*arrow*) in a patient with severe functional tricuspid regurgitation. *RA,* Right atrium; *RV,* right ventricle. **Right,** Severity may be underestimated because of its low velocity and monochromatic appearance.
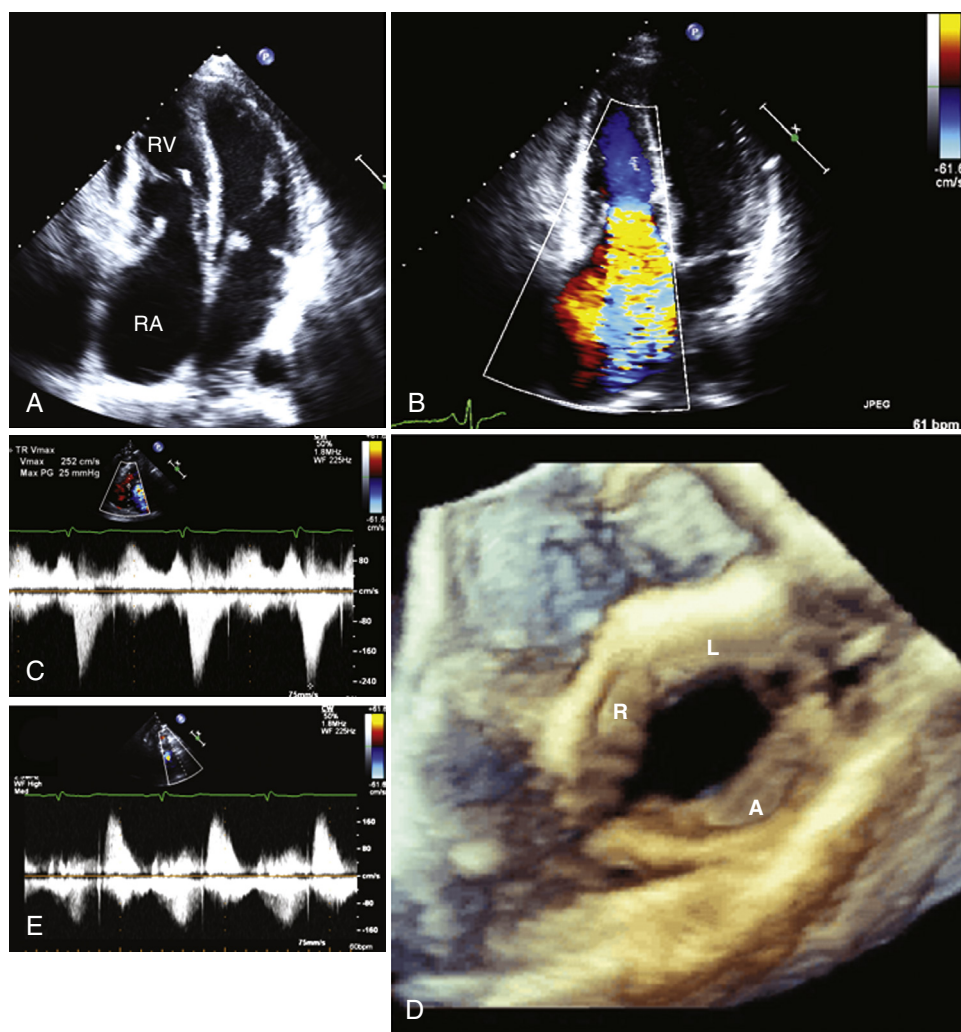


FIGURE 16.49 Carcinoid heart disease. **A**, Apical 4-chamber view, demonstrating the thickened and retracted tricuspid valve, characteristic drumstick-like appearance, frozen in the half-open, half-closed position. The interventricular septum is distended leftwards and the right atrium is severely enlarged. *RA,* Right atrium; *RV,* right ventricle. **B**, Severe tricuspid regurgitation through the wide-open valve (See Video 16.43). **C**, CW Doppler of the tricuspid antegrade and regurgitant flow, illustrating a mildly ste- notic valve but severe tricuspid regurgitation. The remarkably rapid slope of deceleration of the tricuspid regurgitant jet is indica- tive of severely elevated right atrial pressure. **D**, 3D live TEE view from the pulmonary arterial aspect of the similarly thickened and retracted pulmonic valve (*R*, right; *L*, left; *A*, anterior leaflet). **E**, CW Doppler of the pulmonic antegrade and regurgitant flow (from transthoracic echocardiogram), illustrating only a mildly stenotic pulmonic valve but severe pulmonic regurgitation, as evidenced by the dense jet with a very rapid deceleration time.

prostheses. eTable 16.5 provides normal echocardiographic values for the most common implanted valves. More current data, includ- ing recently introduced prosthe- ses, are collated from the literature and valve manufacturers at www. valveguide.ch.[68] A helpful rule of thumb when valve size is unknown is that for common-size prostheses in patients with physio- logic heart rates and SV, the peak transaortic velocity should be less than 3 m/sec and the mean trans- mitral gradient 5 to 6 mm Hg or lower.[68,69] Stentless bioprosthetic valves, which have little or no acoustic shadowing due to lack of a rigid annulus, are designed to have lower hemodynamic profiles (i.e., lower gradients) than their equivalently sized first-generation predecessors and appear useful for implantation in patients with a small annulus or severely reduced LV function.

The echocardiographic approach to prosthetic valves is similar to but often more challenging than that of native valves. Peak and mean gradients are calculated by using the conventional appli- cation of the Bernoulli equation, and effective orifice area may be calculated with the continuity equation. Additionally, the Dop- pler velocity or "dimensionless" index, defined as the ratio of the VTI (or peak velocity) proximal to the valve to that distal to the valve, provides an alternative metric of aortic prosthetic function that is useful when LVOT diameter can- not be measured. A value less than 0.25 is highly suggestive of valvular obstruction. As for native valves, it is critical that LVOT sampling be proximal to the site of flow accel- eration; in the case of transcatheter or sutureless valves, the sampling volume should be proximal to the inlet of the metal frame because in these valves there is acceleration of flow at the inlet, as well as at the level of the cusps. For mitral pros- theses, the comparable measure is the ratio of mitral to aortic VTI with values less than 2.2 consid- ered normal. In the patient with AF, matching of cycle lengths for beats used for LVOT and valvular VTIs is preferred to averaging over multi- ple beats. Beats corresponding to physiologic heart rates should be used if available. Although the PHT may be useful in a relative sense in patients with mitral prostheses (with PHT ≥130 ms considered

**ETABLE 16.5 Normal Values for Implanted Valves**

| AORTIC VALVES | SIZE (mm) | PEAK GRADIENT (mm Hg) | MEAN GRADIENT (mm Hg) | EFFECTIVE ORIFICE AREA (cm²) |
|---|---|---|---|---|
| Carpentier-Edwards Pericardial Stented bovine pericardial | 19 | 32.1 ± 3.4 | 24.2 ± 8.6 | 1.2 ± 0.3 |
| | 21 | 25.7 ± 9.9 | 20.3 ± 9.1 | 1.5 ± 0.4 |
| | 23 | 21.7 ± 8.6 | 13.0 ± 5.3 | 1.8 ± 0.3 |
| | 25 | 16.5 ± 5.4 | 9.0 ± 2.3 | |
| Carpentier-Edwards Standard Stented porcine | 19 | 43.5 ± 12.7 | 25.6 ± 8.0 | 0.9 ± 0.2 |
| | 21 | 27.7 ± 7.6 | 17.3 ± 6.2 | 1.5 ± 0.3 |
| | 23 | 28.9 ± 7.5 | 16.1 ± 6.2 | 1.7 ± 0.5 |
| | 25 | 24.0 ± 7.1 | 12.9 ± 4.6 | 1.9 ± 0.5 |
| | 27 | 22.1 ± 8.2 | 12.1 ± 5.5 | 2.3 ± 0.6 |
| | 29 | | 9.9 ± 2.9 | 2.8 ± 0.5 |
| Hancock Stented porcine | 21 | 18.0 ± 6.0 | 12.0 ± 2.0 | |
| | 23 | 16.0 ± 2.0 | 11.0 ± 2.0 | |
| | 25 | 15.0 ± 3.0 | 10.0 ± 3.0 | |
| Hancock II Stented porcine | 21 | | 14.8 ± 4.1 | 1.3 ± 0.4 |
| | 23 | 34.0 ± 13.0 | 16.6 ± 8.5 | 1.3 ± 0.4 |
| | 25 | 22.0 ± 5.3 | 10.8 ± 2.8 | 1.6 ± 0.4 |
| | 29 | 16.2 ± 1.5 | 8.2 ± 1.7 | 1.6 ± 0.2 |
| Medtronic Mosaic Stented porcine | 21 | | 14.2 ± 5.0 | 1.4 ± 0.4 |
| | 23 | 23.8 ± 11.0 | 13.7 ± 4.8 | 1.5 ± 0.4 |
| | 25 | 22.5 ± 10.0 | 11.7 ± 5.1 | 1.8 ± 0.5 |
| | 27 | | 10.4 ± 4.3 | 1.9 ± 0.1 |
| | 29 | | 11.1 ± 4.3 | 2.1 ± 0.2 |
| Medtronic-Hall Single tilting disc | 20 | 34.4 ± 13.1 | 17.1 ± 5.3 | 1.2 ± 0.5 |
| | 21 | 26.9 ± 10.5 | 14.1 ± 5.9 | 1.1 ± 0.2 |
| | 23 | 26.9 ± 8.9 | 13.5 ± 4.8 | 1.4 ± 0.4 |
| | 25 | 17.1 ± 7.0 | 9.5 ± 4.3 | 1.5 ± 0.5 |
| | 27 | 18.9 ± 9.7 | 8.7 ± 5.6 | 1.9 ± 0.2 |
| St. Jude Medical Standard Bileaflet | 19 | 42.0 ± 10.0 | 24.5 ± 5.8 | 1.5 ± 0.1 |
| | 21 | 25.7 ± 9.5 | 15.2 ±5.0 | 1.4 ± 0.4 |
| | 23 | 21.8 ± 7.5 | 13.4 ± 5.6 | 1.6 ± 0.4 |
| | 25 | 18.9 ± 7.3 | 11.0 ± 5.3 | 1.9 ± 0.5 |
| | 27 | 13.7 ± 4.2 | 8.4 ± 3.4 | 2.5 ± 0.4 |
| | 29 | 13.5 ± 5.8 | 7.0 ± 1.7 | 2.8 ± 0.5 |

| MITRAL VALVES | SIZE (mm) | PEAK GRADIENT (mm Hg) | MEAN GRADIENT (mm Hg) | PEAK VELOCITY (m/sec) | PRESSURE HALF-TIME (msec) | EFFECTIVE ORIFICE AREA (cm²) |
|---|---|---|---|---|---|---|
| Carpentier-Edwards Stented bioprosthesis | 27 | | 6 ± 2 | 1.7 ± 0.3 | 98 ± 28 | |
| | 29 | | 4.7 ± 2 | 1.76 ± 0.27 | 92 ± 14 | |
| | 31 | | 4.4 ± 2 | 1.54 ± 0.15 | 92 ± 19 | |
| | 33 | | 6 ± 3 | | 93 ± 12 | |
| Carpentier-Edwards Pericardial Stented bioprosthesis | 27 | | 3.6 | 1.6 | 100 | |
| | 29 | | 5.25 ± 2.36 | 1.67 ± 0.3 | 110 ± 15 | |
| | 31 | | 4.05 ± 0.83 | 1.53 ± 0.1 | 90 ± 11 | |
| | 33 | | 1 | 0.8 | 80 | |
| Hancock I or not specified Stented bioprosthesis | 27 | 10 ± 4 | 5 ± 2 | | 115 ± 20 | 1.3 ± 0.8 |
| | 29 | 7 ± 3 | 2.46 ± 0.79 | | 95 ± 17 | 1.5 ± 0.2 |
| | 31 | 4 ± 0.86 | 4.86 ± 1.69 | | 90 ± 12 | 1.6 ± 0.2 |
| | 33 | 3 ± 2 | 3.87 ± 2 | | | 1.9 ± 0.2 |
| Hancock II Stented bioprosthesis | 27 | | | | | 2.21 ± 0.14 |
| | 29 | | | | | 2.77 ± 0.11 |
| | 31 | | | | | 2.84 ± 0.1 |
| | 33 | | | | | 3.15 ± 0.22 |
| Medtronic-Hall Tilting disc | 27 | | | 1.4 | 78 | |
| | 29 | | | 1.57 ± 0.1 | 69 ± 15 | |
| | 31 | | | 1.45 ± 0.12 | 77 ± 17 | |
| St. Jude Medical Bileaflet | 23 | | 4 | 1.5 | 160 | 1 |
| | 25 | | 2.5 ± 1 | 1.34 ± 1.13 | 75 ± 4 | 1.35 ± 0.17 |
| | 27 | 11 ± 4 | 5 ± 1.82 | 1.61 ± 0.29 | 75 ± 10 | 1.67 ± 0.17 |
| | 29 | 10 ± 3 | 4.15 ± 1.8 | 1.57 ± 0.29 | 85 ±10 | 1.75 ± 0.24 |
| | 31 | 12 ± 6 | 4.46 ± 2.22 | 1.59 ± 0.33 | 74 ± 13 | 2.03 ± 0.32 |

From Zoghbi WA, John B Chambers, Jean G Dumesnil, et al. Recommendations for evaluation of prosthetic valves with echocardiography and Doppler ultrasound. A report from the American Society of Echocardiography's Guidelines and Standards Committee and the Task Force on Prosthetic Valves. *J Am Soc Echocardiogr*. 2009;22:975. See also www.valveguide.ch for more recent data and models.

suggestive of obstruction),[69] it does not provide a valid measure of effective orifice area.

In many centers, intraoperative TEE is performed routinely during valve procedures, and these studies can both alert the surgeon to remediable complications before chest closure and serve as reference studies for follow-up evaluation. It is also recommended that TTE be performed soon—either before hospital discharge or within 3 months—after implantation to define the baseline appearance and structure with this modality and under more physiologic conditions than those present in the immediate postpump period (see Chapter 79). For all studies, chamber dimensions and function and estimated PASP, as well as heart rate, blood pressure, and BSA, should be included in the report. For postoperative echocardiographic evaluation, it is important to obtain information on valve type and size and details of the valve implantation when possible.

### Abnormalities in Valve Appearance

Abnormalities in valve appearance include evidence of an unusual implantation position or valvular dehiscence, which when extensive is characterized by pathologic valve rocking (Video 16.46). Although extensive bioprosthetic cusp thickening is typically associated with functional disturbance (see later), mild abnormalities may not affect valve function. Similarly, valve vegetation and thrombus may be functionally silent. Therefore, echocardiographic evaluation must focus on structure even when function is normal, with ensuing TEE planned if TTE images are nondiagnostic.

### Approach to Assessing Elevated Prosthetic Gradients

The diagnosis of prosthetic stenosis is suggested when gradients are elevated and the effective orifice area is reduced relative to published norms. Comprehensive guidelines from national echocardiography societies have been published (and more recently reviewed)[69]. For aortic prostheses, a Doppler velocity index less than 0.25 or a ratio of acceleration to ejection times greater than 0.4 supports the diagnosis. For mitral prostheses per ASE guidelines, a PHT >200 msec, peak E wave ≥2.5 m/sec, or $VTI_{MV}/VTI_{LVOT}$ of ≥2.5 suggests severe stenosis vs normal values of less than 130 msec, less than 1.9 and less than 2.2 m/sec respectively. As with native valves, gradients must be interpreted in the context of heart rate. Causes of prosthetic stenosis include restricted leaflet/disc motion because of thrombus (Fig. 16.54 and Video 16.47), pannus ingrowth (Fig. 16.55), vegetation, or in the case of bioprostheses, cusp calcification and degeneration (Fig. 16.56). Differentiation between pannus and thrombus may be challenging, although thrombi tend to have a softer echotexture than pannus and may be larger with extension beyond the sewing ring. Clinical factors suggesting thrombus include the acuity of symptom onset and a history of inadequate anticoagulation. Because the restricted motion may be intermittent, it is important to capture multiple beats if prosthetic dysfunction is clinically suspected. TEE is frequently required to image valves optimally, and fluoroscopy or CTA may be helpful when abnormal occluder motion is suspected in mechanical valves.
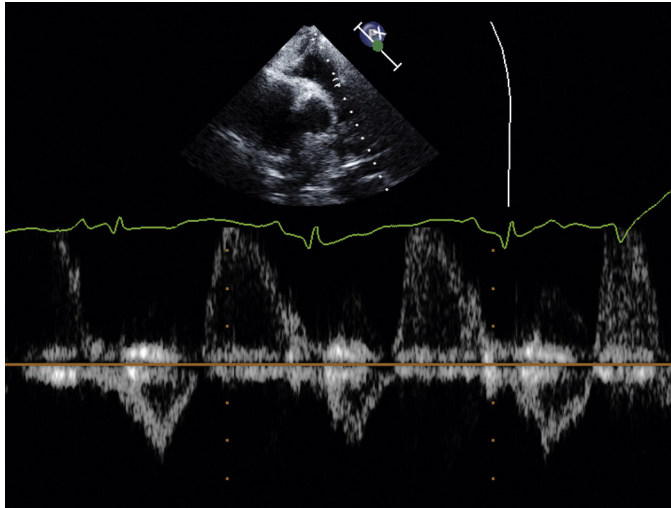


**FIGURE 16.50** PW Doppler interrogation of the RVOT in a patient who has undergone pulmonary valvotomy. There is severe pulmonic regurgitation resulting in a laminar regurgitant signal.
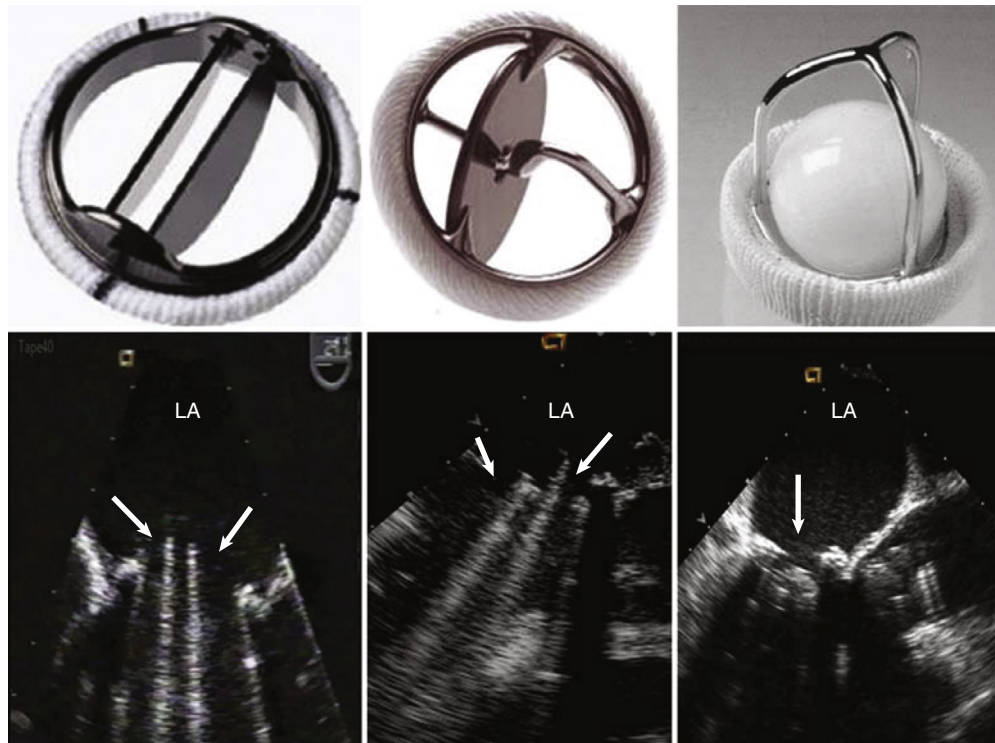


**FIGURE 16.51** Mechanical prostheses and their transesophageal echocardiographic (TEE) appearance when implanted in the mitral position. **Left panels**, St. Jude bileaflet valve. *Arrows* indicate discs in the open position. **Middle panels,** Medtronic-Hall tilting single disc valve. The *right arrow* indicates the disc in the open position, and the *left arrow* indicates reverberation from the central pivot. **Right panels,** Starr Edwards ball-and-cage valve. The *arrow* points to the valve in the open position. *LA,* Left atrium.

Notably, elevated gradients do not always reflect prosthetic stenosis. *Patient-prosthesis mismatch* (PPM) refers to the situation in which the implanted valve, although functioning normally, has elevated gradients (see Chapter 79). This occurs when patient anatomy necessitates the implantation of a smaller-than-ideal valve. The diagnosis is made by confirming that the calculated effective orifice area is consistent with normal function, but the *indexed* orifice area is ≤0.85 cm²/m² for aortic prostheses and less than 1.2 cm²/m² for mitral prostheses. For aortic prostheses an indexed effective orifice area less than 0.65 cm²/m² is considered severe PPM, a phenomenon encountered in 2% to 11% of patients. PPM is best studied for the aortic valve and is reportedly associated with poorer outcomes, although in obese patients it is unclear whether the indexed effective orifice area should be calculated on the basis of lean rather than actual body mass.

Elevated gradients may also be a consequence of significant regurgitation, which when paravalvular in origin may be underappreciated on initial evaluation. A final important cause of elevated gradients in aortic prostheses, *pressure recovery,* refers to the tendency for Doppler-derived gradients to overestimate those registered invasively.

This occurs because Doppler measures the largest gradient, typically encountered at the vena contracta, whereas invasive measurements reflect pressure distal to the valve where there has been recovery either because blood has moved from the narrow valve orifice into the wider aorta (i.e., a flask-shaped aortic root, which is a significant factor only in the setting of aortas measuring <3 cm) or, in the case of bileaflet mechanical valves, because the lower pressure encountered in the central orifice is augmented by higher pressure caused by eddies at the lateral orifices (eFig. 16.31). Pressure recovery is most important clinically in the setting of small (≤21 mm) bileaflet valves in the aortic position. As demonstrated, the measurements most representative of invasive gradients is obtained by carefully interrogating the lateral orifices, but this generally requires TEE. Alternatively, it has been suggested that gradients recorded through the central orifice may be corrected by applying the pressure loss coefficient of 0.64. (Of note, the reported normal values in eTable 16.5 are uncorrected.)

### Prosthetic Regurgitation

Trivial degrees of valvular regurgitation are normal findings, although the location of normal jets varies depending on the valve type. Pathologic regurgitation which is termed *central* (*trans*valvular) originates from within the sewing ring (central, transvalvular origin), which should be distinguished from *para*valvular regurgitation which arises external to the annulus. Valvular regurgitation in mechanical valves typically reflects occluder malfunction as a result of pannus, thrombus, vegetation, or rarely, retained mitral valve apparatus preventing full leaflet closure, whereas in bioprostheses, this is typically a result of cusp degeneration or disruption from endocarditis. Paravalvular regurgitation may be a residual finding resulting from suboptimal implantation or may develop de novo from endocarditis or spontaneous valve dehiscence. Some degree of paravalvular regurgitation is a common finding after transcatheter aortic valve implantation (see Chapter 72), but moderate or greater degrees appear to be associated with a worse prognosis (Fig. 16.57).
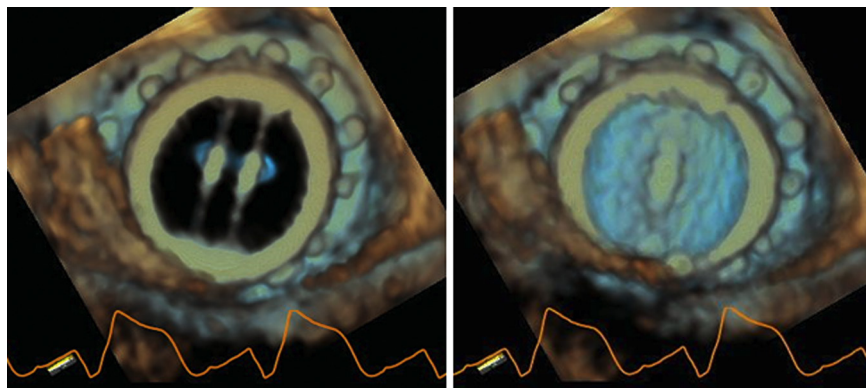


**FIGURE 16.52** Three-dimensional TEE views of a bileaflet mechanical prosthesis as viewed from the left atrial aspect in diastole (**left**, with discs open) and systole (**right**, with discs closed). (See corresponding Video 16.47.)
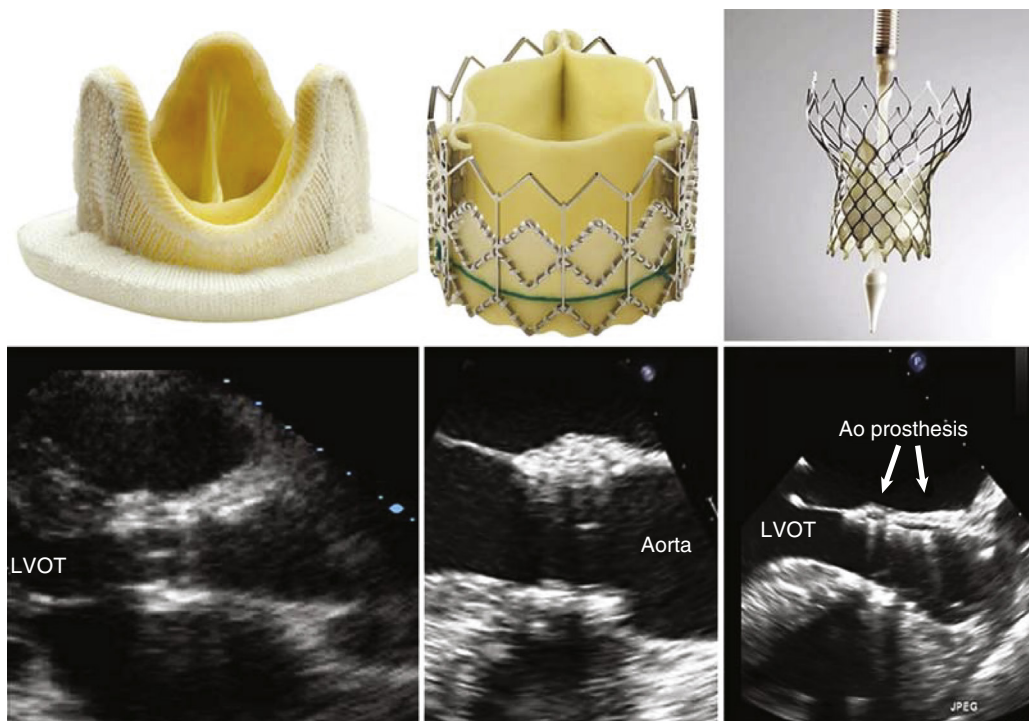


**FIGURE 16.53** Bioprostheses and their echocardiographic long-axis appearance when implanted in the aortic (*Ao*) position. **Left panels,** Heterograft stented bioprosthesis. **Middle panels,** Sapien balloon expandable transcatheter aortic valve. **Right panels,** CoreValve self-expanding transcatheter aortic valve. *LVOT,* Left ventricular outflow tract.
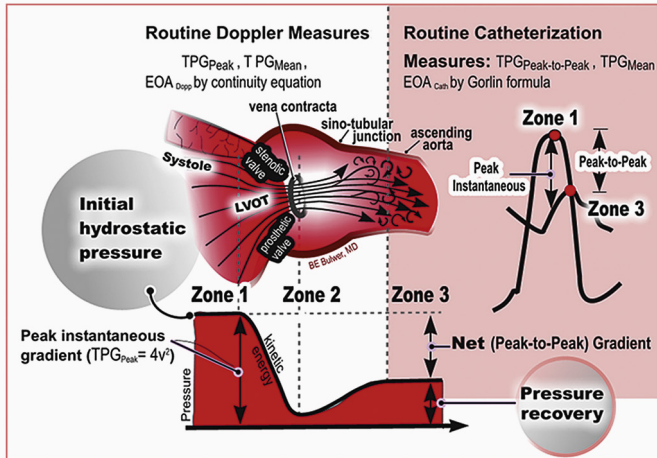
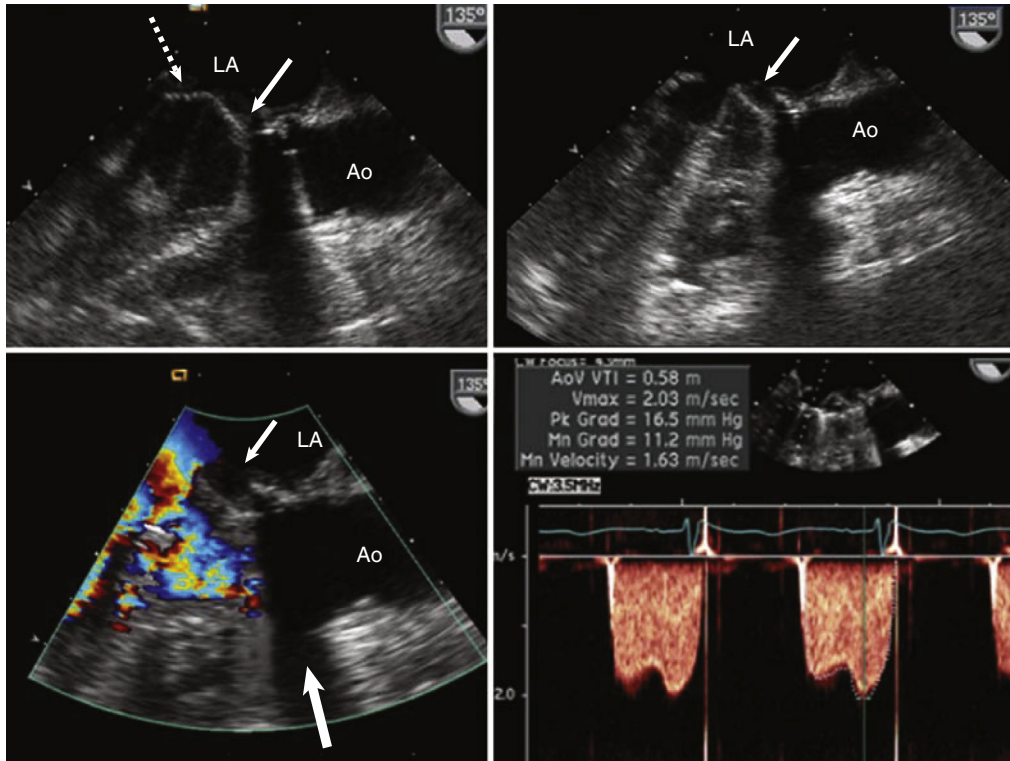**EFIGURE 16.31** The pressure recovery phenomenon.

**FIGURE 16.54** TEE showing a bileaflet mechanical mitral prosthesis in which one disc is immobilized because of thrombus. **Upper left,** Systolic frame showing that neither disc (*arrows*) closes completely. **Upper right,** While the left disc opens fully, the right disc is immobile. **Lower left,** Color flow Doppler demonstrating high-velocity flow through a single orifice. The *large arrow* indicates acoustic shadowing because of the mitral sewing ring. **Lower right,** Doppler demonstrating an elevated transmitral gradient (11 mm Hg at a heart rate of 65 beats/min). *Ao,* Aorta; *LA,* left atrium.
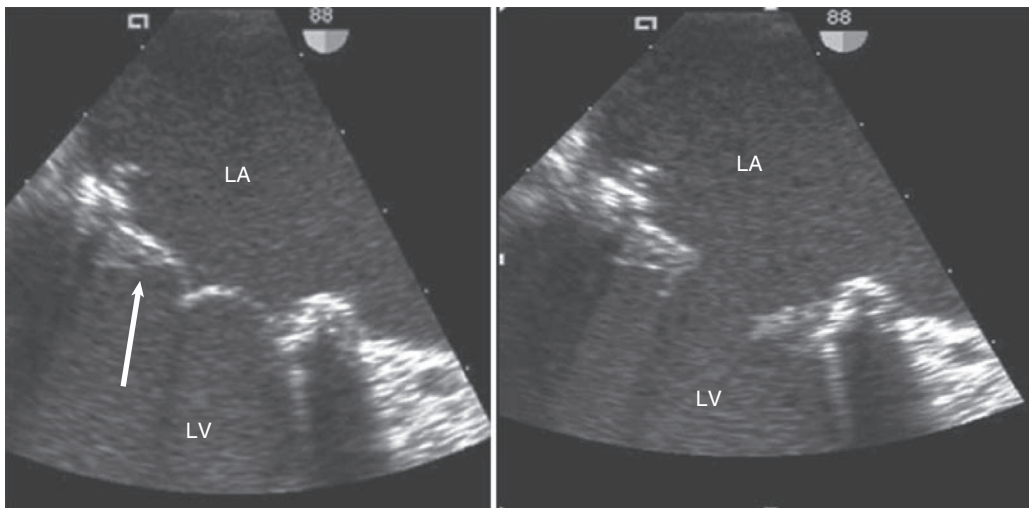


**FIGURE 16.55** TEE appearance of pannus ingrowth (*arrow*) in a mitral bioprosthesis. **Left,** Systole. **Right,** Diastole. The pannus has immobilized the base of the left-sided cusp and created a hinge point midway along the cusp and an narrow orifice. *LA,* Left atrium; *LV,* left ventricle.
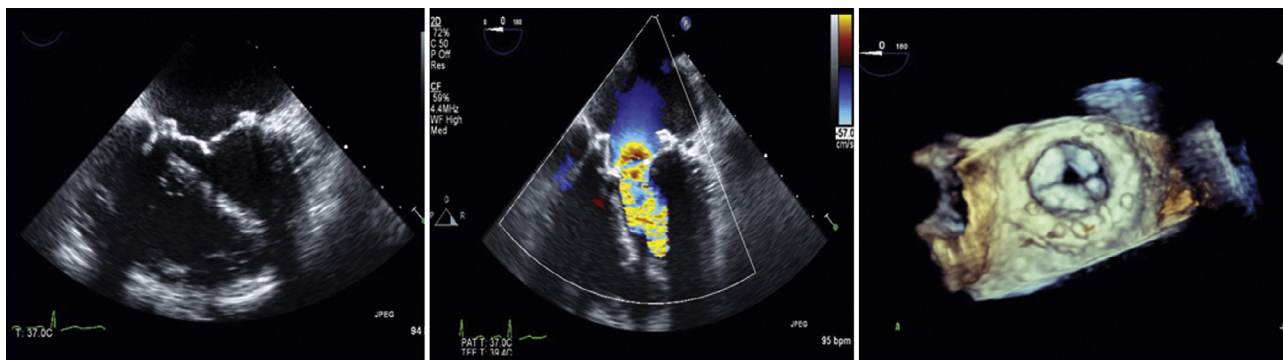


**FIGURE 16.56** TEE demonstrating a degenerated bioprosthesis. **Left,** Diastolic frame showing grossly restricted cusp motion. **Middle,** Color Doppler demonstrating turbulent transmitral flow and an easily identifiable proximal isovelocity hemispheric surface area shell. **Right,** 3D TEE view of the prosthesis from the left atrial perspective. The mitral orifice is greatly restricted.
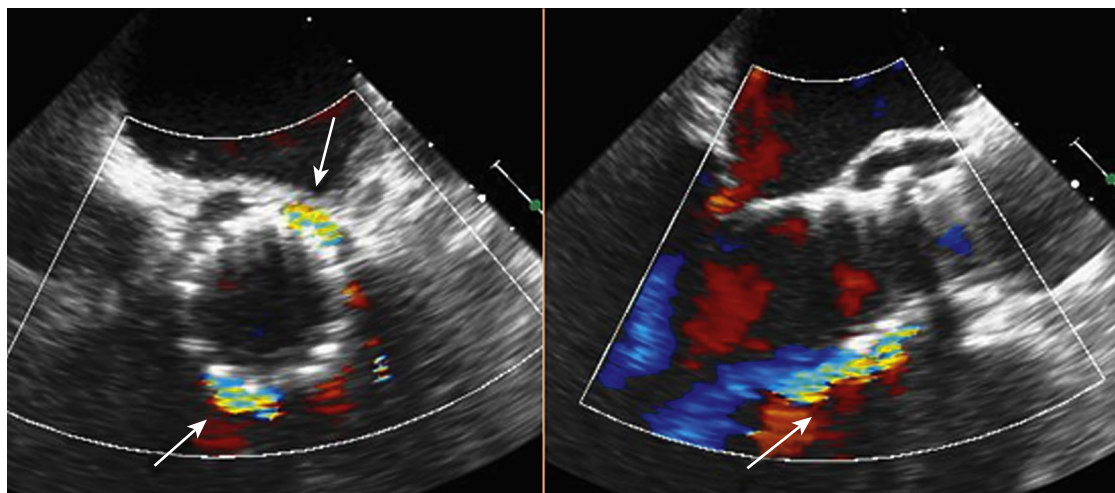
**FIGURE 16.57** Orthogonal TEE views of a balloon-expandable aortic prosthesis (TAVI, CoreValve) with at least two sites of significant paravalvular regurgitation (*arrows*), seen as turbulent diastolic flow on **left panel** (45 degrees) and **right panel** (120 degrees).

Detection of prosthetic regurgitation may require nonstandard views. Quantitation of prosthetic regurgitation may be challenging because jets frequently are highly eccentric and may be multiple, thus limiting the value of approaches based on jet dimensions. For mechanical valves the acoustic shadowing cast by mitral prostheses can greatly limit detection of MR, because the shadowing predictably falls directly over the left atrium in TTE views. The use of TEE is extremely advantageous in this respect since it insonifies the valve from an aspect posterior and directly adjacent to the left atrium. Assessment of paravalvular regurgitation in transcatheter or sutureless valves is particularly difficult because multiple pinhole jets may be present and the stents may obscure portions of the color flow jet.[70] As in native AR, the presence of a shortened PHT (<200 msec) and holodiastolic flow reversal in the descending thoracic or abdominal aorta are clues to significant regurgitation. For mitral prostheses, $VTI_{MV}/VTI_{LVOT}$ of ≥2.8 (as seen in stenotic valves as well), but in particular an elevated E wave (i.e., peak gradient elevated out of proportion to the mean gradient) and pulmonary venous flow reversal in systole, should raise suspicion for significant regurgitation. The quantitative Doppler approach using the pulmonic valve as the reference may also be helpful for aortic prostheses. As in native valvular regurgitation, regurgitant volume values less than 30 mL, 30 to 59 mL, and ≥60 mL and regurgitant fraction values less than 30%, 30% to 50%, and greater than 50% are consistent with mild, moderate, and severe prosthetic AR, respectively. For mitral valves the presence of well-defined flow convergence suggests significant regurgitation, and the PISA approach may be used to quantitate central valvular or well-defined single paravalvular jets. 3D TEE approaches that allow direct planimetry of regurgitant orifices and better localization of paravalvular leaks facilitate these tasks and may be more accurate.

Prosthetic tricuspid and pulmonic valves are much less common than their left-sided counterparts. In general, methods developed for assessment of the mitral and aortic valves are extrapolated to the tricuspid and pulmonic valves, although the evidence base for their use is less robust.



**FIGURE 16.58** Pericardial effusion. A parasternal long-axis view shows both pericardial effusion (*PE*) and pleural effusion (*left arrow*). Note that the descending thoracic aorta (*right arrow*) is displaced from the heart by the pericardial effusion. With isolated pleural effusion, the descending aorta (*Ao*) remains immediately posterior to the heart. In this case the pericardial effusion extends posterior to the left atrium (*LA*), although this is not always the case. *LV,* Left ventricle; *RV,* right ventricle.

## PERICARDIAL DISEASE (SEE CHAPTER 86)

Echocardiography is the imaging modality of choice for the identification of pericardial effusion and is an important tool in the diagnosis of tamponade and pericardial constriction (see Chapter 86).

### Pericardial Effusion

Identification of pericardial effusion was one of the earliest applications of echocardiography.[71,72] The diagnosis is made when an echo-free space separates the visceral and parietal pericardial echoes throughout the cardiac cycle, including diastole (Fig. 16.58). Systolic separation alone may be a normal finding reflecting normal
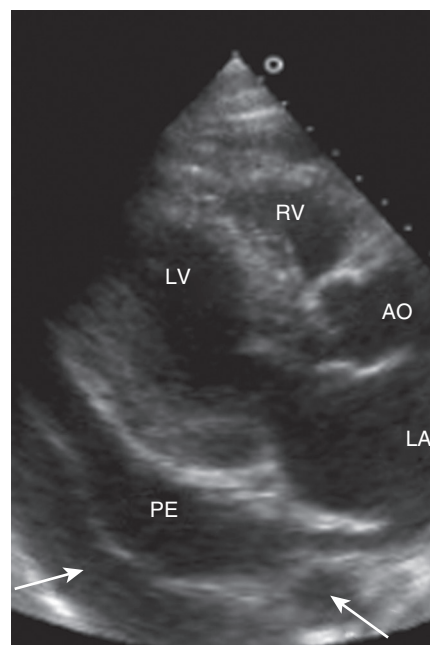
lubricating pericardial fluid. In most cases the diagnosis of pericardial effusion is straightforward because the parietal pericardium is a strong echo reflector and the visceral pericardium is adherent to the epicardial surface of the heart. "Echo free" is defined as having an echotexture that is equivalent to that of the intracardiac blood pool. Although it is typically black, in some cases suboptimal image quality results in both blood pool and pericardial effusion with a grayish or intermediate echotexture. In such cases it may be difficult to differentiate a small pericardial effusion from epicardial fat, although the latter typically has a more reticulated inhomogeneous appearance than a fluid effusion.

Another source of confusion may be left pleural effusion. Differentiating features include displacement of the aorta from the heart by pericardial (but not pleural) fluid and extension of pleural (but not

pericardial) fluid behind the left atrium (see Fig. 16.58). Of the two features, the relative position of the aorta is the most definitive: pericardial effusions may extend cephalad beyond the atrioventricular groove but will be anterior to the aorta, whereas fluid posterior to the aorta is pleural in nature. It is therefore essential that sonographers routinely provide views that demonstrate the descending thoracic aorta and its position relative to the heart. Multiple windows—particularly the subcostal view, because fluid is gravity dependent and thus tends to collect inferiorly—are essential to rule out localized effusions.

Sizing of pericardial effusions is typically somewhat subjective, with the terms *trace, small, medium,* and *large* being used. For reporting the size of effusions when longitudinal comparison will be important, it is helpful to report the maximal diameter of the effusion while noting the view(s) and time of the cardiac cycle (systole versus diastole) when the measurement is taken. Earlier estimates of the volume of the effusion, calculated using linear measures of pericardial and epicardial diameter, relied on a symmetric distribution of fluid and assumptions on the shape of the pericardial sac and heart. Semiquantitatively, systolic separation alone is consistent with a trace (physiologic) collection. Effusions with linear dimensions of less than 1 cm (small) correspond with less than 300 mL of fluid, whereas 1 to 2 cm (moderate) corresponds with 500 mL, and a dimension greater than 2 cm (large) is usually associated with greater than 700 mL of pericardial fluid.[72]

### Pericardial Hematoma

Pericardial hematoma results from bleeding into the pericardial space and may be caused by bleeding along suture lines after open heart surgery, trauma, myocardial rupture, or aortic dissection. It may occur as a complication of catheter-based or surgical intervention. Hematomas typically have an echotexture that is more coalescent and echodense than that of free fluid (Video 16.48). They may be unevenly distributed and localized to the bleeding site, such as the anterior mediastinum post-CABG. When images are obtained in the acute setting, there may be evidence of both clot and free fluid (Fig. 16.59).
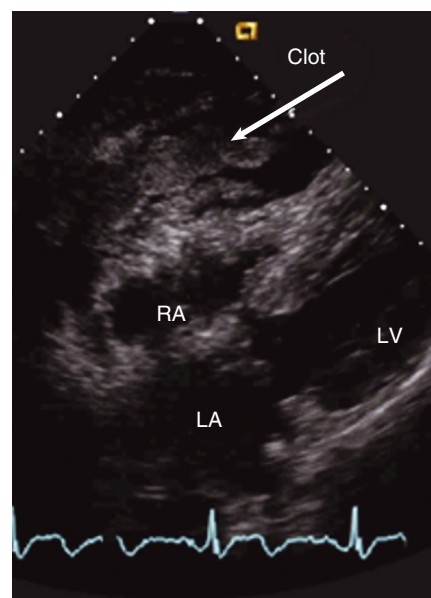
#### Echocardiographic Markers of Tamponade

Echocardiographic markers of cardiac tamponade fall into two categories: (1) cardiac chamber invagination reflecting *elevated intrapericardial pressure* and the resultant pressure gradients across the chamber walls and (2) echocardiographic markers of pulsus paradoxus, which reflect exaggerated respiratory variation in left-sided heart filling and ejection relative to that of the right side of the heart (*ventricular interdependence*).

*Right atrial inversion* is a dynamic phenomenon with onset when RA volume and pressure are lowest: in late ventricular diastole immediately after atrial contraction (Fig. 16.60, left panel, and Video 16.49). Inversion continues through a variable portion of ventricular systole and resolves as the right atrium fills and RA pressure rises. This sign can be detected in any view where the RA wall and adjacent effusion are well seen, typically the parasternal short-axis view at the level of the great vessels and the apical and subcostal four-chamber views. This sign is highly sensitive (100%) but may be present when hemodynamic disturbances are invasively detectable but fall below the threshold for the clinical diagnosis of tamponade, resulting in a specificity for clinical tamponade of 82%. Empirically, an RA inversion time index (readily calculated as number of frames during which the right atrium is inverted divided by number of frames per cardiac cycle) of at least 0.33 is associated with clinically evident tamponade (100% specificity, 95% sensitivity). *Left atrial inversion* as a marker of tamponade is rare and typically occurs in the setting of loculated effusions or those in which the pericardial reflection is relatively high and the left atrium is exposed to the effects of intrapericardial pressure.

*Right ventricular inversion* has its onset when RV volume and pressure are lowest: during isovolumic relaxation (Fig. 16.60, right panel). It continues through a variable portion of ventricular diastole, with the RV contour normalizing as the ventricle fills and RV pressure rises. This sign is most easily detected on the parasternal long-axis view, which displays



FIGURE 16.59 Pericardial hematoma. A subcostal view shows clotted (*arrow*) and free blood (black echotexture) within the pericardial space. In this patient the cause was acute aortic dissection. *LA,* Left atrium; *LV,* left ventricle; *RA,* right atrium.
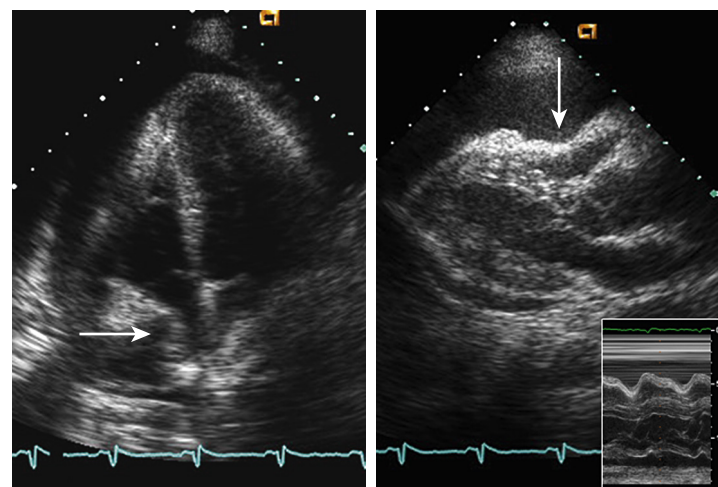


FIGURE 16.60 Signs of cardiac tamponade. **Left,** Apical four-chamber view showing RA inversion (*arrow*), a marker of tamponade. In this case, inversion, which is initiated in late ventricular diastole, has persisted well into ventricular systole. **Right**, Parasternal long-axis view showing RV collapse in diastole (*arrow*). *Inset,* An M-mode cursor placed down the RVOT shows diastolic inversion of the RV wall (note timing with respect to the ECG, closed aortic valve, and open mitral valve). (See Videos 16.49 and 16.50.)

the RVOT (Video 16.50). Its reported sensitivity is 82% to 94%, with a specificity of 88% to 100%.

It is important to note that RA inversion and RV inversion are defined by actual wall invagination rather than by the normal flattening that may occur with respective chamber systole. RA or RV inversion may also be absent (i.e., false-negative) in the setting of underlying right-sided heart dysfunction associated with elevated intracavitary pressure. With pericardial hematoma in which no free blood is present, dynamic inversion of the chambers will not be observed, but the presence of fixed compression and underfilling of the cardiac chambers may be clues to the presence of tamponade physiology (see Video 16.48).

There are echocardiographic correlates to the clinical phenomenon of pulsus paradoxus. In the normal state, a slight increase (up to 17%) in flow velocities through the right heart occurs on inspiration, with a reciprocal but smaller decrease (up to 10%) in flow velocities through the left heart in systole. These tendencies are exaggerated
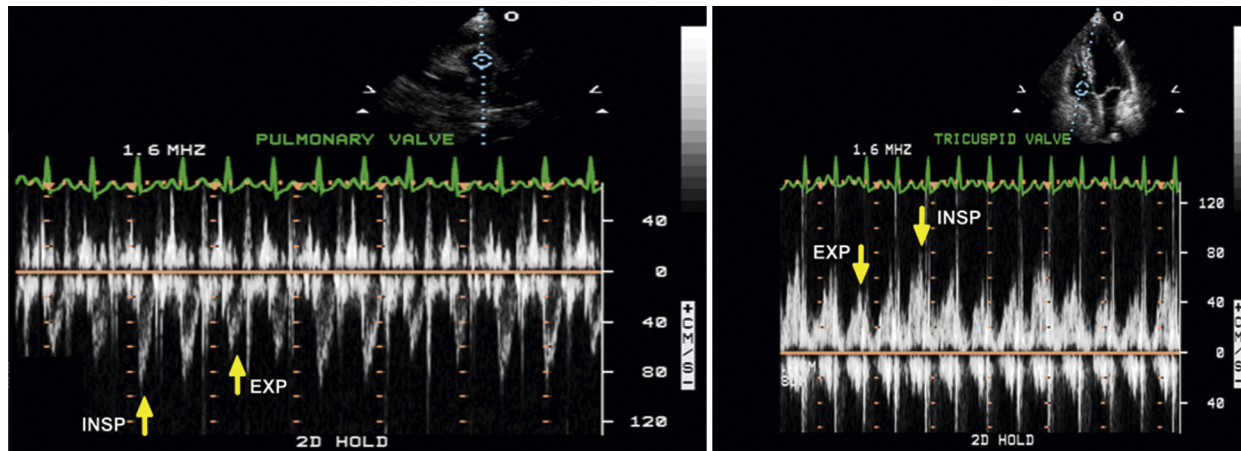
**FIGURE 16.61** Doppler spectra showing the characteristic exaggerated respiratory variation in right-sided pulmonary valve outflow **(left panel)** and tricuspid valve inflow **(right panel)** peak flow velocities. On inspiration, right-sided flow increases. In the left heart, PW tracings of LVOT outflow and mitral valve inflow (not shown) would demonstrate reciprocal reductions in left-sided flow on inspiration. *EXP,* Expiration; *INSP,* inspiration.
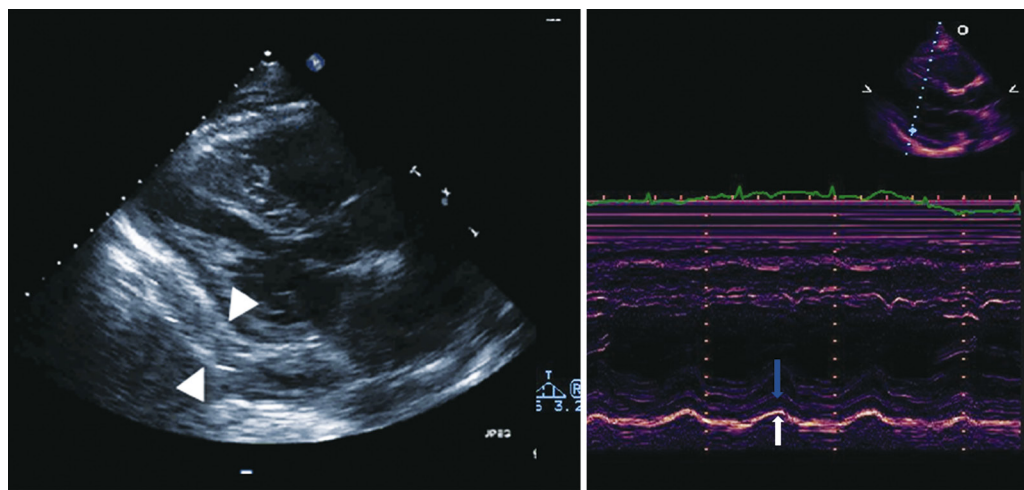


**FIGURE 16.62  Left,** Parasternal long-axis view demonstrating thickened pericardium (between *arrows*). **Right,** M-mode echocardiogram. The bright posterior echo (*white arrow*) representing the parietal pericardium moves in parallel with the visceral pericardial/epicardial echoes (*blue arrow*), a finding indicative of adhesion between the two layers. If the pericardial space were expanded by free fluid (pericardial effusion), the parietal pericardial echo would be relatively stationary (compare with the M-mode *inset* of Fig. 16.60).

## Constrictive Pericarditis

Pericardial constriction occurs when there is thickening, with or without calcification, of the pericardium that results in impaired cardiac diastolic filling, particularly during inspiration (Fig. 16.62). The clinical features mimic those of biventricular heart failure, although the presence of a pericardial knock and Kussmaul sign (inspiratory increase in jugular venous pressure) should raise suspicion for constriction. Frequently, when the patient is referred for echocardiographic evaluation, the clinical differential diagnosis is "restrictive cardiomyopathy" versus pericardial constriction, since EF is generally preserved in both. Pericardial thickening is a hallmark of constriction but is a relatively insensitive finding; furthermore, echocardiography is relatively insensitive for detecting pericardial thickening compared with CT and CMR. When the pericardial space is expanded because of adhesions and fibrous tissue, the visceral and parietal pericardia are separated by tissue of variable echogenicity, unlike the echolucent appearance of pericardial effusion. Also, with effusion the parietal pericardial echo will be relatively stationary, whereas with pericardial thickening, visceral and parietal pericardial echoes will move in tandem. Calcification will result in acoustic shadowing.

Restrictive and constrictive physiology share a mitral diastolic filling pattern characterized by a prominent E wave (E/A ratio >2) and shortened DT caused by rapid early filling, biatrial enlargement, and a fixed dilated IVC that does not change size with a sniff. However, the two may be distinguished by tissue and color Doppler diastolic indices, as well as respirophasic effects on septal motion (ventricular interdependence and septal bounce) that are not seen with restriction. Mitral annular DTI waves generally have normal or increased amplitude in constriction (peak e′ ≥8 cm/sec is reported to be 89% sensitive and 100% specific for constriction), reflecting compensatory exaggerated longitudinal motion of the heart, in contrast to the reduced e′ seen

when a tense, fluid-filled pericardium constrains the overall heart size and increases interdependence between the right and left ventricles. The most widely used signs are an exaggerated (>25%, and often >60% in frank tamponade) inspiratory increase in the tricuspid inflow Doppler E wave peak velocities with a reciprocal decrease (of >30%) in the mitral E wave velocities (Fig. 16.61), as well as corresponding changes in the pulmonic and aortic (or LVOT) systolic Doppler spectra. Additional signs of tamponade include the characteristic appearance of the heart oscillating or "swimming" in the pericardial fluid (see Video 16.49), which has its counterpart in electrical alternans on ECG, and a dilated IVC consistent with elevated RA pressures.

### Pericardiocentesis

Echocardiography may also be useful in guiding needle pericardiocentesis, particularly in the setting of loculated effusions. Imaging may help identify the best puncture site and angle of needle introduction, then confirm that the needle has entered the pericardial space. The latter is accomplished by the injection of a small amount of agitated saline, which will opacify the pericardial effusion with proper needle placement but will result in intracardiac contrast bubbles if the needle inadvertently penetrates the heart. Echocardiography is used to document the reduction in effusion size that should occur with successful drainage.

with restriction. Notably, the peak e′ of the lateral site may be smaller than that of the medial annulus, which is the opposite of the normal pattern; this phenomenon is termed *annulus reversus* and is believed to result from calcification and tethering effects of the pericardium on the lateral heart wall. Color M-mode propagation velocity is typically normal or even increased in constriction but reduced in restriction. In addition, PASP rarely exceeds 50 mm Hg in constriction.

In constriction the rigid pericardium abruptly limits filling to a fixed volume. When inspiration causes increased venous return to the right side of the heart, there is a sudden leftward septal shift and thus obligatory reduction in the amount of blood that the left ventricle can accommodate. The leftward septal shift may be seen on echocardiography during inspiration (Fig. 16.63 and Video 16.51), and often a transient left-right septal "bounce" occurs in both early and late diastole, giving the appearance of a double bounce. This ventricular interdependence occurs in tamponade, but pericardial encasement has the additional effect of isolating the heart chambers (but not pulmonary veins) from swings in intrathoracic pressure. This affects blood flow into the heart:



**FIGURE 16.63** Schematic representing the echocardiographic manifestations of constriction that may be appreciated on the apical four-chamber view and PW Doppler. Mitral (*MV*) and tricuspid (*TV*) valve Doppler spectra are characterized by an increased E/A ratio and shortened deceleration time. With inspiration there is increased venous return to the right side of the heart, which can be accommodated within the rigid pericardium only by displacement of the interventricular septum to the left and reduced left-sided filling. On expiration, left-sided filling increases, the septum moves to the right, and there is flow reversal in the hepatic veins (see Fig. 16.64). *IVC,* Inferior vena cava; *LA,* left atrium; *LV,* left ventricle; *RA,* right atrium; *RV,* right ventricle. (Modified from Bulwer BE, Rivero JM, eds. *Echocardiography Pocket Guide: The Transthoracic Examination*. Burlington, MA: Jones & Bartlett Learning; 2011, 2013:141. Reprinted with permission.)

with inspiration there is a decrease in intrathoracic pressure and hence a reduction in pulmonary venous pressures driving flow into the left heart, and with expiration there is a rise in intrathoracic (and therefore pulmonary venous) pressures, augmenting flow into the left heart but diminishing RV filling due to septal rightwards motion. There are also exaggerated respirophasic changes in the magnitude of the mitral and tricuspid E-waves (in opposing directions, similar to the patterns in tamponade). Additional markers of constriction include premature opening of the pulmonic valve, which is most pronounced with inspiration (reflecting a rapid rise in end-diastolic RV pressure that exceeds pulmonary artery pressure), diastolic MR, and expiratory diastolic hepatic vein flow reversal consistent with venous congestion (Fig. 16.64). In digital echocardiography laboratories where acquisitions are frequently limited to one to three beat clips, it is essential that longer captures with respiratory gating be obtained to assess the impact of respiration.

Parasternal views can be helpful with M-mode echocardiography over multiple cycles to parse the leftward (posterior) motion of the septum on inspiration and the diastolic septal bounce. In addition, diastolic flattening of the posterior myocardial endocardium rather than the normal continued posterior motion during diastole may be present and reflects abrupt ventricular filling. One may also demonstrate two thickened adhered pericardial layers moving in parallel throughout the cardiac cycle (see Fig. 16.62). Strain analysis shows that GLS is often preserved, but regional analysis demonstrates that there is decreased LV lateral wall and RV free wall strain with preserved septal strain ("strain reversus"), which is theorized to be due to myocardial tethering to the pericardium (analogous to the annulus reversus of mitral annular TDI).[71]

Differentiation between constriction and restriction can be further complicated by coexisting pathologies in the patient. Fibrotic involvement extending from the pericardium into the myocardium may result in mixed constrictive-restrictive physiology. Echocardiographic reassessment after removal of the pericardial fluid causing tamponade may unmask underlying constriction (i.e., effusive-constrictive physiology while the effusion was present).

### MALIGNANT INVOLVEMENT OF THE PERICARDIUM
Malignant pericardial disease typically occurs on the basis of local spread or distal metastases, with lung and breast cancer being the most
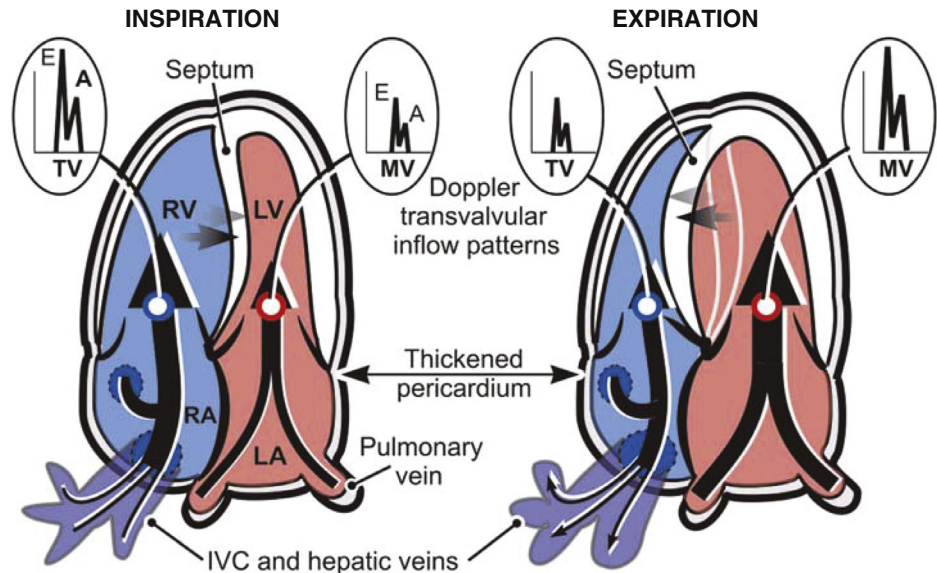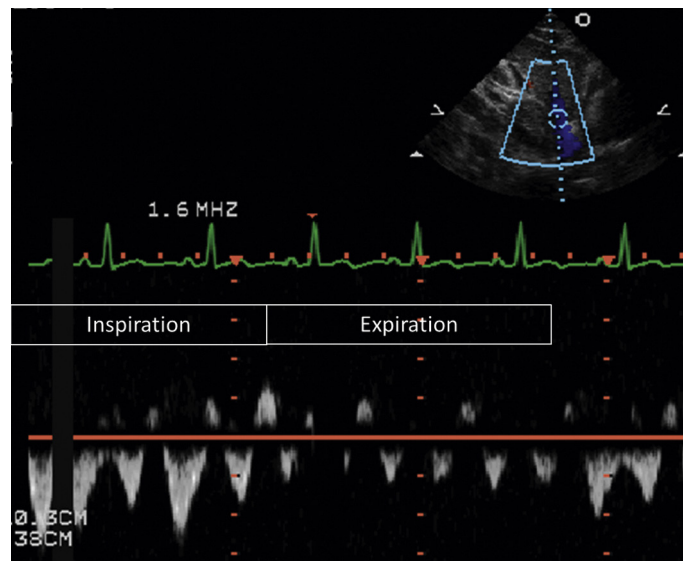


**FIGURE 16.64** Hepatic venous flow recordings demonstrate expiratory diastolic flow reversal, seen in constriction.

common primaries. Primary pericardial tumors are uncommon. The echocardiographic appearance may be that of pericardial effusion and/or solid tumor, which frequently invades locally into the myocardium (Fig. 16.65).

### OTHER PERICARDIAL PATHOLOGY
*Congenital absence of the pericardium* is a rare abnormality that usually involves the left pericardium and is associated with a leftward shift in the position of the heart, as well as exaggerated translation. The net result is an echocardiographic pattern that mimics RV volume overload. A *pericardial cyst* is a benign abnormality that is typically detected as an incidental finding of an echo-free mass adjacent to the heart.
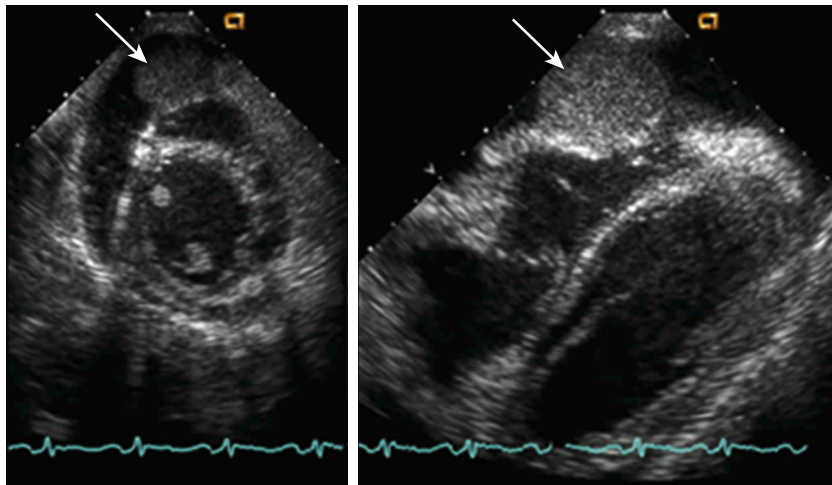
**FIGURE 16.65** Subcostal echocardiograms showing a tumor metastasis *(arrows)* within the pericardial space and invading the right ventricular myocardium. The tumor is surrounded by pericardial effusion.

# DISEASES OF THE AORTA (SEE CHAPTER 42)

TTE is a first-line tool to assess the thoracic aorta for pathologic processes (see Chapter 42).[15,27] TTE can visualize the aortic root and proximal ascending aorta, aortic arch up to the isthmus (takeoff of the left subclavian artery), and limited portions of the descending thoracic and proximal abdominal aorta (Fig. 16.66). TEE can be used to more comprehensively examine the entire thoracic aorta (Fig. 16.67), with the exception of a small area of distal ascending aorta (which is obscured by shadowing from the air-filled trachea interposed between the esophagus and the heart), the so-called echo blindspot. Therefore, for screening purposes and for serially monitoring a known aortic abnormality for stability, TTE may be sufficient. Higher degrees of suspicion for an acute aortic process or for disease extending beyond the TTE windows require TEE evaluation (or alternatively, CT or magnetic resonance angiography [MRA]).[26]

During the standard echocardiographic examination, the normal diameter of the aorta should be assessed at the aortic annulus, sinuses of Valsalva and sinotubular junction (aortic root), and ascending aorta. The upper limit of normal varies with age, sex, and BSA (Table 16.10 and eFig. 16.32). More of the ascending aorta can be viewed by moving the transthoracic probe up one interspace, angling the probe more cephalad, or utilizing right parasternal windows.

## Focal Aortopathies

*Atherosclerotic plaque* can be visualized as irregular, heterogeneous, or echobright calcified foci adherent to the endothelial side of the lumen. These plaques often accumulate at the sinotubular junction and aortic arch. Plaque that is thicker than 5 mm or that has mobile or protruding elements appears to be at higher risk of being associated with stroke (Fig. 16.68A). *Ulcerated aortic plaque* is thought to be a potential precursor to intramural hematomas (see later). In patients with bicuspid valves, the descending aorta should always be evaluated carefully for narrowing and blood flow acceleration at the isthmus, to rule out *aortic coarctation*.

## Aortic Emergencies

*Aortic aneurysms,* technically defined as vessel dilation greater than 50% above the normal diameter of the aorta, may occur anywhere along the course of the aorta (Fig. 16.68B), although they are more common in the abdominal location. Patients with connective tissue syndromes (e.g., Marfan, Loeys-Dietz, Ehlers-Danlos type IV) and patients with bicuspid aortic valves are thought to have defects in the elastic and smooth muscle composition of the aorta which render them prone to the development of ascending aneurysms (generally defined

as ascending aortic diameter >4.0 cm). Marfan syndrome in particular often affects only the sinuses of Valsalva symmetrically, whereas diameters at the sinotubular junction and ascending aorta are relatively preserved. The portion of the aortic wall proximal to the coronary orifices is often elongated, giving the root an "onion-bulb" appearance. If the aneurysm involves the ascending aorta and the proximal root up to and including the annulus (termed *aortoannular ectasia*), the resulting incomplete cusp coaptation may cause aortic insufficiency and necessitate valve repair as well. Isolated *sinus of Valsalva aneurysms* are focal dilations that asymmetrically affect only one sinus (most often the right, as shown in Fig. 16.69). They are usually discovered incidentally, and their cause is uncertain. Although not considered an acute aortic emergency, there have been case reports of rupture of these aneurysms into the right ventricle, right atrium, and other locations. In contrast to *ascending* aneurysms, most *descending* aortic aneurysms are associated with atherosclerosis. Whereas ascending aneurysms are typically fusiform, abdominal aneurysms may be more irregular, focal, and saccular in shape.

The most common emergency indication for echocardiography in patients with aortic diseases is to detect *aortic dissection*, a tear in the aortic intima that enables blood to force its way between the other layers of the vessel wall. Although it can arise de novo, aortic dissection and rupture are the most feared sequelae of aortic aneurysms and thus share the same causative associations and risk factors, including connective tissue disorders, aortic valve disease (personal or family history), hypertension, smoking, and atherosclerosis. Figures 16.66 and 16.67 show examples of aortic dissection and their location and appearance (Videos 16.52 and 16.53). Recent aortic manipulation, such as cardiac catheterization, cardiac surgical bypass, placement of intra-aortic balloon pumps, and intravascular stenting, is also considered a high-risk condition.[26] Serious morbidity from compromised blood flow to the coronary arteries, central nervous system, renal arteries, and other organs may occur, and if the dissection ruptures through all three layers, massive bleeding and death can rapidly ensue. Dissection tends to propagate in antegrade fashion (i.e., from the proximal toward the distal aorta), although retrograde extension may also occur all the way back to the sinuses, causing aortic insufficiency or occluding coronary artery ostia (Video 16.54). The mortality rate is high, and surgical treatment has been shown to be the most effective therapy for patients with ascending (DeBakey types I and II or Stanford type A) dissections. *Blunt chest trauma,* in particular rapid-deceleration injuries such as in motor vehicle accidents, may cause tears at the ligamentum arteriosum (near the aortic isthmus, just distal to the left subclavian artery), which demarcates a hinge point between the relatively tethered descending thoracic aorta and the more mobile arch and ascending aorta. Tertiary syphilis, now a rare disease in the developed world, can cause *aortitis*, that is, inflammation of the aortic adventitia, weakening of the walls, and subsequent development of descending aortic aneurysms and dissections. Rarely, other systemic arteritides, such as giant cell arteritis, can also cause aneurysm formation in the ascending aorta.

TTE has somewhat limited sensitivity for aortic dissection (70% to 80% for all locations with higher sensitivity in type A dissections) and specificity (63% to 93%) because of limited views of the abdominal aorta. TEE has been shown to have a sensitivity reaching 99% and specificity of 89%, particularly with ascending dissections.[26] An aortic dissection flap on echocardiography appears as a linear or thin serpiginous tissue plane extending parallel (in the long-axis plane) (Fig. 16.70A; see also Fig. 16.66A,C) or semicircumferentially (in the short-axis plane) (see Fig. 16.67I) to the aortic walls. It represents the intima that has split from the other layers of the aorta. An acute, unthrombosed flap will undulate independently and usually bulge outward from the true lumen in pulsatile fashion during systole. These characteristics can be demonstrated by M-mode and can be used to distinguish true disease from reverberation artefact. If color Doppler is used to sweep
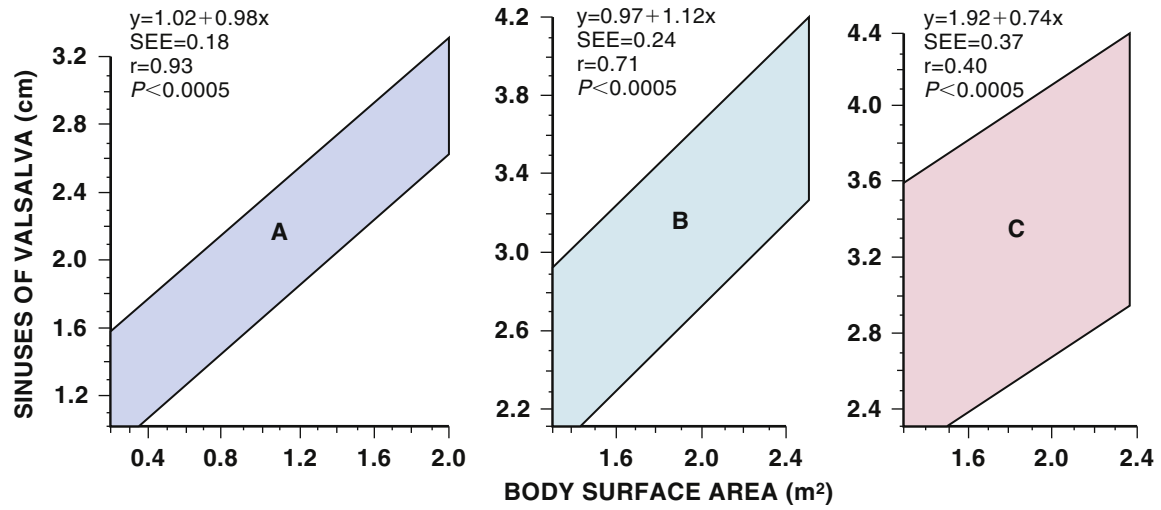
**EFIGURE 16.32** Normal aortic root sizes. The 95% confidence intervals for aortic root diameter at sinuses of Valsalva on the basis of body surface area (BSA) in children and adolescents (**A**), adults age 20 to 39 (**B**), and adults age 40 or older (**C**).
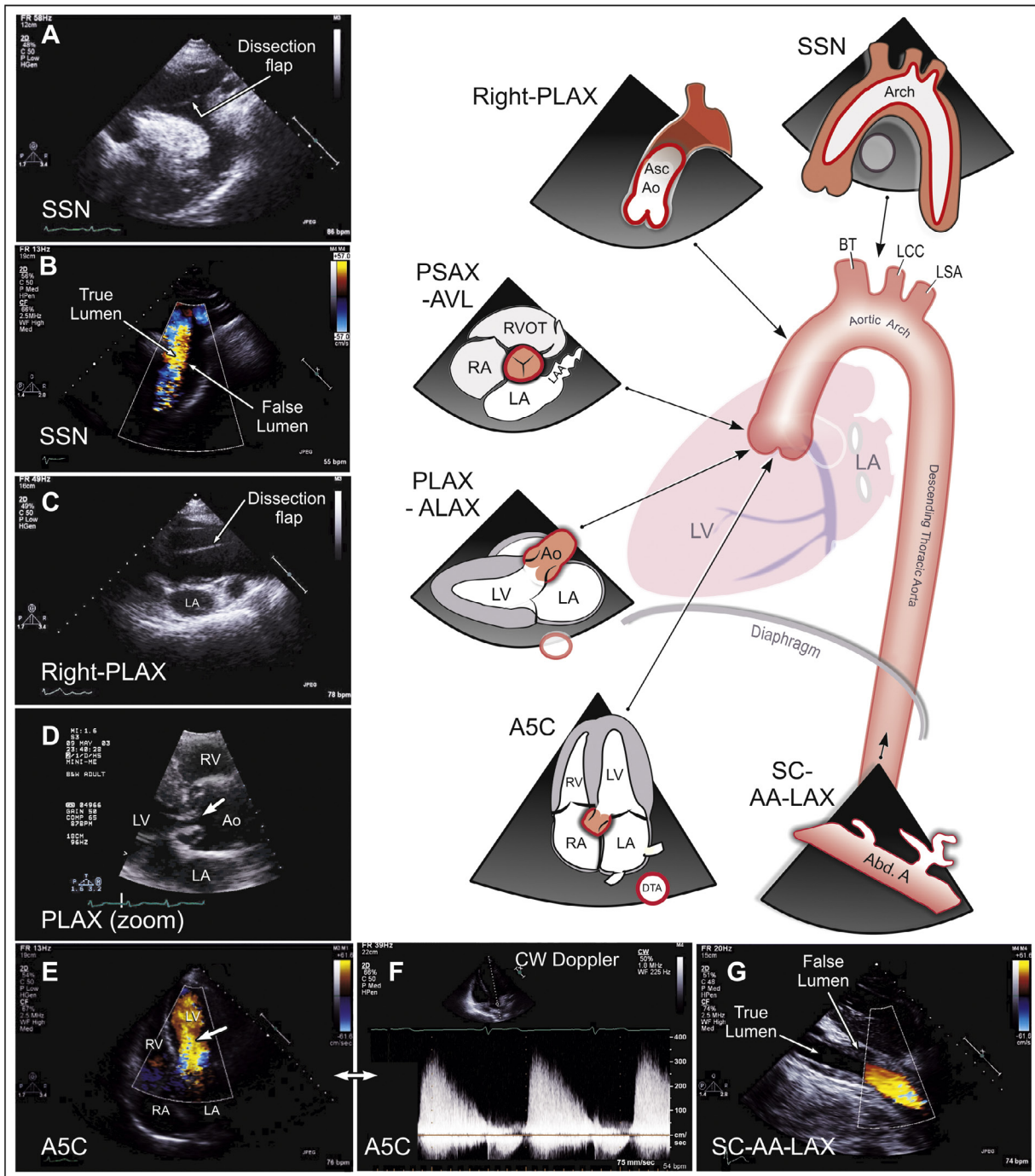
**FIGURE 16.66** Transthoracic views of the aorta and examples of acute aortic pathologies from each window. The composite illustrates **(A, B)** suprasternal notch 2D and color Doppler views of a type A dissection flap that is seen extending into the brachiocephalic artery; **(C, D)** a type A dissection flap that originates at the level of the aortic sinuses, prolapses through the aortic valve, and also extends into the ascending aorta in the parasternal long-axis view (see Video 16.52); **(E, F)** color and spectral Doppler apical five-chamber views illustrating the resultant severe aortic insufficiency (see Video 16.53); and **(G)** an abdominal aortic type B dissection with a small central true lumen and chronic thrombus in the circumferential false lumen in the subcostal long-axis view. *ALAX,* Apical long axis; *PLAX,* parasternal long axis; *PSAX,* parasternal short axis; *SSN,* suprasternal notch; *SC,* subcostal; *Ao,* aorta; *AVL,* aortic valve level; *BT,* brachiocephalic trunk; *DTA,* descending thoracic aorta; *LCC,* left common carotid artery; *LSA,* left subclavian artery; *TL,* true lumen; *FL,* false lumen.

along the flap, one may occasionally be able to identify the site of the primary tear as a communication between the false and true lumen (Video 16.55). The false lumen may be seen to contain more spontaneous echocardiographic contrast or even formed thrombus. By color and spectral Doppler, forward flow in systole can also help identify the true lumen (Fig. 16.70B,E). Complications arising from aortic dissection that may be directly imaged by ultrasound include: (1) extension of the flap into the coronary arteries with loss of the diastolic-dominant coronary flow by spectral and color Doppler and wall motion abnormality signaling MI; (2) AR (see Fig. 16.66E,F) which may be caused by interference with leaflet coaptation due to diastolic prolapse of the

flap across the aortic valve, enlargement of the annulus or root, and/or displacement of the cusps relative to one another; (3) extension of the flap into the carotid arteries (causing stroke) or the innominate or subclavian arteries (see Fig. 16.66A); (4) pericardial effusion, which is frequently frank hemopericardium; (5) pleural effusion, which is more common on the left than on the right side; and (6) periaortic hematoma, signifying a leak into the adventitia and impending complete rupture.

Other aortic emergencies are less common but equally life threatening. *Aortic transection* occurs as a result of severe deceleration injury and consists of complete shearing of the aorta at the isthmus, with the
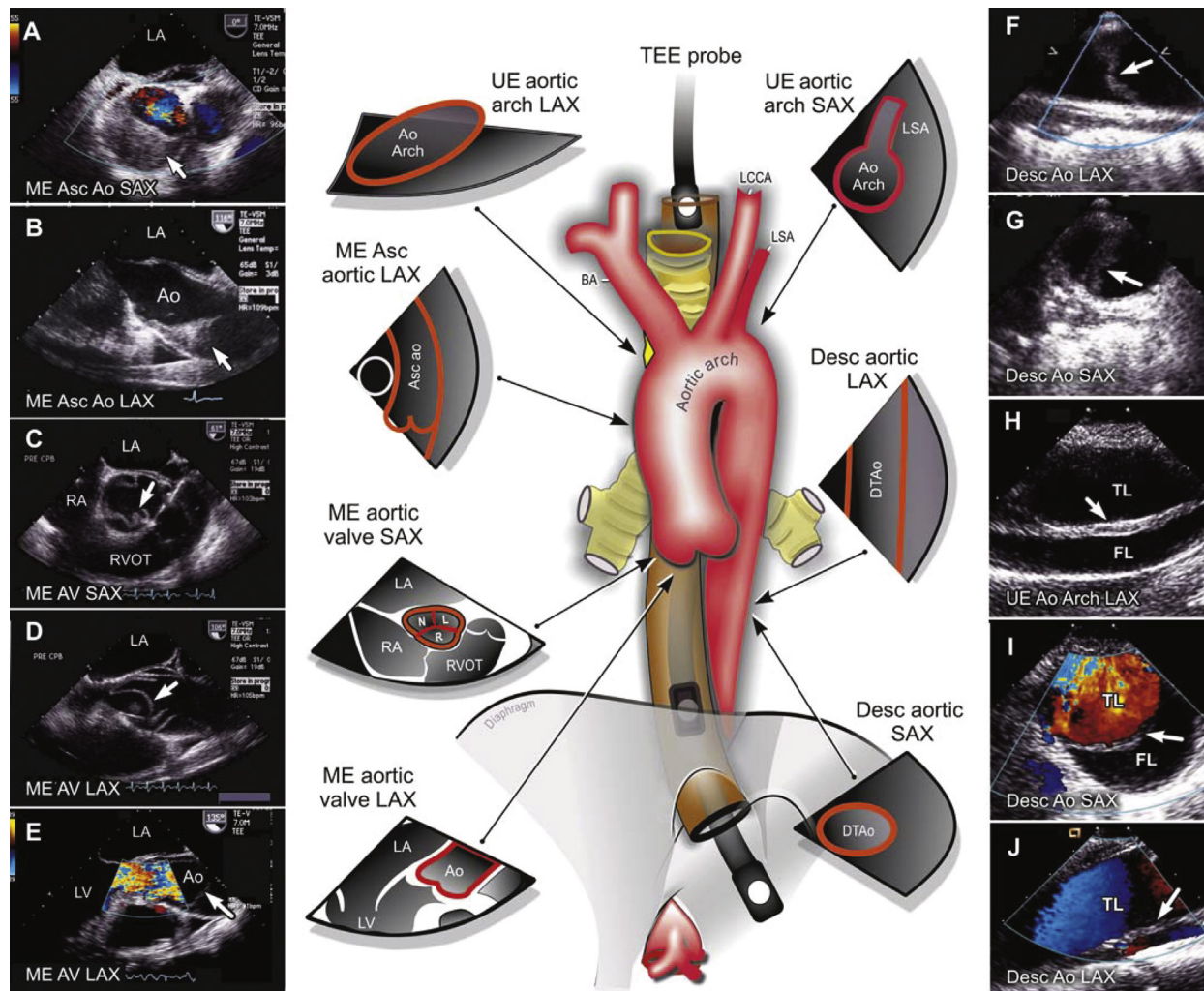
**FIGURE 16.67** This TEE composite illustrates **(A, B)** short- and long-axis views of an intramural hematoma in the ascending aorta (*arrow*); **(C, D)** a type A dissection flap that originates at the level of the aortic sinuses, prolapses through the aortic valve, and also extends into the ascending aorta (see Video 16.54); **(E)** severe aortic insufficiency resulting from dissection in the same patient; **(F, G)** long- and short-axis views of partial aortic transection occurring in the descending thoracic aorta just distal to the origin of the left subclavian artery as a result of sudden deceleration during a motor vehicle accident; and **(H-J)** long- and short-axis views of a type B aortic dissection flap A (*arrow*) visualized in the distal descending thoracic aorta (see Video 16.55). *FL,* False lumen; *TL,* true lumen; *ME,* midesophageal; *ME,* midesophageal; *UE,* upper esophageal.

### TABLE 16.10 Normal Values for Aortic Size in Adults

| | ABSOLUTE VALUES (cm) | | INDEXED VALUES (cm/m²) | |
|---|---|---|---|---|
| **AORTIC ROOT** | **MEN** | **WOMEN** | **MEN** | **WOMEN** |
| Annulus | 2.6 ± 0.3 | 2.3 ± 0.2 | 1.3 ± 0.1 | 1.3 ± 0.1 |
| Sinuses of Valsalva | 3.4 ± 0.3 | 3.0 ± 0.3 | 1.7 ± 0.2 | 1.8 ± 0.2 |
| Sinotubular junction | 2.9 ± 0.3 | 2.6 ± 0.3 | 1.5 ± 0.2 | 1.5 ± 0.2 |
| Proximal ascending aorta | 3.0 ± 0.4 | 2.7 ± 0.4 | 1.5 ± 0.2 | 1.6 ± 0.3 |

From Lang RM, Badano LP, Mor-Avi V, et al. Recommendations for cardiac chamber quantification by echocardiography in adults: an update from the American Society of Echocardiography and the European Association of Cardiovascular Imaging. *J Am Soc Echocardiogr* 2015;28:1.

severed ends of the aorta floating freely within hematoma. This is so lethal that examples are rarely captured on TEE during emergency surgery or endovascular repair, although local containment of blood within the mediastinum can permit a very brief window of survival.

A partial transection is shown in Fig. 16.67F, G. *Aortic intramural hematoma* is an accumulation of blood that remains contained within the aortic media; it accounts for approximately 5% to 20% of acute aortic syndromes (see Fig. 16.67A, B). On echocardiography, intramural hematoma appears as a smooth, homogeneously echogenic bulge within the medial layer of aortic wall. It is hypothesized to arise from rupture of a penetrating atherosclerotic ulcer, spontaneous rupture of the vasa vasorum, or more frequently, blunt trauma. Intramural hematomas are distinguished from atherosclerotic plaque (which is typically focal, echobright, and irregular), in that they lie within the aortic wall and extend smoothly and longitudinally along the aorta. On cross-sectional views the hematoma appears as a crescentic or circular area of homogeneous thickening around the central aortic lumen. Unlike dissection, the intimal layer is still intact and is not mobilized, so there is no detectable intimal tear and no blood flow communication with the aortic lumen. If the intramural hematoma is relatively small, additional imaging with CT or MRA may be required to identify the hematoma definitively and distinguish it from the differential diagnoses of plaque or periaortic fat. Intramural hematomas can arise in either ascending or descending aortic locations and may enlarge or progress to frank aortic dissection and may have similar mortality rates. Thus the principles of medical and surgical management are essentially the same as for typical aortic dissections.[26]
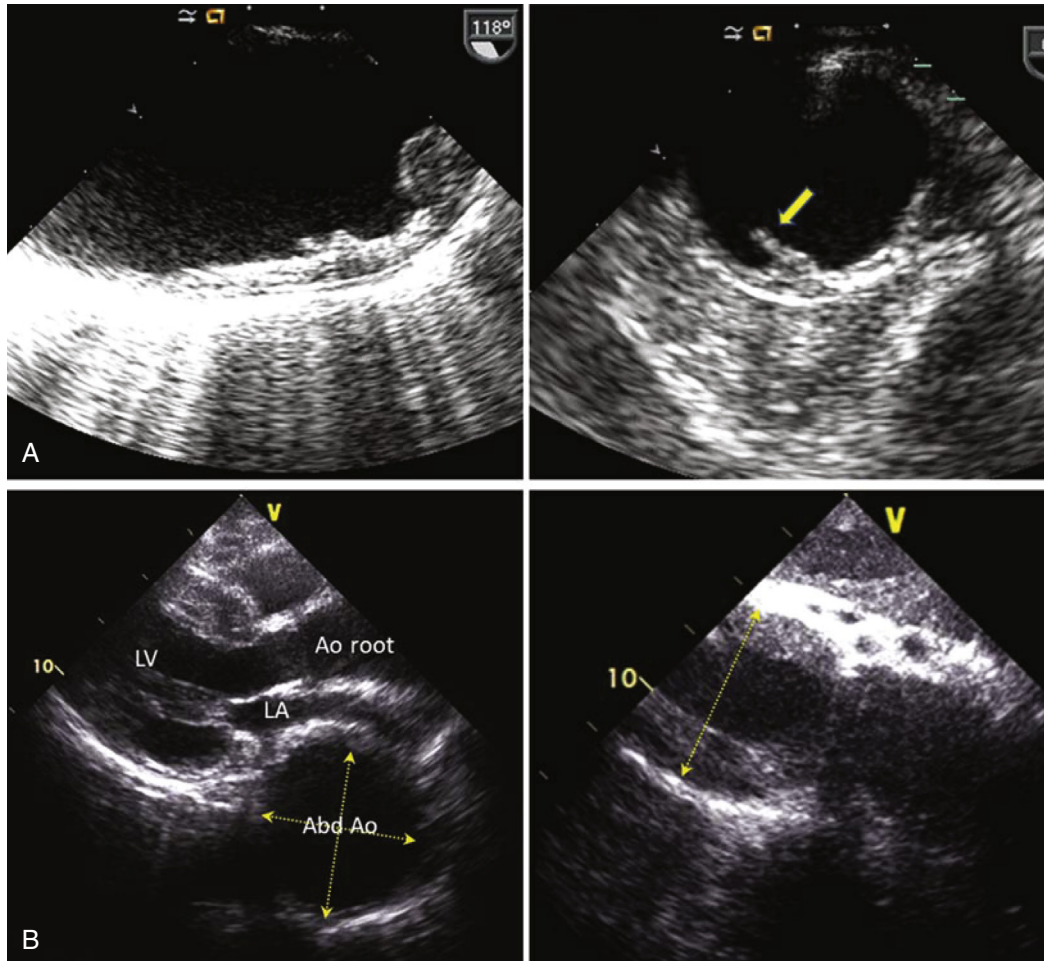
FIGURE 16.68 Aortic atheroma and aneurysm. **A,** TEE views of complex aortic atheroma in the ascending aorta. In the long-axis view **(left),** the atheroma is seen to be irregular and measures up to 1.0 cm in thickness. In the short-axis view **(right),** a protuberant finger-like atheroma is seen and is independently mobile. **B,** Transthoracic parasternal long-axis (**left**) and subcostal (**right**) views of a large 7-cm-diameter descending thoracoabdominal aortic aneurysm (*dotted arrows* spanning the diameter) compressing the posterior aspect of the left atrium (*LA*), within which diffuse circumferential thick mural thrombus is layered. *Ao,* Aortic; *LV,* left ventricle.

## PULMONARY EMBOLISM (SEE CHAPTER 87)

Echocardiography can be extremely useful in the diagnosis and management of acute pulmonary embolism. Indeed, in the acutely unstable patient with known risk factors for hypercoagulability, echocardiographic evidence of RV dysfunction can prompt consideration for immediate reperfusion therapy without further testing.[73] For patients who are hemodynamically stable, however, CT pulmonary angiography is preferred for the definitive diagnosis of pulmonary embolism because of its higher accuracy. Echocardiography provides supplemental information, has prognostic value, and may inform or monitor therapy (particularly if CT angiography is not feasible). Echocardiography performed for other indications, including dyspnea, chest pain, and hypotension, also occasionally leads to the incidental discovery of pulmonary embolus as certain echocardiographic findings can be virtually pathognomonic.

The thrombi of pulmonary embolism generally arise from the deep venous system in the legs. Thus they may have a pathognomonic appearance of sausage-link like casts of the veins from which they have originated. Echocardiography may be used to directly visualize thrombus anywhere from the IVC to the mainstem pulmonary arteries (Fig. 16.71 and Video 16.56). Those in the pulmonary arteries generally can be visualized to just past the bifurcation with TTE; when found, they are associated with RV dysfunction and high early mortality. Although TEE can image slightly farther into the main pulmonary artery branches, it is not sensitive enough to be relied upon as a primary diagnostic modality for pulmonary embolism. The pulmonary artery bifurcation should be carefully assessed from the short-axis views in patients with suspected pulmonary embolism, and it is not uncommon for so-called saddle emboli to become lodged at the bifurcation (Fig. 16.71, right). Putative thrombi must be distinguished

from other cardiac masses, including myxomas, fibroelastomas, and vegetations (see later, Cardiac Masses).

The characteristic echocardiographic findings in pulmonary embolism result in part from the unique physiology of the right ventricle and are summarized in Figure 16.72. The normal right ventricle is generally accustomed to low PVR and thus extremely low afterload, and RV systolic pressure normally is low. In acute pulmonary embolism, PVR rises substantially and abruptly, which results in RV dilation and, in severe cases, failure. Thus, RV dilation is the echocardiographic hallmark of pulmonary embolism, and is found in ≥25% of patients with pulmonary embolus. It is best visualized on the apical four-chamber view, where classic findings include RV diameter greater than LV diameter (ratio >1.0) and a small, underfilled, but normally functioning left ventricle. A distinctive regional wall motion abnormality has been recognized in acute pulmonary embolism in which the free RV midwall becomes dyskinetic, with relative sparing of the apex and base. This pattern, known as the *McConnell sign,* is highly specific for conditions in which PVR increases abruptly[74] but cannot be relied on to distinguish pulmonary embolus from other causes of respiratory decompensation. (eFig. 16.33 and Video 16.57). RV TAPSE may also be decreased in patients with acute pulmonary embolus. Both RV dilation and RV regional dysfunction will be less apparent in patients in whom PVR has been elevated for a longer period, resulting in RV hypertrophy. In these patients, pulmonary pressure will ultimately rise, and the right ventricle may not show evidence of acute dilation or dysfunction in acute pulmonary embolism. Thus the classic echocardiographic RV patterns are of lower sensitivity and have low negative predictive value in patients with longstanding pulmonary hypertension, such as those with chronic obstructive pulmonary disease (COPD) or chronic thromboembolic disease.
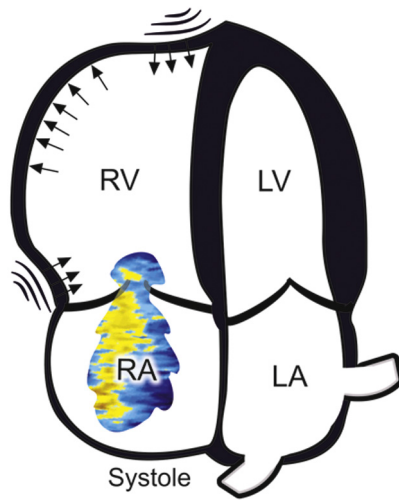
**EFIGURE 16.33** Regional right ventricular dysfunction (McConnell sign) in acute pulmonary embolism. The right ventricle (RV) is enlarged and right ventricular regional function is abnormal, with dyskinesis of the midwall region and relative sparing of the apex and base. Tricuspid regurgitation is usually present. *LA,* Left atrium; *LV,* left ventricle; *RA,* right atrium.
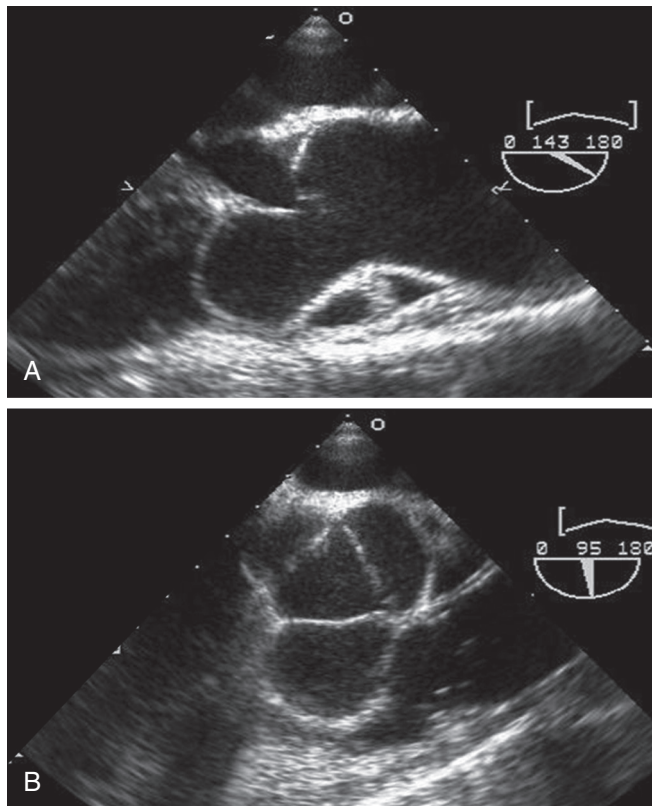
**FIGURE 16.69** Sinus of Valsalva aneurysm. **A,** TEE long-axis view of a right sinus of Valsalva aneurysm (measuring 2.5 × 2.8 cm). **B,** TEE short-axis view of the trileaflet aortic valve in the open position showing the right sinus aneurysm in cross section. The patient had mild aortic insufficiency.

In patients without a previous history of pulmonary hypertension, even in the setting of acute pulmonary embolus, the TR velocity will remain relatively normal, rarely exceeding 3 m/sec. Patients with pre-existing pulmonary vascular disease, however, may have increased TR velocity consistent with elevated pulmonary systolic pressure. Assessment of RV dilation and dysfunction has now been incorporated into treatment algorithms and is particularly useful in triaging highly unstable and intermediate-risk patients.[73] Their presence is an independent predictor of adverse outcomes and short-term mortality, even in hemodynamically stable patients. In terms of response to therapy, improvement in RV function can be seen on echocardiography within several days of successful treatment—reperfusion by either embolectomy or thrombolysis—of pulmonary embolism.

## PULMONARY HYPERTENSION (SEE CHAPTER 88)

Echocardiography can noninvasively assess for pulmonary hypertension and causative conditions. Pulmonary hypertension is defined by a mean pulmonary artery pressure of at least 20 to 25 mm Hg. It is classified as Group 1: pulmonary arterial hypertension; Group 2: due to left heart disease; Group 3: due to lung disease and/or chronic hypoxia; Group 4: due to pulmonary emboli and Group 5: due to blood and other disorders including sickle cell disease, in which pulmonary hypertension is an important cause of morbidity and mortality.

With the exception of some Group 2 cases, the common echocardiographic appearance is an enlarged right side with an intrinsically normal left ventricle but septal flattening in systole and diastole (Fig. 16.73). Echocardiography is well suited to identify underlying left heart pathology as well as other causes of pulmonary hypertension including congenital shunts (VSDs, PDAs or less commonly ASDs). In general, most of the indices of pulmonary artery pressure and right-sided heart failure (e.g., TAPSE, FAC) have been shown to be predictors of mortality in patients with diverse causes of pulmonary hypertension.[75]

2D echocardiographic findings in patients with pulmonary hypertension include flattening of the interventricular septum (predominantly in systole but often, due to concomitant RV dilation, in diastole as well), dilation of the pulmonary artery, RV hypertrophy, RV dilation, and ultimately RV dysfunction. Other signs are enlargement of the right atrium, dilation of the IVC and hepatic veins, loss of respirophasic size variation in the IVC and systolic notching of the pulmonic valve (dubbed the "flying W" sign). Typical Doppler findings include elevated TR velocity (≥3.0 m/sec), which is used to calculate the RVSP (See example in Fig. 16.73D). The calculation is based on the Bernoulli-derived pressure gradient between the right ventricle and right atrium and estimated RA pressure derived from the size and inspiratory collapsibility of the IVC. The equation for estimating PASP is:

$$PASP = 4 \ (TRpeak \ velocity)^2 + RA \ pressure$$

where TRpeak velocity is measured in m/sec and RA pressure in mm Hg. In the absence of right ventricular outflow obstruction, the RVSP equals the PA systolic pressure (PASP). The normal IVC diameter measured 1 to 2 cm from the IVC-RA junction is less than 2.1 cm and normal collapsibility, elicited with a sniff, is at least 50%. If size and collapsibility are normal, the RA pressure is assumed to be 3 mm; if one is abnormal, 8 mm Hg; and if both are abnormal, 15 mm Hg (see Table 16.7).

If TR is not present or the TR jet is acquired off-axis, this measurement will be impossible to make or will underestimate the severity of pulmonary hypertension. Additionally in severe TR, the RA pressure is grossly elevated and the standard approach will underestimate PASP. A shortened PA acceleration time has also been reported as a Doppler marker of pulmonary hypertension but is limited by its reproducibility.

If there is pulmonic regurgitation, PA diastolic pressure can be calculated as the diastolic gradient between the PA and RV plus the RA pressure. Mean PA pressure can be calculated in one of several ways, most commonly by integration of the TR jet to determine mean RV to RA pressure gradient and adding RA pressure. In addition to PA pressure assessment, the PVR in Woods units (PVR) can be calculated noninvasively by using the formula:

$$PASP = 10 \ (TRpeak \ velocity/VTI_{RVOT}) + 0.1$$

where TR peak velocity is measured in m/sec and $VTI_{RVOT}$ in cm. This approach may have utility in distinguishing high PASP caused by increased pulmonary blood flow (as occurs in high-output states such as hyperthyroidism, anemia, and obesity) from that caused by elevated PVR.

Assessment of RV size and function is essential in pulmonary hypertension. RV FAC, TAPSE, RV Tei index, and tricuspid annular systolic velocity (S′) are typical quantitative measures to assess RV function in patients with pulmonary hypertension (see Table 16.6). RV longitudinal and free wall strain, as well as RV EF and increased RV indexed volumes as determined by 3D echocardiography are newer echocardiographic indices that have been shown to predict poor outcome in pulmonary hypertension.[75]

There are several features that may assist in distinguishing between pulmonary hypertension and acute pulmonary embolism on echocardiography. Acute pulmonary embolism is not usually associated with RV hypertrophy, elevation in PAP, or flattening of the interventricular septum in systole, unless there is pre-existing disease (e.g., longstanding thromboembolic disease with resultant pulmonary hypertension). In addition, the regional RV dysfunction in acute pulmonary embolism may spare the apex, whereas there is global RV hypokinesis in pulmonary hypertension.

## INFECTIVE ENDOCARDITIS (SEE CHAPTER 80)

Echocardiography is the first-line modality in the diagnosis, evaluation, and management of endocarditis. The American College of Cardiology/American Heart Association guidelines regard echocardiography as a Class I indication in the following settings: (1) in patients with suspected endocarditis to characterize the hemodynamic severity of valvular lesions, assess ventricular function and pulmonary pressures, and detect complications; (2) TTE and/or TEE are recommended for
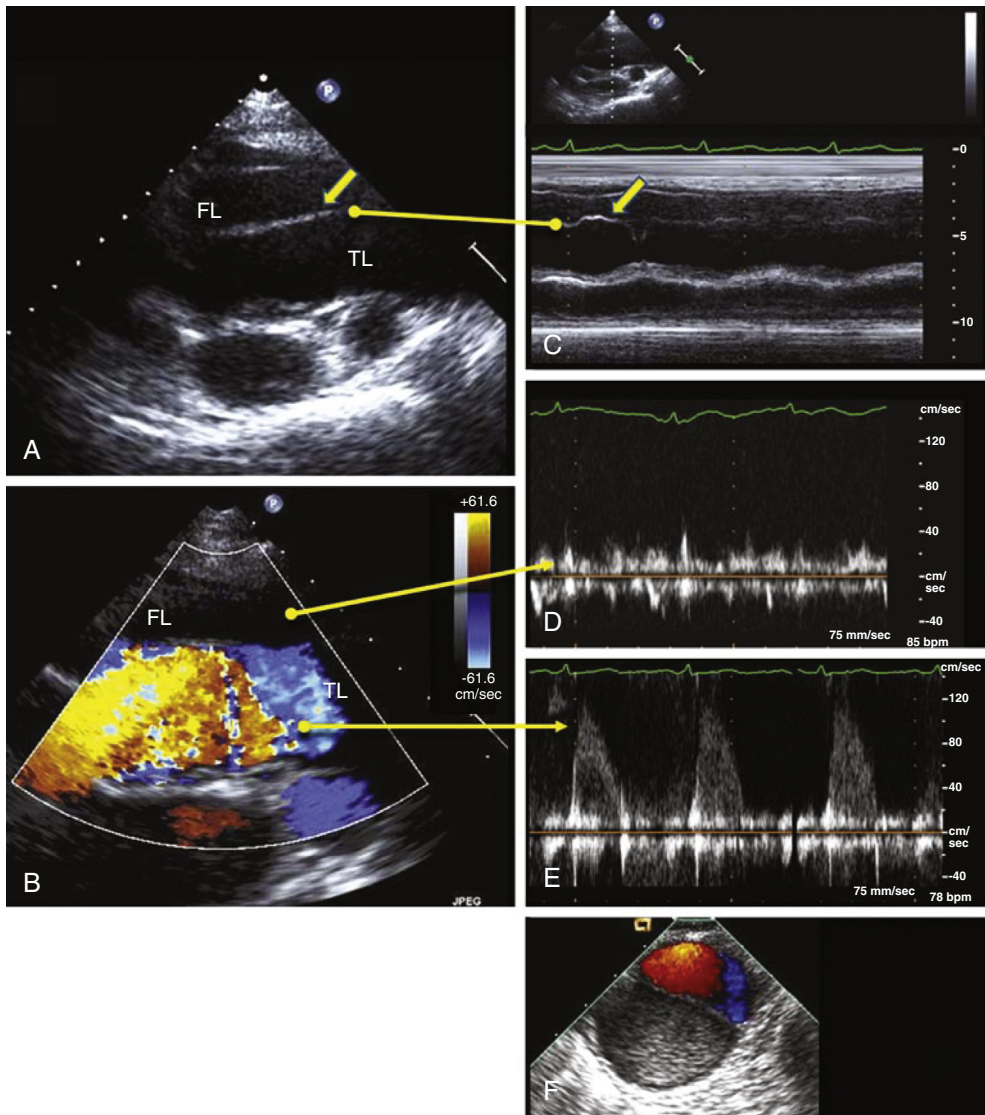
FIGURE 16.70 Aortic dissection demonstrating true and false lumens. **A,** TTE high parasternal long-axis view of a type A aortic dissection. The linear dissection flap is indicated by the *arrow*. *FL,* False lumen; *TL,* true lumen. **B,** TTE view at the same level with color flow Doppler illustrating brisk and turbulent color flow within the true lumen. **C,** M-mode illustrating systolic pulsation of the dissection flap *(arrow)* outward from the true aortic lumen. **D,** Low-velocity spectral Doppler flow without clear cyclic variation in the false lumen. **E,** Systolic forward high-velocity spectral Doppler flow in the true lumen. **F,** TEE short-axis view of the ascending aorta in a different type A dissection case demonstrating spontaneous echocardiographic contrast in the false (larger) lumen and brisk systolic flow in the true (smaller) lumen by color Doppler.
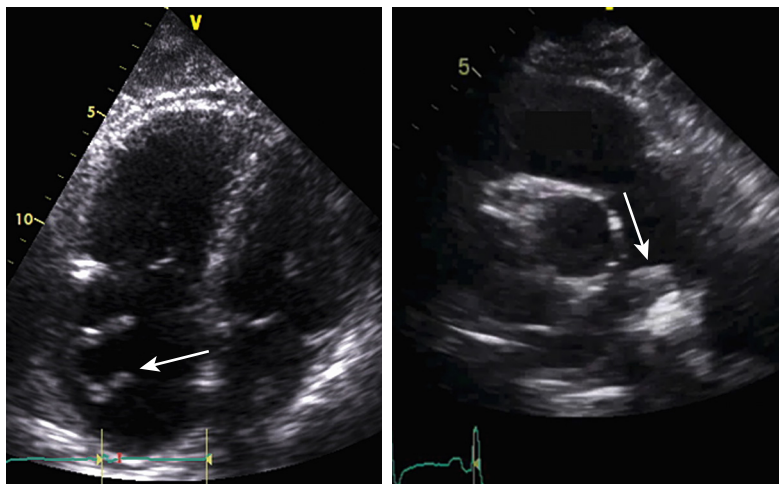


FIGURE 16.71 **Left,** Thromboembolus in the right atrium (*RA*). The *arrow* indicates a serpentine mass that is a thrombotic "cast" of a deep vein of the lower extremities that has embolized to the RA. (See Video 16.56.) Note the right-sided heart dilation and hypokinesis, clues indicating that a significant acute pulmonary embolus has also occurred. **Right,** Saddle embolus at the bifurcation of the pulmonary artery (*arrow*).

re-evaluation of patients with endocarditis who have a change in clinical signs or symptoms (e.g., new murmur, embolism, persistent fever, HF, abscess, or atrioventricular heart block) and in patients at high risk of complications (e.g., extensive infected tissue/large vegetation on initial echocardiogram or staphylococcal, enterococcal, fungal infections); (3) in patients with known or suspected endocarditis, TEE is recommended when TTE is nondiagnostic, when complications have developed or are clinically suspected, or when intracardiac device leads are present; and (4) Intraoperative TEE should be performed for patients undergoing valve surgery for IE.[65,76] Following completion of antibiotic therapy, TTE is also recommended to re-evaluate cardiac and valve structure and function.

Infective endocarditis is definitively diagnosed by culture or pathologic examination of a vegetation (in situ or embolized) or intracardiac abscess. However, many cases are diagnosed on clinical grounds by using the modified Duke criteria as a guideline. The first criterion is positive blood cultures consistent with infective endocarditis. The second major criterion is an echocardiogram demonstrating (1) a vegetation (Fig. 16.74AB, and Video 16.58) (an oscillating intracardiac mass on a valve, in the path of a regurgitant jet, or on implanted material) in the absence of an alternative anatomic explanation, (2) an abscess or pseudoaneurysm (Fig. 16.74C and Video 16.59), or (3) new partial dehiscence of a prosthetic valve (Fig. 16.74D; see Video 16.46).[76] Variations on the extent and location of destroyed endocardial tissue can lead to distinct associated pathologies such as pseudoaneurysms, leaflet aneurysms or perforations, and fistulas between neighboring cavities.

The sensitivity of TTE ranges up to 63% (up to 71% in patients without prosthetic valves), with a specificity close to 100%. Endocarditis of the mitral and aortic valves are unlikely without evidence of regurgitation. The suboptimal sensitivity often results from physical imaging factors causing poor image quality and acoustic shadowing and also depends on the size of the vegetation. Because of its higher 2D resolution and different windows, TEE has much higher sensitivity (94% to 100%) and is especially advantageous in assessing prosthetic valves and diagnosing paravalvular extension of infection with abscess. Thus, a reasonable diagnostic approach is to use TTE as the first-line screening tool; if this is nondiagnostic, one may turn to TEE if clinical suspicion for endocarditis is
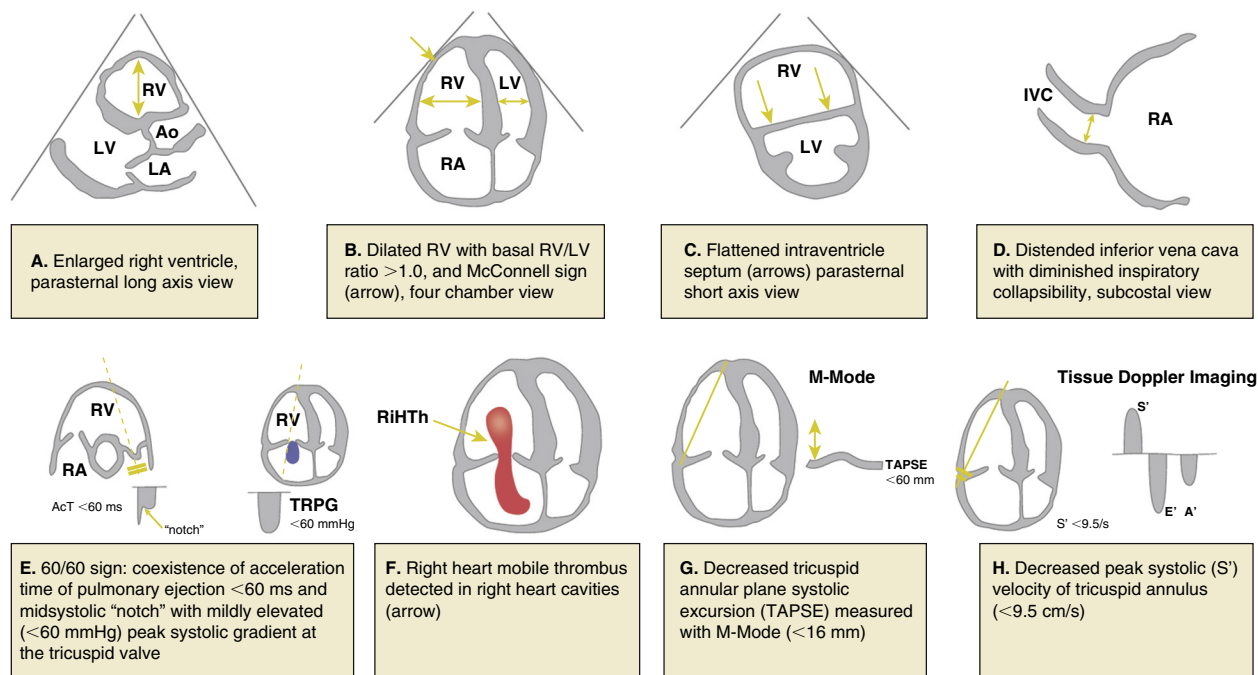
**A.** Enlarged right ventricle, parasternal long axis view

**B.** Dilated RV with basal RV/LV ratio >1.0, and McConnell sign (arrow), four chamber view

**C.** Flattened intraventricle septum (arrows) parasternal short axis view

**D.** Distended inferior vena cava with diminished inspiratory collapsibility, subcostal view

**E.** 60/60 sign: coexistence of acceleration time of pulmonary ejection <60 ms and midsystolic "notch" with mildly elevated (<60 mmHg) peak systolic gradient at the tricuspid valve

**F.** Right heart mobile thrombus detected in right heart cavities (arrow)

**G.** Decreased tricuspid annular plane systolic excursion (TAPSE) measured with M-Mode (<16 mm)

**H.** Decreased peak systolic (S') velocity of tricuspid annulus (<9.5 cm/s)

**FIGURE 16.72** Echocardiographic signs of RV pressure overload that may be associated with pulmonary embolus. A', peak late diastolic (during atrial contraction) velocity of tricuspid annulus by tissue Doppler imaging; AcT, right ventricular outflow Doppler acceleration time; Ao, aorta; E', peak early diastolic velocity of tricuspid annulus by tissue Doppler imaging; IVC, inferior vena cava; LA, left atrium; LV, left ventricle; RA, right atrium; RiHTh, right heart thrombus (or thrombi); RV, right ventricle/ventricular; S', peak systolic velocity of tricuspid annulus by tissue Doppler imaging; TAPSE, tricuspid annular plane systolic excursion; TRPG, tricuspid valve peak systolic gradient. (From Konstantinides SV, Meyer G, Becattini C, et al. 2019 ESC guidelines on the diagnosis and management of acute pulmonary embolism developed in collaboration with the European Respiratory Society (ERS): The Task Force for the diagnosis and management of acute pulmonary embolism of the European Society of Cardiology (ESC). *Eur Heart J.* 2020;41:543.)
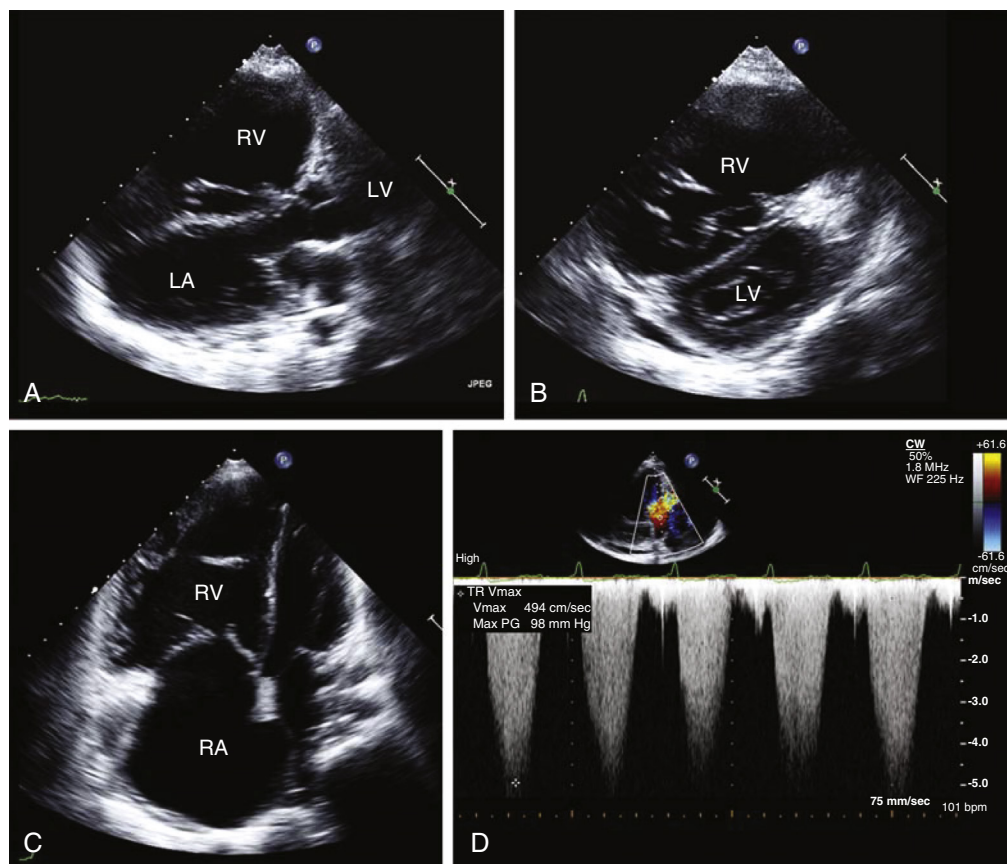


**FIGURE 16.73** Pulmonary hypertension secondary to chronic thromboembolic disease. **A,** Parasternal long-axis view illustrating a small left ventricular cavity and enlarged right ventricular outflow tract. **B,** Parasternal short-axis view demonstrating the D-shaped left ventricular cavity caused by systolic and diastolic septal flattening, i.e., pancyclic elevated right ventricular pressure. **C,** Apical four-chamber view. Note the dilated right atrium and tricuspid annulus with incomplete closure of the tricuspid valve, as well as leftward distention of the interatrial septum. **D,** Severe tricuspid regurgitation (TR) with an elevated TR velocity corresponding to a calculated right ventricular systolic pressure of 98 mm Hg plus right atrial pressure. The upslope of the tricuspid regurgitant jet is slow, indicative of poor right ventricular contractility. *LA,* Left atrium; *LV,* left ventricle; *RA,* right atrium; *RV,* right ventricle.
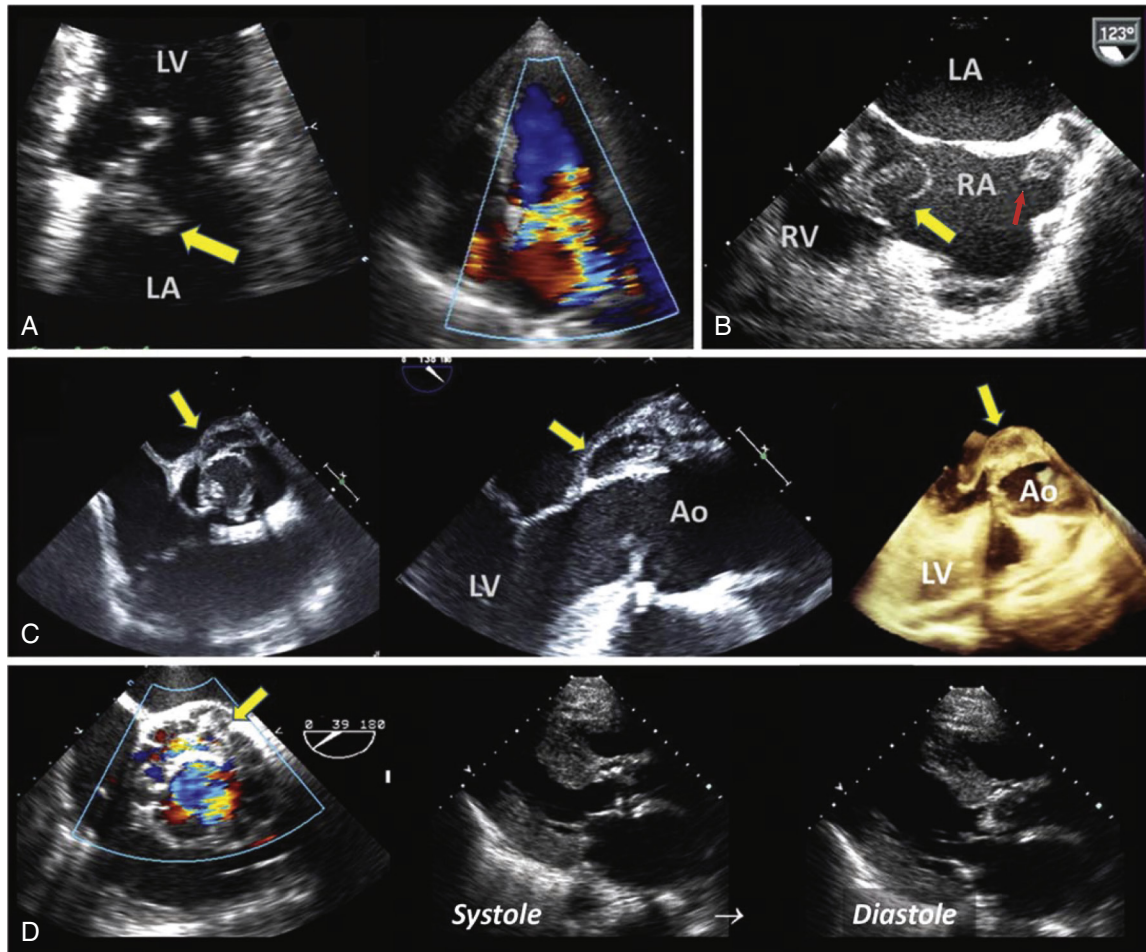
**FIGURE 16.74** Echocardiography in endocarditis. **A,** Vegetation (*arrow*) on the left atrial aspect of a rheumatic mitral valve **(left panel)** with color Doppler demonstration of a second noncentral jet of MR at the base of the leaflet and vegetation indicative of leaflet perforation **(right panel).** (See corresponding Video 16.58.) **B,** Vegetation (*yellow arrow*) on the right atrial aspect of the tricuspid valve on a TEE long-axis view. An additional vegetation (*red arrow*) in the superior vena cava associated with a previous indwelling catheter is noted, and the eustachian valve was also infected in this patient with a history of intravenous drug abuse. **C,** Paravalvular abscess (*arrow*) as indicated by the crescentic echolucent area with thickening from the 11- 1 o'clock position on short-axis **(left panel)** and long-axis **(middle panel)** TEE views anterior to the annulus of a bicuspid aortic valve (open in systole), also visualized on the 3D TEE view **(right panel).** (See Video 16.59.) **D,** Ringlike abscess around the annulus of a bioprosthetic aortic valve as seen on a short-axis TEE view **(left panel).** This causes dehiscence of the valve, as seen on long-axis TEE views **(middle and right panels),** in which it rocks forward in systole and prolapses into the LVOT in diastole. (See Video 16.46.) *Ao,* Aorta; *LA,* left atrium; *LV,* left ventricle; *RA,* right atrium; *RV,* right ventricle.

high, as in the patient with a prosthetic valve or predisposing condition, clinical features suspicious for a complicated endocarditis, or a potential indication for cardiac surgery.[78] Selected patients with suspected endocarditis—often those with obscured areas or acoustic shadowing on echocardiography, degenerative changes that are difficult to distinguish from infectious processes, vascular grafts, or those at high risk of complications during TEE—will benefit from additional imaging with other techniques such as CT angiography, CMR, or metabolic imaging modalities such as FDG PET or white blood cell imaging. These complementary modalities are particularly helpful in the setting of prosthetic valves (see Multimodality Imaging and Future Directions).

Vegetations appear as discrete echogenic masses that are adherent to but have motion that is distinct from that of valve itself. A typical mitral vegetation is shown in Fig. 16.74A; see Video 16.58. Characteristics of vegetations that aid in distinguishing them from other masses include localization, texture, motion, shape, and associated abnormalities. Vegetations are typically located on the upstream, or low-pressure, sides of valves (i.e., the atrial aspect of atrioventricular valves or the ventricular aspect of semilunar valves); less often, they are attached to the periphery of septal defects (on the low-pressure side), to chordae, or to the mural endocardium. The *echodensity* of a vegetation is usually similar to that of myocardium, although advanced vegetations can be inhomogeneous, with findings indicative of liquefaction (which is echolucent) or fibrosis/calcification (which is echodense or bright). Independent *motion* of vegetations is often described as oscillating or erratic. Large vegetations can create a "ball-and-chain"

effect that causes leaflet prolapse and flail into the upstream chamber and consequent regurgitation. Vegetations vary tremendously in *shape* but often appear as compact multilobulated or pedunculated, amorphous, and friable agglomerations compared with tumor tissue or thrombus. The vegetation can extend some distance from the valve to which it is tethered and may occur in multiples on the same or different valves. *Associated abnormalities* such as regurgitation, abscesses, leaflet perforation, and intracardiac fistulas can accompany advanced endocarditis. 3D TEE appears to provide more accurate assessment of overall vegetation size, and in some cases can better visualize and define the extent of complications involving valves and surrounding anatomic structures.[78] There are no distinguishing characteristics that are organism specific, although staphylococcal infections (particularly methicillin-resistant *Staphylococcus aureus* and *S. lugdunensis*) tend to be more destructive and form abscesses, and fungal infections are often impressively large and dendritic in appearance.

Vegetations devoid of microorganisms are the hallmark of *noninfectious endocarditis*, also called "nonbacterial thrombotic" or "nonbacterial marantic" endocarditis (see Chapter 80). The typical lesions are small (1 to 5 mm), verrucous, nondestructive nodules that adhere to the upstream side of the valve (typically mitral or aortic) along the line of closure and contain only cellular and fibrin elements. These aseptic lesions are seen in up to 43% of patients with systemic lupus erythematosus (SLE) and 29% of those with antiphospholipid syndrome (APS), in whom they can cause cerebral embolization. These also occur in patients with advanced neoplasms, sepsis, and prothrombotic

tendencies in association with clinical features indistinguishable from those of typical infective endocarditis (see later, Systemic Diseases and Echocardiography).[77]

It is important to note that the presence of preexisting thickening and degenerative changes in leaflets can render the diagnosis challenging. On occasion, myxomatous leaflets, ruptured chordae, calcified structures, and fibrin strands can either mask or mimic a vegetation. Papillary fibroelastomas and thrombi can resemble valvular vegetations. In these circumstances, clinical correlation with other Duke diagnostic criteria is important. Comparison with previous echocardiograms should also be undertaken; a stable finding over years is unlikely to represent a vegetation. Use of TEE for higher-resolution images is often indicated, particularly if a cardiac device is involved, a complication (e.g., embolization, valve destruction, abscess) is suspected or an aggressive organism such as *S. aureus* is involved[78,79]

Among patients with endocarditis, 66% to 75% have risk factors for infection, and echocardiography should be used to scrutinize the relevant structures at risk particularly carefully. Patients with any type of prosthetic valve or closure device, complex cyanotic congenital heart disease, and surgical systemic-pulmonary shunts are at relatively high risk. Previous endocarditis and IV drug abuse are strong predisposing factors for tricuspid and pulmonic valve endocarditis. Those with bicuspid aortic valves, rheumatic heart disease, or mitral valve prolapse are predisposed but at lower risk. Other intracardiac structures that are prone to infection, usually at the time of placement or access, include defibrillator/pacemaker wires and chronic indwelling IV catheters, particularly when used for total parenteral nutrition or hemodialysis in immunocompromised patients. Echocardiographic characteristics associated with a poorer prognosis and/or embolization include vegetation size greater than 1.0 cm on 2D images (which confers a 2.5-fold higher risk for embolization, especially if on the mitral valve), increasing size of the vegetation over time despite therapy, very mobile vegetation, and paravalvular abscess. The latter is more common with prosthetic valves and increases mortality twofold. Other findings such as severe left-sided regurgitation or prosthetic valve dysfunction, low LVEF, pulmonary hypertension, and premature mitral valve closure or other signs of elevated diastolic pressures also portend poor outcome.[76,79]

The natural history of vegetations after medical therapy is of interest because most will still be apparent on follow-up echocardiography in 1 to 2 months, even after successful medical treatment. Approximately half will become more echodense over time. These observations probably reflect the varied components of the vegetation, which include not only bacteria but also inflammatory cells, fibroblasts, and extracellular matrix. Growth of a vegetation over time and increasing valvular regurgitation are additional poor prognostic signs. However, the mere persistence of vegetations in the absence of symptoms or positive blood cultures is not associated with increased clinical complications. Thus, treatment of endocarditis should not be guided by the echocardiographic morphology of the vegetation over time but by clinical response to therapy.

## Role of Echocardiography in Surgery for Endocarditis

If left untreated, infective vegetations are destructive via pathways that are apparent on echocardiograms and ECGs and by clinical sequelae. If present, these sequelae are indications for surgery, particularly if recalcitrant to medical therapy. Indications include (1) embolism to the coronary arteries, brain, lungs, spleen, kidney, or extremities; (2) severe valvular regurgitation and heart failure secondary to leaflet malcoaptation, perforations, or flail; (3) abscess, which may invade the cardiac conduction system; (4) mycotic aneurysms of vessels and valves; (5) pseudoaneurysms or fistulas of the heart; and (6) suppurative or hemorrhagic pericarditis.

Typical paravalvular extension patterns can be detected on echocardiograms (and ECGs). At the *aortic valve*, involvement of the right cusp can lead to necrosis of the membranous interventricular

septum, aneurysm of the right sinus of Valsalva, and, prosthetic valve dehiscence. Embolization into the RCA can also occur and cause MI. Involvement of the left cusp can affect the intervalvular fibrosa and extend to infect the base of the anterior mitral valve leaflet. There is also the potential to form an aortic-to-LVOT fistula, or prosthetic paravalvular leak. Involvement of the noncoronary cusp can extend to the posterior interventricular septum, where the His conduction fibers are located, which can lead to the development of an intra- or infra-hisian block (third-degree atrioventricular block) or bundle branch block.

Severe infection of the *mitral valve* less frequently leads to conduction disturbances. Although first- or second-degree atrioventricular block can occur, supraventricular tachycardias are more common. *Tricuspid valve* infection can extend to involve the tricuspid annulus and eustachian valves (Fig. 16.74B), seed the pulmonic valve, and cause septic pulmonary emboli in 25% to 80% of cases.

### SYSTEMIC DISEASES AND ECHOCARDIOGRAPHY

Aside from conditions that directly affect the heart itself, many systemic diseases with cardiac manifestations are detectable on echocardiography. Uncontrolled hypertension causes symmetrically increased wall thickness and LV hypertrophy in association with LA enlargement and diastolic dysfunction. Renal disease causes early calcification of the valves and potentially uremic pericardial effusions. Hypothyroidism can be associated with a myxedematous pericardial effusion. COPD can cause conspicuous right-sided heart enlargement, RV hypertrophy, elevated TR velocity, and a prominent pericardial fat pad secondary to corticosteroid treatment.

There are diseases that affect all tissue layers of the heart. Amyloidosis is notorious for causing restrictive cardiomyopathy (see earlier and Fig. 16.27F), but also frequently causes valvular thickening and pericardial effusions. Infiltration of amyloid into the atrial walls leads to poor atrial contractility and a high prevalence of atrial thrombi, even when sinus rhythm is still present.[47] Granulomatous diseases such as sarcoidosis can cause a focal myocarditis with granulomas (eFig. 16.34), which results in very localized areas of akinesis in a noncoronary distribution (see Video 16.18). Pericarditis, valvulitis, and also coronary and aortic arteritis have been reported with Wegener granulomatosis. Although scleroderma is known to cause direct myocardial fibrosis histologically, on echocardiography this becomes apparent in only a minority of patients, usually late in the course of disease. Instead, the most common echocardiographic abnormalities in scleroderma are elevated RV systolic pressure, RV dilation, and pericardial effusion, as well as LA enlargement and diastolic dysfunction.

Other diseases that have echocardiographic manifestations include human immunodeficiency virus (HIV) infection (see Chapter 85), in which the most common abnormalities are dilated cardiomyopathy, pericardial effusion (seen in 12% to 25% of cases), and also HIV-related pulmonary hypertension and cardiac lymphomas. The prolonged duration of HIV infection and combination antiretroviral therapy regimens may contribute directly and indirectly (via lipodystrophic effects and chronic inflammation) to both cardiomyopathy and the excess risk of CAD in this population. Overall however, with increasing access to combination antiretroviral therapy, the prevalence of clinically significant HIV-associated cardiomyopathy and pericardial effusions appears to be decreasing.[80]

Similarly, even when cancers spare the heart by way of direct involvement, the radiation and chemotherapy regimens used to attack the neoplasms can have cardiac effects (see Chapters 56 and 57). Ideally, the early detection of cardiomyopathy in patients who receive chemotherapy, particularly with anthracyclines (as well as tyrosine kinase inhibitors and immunomodulators), allows modification of the protocol before irreversible damage occurs. Screening for LVEF is the most widely used strategy (with a suggested cutoff of decline in LVEF ≥10% to an absolute value < 53% as a sign of LV dysfunction), but a decrease in peak systolic GLS (>15% change from baseline) is a more sensitive and earlier predictor of cardiotoxicity.[81,82] Baseline and serial determination of GLS is becoming more widely accepted as reproducibility improves and vendors converge to standardize measurements. It is not yet known if decrements in GLS during chemotherapy will predict chronic irreversible heart failure, and thus it remains to be seen if cancer treatment should be altered based on a new reduction in GLS alone. Aside from chemotherapy damage, survivors of Hodgkin disease also frequently have early thickening and stenosis of the aortic and less commonly mitral valves, as well as accelerated CAD from radiotherapy. Hence, screening echocardiograms for even asymptomatic patients who have had radiation therapy are recommended at 10 years post-radiation and
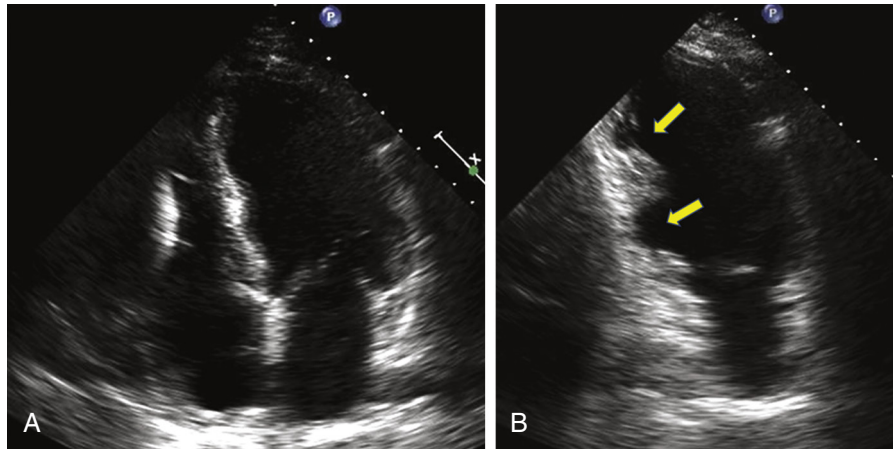
**EFIGURE 16.34** Sarcoidosis. **A,** Apical four-chamber view illustrating the right-sided heart enlargement (containing a pacemaker wire) and the septal focal wall motion abnormalities in the left ventricle ("scalloping") typically seen in sarcoid heart disease. RV dilation is often secondary to pulmonary hypertension from sarcoid lung involvement. **B,** Apical two-chamber view illustrating very focal areas of thinning and akinesis (*arrows*) in the inferior LV wall because of sarcoid granulomas and/or myocardial scarring. (See corresponding Video 16.14.)

every 5 years thereafter. For symptomatic patients with valvular disease, echocardiography is suggested annually.

Several other conditions predispose to valvular abnormalities (see earlier, Valvular Heart Disease). Rheumatic carditis and its sequelae are well-known historical examples and are still a significant cause of heart disease in developing nations (see Chapter 81). Up to 60% of patients with carcinoid tumors have cardiac involvement in which plaquelike deposits build up on the right-sided heart valves (typically the ventricular aspect of the tricuspid valve and the arterial aspect of the pulmonic valve). This causes a characteristic retracted fixed, "half-open" appearance of the tricuspid and pulmonary leaflets and a combination of valvular stenosis and regurgitation (see Fig. 16.49; see Video 16.43). Cardiac involvement confers a worse median survival time for carcinoid. The hematologic malignancies and any thrombophilic state (e.g., sepsis, disseminated intravascular coagulation, SLE, APS) can cause nonbacterial marantic endocarditis in which the sterile vegetations and fibrin strands undergo frequent cycles of growth and subsequent fragmentation and embolization, with associated valvulitis and leaflet destruction. The systemic vasculitides such as Takayasu arteritis and Behçet disease are notable causes of AR and aortic root dilatation, particularly in younger patients.[83]

## CARDIAC MASSES (SEE CHAPTER 98)

Cardiac tumors are relatively rare, ranging from an incidence of 1% to 2% in general autopsy series but up to 4% to 8% in cancer patient autopsies, so routine screening is not recommended. Among primary tumors of the heart, up to 90% or more are detected incidentally and three quarters are benign. It is the location of an intracardiac or extracardiac mass—in the context of the patient's age, clinical findings, and comorbidities—that is often the best indicator of the type of tumor; morphologic features of the mass play a secondary role in identification (Table 16.11).[84]

Nonetheless, the overall appearance of the mass (with respect to size, solid versus cystic, shape, degree of independent mobility, and fragility), its attachments, and the extent of myocardial, endocardial, or pericardial invasion can offer clues to its nature. Calcified or fibrotic areas appear echobright, whereas cystic degeneration causes echolucent foci on echocardiography. Obstruction to caval or valvular inflow will cause increases in peak spectral Doppler velocities, often with a mosaic color Doppler pattern signifying turbulent flow. MS and MR caused by an LA myxoma prolapsing across the mitral valve is a classic example (Fig. 16.75 and Video 16.60). When myxomas present this way, the echocardiographic appearance of this entity may be so pathognomonic that no further workup is required before surgical resection. Although 70% of myxomas originate from the left side of the fossa ovalis, they may arise in other locations and may be multiple, so that complete echocardiographic evaluation of the heart is indicated. Similarly, papillary fibroelastomas occur so characteristically on the aortic and mitral valves and are so commonly seen as filamentous or amorphous growths that shimmer, undulate, and prolapse, that further assessment may not be required before surgery (Fig. 16.76 and Video 16.61). However, the smaller lesions may be difficult to differentiate from highly mobile Lambl excrescences or even vegetation.

In select patients, to refine the diagnostic possibilities, IV echocardiographic contrast material may be used to determine whether a tumor hyperenhances. Hyperenhancement indicates that the mass is neovascularized and thus more likely to be malignant than a benign stromal tumor or thrombus.[21] One can also use 3D echocardiography to better illustrate the overall size, location, and attachments of intracavitary masses. Following diagnosis, echocardiography is a convenient way to monitor for recurrence, growth, or adverse sequelae after excision or treatment.[85]

### COMMON PRIMARY TUMORS

*Myxoma* accounts for more than 50% of primary cardiac tumors in adults, followed by papillary fibroelastomas and lipomas. Myxoma is a primary benign tumor believed to arise from mesenchymal (endocardial) cells. It typically arises in the left atrium (75% of cases, with the other 20% occurring in the right atrium and 5% in the ventricles) and is attached to the interatrial septum near the fossa ovalis by a stalklike pedicle. Attachments to the mitral valve have been described in a small

percentage of cases. Grossly and on echocardiography, myxoma frequently appears as a gelatinous, compact mass, but there is a spectrum of morphologies. Smaller tumors tend to be more papillary or villous and are friable and thus prone to embolize. Larger myxomas have a smoother, globular, or grape cluster–like appearance and can grow large enough to fill the left atrium and cause both MS and a renowned tumor "plop" on auscultation as the mass prolapses into the left ventricle in diastole (see Fig. 16.75 and Video 16.60). Approximately 7% of cases result from an autosomal dominant mutation and are part of the "Carney complex" syndrome, associated with skin lentiginosis and endocrine disorders.[85]

In adults, *papillary fibroelastomas* are the next most common cardiac benign tumors and the most common valvular tumor. Most (>80%) are found on left-sided (aortic or mitral) valves, although any valve may be affected, and 9% occur as multiple lesions. Pathologists usually classify fibroelastomas as an advanced or more florid form of *Lambl excrescences,* which are degenerative changes in the valves. Fibroelastomas tend to appear on either side of the aortic valve or on the atrial side of the mitral valve. Less frequently, they have also been known to arise on mitral chordae or papillary muscles. On echocardiography, papillary fibroelastomas appear round, oval, or irregular in shape and homogeneous in texture (see Fig. 16.76 and Video 16.61). Almost half have a short stalk, which confers more mobility. Fibroelastomas are found most frequently in older adults as solitary lesions. Shedding of the threadlike elements and associated clot accounts for their frequent manifestation as embolization (transient ischemic attack or stroke, angina, or sudden death).[84,85]

*Lipomas* are encapsulated collections of benign fat cells that tend to occur in subepicardial or subendocardial locations and may grow into the pericardial space. Although benign, usually discovered incidentally, and easily distinguished by CMR characteristics (see Chapter 19), these tumors tend to increase progressively and can cause mass effect, heart block, or tachyarrhythmias. *Lipomatous hypertrophy of the interatrial septum* is a generally benign finding, particularly in elderly or obese patients and is technically hyperplasia of epicardial adipocytes within the groove between the LA and RA walls and inferior pyramidal space, which spares the fossa ovalis and produces a characteristic dumbbell-shaped mass. Although lipomatous hypertrophy is unencapsulated and may reach an impressive thickness (1 to 2 cm or more), if the location is typical and no associated atrial arrhythmias or caval obstruction are present, no treatment is indicated.[86]

*Pericardial cysts* are benign fluid-filled tumors of the parietal pericardium and are thought to be a congenital abnormality.[72,87] They may be solitary or multilocular, and some have been documented to grow to massive (>20 cm) size. They account for approximately 20% of benign primary cardiac masses (overall incidence of 1 in 10,000) and usually occur near the cardiophrenic borders (right more often than the left). This gives the appearance of cardiomegaly on chest radiographs and an encapsulated echolucent mass on echocardiography. Among known cases, 75% are asymptomatic. If large, however, pericardial cysts may cause atypical chest pain, breathlessness, AF, persistent cough, or compressive problems such as RVOT obstruction. Rare cases of cardiac tamponade secondary to intrapericardial rupture and hemorrhage have been reported.

*Rhabdomyomas* are the most common primary cardiac neoplasm in children and are usually found during the first year of life. They tend to be solid intramyocardial lesions containing striated myocyte fibers, and 90% occur as multiple tumors. Although most patients are asymptomatic, larger tumors have been known to cause arrhythmias, LVOT obstruction, and heart failure. Half the cases are associated with tuberous sclerosis. Most regress spontaneously, and overall these tumors are rare in young adults.[84,85]

*Fibromas* are the second most common pediatric cardiac neoplasm. They arise in the ventricular myocardial layer, are five times more common in the left ventricle, and consist of solid tumors containing fibroblasts. These tumors often occur in the LV septum or free wall, where they appear broad-based and can become quite large and develop calcific foci (eFig. 16.35). Unlike rhabdomyomas, fibromas do not spontaneously regress and may grow to a size that obliterates the heart chamber, interferes with valvular function, or causes arrhythmia and thus necessitates surgical resection.[85]

## Secondary Tumors

Secondary cardiac tumors outnumber primary ones by 20 to 40 to 1. In principle, any malignant tumor may metastasize to the heart. The most
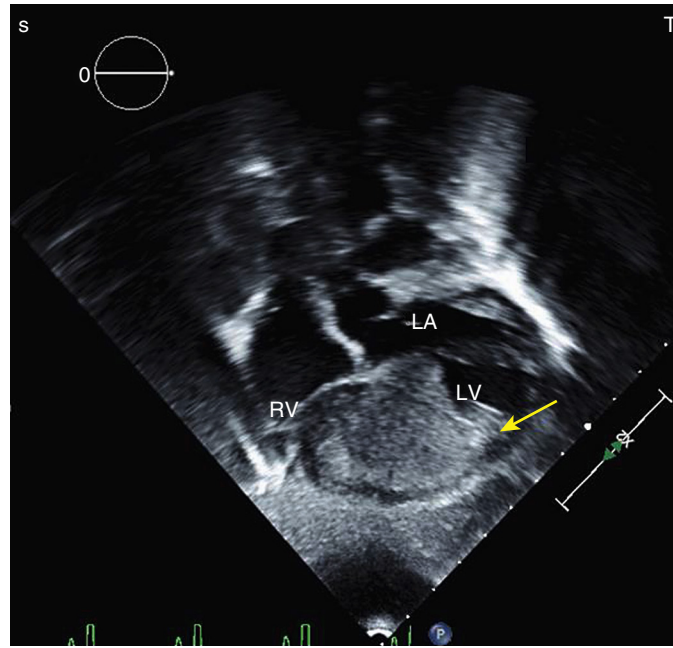
Fibroma

**EFIGURE 16.35** Fibroma. Transthoracic pediatric echocardiogram five-chamber view showing a large (5-cm) fibroma (*arrow*) arising in the distal left ventricle and exerting mass effect on the right ventricle.

**TABLE 16.11 Site-Specific Differential Diagnosis of Cardiac Tumors**

| SITE | ONCOLOGIC | ALSO CONSIDER NON-NEOPLASTIC MASSES | NORMAL OR VARIANT STRUCTURES |
|---|---|---|---|
| Left atrium | Myxoma<br>Lipoma<br>Bronchogenic carcinoma<br>Sarcoma (involving the wall/pericardium)<br>Hemangioma<br>Paraganglioma | Thrombus<br>Endocardial blood cyst | Lipomatous hypertrophy of interatrial septum<br>External compression (by hernia, thoracic aorta, bezoar)<br>Echocardiographic artefact: left upper pulmonary vein limbus ("Coumadin ridge")<br>Appendage pectinate muscles<br>Atrial suture anastomosis after heart transplantation<br>Inverted LA appendage (postoperative)<br>Aberrant LA chorda |
| Right atrium | Myxoma<br>Nephroblastoma, renal cell cancer<br>Hepatocellular carcinoma<br>Sarcoma (angiosarcoma)<br>Paraganglioma<br>Adrenal tumors | Thrombus (deep venous or in situ) or fibrin casts (of previous indwelling catheter/wire)<br>Vegetation (on pacer/ICD wires)<br>Lipomatous hypertrophy of interatrial septum | Eustachian valve<br>Chiari network<br>Crista terminalis<br>Interatrial septal aneurysm<br>Pectus excavatum |
| Left ventricle | Rhabdomyoma (often multiple)<br>Fibroma<br>Hamartomas<br>Purkinje cell tumors (usually infants) | Thrombus<br>Apical hypertrophic cardiomyopathy<br>Subaortic membrane | Calcified or multilobed papillary muscles<br>Redundant or severed mitral chordae<br>Trabeculations, false tendons<br>Focal upper septal hypertrophy<br>Swirling from inhomogeneous intravenous echocardiographic contrast distribution |
| Right ventricle | Rhabdomyoma<br>Fibroma | Thrombus | Redundant tricuspid chordae<br>Tricuspid papillary muscle<br>Moderator band |
| Valves/annuli | Papillary fibroelastoma<br>Myxoma<br>Hamartoma<br>Lipomas | Lambl excrescences<br>Focal or caseous mitral annular calcification<br>Vegetation<br>Marantic endocarditis<br>Thrombus (especially on prosthetics) Pannus (especially on prosthetics)<br>Abscess<br>Blood cyst<br>Rheumatoid nodule | Nodules of Arantius<br>Myxomatous/degenerative changes<br>Pannus; loose suture; bioglue or pledgets around prosthetic valves |
| Pericardium | Malignant involvement from lung, breast, lymphoma/leukemia, or gastrointestinal tract melanoma<br>Mesothelioma<br>Primary: spindle cell tumor, fibrous tumors, lipoma, liposarcoma, teratoma<br>Paraganglioma | Pericardial or bronchogenic cyst<br>Rheumatoid nodule<br>Thrombus<br>Hydatid cyst (Echinococcus) | Epicardial or mediastinal fat<br>Pectus excavatum<br>Atelectatic lung or fibrin in pleural/peritoneal spaces<br>Vascular pseudoaneurysm<br>Thymus (in infants) |

*ICD,* Implantable cardioverter-defibrillator; *LA,* left atrial.
Modified from Wu J. Cardiac tumors and masses. In: Stergiopoulos K, Brown DL, eds. *Evidence-Based Cardiology Consult*. New York: Springer Science + Business Media; 2014.

common site of involvement is the pericardium, with invasion of the myocardium seen next in frequency.[84]

*Pericardial involvement* in cancers may arise from direct invasion of tumor from adjacent lung or mediastinum (e.g., mesothelioma, lymphoma), or there may be more diffuse involvement and effusive/constrictive changes. The most frequent sources of malignant pericardial disease are lung cancer, lymphoma/leukemia, and breast cancer because of their relatively high prevalence, and proximity to the heart. Metastatic pericardial disease may invade the myocardium as well. Of all malignancies, *melanoma* has the highest predilection to metastasize to the heart and pericardium. Cardiac metastases from any source typically are small and multiple or cause effusion or diffuse thickening of the pericardium. However, bulky large solitary tumor lesions may also occur and, unlike benign tumors, may extend from the blood pool into the myocardium or pericardium (see Fig. 16.65).

Secondary tumors may also invade the heart by direct extension[85]: renal cell carcinoma, Wilms tumor, uterine leiomyosarcoma, hepatomas, angiosarcomas, and adrenal tumors can be detected extending into the right atrium via the IVC on echocardiography. Bronchogenic carcinomas can invade the left atrium through the pulmonary veins. An important teaching point is that all four pulmonary veins should be comprehensively evaluated when a left atrial mass is identified.
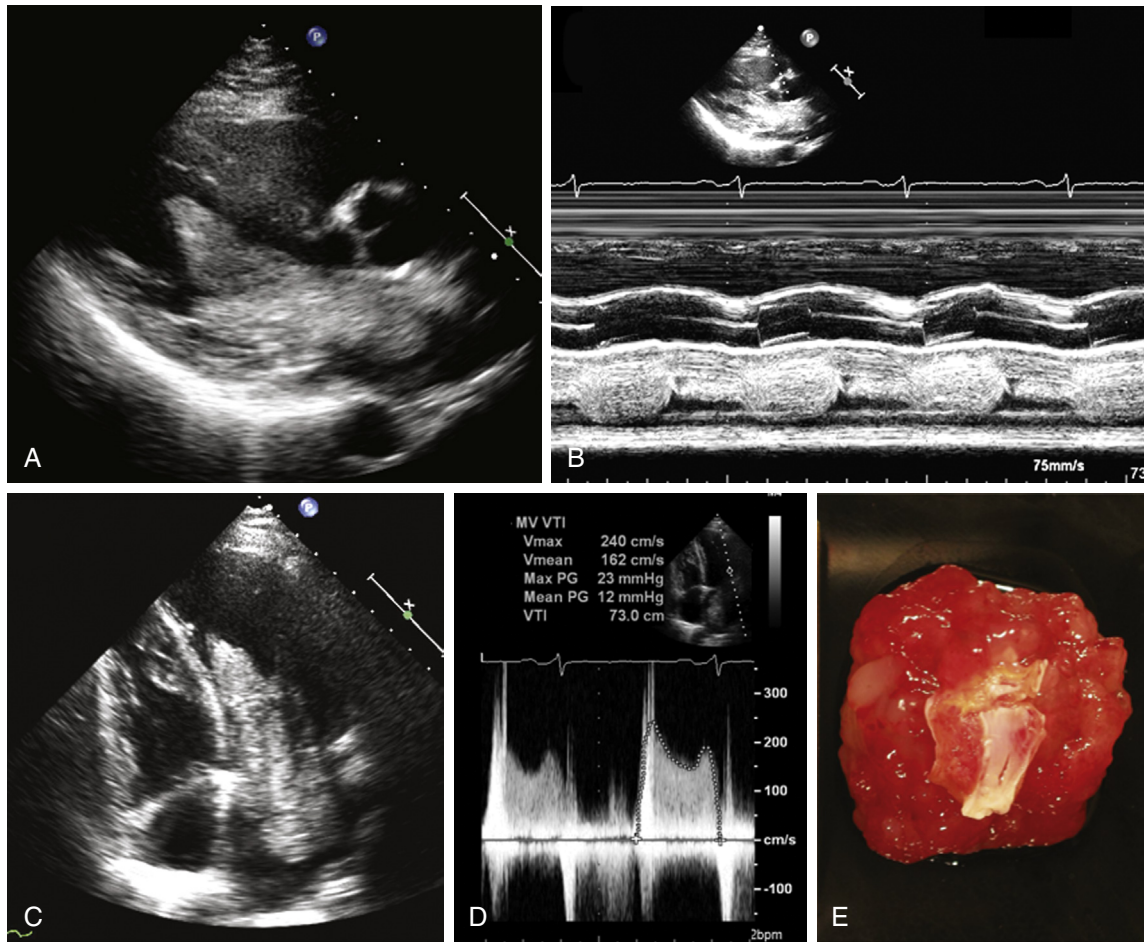
**FIGURE 16.75** Left atrial myxoma. **A,** Parasternal long-axis view. **B,** M-mode view showing the mass prolapsing through the mitral valve into the left ventricle in diastole. **C,** Apical 4-chamber view. **D,** Transmitral gradients (mitral stenosis) as shown by CW Doppler, with peak and mean gradients of 23 and 12 mm Hg. **E,** Gross pathological specimen. (Modified from Wu J. Cardiac tumors and masses. In Stergiopoulos K, Brown DL, eds. *Evidence-Based Cardiology Consult*. New York: Springer Science + Business Media; 2014.)
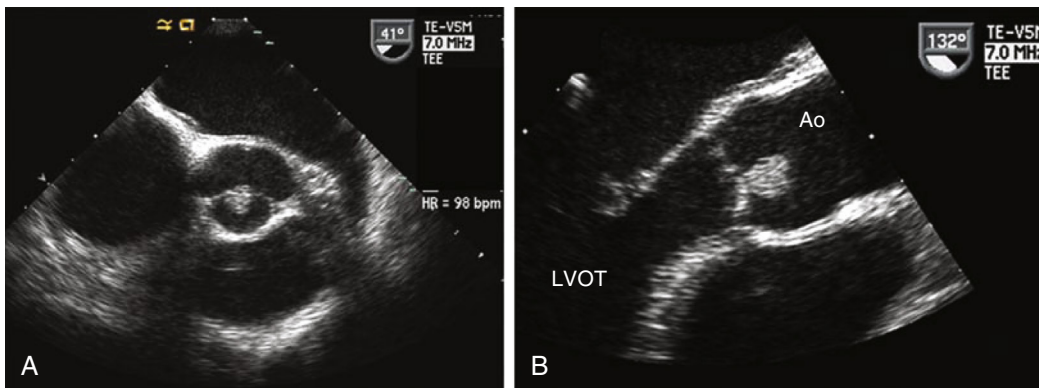


**FIGURE 16.76** Papillary fibroelastoma on the aortic valve. **A,** TEE short-axis view showing the mass on the aortic aspect of the noncoronary cusp. **B,** TEE long-axis view. *Ao,* Aorta; *LVOT,* left ventricular outflow tact. (See Video 16.61.) (Modified from Wu J: Cardiac tumors and masses. In: Stergiopoulos K, Brown DL, eds. *Evidence-Based Cardiology Consult*. Springer Science + Business Media, Inc., 2014.)

Evidence of pulmonary venous involvement is pathognomonic of a malignant process. Lymphatic and hematogenous routes are also pathways to the heart. The location and mass effect of the metastases, rather than type of primary, tend to determine the patient's symptomatology.

## Alternative Diagnoses
### Pseudoneoplasms
With the abundance of cardiac imaging being performed by various modalities, it is inevitable that normal or slight variants of normal structures, degenerative or benign acquired lesions, and nonneoplastic masses may be detected. The onus is on the cardiologist or radiologist to distinguish between the following entities (listed in Table 16.11) and a true neoplasm.

### Intracardiac Thrombus
Masses such as thrombi and vegetations have obvious clinical implications. On echocardiography, formed thrombi appear relatively homogeneous in echodensity and have a gel-like or deformable appearance (Fig. 16.77B). Old thrombi may have more echobright regions and a compact immobile or laminated appearance (see Fig. 16.27A). Clues that a mass is actually a thrombus include residence in areas of stasis (e.g., tip of LA appendage or within LV aneurysm), "wisps" of spontaneous echocardiographic contrast associated with the surface (Fig. 16.77A and Video 16.62), and associated predisposing cardiac conditions, including MS, prosthetic valves, cardiomyopathy, aneurysms of any chamber, or AF (Video 16.63). Ropelike vacillating masses in the right side of the heart often represent thromboemboli from the deep venous system (see Fig. 16.71, left, and Video 16.56). If one is found, then the IVC, as well as the pulmonary arteries, should be inspected for
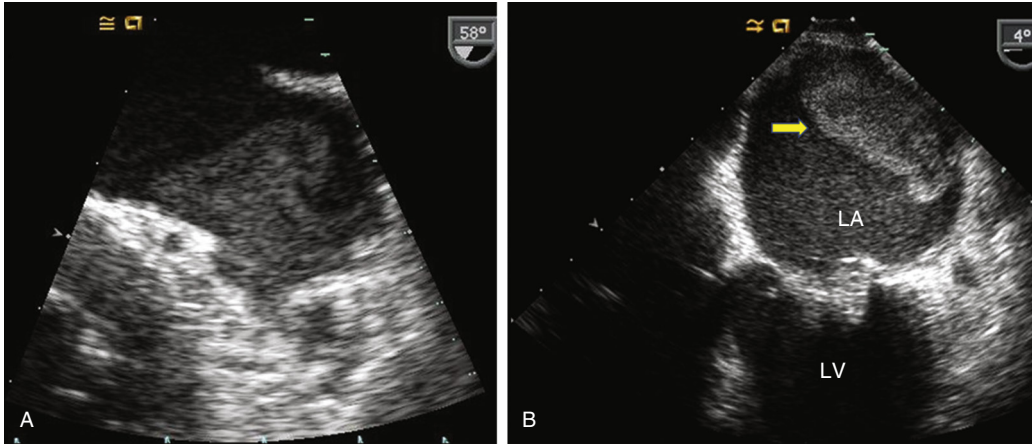
**FIGURE 16.77** Spontaneous echocardiographic contrast and left atrial appendage thrombus. **A,** Zoomed TEE view of spontaneous echocardiographic contrast in the left atrial appendage in a patient with a bileaflet mechanical mitral prosthesis who was subtherapeutic with warfarin treatment (See Video 16.62). **B,** TEE view of organized thrombus (*arrow*) in the left atrial appendage in a patient following mitral annuloplasty. *LA,* Left atrium; *LV,* left ventricle. (See Videos 16.63.)

indenting the posterior wall of left atrium) can give the appearance of a large mass when viewed in only one plane. In the case of a hiatal hernia, having the patient ingest a carbonated beverage to create "contrast" in the hernia can be diagnostic. Knowledge of the typical appearance of these abnormalities, use of echocardiographic enhancing agents, and either careful tilting and sweeping of the transducer plane or use of 3D echocardiography to track the boundaries and attachments of these entities can reveal their true nature.

## ADULT CONGENITAL HEART DISEASE (SEE CHAPTER 82)

Echocardiography plays a critical role in the evaluation and management of both children and adults with congenital heart disease. Consequently, this section focuses on the role of echocardiography in diagnosing common shunts (ASDs and VSDs), as well as transposition of the great arteries (TGA) and tetralogy of Fallot, complex lesions that may be seen by cardiologists caring for adults. The use of echocardiography for the selection and implantation of ASD closure devices is also covered.

### Atrial Septal Defect

ASDs account for approximately 10% of all congenital heart disease and 20% to 40% of congenital heart disease occurring in adulthood. The initial diagnosis of ASD is often made during echocardiography for nonspecific symptoms or for a heart murmur in an asymptomatic individual.

#### General Imaging Principles

Figure 16.78 provides the anatomic classification of ASDs. Although secundum defects are often isolated anomalies, ASDs of other types are frequently associated with other structural anomalies. Multiple ASDs may be encountered in the same patient. Secundum and primum ASDs can generally be diagnosed with 2D TTE, but TEE is typically required to detect sinus venosus and coronary sinus defects. On TTE, although parasternal and apical views are useful, the subcostal view is particularly important because it optimizes the Doppler detection of shunts and minimizes the chance that normal thinning of the fossa will be mistaken for a secundum defect. In the absence of significant pulmonary hypertension, ASD flow is typically left to right, reflecting normal intracardiac pressures. However, agitated saline injections may demonstrate the transient right-to-left shunts that can occur in patients with ASDs or show negative contrast enhancement ("ghosting") when the shunt flow from the left atrium meets the contrast-enhanced RA blood pool.

Regardless of location, hemodynamically significant ASDs will be associated with evidence of RV volume overload, characterized by RV enlargement and diastolic flattening of the interventricular septum. Pulmonary hypertension, which may complicate large defects, will result in flattening that persists through systole. This 2D appearance of RV volume overload and right-sided heart enlargement is considered evidence of a hemodynamically significant shunt ($Q_p/Q_s \geq 1.5:1$). For ASDs, $Q_p/Q_s$, or the ratio of pulmonic to systemic flow is the ratio of RV output (RV SV) to LV output (LV SV) and may be calculated directly by applying the principles of the continuity equation:

$$Q_p/Q_s = \left( \pi[D_{RVOT}/2]^2 \times VTI_{RVOT} \right) / \left( \pi[D_{LVOT}/2]^2 \times VTI_{LVOT} \right)$$

where D indicates the diameter of the RVOT and LVOT, respectively (Fig. 16.79). Additionally, PVR can be calculated in Wood units (see earlier, Pulmonary Hypertension); normal PVR is 0.5 to 1.5 Wood units.[75]
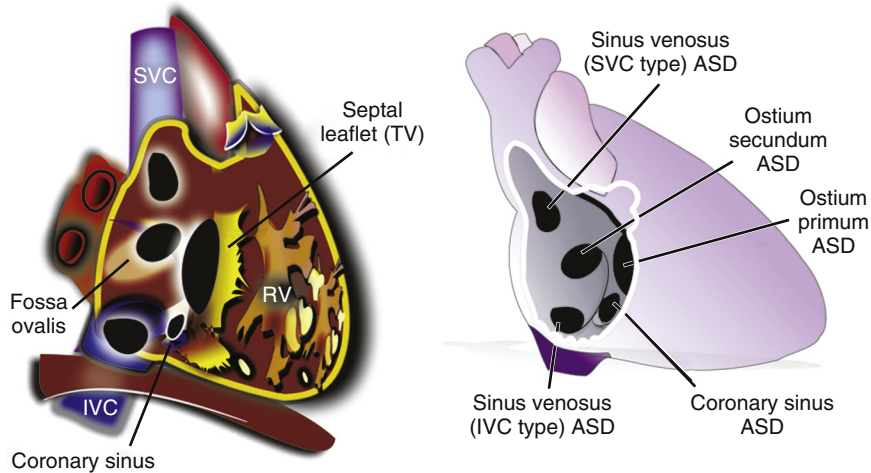
portions of the same clot. With anticoagulation, intracardiac thrombi frequently regress or remain stable.

The presence of LV aneurysms or severe dilated cardiomyopathy should always prompt vigilance for thrombi. Conversely, it would be highly unusual for a thrombus to form in an area with normal wall motion. Use of a high-frequency (7 to 8 MHz) probe to focus on the cardiac apex, angling it at unconventional views and sweeping across the field as needed, can better distinguish thrombus versus myocardium or trabeculations and will also decrease noise and reverberation artefact. Ultrasound enhancing agents are often the key, particularly when endocardial border or thrombus definition is poor.

With its higher resolution and proximity to the base of the heart, TEE plays a major role in ruling out intracardiac thrombi (or other sources of emboli, such as atheroma or vegetation) when no identifiable source is found after TTE and after imaging the head and neck arteries. An embolic stroke or unusually high transvalvular gradients in a patient with a mechanical (or even bioprosthetic) valve should prompt referral for TEE, contingent on the assumption that the findings on TTE were nondiagnostic and that they would alter management. TEE is also frequently used to facilitate the decision to anticoagulate, cardiovert, or perform radiofrequency ablation of a tachyarrhythmia, particularly in high-risk patients (i.e., those with the predisposing cardiac conditions mentioned earlier or those found to be underanticoagulated before a planned procedure). TEE should be performed before percutaneous mitral valvuloplasty for rheumatic MS to rule out LA thrombus (as well as to better define the mitral anatomy and degree of regurgitation) and thus avert potentially catastrophic embolic complications.[15,26,77]

#### Vegetations and Pannus

Vegetations tend to arise on the lower pressure (regurgitant) side of valves or at areas of flow turbulence. Valves with degenerative changes, prosthetic valves, and indwelling catheters or pacemaker/defibrillator wires are well-recognized nidi for infection. Thick, immobile, heaped-up irregular masses affixed to the annuli of older prosthetic valves may represent pannus (fibrovascular granulation tissue) (see Fig. 16.55). For both thrombi and vegetations, the larger and/or highly mobile masses that threaten the pulmonary, systemic, or cerebral circulation with embolization or cause severe valvular dysfunction may compel emergency surgical resection (see earlier, Infective Endocarditis).

#### Normal Variants and Artefacts

Normal or mild variants of normal structures have also been mistaken for neoplasms on echocardiography (see Table 16.11). The most common are lipomatous hypertrophy, upper septal hypertrophy, redundant and/or calcified mitral chordae, prominent/multilobed papillary muscle, interatrial septal aneurysm, or pericardial fat. Degenerative changes such as valvular calcification or external compression of chambers of the heart by adjacent structures (e.g., from esophageal hernia

**FIGURE 16.78** Classification of atrial septal defects (ASDs). *IVC, SVC,* Inferior, superior vena cava; *RV,* right ventricle; *TV,* tricuspid valve.
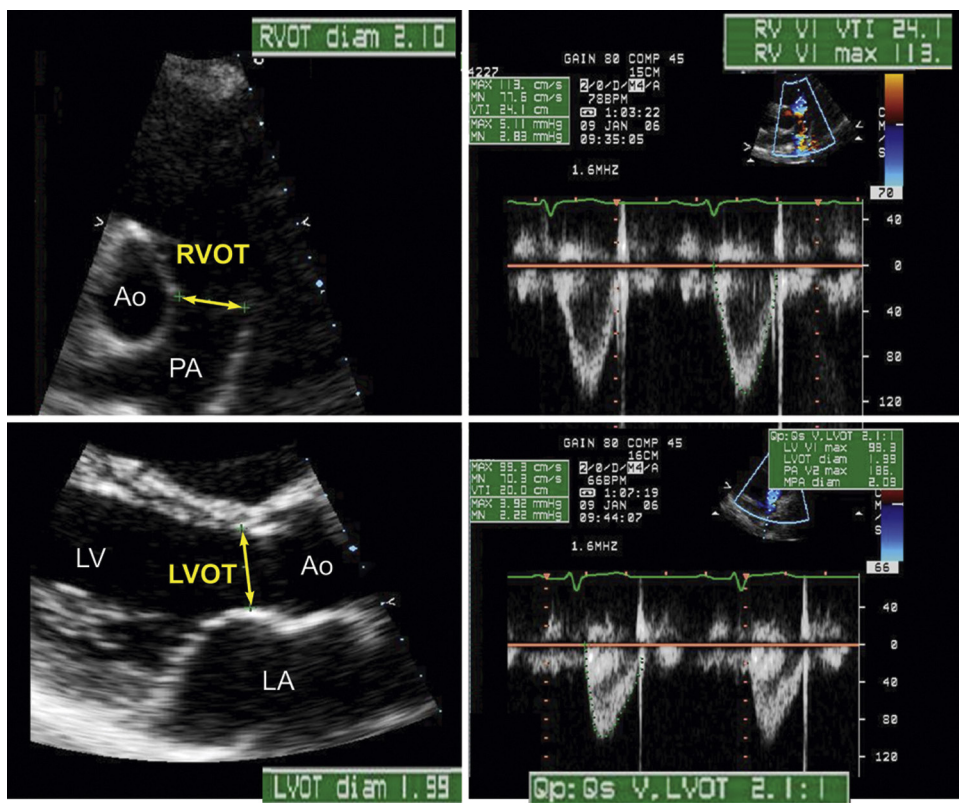


**FIGURE 16.79** $Q_p/Q_s$ calculation. For ASDs, $Q_p$ is equivalent to RV stroke volume (SV), which equals $CSA_{RVOT} \times VTI_{RVOT}$, in which $CSA_{RVOT} = \pi(D/2)^2$. $Q_s$ is equivalent to LV SV calculated as $CSA_{LVOT} \times VTI_{LVOT}$, where $CSA_{LVOT} = \pi(D/2)^2$. The **upper and lower panels** illustrate the derivation of RV and LV SV, respectively, from echo data. *Ao,* Aorta; *LA,* left atrium; *PA,* pulmonary artery.
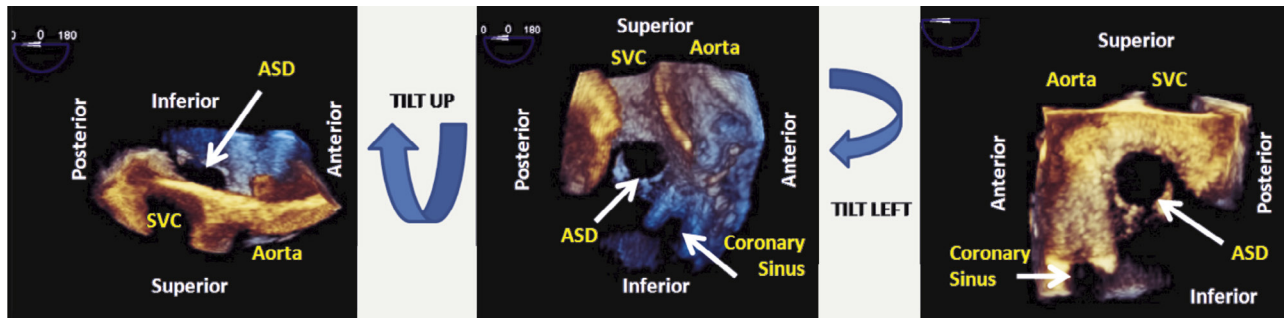
## Secundum Atrial Septal Defect

Secundum ASDs account for 75% of all ASDs and 30% to 40% of congenital disease seen in patients older than 40 (see Chapter 82). Figures 16.80 and 16.81 show the 2D TTE and TEE echocardiographic appearance of these defects. They are the only ASDs that are eligible for catheter-based closure. In planning transcatheter closure, TEE is used to (1) ensure that only one (or more) secundum ASDs is present, excluding other interatrial shunts that cannot be closed percutaneously, (2) size the defect, and (3) ensure that there is enough adjacent tissue rim to anchor the device. 3D TEE is especially advantageous for displaying en face displays of the septum before and during implantation

(eFig. 16.36).[77,88] Of the two devices currently approved by the U.S. Food and Drug Administration, the Amplatzer may be used for defects up to 38 mm, whereas the Cardioform device may be used only for defects up to 17 to 18 mm, although it may be placed successfully in patients with deficient anterior rims.

With 2D TEE, orthogonal diameters are recorded during ventricular systole, and a screen for presence of fenestrations is performed. 3D echocardiography allows en face displays of the entire defect in relation to the surrounding landmarks; measurements can be performed online with less risk of undersizing the defect compared to standard 2D imaging, particularly in those of irregular shape (see Fig. 16.81). Acceptable rim margins are at least 3 mm for the anterior rim and 5 mm for all other rims. Deficiency of the anterior rim is the most common (Fig. 16.81, right, and Fig. 16.82).

Device closure is guided by either TEE or intracardiac echocardiography (ICE). In sequential order, the key steps are placement of the guidewire across the defect (avoiding any smaller secondary fenestrations), balloon sizing of the defect, occluder placement followed by a tug to ensure optimal seating, assessment for residual shunt by color Doppler, and a survey for any complications such as pericardial effusion. Small residual shunts may be present immediately following deployment but often resolve after endothelialization of the device. Fig. 16.83 illustrates the 2D and 3D TEE appearance of a successfully deployed Amplatzer device. The occluder halves should appear well-apposed and aligned on both sides of the interatrial septum, without unusual tilting or prolapse of any portion through the defect, and ideally with no significant shunting by color Doppler or saline contrast. If there is misalignment of the device, particularly causing it to impinge upon the aortic root, there is a risk of erosion through the tissue.[88]

A *patent foramen ovale* (PFO) is a related condition characterized by incomplete fusion of the septum primum and septum secundum following birth. It may be detected by saline contrast demonstration of a right-to-left interatrial shunt, typically with maneuvers that raise RA pressure (cough, Valsalva or Müller maneuver). PFO is a very common condition that occurs in 20% to 35% of the normal population. It is also frequently associated with aneurysm of the interatrial septum. Echocardiography with saline contrast injection is often used to elucidate a PFO that could allow a paradoxical embolism to occur in patients without a clear source of left-sided embolic events, i.e., cryptogenic stroke. Video 16.64 shows both a PFO (positive bubble study) and an interatrial septal aneurysm. Evaluation for a PFO is one reason for performing TTE and TEE in patients with transient ischemic attacks, embolic stroke, or other embolic events.[79]

EFIGURE 16.36 Three-dimensional TEE imaging of atrial septal defects (ASDs). The TUPLE maneuver provides an easy method to image the right and left sides of the interatrial septum. The initial image is a zoomed 3D volume set acquired from a midesophageal zero-degree window. (From Saric M, Perk G, Purgess JR, Kronzon I. Imaging atrial septal defects by real-time three-dimensional transesophageal echocardiography: step-by-step approach. *J Am Soc Echocardiogr.* 2010;23:1128.)
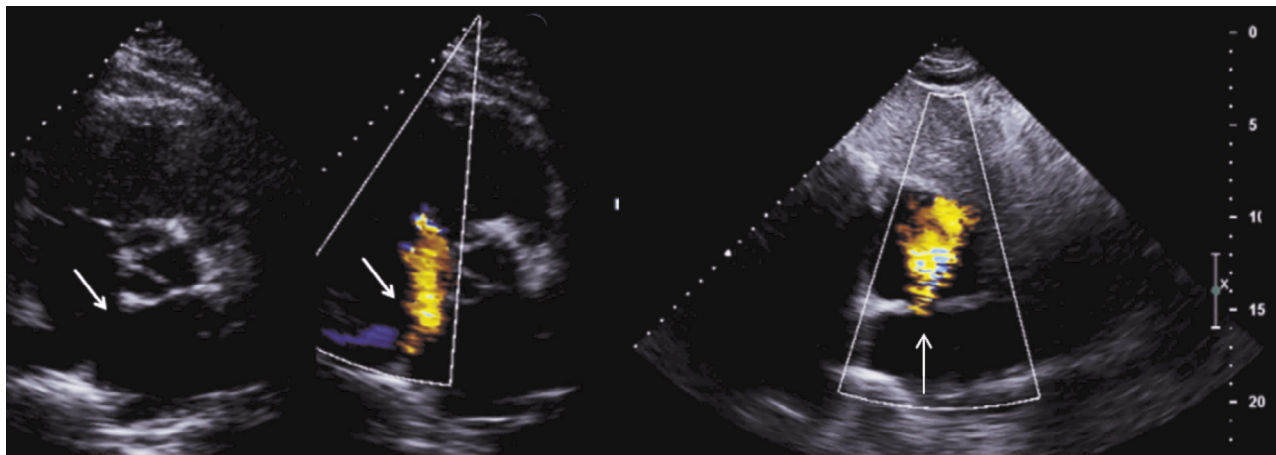
**FIGURE 16.80** Parasternal **(left and middle panels)** and subcostal **(right panel)** images of a secundum ASD and its associated left-to-right shunt (*arrows*).
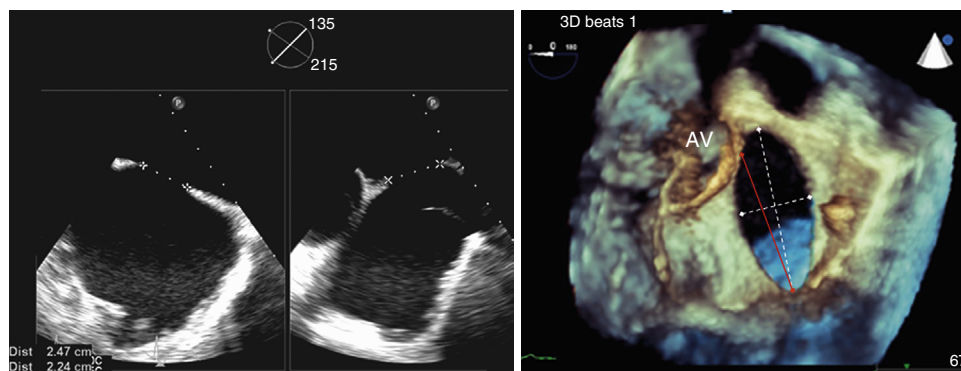


**FIGURE 16.81** Biplane two- and three-dimensional TEE measurement of ASD dimensions. **Left**, Biplane 2D TEE measurement of ASD dimensions. The 0 to 45-degree midesophageal view can be used to measure the anterior (toward aorta) and posterior (toward pulmonary veins) rims, whereas the 90- to 120-degree view images the superior (toward SVC) and inferior (toward IVC) rims. **Right**, Large secundum ASD viewed by 3D TEE from the left atrial perspective. Note that the 2D TEE–measured diameter (*red line*) is typically smaller than that measured by 3D TEE (*white dotted lines*). Also note that there is a deficient anterior rim, i.e., no separation between the defect and the aortic valve (*AV*).
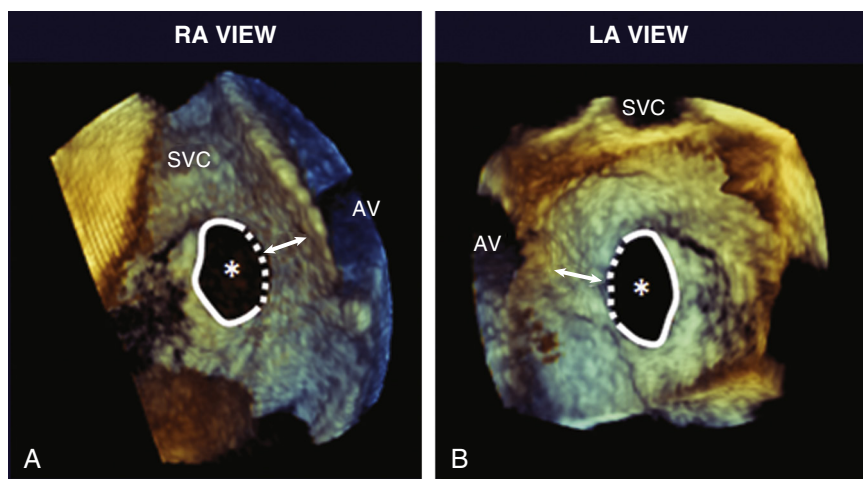


**FIGURE 16.82** Assessment of ASD rims with 3D TEE in **A,** right atrial (RA) and **B,** left atrial (LA) views. The anterior rim is represented as the distance between the *dotted line* and the aorta (*arrow*). *Asterisk*, secundum ASD. *AV,* Aortic valve. (From Saric M, et al. Imaging atrial septal defects by real-time three-dimensional transesophageal echocardiography: step-by-step approach. *J Am Soc Echocardiogr.* 2010;23:1128.)
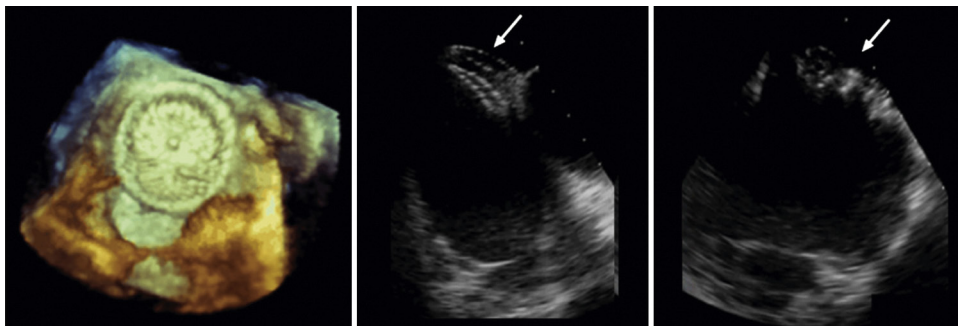
accompanied by inlet VSDs (complete atrioventricular canal defect). Partial atrioventricular canal defects typically have an associated cleft mitral valve. In complete atrioventricular canal defects there is a common single atrioventricular valve. atrioventricular canal defects are the most common congenital heart abnormality in Down syndrome. Primum defects can be seen on apical or subcostal views if posterior angulation is ensured to demonstrate the inlet portion of the ventricular septum (Fig. 16.84). These defects must be closed surgically.

**Sinus Venosus Atrial Septal Defect**

Sinus venosus ASDs account for 2% to 10% of ASDs and occur in two locations. The SVC type creates a confluence among the left atrium, right atrium, and SVC as it enters the right atrium. It is frequently accompanied by partial anomalous drainage of the right upper pulmonary vein, which is created when this vein enters the confluence. Partial anomalous drainage contributes to the left-to-right shunt. IVC-type defects are less common and create a confluence among the left atrium, right atrium, and IVC as it enters the right atrium. They may be accompanied by partial anomalous drainage of the right lower pulmonary vein. These defects should be suspected in patients with markers of RV volume overload without apparent cause. Typically, TEE is required to make the diagnosis, although SVC-type defects may be demonstrated with subcostal TTE. Figure 16.85 shows the TEE appearance of a sinus venosus ASD with partial anomalous pulmonary venous drainage. Sinus venosus ASDs must be closed surgically.

## Primum Atrial Septal Defect

Primum ASDs account for 15% to 20% of ASDs and occur as part of the spectrum of atrioventricular canal defects. They may occur as isolated defects (partial atrioventricular canal defect) or may be

## Coronary Sinus Atrial Septal Defect

Coronary sinus ASDs are rare and may be associated with fenestrations or complete unroofing of the coronary sinus into the left atrium. They are frequently associated with a persistent left SVC, a more frequent

FIGURE 16.83 Postimplantation appearance of an Amplatzer ASD closure device. **Left panel,** 3D left atrial perspective. **Middle** and **right panels,** Orthogonal 2D TEE views. The *arrow* points to the left atrial disc.
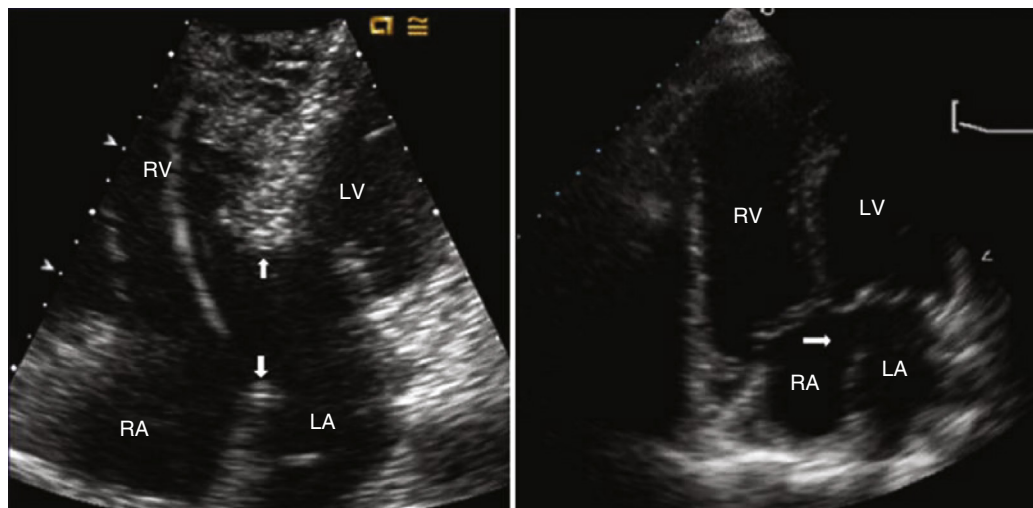


FIGURE 16.84 Apical four-chamber views showing complete **(left)** and partial **(right)** atrioventricular canal defects. In the **left panel,** *arrows* outline a large defect with atrial and ventricular components. In the **right panel** there is a primum ASD (*arrow*) with an intact ventricular septum. *LA,* Left atrium; *LV,* left ventricle; *RA,* right atrium; *RV,* right ventricle.
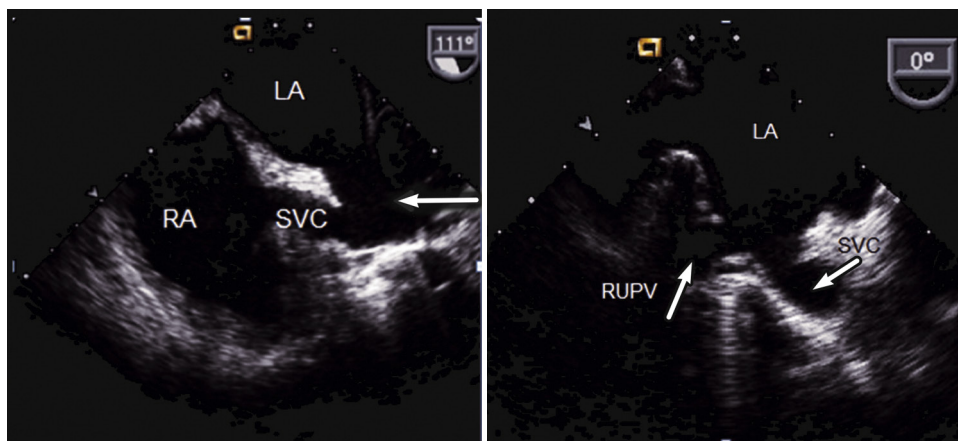


FIGURE 16.85 TEE images of a sinus venosus ASD (SVC type) with anomalous drainage of the right upper pulmonary vein (*RUPV*). A confluence is created between the superior vena cava (*SVC*), RUPV, and adjoining atria. *LA,* Left atrium; *RA,* right atrium.

finding (0.3% of the general population) and the most common cause of a dilated coronary sinus in general. The diagnosis is facilitated with TEE. Isolated persistent left SVC can be easily confirmed by TTE by injecting agitated saline contrast into a left cubital vein and demonstrating opacification of the coronary sinus first, followed by contrast within the right atrium (Video 16.65). It is usually an incidental finding that is generally not clinically important, but it can complicate transvenous placement

of catheters or pacemaker/AICD leads if not recognized.

## Ventricular Septal Defect

There are a number of classifications for VSDs. Figure 16.86 shows one anatomic classification, and Figure 16.87 outlines the division of the interventricular septum into its membranous, inlet, outlet, and trabecular portions along with the echocardiographic views that may be used to identify defects in each of these locations. VSDs vary in size and are considered to be small (restrictive) when less than half the size of the aortic root and when the LV-RV pressure gradient is greater than 64 mm Hg. Moderately restrictive VSDs are approximately half the size of the root, with gradients of approximately 36 mm Hg. With larger nonrestrictive defects, LV and RV systolic pressures are equalized. These latter defects are those that most often result in irreversible pulmonary vascular changes (Eisenmenger syndrome). Echocardiography may be used to size defects and LV-RV gradients. Shunting may be assessed by both color flow mapping and $Q_p/Q_s$ calculated with the continuity equation. Although chamber size may be normal in the setting of small defects, LV and LA enlargement is expected in those that are hemodynamically significant.

### Membranous (Paramembranous) and Outlet Ventricular Septal Defects

Eighty percent of VSDs involve the membranous septum. They vary in size, but even small defects can generally be detected on the parasternal long-axis view, as revealed by a high-velocity color Doppler jet. Membranous defects may be associated with wind-sock aneurysms that reflect varying degrees of spontaneous closure (Fig. 16.88). Even though the jets of membranous and outlet (supracristal) defects appear similar on the parasternal long-axis view, these defects may be distinguished from one another on short-axis views at the level of the great vessels. Membranous defects will be directed toward the septal leaflet of the tricuspid valve (10 to 11 o'clock position on the short-axis clock face), whereas outlet defects will be associated with jets that are directed toward the pulmonic valve (at 2 to 3 o'clock on the short axis clock face) (Fig. 16.87 and 16.89). Either defect may be accompanied by aortic cusp prolapse and consequent AR.
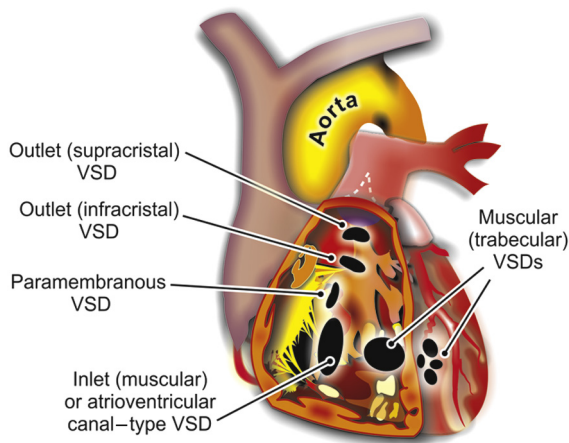
**FIGURE 16.86** Anatomic classification system for ventricular septal defects (VSDs).

## Inlet Ventricular Septal Defects

Inlet defects have been addressed in the preceding discussion of complete atrioventricular canal defects. Although often easily detected (see Fig. 16.84, left panel), inlet VSDs may be partially closed by adjacent atrioventricular valve tissue. In such situations, nonstandard views and TEE may be required to detect the ventricular component of the atrioventricular canal defect.

## Muscular Ventricular Septal Defects

Muscular defects vary considerably in size and location and may be multiple. When small and serpiginous, they may easily be missed with conventional echocardiographic views. Because these small defects are associated with loud murmurs with or without a thrill, a detailed evaluation using nonstandard views, such as sliding/tilting the transducer systematically down the barrel of the left ventricle with color Doppler sweeps, is warranted in any patient with these clinical manifestations (Fig. 16.90).

### TRANSPOSITION OF THE GREAT ARTERIES

TGA arises from failure of the aorticopulmonary septum to take its normal spiraling course (see Chapter 82). In dextro (D)–TGA the aorta lies anterior and to the right of the pulmonary artery and arises from the right ventricle, with the pulmonary artery arising from the left ventricle (eFig. 16.37, middle panel). D-TGA accounts for 5% to 7% of all congenital heart disease and, in the absence of shunting (VSD, ASD, patent ductus arteriosus) or surgery, D-TGA would be fatal. The most common associated anomalies are VSD (30% to 45%), pulmonary outflow tract obstruction (25%), and coarctation. Patients seen by cardiologists treating adults with congenital heart disease will have undergone corrective surgery consisting of either an atrial baffle/switch (Mustard or Senning) procedure in the past (up until ~1985), or more recently an arterial switch procedure.[89]

With baffle procedures the systemic venous baffle directs deoxygenated blood across the mitral valve into the left ventricle, from which it is ejected into the pulmonary artery. The pulmonary venous baffle directs oxygenated blood returning from the lungs to the tricuspid valve and into the right ventricle, from which it is pumped into the aorta. The end result is a "physiologic" circulation. Although short- and mid-term results are good, the right ventricle ultimately fails because of its inability to sustain its role as the systemic ventricle. Other complications detectable by echocardiography include baffle obstruction, baffle leaks, and pulmonary hypertension (the cause of which is incompletely understood).

The echocardiographic hallmark of transposition is parallel orientation of the great vessels, best appreciated on parasternal long-axis or apical views (Fig. 16.91). The diagnosis can be confirmed by demonstrating that the posterior great vessel (the pulmonary artery) bifurcates and the anterior aorta gives off arch vessels. In patients with D-TGA who have undergone atrial switch surgery, the baffles can be traced as they crisscross the atrium, with color flow mapping and spectral Doppler identifying areas of obstruction and baffle leak. The hypertrophied right ventricle has the rounded contour typically associated with the left ventricle, whereas the left ventricle is crescentic, a result of reversal of the

normal septal curvature because of systemic RV pressures. RV systolic function may be reduced with accompanying functional TR.

Levo (L)–TGA, also termed *congenitally corrected transposition,* is rare and accounts for less than 1% of all congenital heart disease. In L-TGA, transposition, with the aorta anterior and typically to the left of the pulmonary artery, is also accompanied by ventricular inversion. Thus, systemic venous blood returning to the right atrium drains into the morphologic left ventricle and is pumped into the pulmonary artery. Pulmonary venous blood returning to the left atrium crosses the tricuspid valve into the morphologic right ventricle, from which it is ejected into the aorta. Therefore the circulation is "normalized" (see eFig. 16.37, right panel). Associated abnormalities are common and include VSD (70% of patients), pulmonary outflow tract obstruction that is typically subvalvular (40%), and abnormalities of the tricuspid (systemic atrioventricular) valve (90%). Patients, particularly those without associated anomalies, may remain undiagnosed until adulthood, but eventually the morphologic right ventricle will fail because it cannot meet the pressure demands of the systemic circulation.

Echocardiographic features of L-TGA again include parallel orientation of the great vessels as with all cases of transposition, but on apical views, ventricular inversion becomes apparent. Ventricular morphology may be determined by the structure of its atrioventricular valve and the pattern of trabeculation. The morphologic right ventricle is associated with a tricuspid atrioventricular valve, which is identified by the presence of three leaflets and leaflet insertion that is apical to that of the mitral valve. The morphologic right ventricle is coarsely trabeculated with a moderator band, whereas the morphologic left ventricle is smooth walled and has two discrete papillary muscles. In assessing ventricular morphology by the four-chamber view, it is essential to maintain standard transducer orientation and avoid rotating the transducer so that an image is created in which the right and left ventricles occupy their expected positions. Figure 16.92 illustrates ventricular inversion in a patient with L-TGA. As with D-TGA, the morphologic right ventricle is hypertrophied with a round contour, and the morphologic left ventricle is crescentic. The septal curvature is reversed, consistent with the systemic pressure in the morphologic right ventricle.[89]

### TETRALOGY OF FALLOT

Tetralogy of Fallot is the most common form of cyanotic congenital heart disease and accounts for 10% of all congenital heart cases. The tetralogy of abnormalities consists of an overriding aorta, nonrestrictive subaortic VSD, RVOT obstruction (typically infundibular with variable valvular abnormalities), and secondary RV hypertrophy. Each of these features is readily identifiable with echocardiography (Fig. 16.93). *Pentalogy of Fallot* refers to the condition in which an ASD is also present.

Surgery for tetralogy consists of patching the VSD and a tailored approach to relieving the RVOT obstruction. Pulmonic regurgitation, sometimes severe, is a frequent finding after surgery for tetralogy of Fallot and may drive the need for repeated surgery. Other problems to remain vigilant for in the years after surgery include residual infundibular (subvalvular) and supravalvular pulmonic stenosis, as well as aneurysmal degeneration of the patch used to open up the infundibulum and/or pulmonary artery.[90]

# TRANSCATHETER INTERVENTIONS (SEE CHAPTERS 74 AND 78)

Transcatheter intervention for the treatment of structural heart disease has been a rapidly evolving field with an expanding number of devices and applications.[70] Throughout every phase in the development and clinical application of these procedures, echocardiography has remained indispensable in selecting candidates with suitable anatomy and pathophysiology, guiding device selection, and providing both intra-procedural guidance and post-procedure assessment. This has held true for older devices (plugs and occluders) used to treat paravalvular leaks and shunts as well as ever-expanding options for valvular disease that have emerged in recent decades, including transcatheter aortic valve replacement (TAVR), mitral and tricuspid repair/replacement, and atrial appendage occlusion.

Currently, TAVR using either balloon-expandable or self-expanding valves is widely available for symptomatic AS. Since 2017, TAVR has surpassed the number of standard surgical aortic valve replacements for AS in Europe and North America. Much less commonly, it is used for bioprosthetic or native valve aortic insufficiency. While TAVR is typically a percutaneous transfemoral procedure, more invasive alternative access sites, including trans-axillary and trans-aortic, may be used.
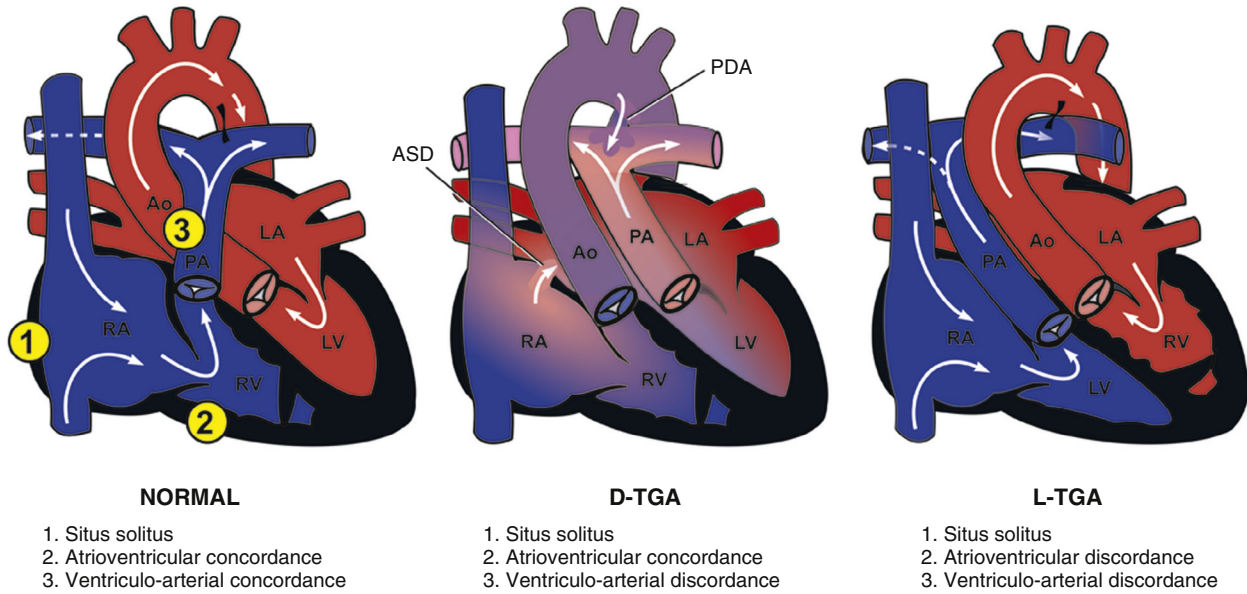
**EFIGURE 16.37** Schematic representation of blood flow through hearts with D-transposition of the great arteries (TGA) and L-TGA.

**NORMAL**
1. Situs solitus
2. Atrioventricular concordance
3. Ventriculo-arterial concordance

**D-TGA**
1. Situs solitus
2. Atrioventricular concordance
3. Ventriculo-arterial discordance

**L-TGA**
1. Situs solitus
2. Atrioventricular discordance
3. Ventriculo-arterial discordance

The latter have largely replaced the trans-apical approach used in early TAVR experience. Pre-procedural assessment routinely includes TTE to verify AS severity, provide input into device selection (type and size) and identify features that would constitute a hostile landing zone for the valve, such as extensive annular or LVOT calcification. Pre-procedural CTA is routinely used to assess vascular access and aortic annular and root size, but in cases where there are contraindications to CT, 3D TEE may be used. 3D capability is important to accurately size the annulus given its non-circularity and is uniquely able to determine the height of the coronary arteries relative to the annulus based on reconstructed views. The latter is important since low coronary ostia pose a risk of occlusion by displaced native leaflets at the time of implantation. Analytic enhancements incorporating artificial intelligence permit detailed online and offline measurements throughout the cardiac cycle (4D TEE) and volume reconstruction at the bedside (eFig. 16.38).

Intraprocedural TEE may be used to ensure that the stented valve is properly seated across the aortic annulus and to immediately assess for complications. Many experienced structural heart programs have transitioned from routine intra-procedural TEE to intraprocedural fluoroscopy alone with immediate post-procedural TTE, reserving planned intra-procedural TEE for patients at higher risk for complications but having TEE on standby should a complication occur.
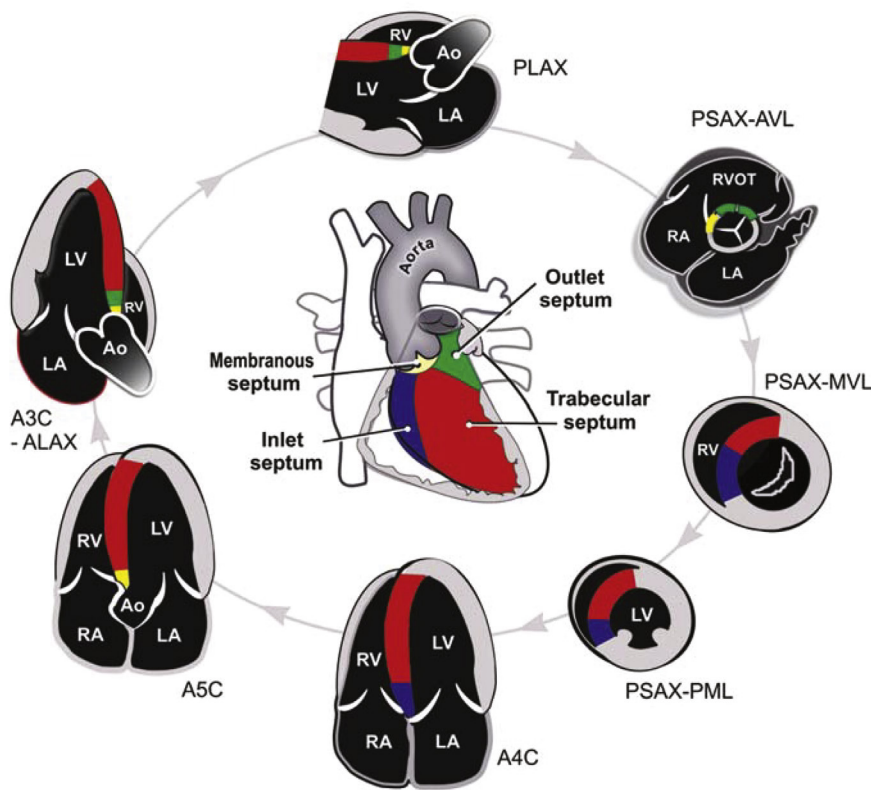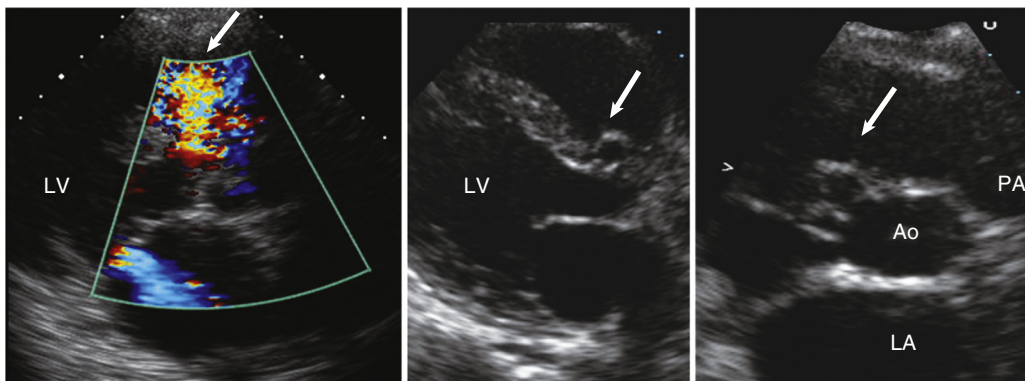


**FIGURE 16.87** Echocardiographic views used in imaging the interventricular septum. *A3C,* Apical three-chamber view; *Ao,* aorta; *AVL,* aortic valve level; *LA,* left atrium; *LV,* left ventricle; *MVL,* mitral valve leaflet; *PLAX,* parasternal long-axis view; *PML,* papillary muscle level; *RA,* right atrium; *RV,* right ventricle. (Modified from Bulwer BE, Rivero JM, eds. *Echocardiography Pocket Guide: The Transthoracic Examination*. Burlington, MA: Jones & Bartlett Learning; 2011, 2013:142. Reprinted with permission.)



**FIGURE 16.88** Parasternal views of a membranous VSD partially closed with a wind-sock aneurysm. **Left,** A systolic left-to-right jet is identified. **Middle,** With slight angulation, a wind-sock aneurysm representing partial spontaneous closure of the defect is identified. *LV,* Left ventricle. **Right,** In the short-axis view, the wind sock helps localize the VSD to the 11 o'clock position, as opposed to outlet defects, which are seen in the 12 to 2 o'clock position (compare with Fig. 16.89). *Ao,* Aorta; *LA,* left atrium; *PA,* pulmonary artery.
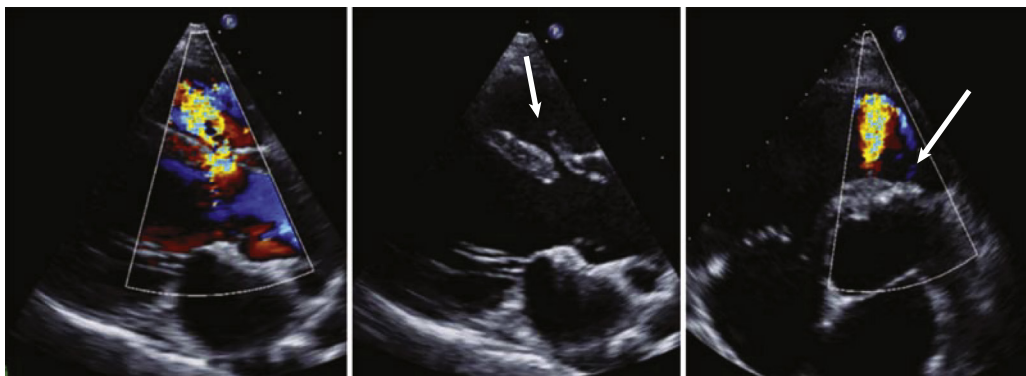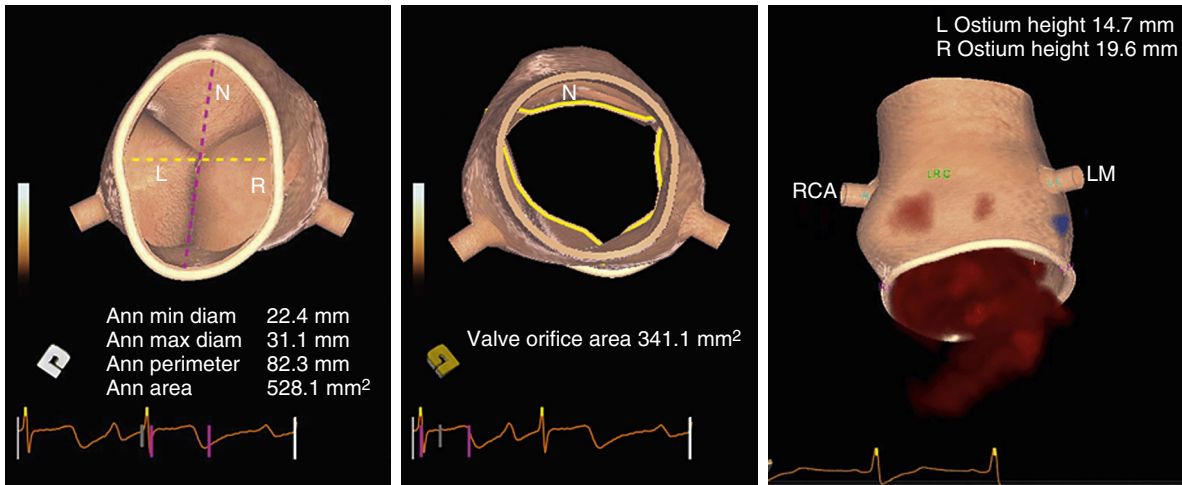


**FIGURE 16.89** Parasternal images illustrating an outlet VSD. In the parasternal long-axis view **(left** and **middle panels)**, the VSD jet and the defect (*arrow*) may be indistinguishable from those of a membranous defect. However, in the short axis **(right panel)**, the jet is seen at the 12 o'clock position immediately next to the pulmonic valve (*arrow*). (Compare with Fig. 16.89.)

EFIGURE 16.38  Three-dimensional TEE volume-rendered still frames of a normal aortic root. **Left,** The true orthogonal long and short axes of the annulus may be determined, as well as annular area. **Middle,** Valve orifice area and leaflet lengths. **Right,** Heights of the coronary ostia from the annulus (which is of particular importance in planning for TAVI).

Post-deployment paravalvular aortic insufficiency is not uncommon, though seen less frequently with newer generation valves (see Fig. 16.57); if the degree is significant, further re-expansion of the stented valve or even implantation of a second valve within the first one may solve the problem. Intra- or post-procedural echocardiography also serves to survey for iatrogenic complications such as acute infarcts caused by coronary ostial inclusion, annular rupture, MR, and pericardial effusion.[70] As experience has grown, TAVR is now used successfully in some patients with bicuspid valves although associated aortopathy can preclude its use in some patients.

Post-procedure follow-up is similar to that for surgical bioprostheses with the exception that TAVR valve design results in acceleration of flow at two levels—the first at the level of the stent frame inlet and the second at the level of the valve cusps. For this reason, care must be taken to record LVOT velocity proximal to the valve inlet. LVOT diameter is typically measured as the outer to outer edge diameter of the lower end of the valve frame (eFig. 16.39). The identification of paravalvular regurgitation also requires some attention to detail; jets may be seen on color Doppler short axis images outside the perimeter of the frame that are trapped within the device skirt and do not actually reach the left ventricle. To be considered paravalvular regurgitation, jets must be demonstrated to reach the LV. Quantitation based on color jet dimensions may be challenging due to the frequent jet eccentricity.

Additionally, valve in valve procedures (TAVR implanted into another TAVR or surgical bioprosthetic AVR) may be performed for initially failed TAVR attempts or subsequent TAVR or surgical valve degeneration. Along the same lines, valves designed for aortic implantation may be used to address mitral bioprosthetic dysfunction (typically MR) or, rarely, mitral
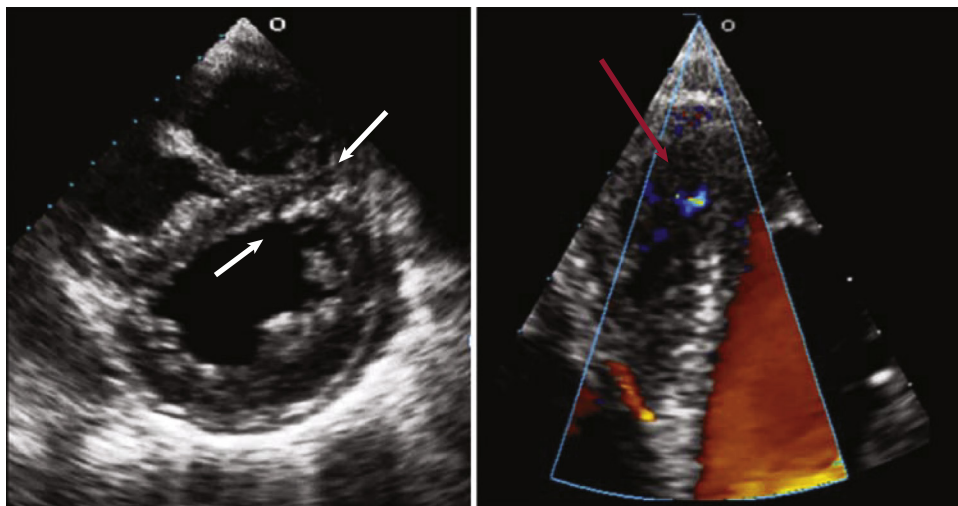


**FIGURE 16.90** Parasternal short-axis **(left)** and off-axis apical **(right)** views demonstrating a serpiginous muscular VSD. The *white arrows* point to LV and RV entry points. The *red arrow* identifies a small left-to-right shunt.
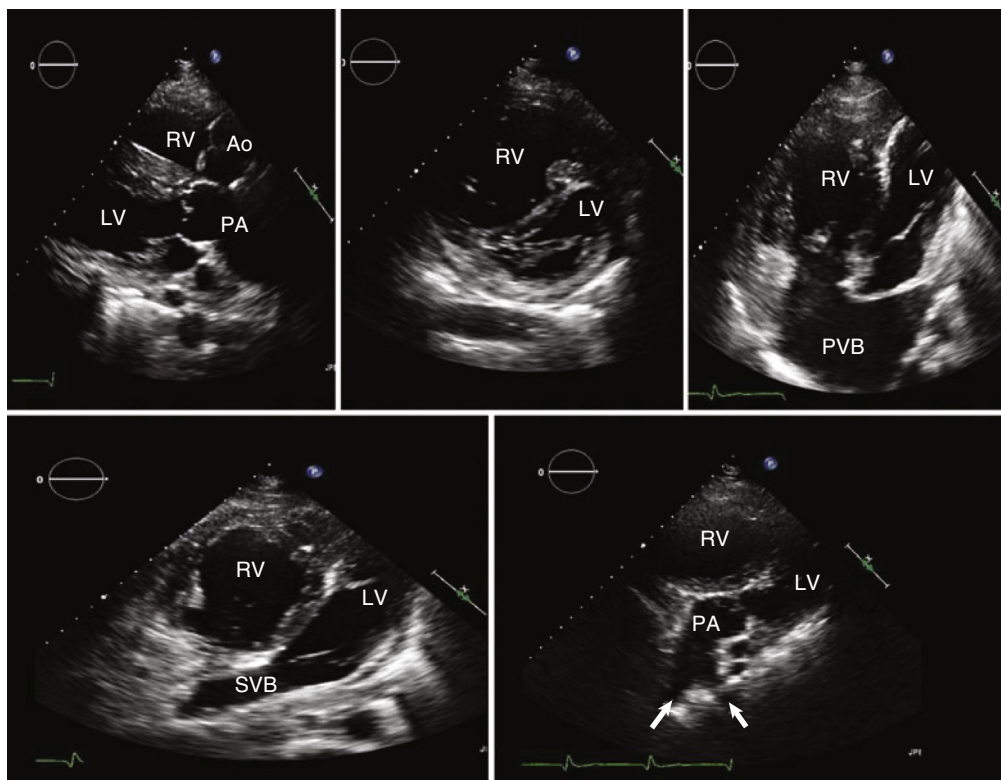


**FIGURE 16.91** ᴅ-Transposition of the great arteries after Mustard baffle surgery. **Top left,** Parasternal long-axis view showing parallel orientation of the aorta (*Ao*) and pulmonary artery (*PA*). The aorta is anterior. **Top middle,** Parasternal short-axis view showing septal inversion reflecting the fact that the right ventricle (*RV*) is the systemic ventricle. **Top right,** Apical four-chamber view showing the pulmonary venous baffle (*PVB*), which directs pulmonary venous flow across the tricuspid valve into the RV. **Bottom left,** The four-chamber view has been angulated to demonstrate the systemic venous baffle (*SVB*), which directs systemic venous return across the mitral valve into the left ventricle (*LV*). Note the right ventricular hypertrophy and enlargement. **Bottom right,** The four-chamber view is angulated anteriorly to demonstrate the connection between the LV and PA. *Arrows* point to the PA bifurcation.
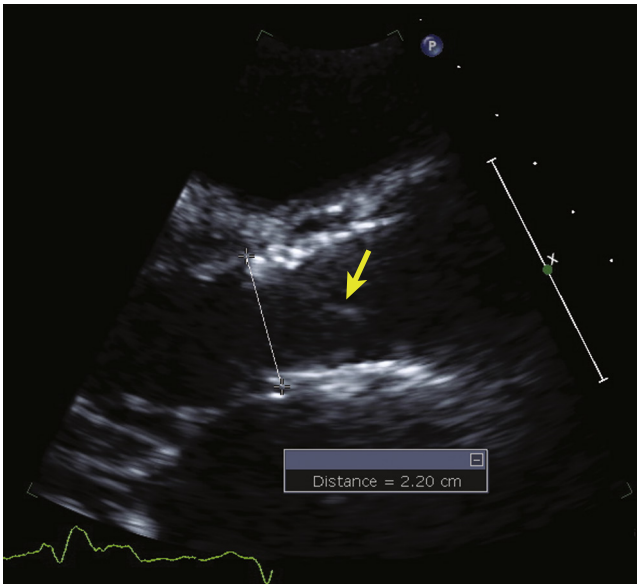
**EFIGURE 16.39** TAVR on parasternal long-axis window. The LVOT diameter should be measured as the outer to outer edge diameter at the lower end of the valve stent frame. *Arrow* indicates the aortic valve leaflets within the TAVR frame.
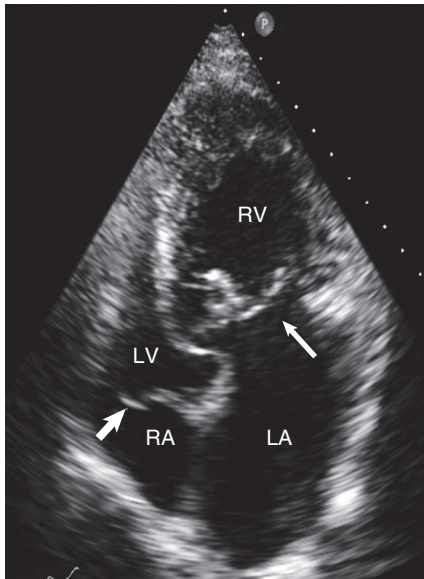
FIGURE 16.92 Apical four-chamber view in patient with L-transposition of the great arteries. The ventricles are inverted with the right ventricle (*RV*) to the right, identified on the basis of its heavy trabeculation and tricuspid atrioventricular valve (*thin arrow*). Although the insertion of the tricuspid valve is always apical to that of the mitral valve, in this case the offset is accentuated, consistent with the Ebstein anomaly. Unlike isolated Ebstein anomaly, that seen with L-TGA does not have a sail-like leaflet or adherence of the septal leaflet to the septum. The *thick arrow* points to the mitral valve. *LA,* Left atrium; *LV,* left ventricle; *RA,* right atrium.

annular calcification (Video 16.66). *Transcatheter pulmonary valve implantation* with balloon expandable valves is now routine in pediatric centers experienced in congenital heart disease.

Balloon valvuloplasty for MS is a relatively common procedure in parts of the world where rheumatic disease is still prevalent. As previously discussed (see Mitral Stenosis), echocardiographic scoring systems may help with patient selection and TEE is used to exclude intra-atrial thrombus.[65] Intra-procedural guidance includes fluoroscopy and TEE, the latter preferentially performed with 3D or intracardiac ultrasound. Measures of success include a decrease in mean gradient without an increase in degree of MR. Of note, the PHT is invalid for calculating MVA in the early post-valvuloplasty period, due to acute changes in left atrial and ventricular compliance.

Interventions for MR can be divided into repair and replacement with options for repair further divided into those procedures that directly alter the leaflets or their chordal support and annuloplasty (direct or indirect). To date, these approaches have been modeled on established surgical techniques. Currently, the only FDA-approved device is the mitral clip edge-to-edge repair system (MitraClip) although others are at varying stages of investigation. An array of devices for transcatheter mitral valve replacement are being evaluated.

The mitral clip (MitraClip) is modeled on the surgical Alfieri procedure and joins the anterior and posterior leaflets, typically at their mid portion, to create a double orifice valve. It may be used for both degenerative and secondary MR and echocardiography plays a critical role in patient selection. Implantation is done under fluoroscopic and TEE guidance ideally with 3D. Key steps are transseptal puncture, orienting the device so that it is aligned with the target jet (ideally P2-A2), advancing the device into the left ventricle, grasping the leaflets with
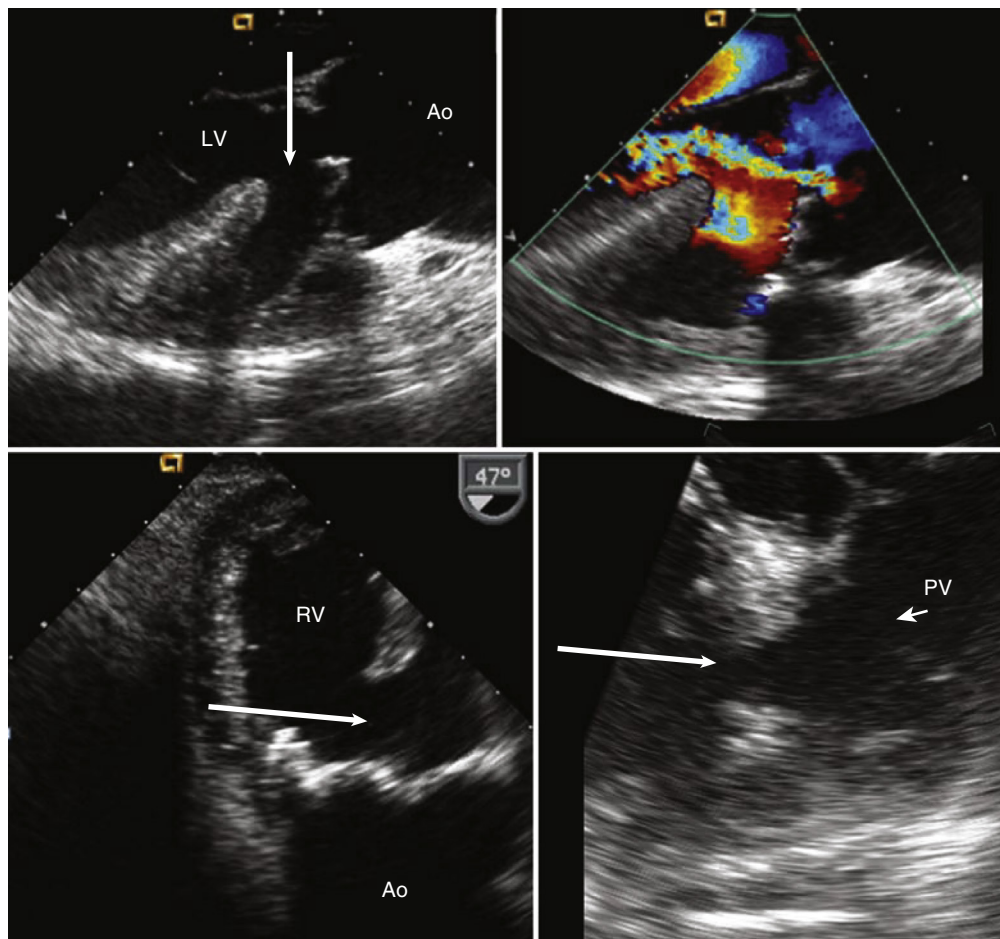


FIGURE 16.93 TEE images of a patient with tetralogy of Fallot. **Upper left,** Midesophageal image showing the aorta (*Ao*) overriding a large (nonrestrictive) VSD (*arrow*). **Upper right,** There is mild aortic regurgitation. **Lower left,** From a deep transgastric view, severe right ventricular hypertrophy is seen. The *arrow* points to the VSD. **Lower right,** In this midesophageal view, focal infundibular narrowing is seen (*arrow*). The pulmonic valve (*PV*) is not well seen but, in other views, was shown to be normal. *LV,* Left ventricle; *RV,* right ventricle.

**FIGURE 16.94** MitraClip repair of posterior mitral valve leaflet flail. 2- and 3-D TEE images in a patient with posterior mitral leaflet flail (**Left panels, yellow arrows**) followed by MitraClip placement (**Right panels, white arrow**). **A,** Posterior leaflet flail segment with ruptured chordae. **B,** Corresponding eccentric severe MR. **C,** 3D TEE view as viewed from the left atrial aspect; **D,** MitraClip is seen attached to both leaflets in the LV. **E,** with reduced M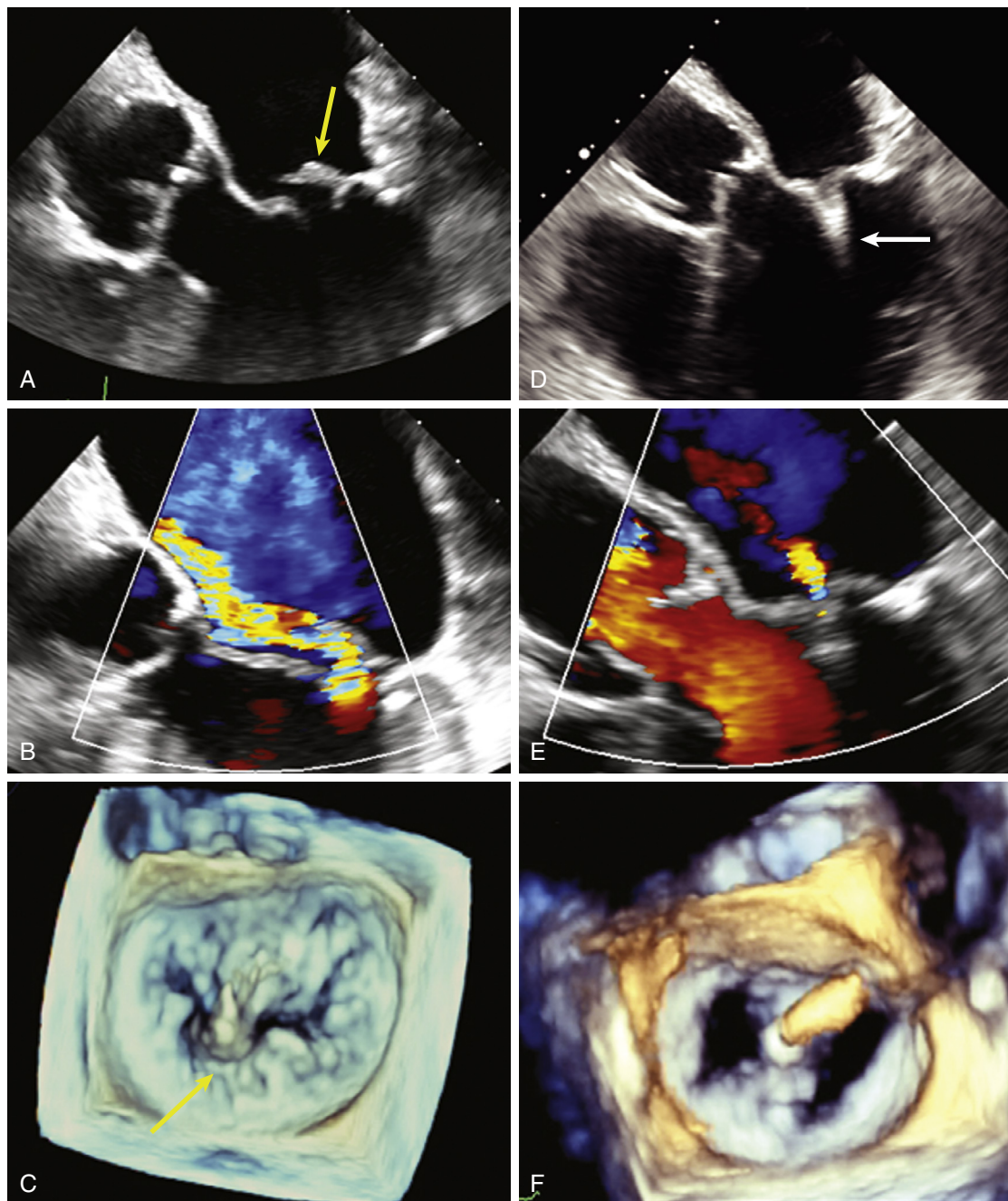R on color Doppler. **F,** 3D TEE view of the double orifice created by the MitraClip (note the delivery catheter is still attached on the left atrial side. (See corresponding Videos 16.66 for pre-MitraClip and 16.67 post-MitraClip.)

device grippers and subsequently device arms, assessing residual MR and degree of MS and excluding complications including pericardial effusion. Intra-procedure assessment of MR relies on color jet dimensions, pulmonary venous flow, 3D planimetered EROA and pulmonary artery pressure. Real-time multiplanar reconstruction, a recent advance in 3D technology is particularly helpful during these procedures[70] (Fig. 16.94 and Videos 16.67 and 16.68). Multiple MitraClips may be placed in a valve with a large orifice as needed to reduce MR, but antegrade mitral gradients and estimated PASP must be followed to prevent iatrogenic MS.

Transcatheter tricuspid valve interventions have emerged more recently, with strategies of leaflet approximation, annuloplasty, or total valve replacement. These are all in clinical trials currently. Procedural success will likely be heavily dependent upon pre-procedural evaluation of the tricuspid valve, TR, and the right heart.[92]

In the subspecialty of electrophysiology, occlusion of the LA appendage is possible with a variety of devices and is targeted toward patients at high risk for recurrent strokes (despite anticoagulation or unable to take anticoagulants) (eFig. 16.40). TEE is performed before the procedure primarily to size the LA appendage and ensure that it can receive an appropriately sized device, as well as to exclude appendage thrombus. For the Watchman device, the ostia of the appendage diameters are measured at several angles, and the appendage must be longer than its width to properly select and seat the occluder. ICE may alternatively be used for transseptal puncture and to guide device delivery.[93] Post-procedure surveillance is performed by TEE in the 1 to 2 months following implantation to assess for any residual flow between the appendage and left atrial body.

There is a small cautionary note to the exponential increase in transcatheter interventions: While generally safe and absolutely essential to
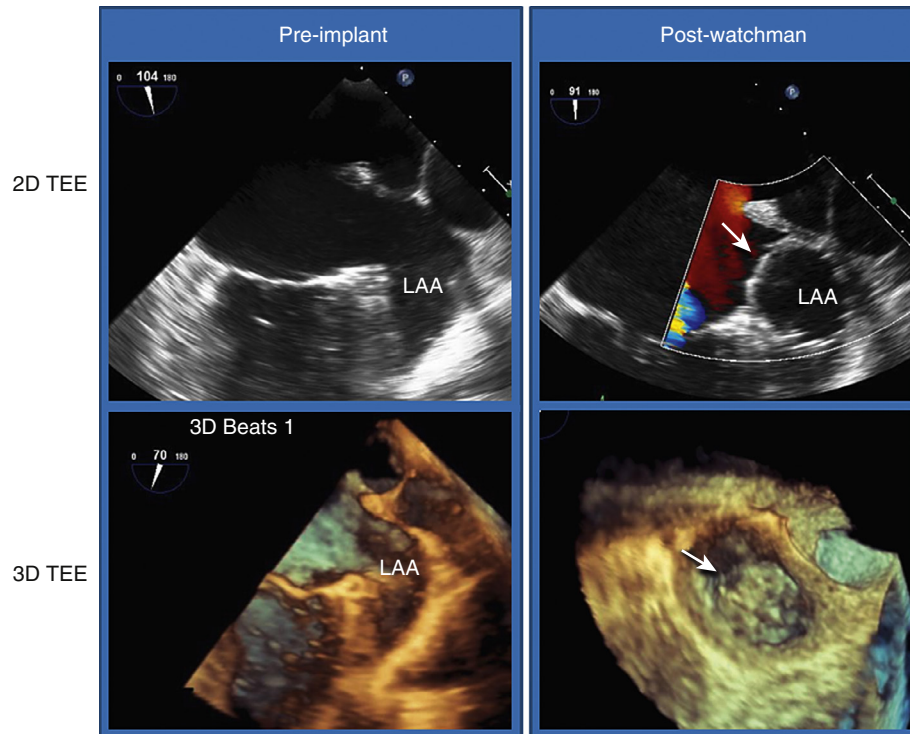
**EFIGURE 16.40** The Watchman device to occlude the left atrial appendage (LAA) for stroke prevention. **Left panels,** 2D and 3D TEE views of the LAA before implantation. Measurements of the LAA ostia taken at multiple angles for selection of the appropriate Watchman device. The appendage length must be longer than its width to accommodate device implantation. **Right panels,** Appendage occluder device (*arrow*) well seated at the neck of the appendage, with no residual flow around the device by color Doppler; **top panel,** 2D view; **bottom panel,** 3D en face view).

deployment of many of these devices, recently there has been increasing recognition that the constant probe manipulation during TEE-guided procedures engenders a potential for esophageal injury. This is particularly true with mitral clip placement, long procedure times, and in patients with risk factors such as prior GI bleed, low body weight, and chronic immunosuppressive medications such as steroids.[19,91] These risks underscore the importance of pre-screening patients, giving appropriate informed consent, and strategizing TEE mechanics (eTable 16.4). The risks may potentially be mitigated by the use of real time 3D-TEE and fusion imaging (see next), which allows for faster and more intuitive display of the device with respect to cardiac structures.

## Future Directions
### Multimodality and Fusion Imaging
Simultaneous advances in nuclear medicine and radiology have occurred hand-in-hand with the clinical implementation of the above transcatheter devices. Although TTE and TEE give real-time information particularly on the dynamic function of the heart chambers and valves, there are specific areas that may not be accessible for ultrasound imaging due to acoustic shadowing (e.g., portions of the aorta, mechanical valve or VAD artefacts, extracardiac structures). Furthermore, TEE is semi-invasive, usually requires at least IV conscious sedation with its inherent risks, and is an aerosol-generating procedure with the potential for airborne transmission of respiratory pathogens. The latter was of particular concern with the COVID-19 pandemic, and prompted an appropriate shift to alternative modalities such as CT angiography, MRI, and nuclear/PET scanning in selected cases.

Common clinical indications in which alternative or adjunct modalities to echocardiography are helpful follow: For aortic disease such as aneurysm and dissection, it is recommended the imaging modality able to visualize the affected segments with the lowest iatrogenic risk be used. Hence TTE and TEE are useful for first-line screening and following chronic disease in the aortic root and proximal ascending aorta. For acute aortic syndromes, CT angiography is often used due to the ability to image the complete aorta, speed, and sensitivity. If there is renal insufficiency, pregnancy, or an allergy to iodinated contrast, the modality with the least radiation exposure is recommended except in the case of emergency. For long-term follow-up, the same modality should be used in order to compare similar measurements, but repetitive radiation exposure in younger adults is to be avoided.[15,94]

TTE followed by TEE remains the mainstay for diagnosing endocarditis. However, in carefully selected cases, particularly those involving prosthetic valves or other implanted devices, CT angiography, metabolic imaging (with ^{18}F-FDG-PET scanning), and radionuclide-labeled white blood cell imaging which detects areas of inflammation are useful ancillary diagnostic tools that can be used to circumvent some of the limitations of echocardiography (see Infective Endocarditis). These radiologic modalities should also be considered in conditions where TEE is impractical or risky for either the patient or the provider. Cardiac PET and CTA images may be fused to confirm which cardiac structures are infected, which is particularly useful if vascular grafts are involved or there is extensive degenerated tissue. Although echocardiography permits high resolution 2D and moving 3D images of highly mobile or tiny structures in the heart, CMR has the advantage of more detailed tissue characterization and less angle dependence than ultrasound. Hence it is very useful for characterizing masses and discerning between myocardial damage, edema, and fibrosis. In many cases of endocarditis, it is very appropriate to use two or more modalities to examine the heart.[15,76,95]

## Handheld Echocardiography (Point of Care Ultrasound)
The era of miniaturization has ushered in increasingly smaller and capable portable ultrasound machines, which were introduced commercially in 2004. Current laptop-size devices are a lightweight alternative to the traditional 400-lb full-size machines and have virtually all the same capabilities, including Doppler and strain imaging, stress and TEE studies, automatic quantification of LVEF, and 4D imaging. They

can operate wirelessly. Many systems allow the performance of vascular, abdominal, and obstetric ultrasound on the same machine and can accommodate a wide range of transducers, including pediatric ones. There are miniaturized disposable TEE probes, designed to stay in patients for up to 72 hours, which may prove useful in the care of ICU patients after cardiac surgery.

The Covid-19 pandemic ignited a rocketing demand for handheld ultrasound devices to perform studies at the bedside (point-of-care ultrasound, or POCUS; see Chapter 94). These devices, developed over the last 20 years, are similar in size to a cellphone and can fit in the physician's coat pocket. Some models consist of a standalone transducer (which may be interchangeably cardiac, vascular, abdominal, or obstetric) which is plugged into a smartphone or tablet that serves as the display. One model uses a silicon chip that produces a 2D array of microsensors in lieu of piezocrystals, giving it the unique capability to act as multiple transducers in a single unit. In the hands of experienced sonographers, the current devices offer 2D and color Doppler imaging with adequate image quality and accuracy compared with conventional machines.[96] Currently, none of the handhelds support spectral Doppler and thus cannot perform quantification of valve stenosis or assess intracardiac pressures. Additionally, without the specialized presets of full-featured systems, echocardiographic enhancing agents (contrast) are less effective. Features of various models include wireless data transmission (in some cases to the cloud), as well as the ability to connect and share real-time images at the bedside for interpretation, teleguidance, and even remote control of settings by an expert consultant. At least one system has piloted an artificial intelligence feature to help the user correctly capture heart images and automatically computes an LVEF.

In COVID-19, SARS-CoV-2 primarily affects the lungs but also causes right and left heart failure, thrombosis, and acute kidney injury, a single streamlined instrument that could rapidly assess the heart, lungs, and blood vessels suddenly became ideal. POCUS units, being easier to carry, use, and disinfect, enabled frequent serial exams at the bedside while reducing the risk of viral transmission and conserving resources. A single focused exam can help distinguish between pneumonia and heart failure, as well as crudely estimate RA filling pressures. Apart from its unique utility in epidemics, handheld ultrasound clearly has the potential to extend the physical exam, educate others, and obtain quantitative serial data at the bedside. From a more global aspect, the affordability and portability of these POCUS units also renders echocardiography more accessible for health care outside the hospital and in underdeveloped regions.

Despite these remarkable developments in handheld units, POCUS is operator-dependent and, like conventional echocardiography, requires an understanding of cardiac anatomy and physiology as well as training in image interpretation for optimal use by noncardiologists.[97] With sufficient user experience and continual improvements in design and function, these instruments will likely become a bedside tool as familiar as the stethoscope in clinical settings. At present, however, they do not supplant a complete formal echocardiographic study with a high-end machine and experienced sonographer.

## Recent Echocardiography Techniques
Echocardiography has evolved over five decades to become a cornerstone in cardiac imaging. Although its fundamentals are based on the immutable physics of ultrasound, revolutionary advances in the processing and application of data continue to not only improve imaging, but also to provide more functional cardiac evaluation and applicability to clinical treatment. 4D imaging and speckle-based strain measurements have moved into the clinical realm. The potential utility of these techniques is being explored in avenues such as valvular, ischemic, and oncologic heart disease.[98] Strain and strain rate measurements in the right ventricle and left atrium may be more discerning indicators of function and filling pressures than our current parameters. 3D strain, the analysis of myocardial deformation in all vectors, is a recent development that may prove useful in cardio-oncology and heart failure. These measurements are currently hampered by limits in temporal and spatial resolution, and need validation and standardization, but research into their clinical and prognostic potential is ongoing. With regard specifically to

valvular disease, the high prevalence of TR that persists or worsens after interventions on the left heart, has spurred a new interest in evaluating patients for TV surgical or transcatheter intervention.

Fusion imaging, in which two or more imaging modalities are combined to form one image (see Echocardiography in the Context of Cardiac Imaging), has already demonstrated utility in endocarditis cases where areas of inflammation (by FDG-PET) can be localized to infected valves or tissue (seen on CT angiography). Using software, it is also possible to overlay 3D echo images with cardiac CT to demonstrate the functional abnormalities (in LV wall motion or strain) that correlate with coronary artery stenoses as well as structural abnormalities such as shunts and defects. 3D TEE images may also be integrated with fluoroscopic markers to more accurately guide transcatheter interventions such as ASD closure, LAA occlusion, and potentially valvular interventions.[99]

## Artificial Intelligence (see Chapter 11)

Artificial intelligence (AI), in the sense of automating tedious or complicated tasks, is already in use in echocardiography: automated endocardial border detection and EF calculation, 2- and 3D strain analysis and calculation of GLS, and automatic calculations of EROAs and volumes on 3D echos are some examples. For handheld ultrasounds, AI can be used to assist a novice in scanning, by combining real-time image assessment with adaptive anatomic guidance. Machine learning algorithms can be automated to expedite the analyses of ventricular size, mass, and global/regional function, but also could demonstrably automate complex assessments of valvular stenoses and regurgitation and diastolic function (by grouping relevant images together, and quantitatively assessing the multiple quantitative and semi-quantitative parameters). One could envision that the integrated data may populate reporting templates and trigger corresponding statements and conclusions.

However, in the context of actual machine learning, the full potential of AI is yet to be realized. AI can theoretically be used for large-scale screening of diseases such as dilated or HCM, amyloidosis, or pulmonary hypertension. Using cluster analysis and additional clinical data, it appears that computers can be tasked, unsupervised, to parse complex echocardiographic phenotypes or subtle characteristics—perhaps too indistinct for the human eye to easily discern, as in the case of strain—in order to identify subgroups of patients with propensity to poor outcomes (e.g., male diabetics with LV hypertrophy and systolic dysfunction). Given the human skills, training, and nuances currently required to perform and interpret echocardiograms, there are obviously limitations to AI. AI presently cannot substitute for an echocardiologist's experience and ability to integrate clinical data in a specific patient, but is undoubtedly poised to enhance the accuracy, efficiency, and utility of echocardiography in clinical practice, education, and research.[100,101]

# APPROPRIATE USE CRITERIA

See the online chapter.

## REFERENCES

### Principles of Ultrasound Imaging

1. Cikes M, D'hooge J, Solomon SD. Physical principles of ultrasound and generation of images. In: Solomon SD, ed. *Essential Echocardiography*. Philadelphia, PA: Elsevier, Inc; 2019.
2. Lang RM, Badano LP, Mor-Avi V, et al. Recommendations for cardiac chamber quantification by echocardiography in adults: an update from the American Society of Echocardiography and the European Association of Cardiovascular Imaging. *J Am Soc Echocardiogr*. 2015;28:1.
3. Mitchell M, Rahko PS, Blauwet LA, et al. Guidelines for performing a comprehensive transthoracic echocardiographic examination in adults: recommendations from the American Society of Echocardiography. *J Am Soc Echocardiography*. 2019;32:1.
4. Mizukoshi K, Takeuchi M, Nagata Y, et al. Normal values of left ventricular mass index assessed by transthoracic three-dimensional echocardiography. *J Am Soc Echocardiogr*. 2016;29:51.
5. Stewart MH, Lavie CJ, Shah S, et al. Prognostic implications of left ventricular hypertrophy. *Progress in Cardiovasc Dis*. 2018;61:446.
6. Guta AC, Badano LP, Ochoa-Jimenez RC, et al. Three-dimensional echocardiography to assess left ventricular geometry and function. *Expet Rev Cardiovasc Ther*. 2019;17:11.
7. Cole GD, Dhutia NM, Shun-Shin JG, et al. Defining the real-world reproducibility of visual grading of left ventricular function and visual estimation of left ventricular ejection fraction: impact of image quality, experience and accreditation. *Int J Cardiovasc Imaging*. 2015;31:1303.
8. Hernandez-Suarez DF. Strain imaging echocardiography: what imaging cardiologists should know. *Curr Cardiol Rev*. 2017;13(2):118–129.
9. Tops LF, Delgado V, Marsan NA, et al. Myocardial strain to detect subtle left ventricular systolic dysfunction. *Eur J Heart Fail*. 2017;19:307.
10. Stöhr EJ, Shave RE, Baggish AL. Left ventricular twist mechanics in the context of normal physiology and cardiovascular disease: a review of studies using speckle tracking echocardiography. *Am J Physiology-Heart Circulatory Physiol*. 2015;311:H633.
11. Nagueh SF, Smiseth OA, Appleton CP, et al. Recommendations for the evaluation of left ventricular diastolic function by echocardiography: an update from the American Society of Echocardiography and the European Association of Cardiovascular Imaging. *J Am Soc Echocardiogr*. 2016;29:277.
12. Nagueh SF. Left ventricular diastolic function: understanding pathophysiology, diagnosis, and prognosis with echocardiography. *J Am Coll Cardiol Img*. 2020;13:228.
13. Rallidi LS, Makavos G, Nihoyannopoulos P. Right ventricular involvement in coronary artery disease: role of echocardiography for diagnosis and prognosis. *J Am Soc Echocardiogr*. 2014;27:223.
14. Porter TR, Shillcutt SK, Adams MS, et al. Guidelines for the use of echocardiography as a monitor for therapeutic intervention in adults: a report from the American Society of Echocardiography. *J Am Soc Echocardiogr*. 2015;28:40.
15. Doherty JU, Kort S, Mehran R, et al. ACC/AATS/ AHA/ASE/ASNC/HRS/SCAI/SCCT/SCMR/STS 2019 appropriate use criteria for multimodality imaging in the assessment of cardiac structure and function in nonvalvular heart disease: a report of the American College of Cardiology appropriate use criteria task force, American Association for Thoracic Surgery, American Heart Association, American Society of Echocardiography, American Society of Nuclear Cardiology, Heart Rhythm Society, Society for Cardiovascular Angiography and Interventions, Society of Cardiovascular Computed Tomography, Society for Cardiovascular Magnetic Resonance, and Society of Thoracic Surgeons. *J Am Coll Cardiol*. 2019;73:488.
16. Doherty JU, Kort S, Mehran R, Schoenhagen P, et al. ACC/AATS/ AHA/ASE/ASNC/HRS/SCAI/SCCT/SCMR/STS 2017 appropriate use criteria for multimodality imaging in valvular heart disease: a report of the American College of Cardiology appropriate use criteria task force, American Association for Thoracic Surgery, American Heart Association, American Society of Echocardiography, American Society of Nuclear Cardiology, Heart Rhythm Society, Society for Cardiovascular Angiography and Interventions, Society of Cardiovascular Computed Tomography, Society for Cardiovascular Magnetic Resonance, and Society of Thoracic Surgeons. *J Am Soc Echocardiog*. 2018;31:381.
17. Thaden JJ, Malouf JF, Rehfeldt KH, et al. Adult intraoperative echocardiography: a comprehensive review of current practice. *J Am Soc Echocardiogr*. 2020;33:735.
18. Purza R, Ghosh S, Walker C, et al. Transesophageal echocardiography complications in adult cardiac surgery: a retrospective cohort study. *Annals Thoracic Surg*. 2017;103:795.
19. Freitas-Ferraz AB, Rodés-Cabau J, Junquera V, et al. Transesophageal echocardiography complications associated with interventional cardiology procedures. *Am Heart J*. 2020;221:19.
20. Porter TR, Mulvagh SL, Abdelmoneim SS, et al. Clinical applications of ultrasonic enhancing agents in echocardiography: 2018 American Society of Echocardiography guidelines update. *J Am Soc Echocardiog*. 2018;31:241.
21. Seol SH, Lindner JR. A primer on the methods and applications for contrast echocardiography in clinical imaging. *J Cardiovasc Ultrasound*. 2014;22:101.
22. Bruun NE, Habib G, Thuny F, et al. Cardiac imaging in infectious endocarditis. *Eur Heart J*. 2014;10:624.
23. Saw J, Lopes JP, Reisman M, McLaughlin P, et al. Cardiac computed tomography angiography for left atrial appendage closure. *Can J Cardiol*. 2016;32:1033.
24. Klein AL, Abbara S, Agler DA, et al. American Society of Echocardiography clinical recommendations for multimodality cardiovascular imaging of patients with pericardial disease. *J Am Soc Echocardiogr*. 2013;26:965.
25. Sicari R, Cortigiani L. The clinical use of stress echocardiography in ischemic heart disease. *Cardiovasc Ultrasound*. 2017;15:7.
26. Erbel R, Aboyans V, Boileau C, et al. 2014 ESC Guidelines on the diagnosis and treatment of aortic diseases: document covering acute and chronic aortic diseases of the thoracic and abdominal aorta of the adult. The Task Force for the Diagnosis and Treatment of Aortic Diseases of the European Society of Cardiology (ESC). *Eur Heart J*. 2014;35:2873.
27. Clavel MA, Pibarot P, Messika-Zeitoun D, et al. Impact of aortic valve calcification, as measured by MDCT, on survival in patients with aortic stenosis: results of an international registry study. *J Am Coll Cardiol*. 2014;64:1202.
28. Balzer J, Zeus T, Veulemans V, et al. Hybrid imaging in the catheter laboratory: real-time fusion of echocardiography and fluoroscopy during percutaneous structural heart disease interventions. *Interv Cardiol*. 2016;11:59.
29. Afzal S, Piayda K, Maier O, et al. Current and future aspects of multimodal imaging, diagnostic, and treatment strategies in bicuspid aortic valve and associated aortopathies. *J Clin Med*. 2020;9:662.
30. Amzulescu MS, De Craene M, Langet H, et al. Myocardial strain imaging: review of general principles, validation, and sources of discrepancies. *Eur Heart J - Cardiovasc Imaging*. 2019;20:605.

### Myocardial Infarction

31. Prastaro M, Pirozzi E, Gaibazzi N, et al. Expert review on the prognostic role of echocardiography after acute myocardial infarction. *J Am Soc Echocardiog*. 2017;30:431.
32. Lancellotti P, Price S, Edvardsen T, et al. The use of echocardiography in acute cardiovascular care: recommendations of the European Association of Cardiovascular Imaging and the acute cardiovascular care association. *Eur Heart J*. 2015;16:119.
33. Roifman I, Connelly KA, Wright GA, et al. Echocardiography vs. Cardiac magnetic resonance imaging for the diagnosis of left ventricular thrombus: a systematic review. *Can J Cardiol*. 2015;31:785.
34. Dudzinski DM, Hung J. Echocardiographic assessment of ischemic mitral regurgitation. *Cardiovasc Ultrasound*. 2014;12:46.
35. Malhotra S, Canty JM. Structural and physiological imaging to predict the risk of lethal ventricular arrhythmias and sudden death. *JACC Cardiovasc Imaging*. 2019;12:2049.
36. Cikes M, Solomon SD. Beyond ejection fraction: an integrative approach for assessment of cardiac structure and function in heart failure. *Eur Heart J*. 2016;37:1642.

### Cardiomyopathies

37. Nunes MCP, Badan LP, Marin-Neto JA, et al. Multimodality imaging evaluation of Chagas disease: an expert consensus of Brazilian Cardiovascular Imaging Department (DIC) and the European Association of Cardiovascular Imaging (EACVI). *Eur Heart J Cardiovasc Imaging*. 2018;19:459.
38. Citro R, Lyon AR, Meimoun P, et al. Standard and advanced echocardiography in takotsubo (stress) cardiomyopathy: clinical and prognostic implications. *J Am Soc Echocardiogr*. 2015;28:57.
39. Omar AM, Bansal M, Sengupta PP. Advances in echocardiographic imaging in heart failure with reduced and preserved ejection fraction. *Circ Res*. 2016;119:357.
40. Katbeh A, Van Camp G, Barbato E, et al. Cardiac resynchronization therapy optimization: a comprehensive approach. *Cardiology*. 2019;142:116.
41. Parato VM, Antoncecchi V, Sozzi F, et al. Echocardiographic diagnosis of the different phenotypes of hypertrophic cardiomyopathy. *Cardiovasc Ultrasound*. 2016;14:30.
42. Maron BJ. Clinical course and management of hypertrophic cardiomyopathy. *N Engl J Med*. 2018;379:655.
43. Asatryan B, Marcus FI. The ever-expanding landscape of cardiomyopathies. *J Am Coll Cardiol Case Rep*. 2020;2:361.
44. Oechslin E, Jenni R. Left ventricular noncompaction: from physiologic remodeling to noncompaction cardiomyopathy. *J Am Coll Cardiol*. 2018;71:723.

45. Towbin JA, McKenna WJ, Abrams DJ, et al. 2019 HRS expert consensus statement on evaluation, risk stratification, and management of arrhythmogenic cardiomyopathy: executive summary. *Heart Rhythm*. 2019;16:e373.
46. Dorbala SD, Cuddy S, Falk RH. How to image cardiac amyloidosis: a practical approach. *J Am Coll Cardiol: Cardiovasc Imaging*. 2019;13:1368.
47. Perry R, Selvanayagam JB. Echocardiography in infiltrative cardiomyopathy. *Heart Lung Circ*. 2019;28:1365.
48. Gorscan J, Bhupendar T. Newer echocardiographic techniques in cardiac resynchronization therapy. *Heart Fail Clin*. 2017;13:53.
49. Ponikowski P, Voors AA, Anker SD, et al. 2016 ESC Guidelines for the diagnosis and treatment of acute and chronic heart failure: the Task Force for the diagnosis and treatment of acute and chronic heart failure of the European Society of Cardiology (ESC) Developed with the special contribution of the Heart Failure Association (HFA) of the ESC. *Eur Heart J*. 2016;37:2129.
50. Ingvarsson A, Werther Evaldsson A, Waktare J, et al. Normal reference ranges for transthoracic echocardiography following heart transplantation. *J Am Soc Echocardiog*. 2018;31:349.
51. Clemmensen TS, Løgstrup BB, Eiskjær H, et al. Changes in longitudinal myocardial deformation during acute cardiac rejection: the clinical role of two-dimensional speckle-tracking echocardiography. *J Am Soc Echocardiogr*. 2015;28:330.
52. Badan LP, Miglioranza MH, Edvardsen T, et al. European Association of Cardiovascular Imaging/ Cardiovascular Imaging Department of the Brazilian Society of Cardiology recommendations for the use of cardiac imaging to assess and follow patients after heart transplantation. *Eur Heart J Cardiovasc Imaging*. 2015;16:919.
53. Olymbios M, Kwiecinski J, Berman DS, et al. Imaging in heart transplant patients. *J Am Coll Cardiol Cardiovasc Imaging*. 2018;11:1514.
54. Elkaryoni A, Abu-Sheasha G, Altibi AM, et al. Diagnostic accuracy of dobutamine stress echocardiography in the detection of cardiac allograft vasculopathy in heart transplant recipients: a systematic review and meta-analysis study. *Echocardiography*. 2019;36:528.
55. Stainback RF, Estep JD, Agler DA, et al. Echocardiography in the management of patients with left ventricular assist devices: recommendations from the American Society of Echocardiography. *J Am Soc Echocardiogr*. 2015;28:853.
56. Bouchez S, Van Belleghem Y, De Somer F, et al. Haemodynamic management of patients with left ventricular assist devices using echocardiography: the essentials. *Eur H J Cardiovasc Imaging*. 2019;20:373.
57. Platz E, Campbell RT, Claggett B, et al. Lung ultrasound in acute heart failure. *J Am Coll Cardiol Heart Failure*. 2019;7:849.
58. Baggish AL, Battle RW, Beaver TA, et al. Recommendations on the use of multimodality cardiovascular imaging in young adult competitive athletes: a report from the American Society of Echocardiography in collaboration with the society of cardiovascular computed tomography and the society for cardiovascular magnetic resonance. *J Am Soc Echocardiog*. 2020;33:523.
59. Wasfy MM, Weiner RB. Differentiating the athlete's heart from hypertrophic cardiomyopathy. *Curr Opin Cardiol*. 2015;30:500.

### Stress Echocardiography

60. Pellikka P, Arruda-Olson A, Chaudhry FA, et al. Guidelines for performance, interpretation, and application of stress echocardiography in ischemic heart disease: from the American Society of Echocardiography. *J Am Soc Echocardiog*. 2020;33:1.
61. Garbi M, Chambers J, Vannan MA, et al. Valve stress echocardiography: a practical guide for referral, procedure, reporting, and clinical implementation of results from the HAVEC Group. *JACC Cardiovasc Imaging*. 2015;8:724.
62. Clavel MA, Burwash IG, Pibarot P. Cardiac imaging for assessing low-gradient severe aortic stenosis. *J Am Coll Cardiol Cardiovasc Imag*. 2017;10:185.
63. Delgado V, Clavel MA, Hahn RT, et al. How do we reconcile echocardiography, computed tomography, and hybrid imaging in assessing discordant grading of aortic stenosis severity? *J Am Coll Cardiol Cardiovasc Imaging*. 2019;12:267.
64. Lancellotti P, Pellikka PA, Budts W, et al. The clinical use of stress echocardiography in non-ischaemic heart disease: recommendations from the European Association of Cardiovascular Imaging and the American Society of Echocardiography. *J Am Soc Echocardiogr*. 2017;30:101.

### Valvular Heart Disease

65. Otto CM, Nishimura RA, Bonow RO, et al. 2020 ACC/AHA Guideline for the management of patients with valvular heart disease. A Report of the American College of Cardiology/ American Heart Association Joint Committee on Clinical Practice Guidelines. *Circulation*. 2021;143(5):e35–e71.
66. Zoghbi WA, Adams D, Bonow RO, et al. Recommendations for noninvasive evaluation of native valvular regurgitation: a report from the American Society of Echocardiography developed in collaboration with the society for cardiovascular magnetic resonance. *J Am Soc Echocardiogr*. 2017;30:303.
67. Baumgartner H, Hung J, Bermejo J, et al. Recommendations on the echocardiographic assessment of aortic valve stenosis: a focused update from the European Association of Cardiovascular Imaging and the American Society of Echocardiography. *J Am Soc Echocardiogr*. 2017;30:372.
68. Frank M, Ganzoni G, Starck C, et al. Lack of accessible data on prosthetic heart valves. *Int J Cardiovasc Imaging*. 2016;32:439.
69. Blauwet LA, Miller Jr FA. Echocardiographic assessment of prosthetic heart valves. *Prog Cardiovasc Dis*. 2014;57:100.
70. Zamorano J, Goncalves A, Lancellotti P, et al. The use of imaging in new transcatheter interventions: an EACVI review paper. *Eur Heart J Cardiovasc Imag*. 2016;17:835.

### Pericardial Disease

71. Chetrit M, Xu B, Verma BR, et al. Multimodality imaging for the assessment of pericardial diseases. *Curr Cardiol Rep*. 2019;21:41.
72. Cosyns B, Plein S, Nihoyanopoulos P, et al. European Association of Cardiovascular Imaging (EACVI) position paper: multimodality imaging in pericardial disease. *Eur Heart J Cardiovasc Imaging*. 2015;16:12.

### Pulmonary Embolism

73. Konstantinides SV, Meyer G, Becattini C, et al. 2019 ESC guidelines on the diagnosis and management of acute pulmonary embolism developed in collaboration with the European Respiratory Society (ERS): the Task Force for the diagnosis and management of acute pulmonary embolism of the European Society of Cardiology (ESC). *Eur Heart J*. 2020;41:543.
74. Mediratta A, Addetia K, Medvedofsky D, et al. Echocardiographic diagnosis of acute pulmonary embolism in patients with McConnell's sign. *Echocardiography*. 2016;33:696.

### Pulmonary Hypertension

75. Cordina RL, Playford D, Lang I, Celermajer DS. State-of-the-Art review: echocardiography in pulmonary hypertension. *Heart Lung Circ*. 2019;28:1351.

### Infective Endocarditis

76. Habib G, Lancellotti P, Antunes MJ, et al. 2015 ESC guidelines for the management of infective endocarditis. The task force for the management of infective endocarditis of the European Society of Cardiology (ESC). Endorsed by the European Association for Cardio-Thoracic Surgery (EACTS) and the European Association of Nuclear Medicine (EANM). *Eur Heart J*. 2015;36:3075.
77. Flachskampf FA, Wouters PF, Edvardsen T, et al. Recommendations for transoesophageal echocardiography: EACVI update 2014. *Eur Heart J Cardiovasc Imaging*. 2014;15:353.
78. Sedgwick JF, Scalia GM. Advanced Echocardiography for the Diagnosis and Management of Infective Endocarditis. Firstenberg MS (ed). Contemporary Challenges in Endocarditis. 2016 In Tech.
79. Saric M, Armour AC, Anaout MS, et al. Guidelines for the use of echocardiography in the evaluation of a cardiac source of embolism. *J Am Soc Echocardiogr*. 2016;29.

### Systemic Disease and Echocardiography

80. Manga P, McCutcheon K, Tsabede N, et al. HIV and nonischemic heart disease. *J Am Coll Cardiol*. 2017;69:83.
81. Plana JC, Galderisi M, Barac A, et al. Expert consensus for multimodality imaging evaluation of adult patients during and after cancer therapy: a report from the American Society of Echocardiography and the European Association of Cardiovascular Imaging. *J Am Soc Echocardiogr*. 2014;27:911.
82. Kang Y, Scherrer-Crosbie M. Echocardiography imaging of cardiotoxicity. *Cardiol Clinics*. 2019;37:419.
83. Bois J, Anand V, Anavekar N. Detection of inflammatory aortopathies using multimodality imaging. *Circ: Cardiovasc Imaging*. 2019;12:e008471.

### Cardiac Masses

84. Wu JC. Cardiac tumors and masses. In: Stergiopoulos K, Brown DL, eds. *Evidence-Based Cardiology Consult*. New York: Springer Science+Business Media; 2014.
85. Palaskas N, Thompson K, Gladish G, et al. Evaluation and management of cardiac tumors. *Curr Treatment Options Cardiovasc Med*. 2018;20:29.
86. Laura DM, Donnino R, Kim EE, et al. Silbiger JJ, Bazaz R, Trost B. Lipomatous atrial septal hypertrophy: a review of its anatomy, pathophysiology, multimodality imaging, and relevance to percutaneous interventions. *J Am Soc Echocardiog*. 2016;29:717.
87. Tower-Rader A, Kwon D. Pericardial masses, cysts and diverticula: a comprehensive review using multimodality imaging. *Prog Cardiovasc Dis*. 2017;59:389.

### Congenital Heart Disease in Adults

88. Akagi T. Current concept of transcatheter closure of atrial septal defect in adults. *J Cardiol*. 2015;65:17.
89. Cohen MS, Eidem BW, Cetta F, et al. Multimodality imaging guidelines of patients with transposition of the great arteries: a report from the American Society of Echocardiography developed in collaboration with the society for cardiovascular magnetic resonance and the society of cardiovascular computed tomography. *J Am Soc Echocardiogr*. 2016;29:571.
90. Valente AM, Cook S, Festa P, et al. Multimodality imaging guidelines for patients with repaired tetralogy of Fallot: a report from the American Society of Echocardiography developed in collaboration with the society for cardiovascular magnetic resonance and the society for pediatric radiology. *J Am Soc Echocardiogr*. 2014;27:111.

### Transcatheter Interventions

91. Freitas-Ferraz AB, Bernier M, Vaillancourt, et al. Safety of transesophageal echocardiography to guide structural cardiac interventions. *J Am Coll Cardiol*. 2020;75:3174.
92. Hahn RT, Nabauer M, Zuber M, et al. Intraprocedural imaging of transcatheter tricuspid valve interventions. *J Am Coll Cardiol Cardiovasc Imaging*. 2019;12:532.
93. Vainrib AF, Harb SC, Jaber W, et al. Left atrial appendage occlusion/exclusion: procedural image guidance with transesophageal echocardiography. *J Am Soc Echocardiogr*. 2018;31:454.

### Future Directions
#### Multimodality Imaging

94. Rozado J, Martin M, Pascual I, et al. Comparing American, European and Asian practice guidelines for aortic diseases. *J Thorac Dis*. 2017;9:S551.
95. Afonso L, Kottam A, Reddy V, et al. Echocardiography in infective endocarditis: state of the art. *Echocardiogr*. 2017;19:127.

#### Handheld Echocardiography (Point of Care Ultrasound)

96. Cahmsi-Pasha MA, Sengupta PP, Zoghbi WA. Handheld echocardiography: current state and future perspectives. *Circulation*. 2017;136:2178.
97. Cardim N, Dalen H, Voigt J-U, et al. The use of handheld ultrasound devices: a position statement of the European Association of Cardiovascular Imaging (2018 update). *Eur Heart J Cardiovasc Imag*. 2019;20:245.

#### Newer Techniques

98. Voigt J-U, Cvijic M. 2- and 3-dimensional myocardial strain in cardiac health and disease. *J Am Coll Cardiol Cardiovasc Imaging*. 2019;12:1849.
99. Takaya Y, Ito H. New horizon of fusion imaging using echocardiography: its progress in the diagnosis and treatment of cardiovascular disease. *J Echocardiog*. 2020;18:9.

#### Artificial Intelligence

100. Dey D, Slomka PJ, Leeson P, et al. Artificial intelligence in cardiovascular imaging: JACC state-of-the-art review. *J Am Coll Cardiol*. 2019;73:1317.
101. Narang A, Lang RM. Artificial Intelligence and Echocardiography. Expert Analysis. https://www.acc.org/latest-in-cardiology/articles/2019/06/18/07/43/artificial-intelligence-and-echocardiography.

# APPROPRIATE USE CRITERIA

## Echocardiography

*Scott D. Solomon and Robert O. Bonow*

During the past three decades, there has been explosive growth in the use of cardiac imaging, particularly in the applications of echocardiography, Doppler echocardiography, and stress and strain echocardiography. Echocardiography remains the most accessible and highest volume cardiac imaging test, but there is much growth also in radiologic imaging modalities. The American College of Cardiology and American Heart Association (ACC/AHA) have jointly produced guidelines for the use of echocardiography since 1980. In 2003, the ACC spearheaded the delivery of appropriate use criteria (AUC) for imaging, which are designed to define the appropriate test for the appropriate indication in the appropriate patient. The process used for development of appropriateness criteria is evidence based, where possible, but is also heavily weighted by expert consensus.

The AUC for imaging modalities are based on a number of common clinical scenarios in which imaging is often used. These scenarios are then rated by a panel with a broad array of expertise (i.e., not just imaging experts, but also practicing physicians, statisticians, and clinical trialists) to evaluate the "appropriateness" of the study in each situation in terms of the following definition: "An appropriate imaging study is one in which the expected incremental information, combined with clinical judgment, exceeds the expected negative consequences by a sufficiently wide margin for a specific indication that the procedure is generally considered acceptable care and a reasonable approach for the indication." Rating scores are made on a scale of 1 to 9, in which higher scores indicate more appropriate use of testing. The scale is then divided in thirds, to correspond with conclusions of: R, rarely appropriate (1 to 3); M, may be appropriate (4 to 6); A, appropriate (7 to 9). The AUC are practical standards intended to help guide the rational and efficient use of these imaging technologies. AUC development is an ongoing process based on the current technical capabilities and when possible, indications are mapped to published society guidelines.[1]

The original AUC for echocardiography and stress echocardiography were published beginning in 2007.[2] Since 2013, the more recent AUC documents for multimodality imaging in patients with predispositions for structural heart disease, arrhythmias, hypertension, chest pain, ischemic heart disease, and heart failure now conform to the updated terminology and provide criteria for the use of echocardiography in these condition as well as other imaging modalities (CMR, CT, and SPECT/PET imaging).[3–6] This more accurately reflects the real-world where multiple different tests are available to the clinician. These AUC have been published as 2 separate companion consensus statements on Appropriate Use Criteria for Multimodality Imaging in the Assessment of Cardiac Structure and Function in Valvular Heart Disease (2017)[5] and likewise in Nonvalvular Heart Disease (2019)[6] (**see Chapter 18** Appropriate Use Criteria). These comprehensive documents include AUC for each indication with respect to transthoracic echocardiography (2 and 3D-imaging), transesophageal echocardiography, stress echocardiography, and strain imaging. In addition, heart and echocardiography society recommendations for the assessments of disease states such as valvular stenoses, regurgitation, and ischemia which are dedicated to transthoracic, transesophageal, and stress echocardiography are helpful for guidance and quality control specifically within the echocardiography laboratory.

## REFERENCES

1. Hendel RC, Lindsay BD, Allen JM, et al. ACC appropriate use criteria methodology: 2018 update: a report of the American College of Cardiology appropriate use criteria task force. *J Am Coll Cardiol*. 2018;71:935.
2. Patel MR, White RD, Abbara S, et al. 2013 ACCF/ACR/ASE/ASNC/SCCT/SCMR appropriate utilization of cardiovascular imaging in heart failure. A joint report of the American College of Radiology appropriateness criteria committee and the American College of Cardiology foundation appropriate use criteria task force. *J Am Coll Cardiol*. 2013;61:2207.
3. Wolk MJ, Bailey SR, Doherty JU, et al. ACCF/AHA/ASE/ASNC/HFSA/HRS/SCAI/SCCT/SCMR/STS 2013 multimodality appropriate use criteria for the detection and risk assessment of stable ischemic heart disease. A report of the American College of Cardiology foundation appropriate use criteria task force, American Heart Association, American Society of Echocardiography, American Society of Nuclear Cardiology, Heart Failure Society of America, Heart Rhythm Society, Society for Cardiovascular Angiography and Interventions, Society of Cardiovascular Computed Tomography, Society for Cardiovascular Magnetic Resonance, and Society of Thoracic Surgeons. *J Am Coll Cardiol*. 2014;63:380.
4. Rybicki FJ, Udelson JE, Peacock WF, et al. 2015 ACR/ACC/AHA/AATS/ACEP/ASNC/NASCI/SAEM/SCCT/SCMR/SCPC/SNMMI/STR/STS appropriate utilization of cardiovascular imaging in emergency department patients with chest pain. A joint document of the American College of Radiology appropriateness criteria committee and the American College of Cardiology appropriate use criteria task force. *J Am Coll Cardiol*. 2016;67:853.
5. Doherty JU, Kort S, Mehran R, et al. 2017 ACC/AATS/AHA/ASE/ASNC/HRS/SCAI/SCCT/SCMR/STS 2017 appropriate use criteria for multimodality imaging in valvular heart disease: a report of the American College of Cardiology appropriate use criteria task force, American Association for Thoracic Surgery, American Heart Association, American Society of Echocardiography, American Society of Nuclear Cardiology, Heart Rhythm Society, Society for Cardiovascular Angiography and Interventions, Society of Cardiovascular Computed Tomography, Society for Cardiovascular Magnetic Resonance, and Society of Thoracic Surgeons. *J Am Soc Echocardiogr*. 2018;31:381.
6. Doherty JU, Kort S, Mehran R, et al. 2019. ACC/AATS/ AHA/ASE/ASNC/HRS/SCAI/SCCT/SCMR/STS 2019 appropriate use criteria for multimodality imaging in the assessment of cardiac structure and function in nonvalvular heart disease: a report of the American College of Cardiology appropriate use criteria task force, American Association for Thoracic Surgery, American Heart Association, American Society of Echocardiography, American Society of Nuclear Cardiology, Heart Rhythm Society, Society for Cardiovascular Angiography and Interventions, Society of Cardiovascular Computed Tomography, Society for Cardiovascular Magnetic Resonance, and Society of Thoracic Surgeons. *J Am Coll Cardiol*. 2019;73:488.